Identifying New Genes and Molecular Mechanisms in Mitochondrial Disease

Ruth Inge Carlton Glasgow

Supervisors:

Professor Robert W. Taylor

Professor Robert McFarland

Dr. Kyle Thompson

This thesis is submitted for the degree of Doctor of Philosophy

Wellcome Centre for Mitochondrial Research

Translational and Clinical Research Institute

August 2020

Abstract

An estimated 1158 nuclear encoded proteins function within mammalian mitochondria. Over the past ten years the increased implementation of next generation sequencing-driven diagnostics, particularly whole exome sequencing (WES), has resulted in the identification of over 150 nuclear genes not previously implicated in mitochondrial disease, necessitating extensive functional studies to determine and confirm pathogenicity. Over one third of reported mitochondrial disease-causing nuclear genetic variants reside in genes encoding proteins with a role in mtDNA gene expression. The overarching aim of my research project was to functionally validate novel candidate mitochondrial disease variants, focusing on those identified in genes encoding proteins with roles in mitochondrial translation, in order to achieve genetic diagnoses for affected patients.

WES of two unrelated patients with early-onset neurological disease presentations identified different and previously unreported variants in the *GFM2* gene encoding ribosome recycling factor mtEFG2. Differential and tissue-specific patterns of combined OXPHOS defects were identified in each patient. Novel compound heterozygous variants in the *TSFM* gene, encoding the elongation factor mtEF-Ts, were identified in a single patient presenting with adult-onset hypertrophic cardiomyopathy. The abundance of mtEF-Ts was significantly decreased in patient fibroblasts and cardiac tissue. The resulting OXPHOS deficiency was most severe in cardiac tissue, accompanied by decreased levels of elongation factor mtEF-Tu.

A homozygous nonsense mutation in the *MRPL47* gene, encoding a mitoribosomal large subunit (LSU) protein, was identified in three unrelated paediatric patients presenting with metabolic acidosis, epilepsy and liver involvement. Patient fibroblasts exhibited disorders of translation and combined OXPHOS defects. Some truncated MRPL47 protein was visualised within the destabilised LSU. Variants in *MRPL65*, a second LSU gene, were identified in five paediatric patients presenting with overlapping clinical features including developmental delay, ataxia and nystagmus. Attempts to generate a CRISPR/Cas9 *MRPL65* knock-out cell line were unsuccessful due to polyploidy of the target genomic region, highlighting the importance of

karyotyping in gene editing studies. *MRPL65* cDNA analysis in a single patient identified retention of intronic sequence due to a +5 splice variant. Patient fibroblasts displayed normal levels of MRPL65 and OXPHOS proteins, but appeared to exhibit a defect in mitochondrial translation alongside some abnormal assembly of the LSU.

This work expands upon our current knowledge of Mendelian mitochondrial disorders, adding to a growing list of nuclear genes implicated in disorders of translation and achieving genetic diagnosis in the presented families. Tissue-specific defects illustrate the complexity of the pathomechanisms underlying these disorders and highlight the gaps in our understanding of adaptive compensatory mechanisms employed in different tissues. This research also emphasises the importance of identifying and characterising multiple families when assigning pathogenicity to novel disease-causing variants.

Acknowledgements

Firstly, I must thank my supervisors Professor Robert Taylor, Professor Robert McFarland and Dr Kyle Thompson for providing me with the opportunity to carry out this PhD and their continued support and guidance throughout. Rob's direction and advice, Bobby's help with all things clinical and Kyle's patience and expertise in the lab have been invaluable. I feel very thankful to have found myself in your team for my six week undergraduate research project, and for every fantastic opportunity that has followed.

Secondly, I would like to thank the rest of the Taylor lab for generating such a warm, helpful and exciting working environment. A special thanks to Monika who has been like a fourth supervisor to me and who's knowledge and guidance has helped shape my entire project. Thank you to Angela for having an answer to every conceivable silly lab question and to Charlotte for all of her genetics mastery. Thanks must also go to others in the Diagnostics team, including Gavin and Laura, who have been extremely accommodating in making cells and tissues available for my use.

I feel fortunate to have not only worked within a fantastic group of scientists at the WCMR, but also to have made some wonderful friendships along the way. To the VIP office members past and present, Hannah, Carla, Ahmad, Megan, Jack (my forever lab husband), Matt, Róisín and Imogen, I can't imagine having gone through this without you. Thank you all for the many, many laughs and for also being there during the very occasional cry. Thanks also to Charlotte and Yasmin for being around to share the highs and lows of our mitochondrial PhD journey as part of the Clayton Park Trio and to Tasnim and Shane for being friends from day one.

The encouragement provided by my friends and family throughout this challenging process has meant so much. My lovely friends Rosie and Lottie D have been a steady source of strength, love and matching wellies. Lottie R has always been on hand for some female empowerment. Having the OG Genetics Squad with Dimitra, Bronwyn and Anna still going strong has brought about so many happy times. Carl has given

me a huge amount motivation during these strange thesis-writing months. Sophie came into my life at the perfect time and has been the sister I didn't know I needed! I am incredibly lucky to have many inspirational and supportive women in my life, including my godmother Chrissie, cousin Abi, auntie Ruth and my honorary 'auntie' Julie. They are wonderful role models and have always been on hand for help when I needed it.

I want to thank my Grandma and Grandad Glasgow for always having faith in me. Thanks to my brothers, Jonathan and Lewis, are also required. They have put up with my PhD induced mood-swings and kept the family group chat a constant source of entertainment. I would not have reached this milestone were it not for my brilliant and unwaveringly supportive parents. I have my Dad to thank for the provision of New Scientist magazines as toilet reading material in childhood, surely sowing the seeds for a scientific career! My Mum has provided me with the blueprints to becoming a strong, intelligent and successful woman while also being the kindest person I know. Making the both of you proud has been my greatest motivation and I love you very much.

It is with huge gratitude that I thank the Lily Foundation for funding my PhD studentship, making this project possible. The work they carry out to fund research that furthers our scientific understanding of mitochondrial disease, and support those affected, is very special. I feel honoured to have been involved in their family weekends throughout my time as a Lily-funded scientist. My final and heartfelt thanks go to the patients and family members who kindly gave their consent to the work presented within this thesis. I very much hope that continued research into mitochondrial disease will improve the lives of all who are impacted by this group of disorders.

Publications

Glasgow, R. I. C., Thompson, K., Barbosa, I. A., He, L., Alston, C. L., Deshpande, C., Simpson, M. A., Morris, A. A. M., Neu, A., Lobel, U., Hall, J., Prokisch, H., Haack, T. B., Hempel, M., McFarland, R. and Taylor, R. W. (2017) 'Novel GFM2 variants associated with early-onset neurological presentations of mitochondrial disease and impaired expression of OXPHOS subunits', *Neurogenetics,* 18(4), pp. 227-235.

Alston, C. L., Heidler, J., Dibley, M. G., Kremer, L. S., Taylor, L. S., Fratter, C., French, C. E., **Glasgow, R. I. C.**, Feichtinger, R. G., Delon, I., Pagnamenta, A. T., Dolling, H., Lemonde, H., Aiton, N., Bjornstad, A., Henneke, L., Gartner, J., Thiele, H., Tauchmannova, K., Quaghebeur, G., Houstek, J., Sperl, W., Raymond, F. L., Prokisch, H., Mayr, J. A., McFarland, R., Poulton, J., Ryan, M. T., Wittig, I., Henneke, M. and Taylor, R. W. (2018) 'Bi-allelic Mutations in NDUFA6 Establish Its Role in Early-Onset Isolated Mitochondrial Complex I Deficiency', *Am J Hum Genet,* 103(4), pp. 592-601.

Perli, E., Pisano, A., **Glasgow, R. I. C.**, Carbo, M., Hardy, S. A., Falkous, G., He, L., Cerbelli, B., Pignataro, M. G., Zacara, E., Re, F., Della Monica, P. L., Morea, V., Bonnen, P. E., Taylor, R. W., D'Amati, G. and Giordano, C. (2019) 'Novel compound mutations in the mitochondrial translation elongation factor (TSFM) gene cause severe cardiomyopathy with myocardial fibro-adipose replacement', *Scientific Reports,* 9(1).

Thompson, K., Collier, J. J., **Glasgow, R. I. C.**, Robertson, F. M., Pyle, A., Blakely, E. L., Alston, C. L., Olahova, M., McFarland, R. and Taylor, R. W. (2019) 'Recent advances in understanding the molecular genetic basis of mitochondrial disease', *J Inherit Metab Dis,* 43(1), pp. 36-50.

Glasgow, R. I. C., Lim, A. Z., Nicholls, T. J., McFarland, R., Taylor, R. W. and Oláhová, M. (2020) 'Nuclear genetic disorders of mitochondrial DNA gene expression', in Gasparre, G. and Porcelli, A.M. (eds.) *The Human Mitochondrial Genome*: Academic Press, pp. 375-409.

Table of Contents

List of Figures

List of Tables

Abbreviations

aa-Rs	Aminoacyl-tRNA synthetase
ATP	Adenosine triphosphate
ATPase	Adenosine triphosphate synthase
BN-PAGE	Blue native polyacrylamide gel electrophoresis
bp	Base pair
cDNA	Complementary DNA
COX	Cytochrome oxidase
CRISPR	Clustered regularly interspaced palindromic repeats
crRNA	CRISPR RNA
Cryo-EM	Cryogenic electron microscopy
D-loop	Displacement loop
DNA	Deoxyribonucleic acid
dNTP	Deoxynucleoside triphosphate
DSB	Double strand break
EF	Ejection fraction
ETC	Electron transport chain
FAD	Flavin adenine dinucleotide
Fe-S	Iron-Sulphur
FH	Failing heart
gDNA	Genomic DNA
GDP	Guanosine diphosphate
GFP	Green fluorescent protein
GTP	Guanosine triphosphate

H&E	Haematoxylin and eosin
HDR	Homology directed repair
HSP	Heavy strand promoter
IMM	Inner mitochondrial membrane
IMS	Intermembrane space
iPSC	Induced pluripotent stem cell
Kb	Kilobase
KSS	Kearns-Sayre syndrome
LSP	Light strand promoter
LSU	Large subunit
LV	Left ventricle
LVDD	Left ventricle end diastolic diameter
M	Molar
MCU	Mitochondrial calcium uniporter
MELAS	Mitochondrial encephalopathy, lactic acidosis and stroke-like episodes
MIA	Mitochondrial import and assembly
MIDD	Maternally inherited deafness and diabetes
mL	Millilitre
MRI	Magnetic resonance imaging
mt-mRNA	Mitochondrial messenger RNA
mt-tRNA	Mitochondrial transfer RNA
mtDNA	Mitochondrial DNA
MTS	Mitochondrial targeting sequence
NAD	Nicotinamide adenine dinucleotide
NCR	Non-coding region

nDNA	Nuclear DNA
NFH	Non-failing heart
NGS	Next generation sequencing
NHEJ	Non-homologous end joining
nM	Nanomolar
NMD	Nonsense mediated decay
NUMTs	Nuclear encoded mitochondrial segments
O_H	Origin of heavy strand replication
O_L	Origin of light strand replication
OMM	Outer mitochondrial membrane
OXPHOS	Oxidative phosphorylation
PAM	Protospacer adjacent motif
PCR	Polymerase chain reaction
PEO	Progressive external ophthalmoplegia
PoTC	Post-termination complex
PPR	Pentatricopeptide repeat
PTC	Peptidyl transfer centre
Q	Ubiquinone
RITOLS	Ribonucleotide incorporation throughout lagging strand
RNA	Ribonucleic acid
ROS	Reactive oxygen species
RRF	Ragged red fibres
RV	Right ventricle
SAM	Sorting and assembling machinery
SDS-PAGE	Sodium dodecyl sulphate polyacrylamide gel electrophoresis

sgRNA	Short guide RNA
siRNA	Small interfering RNA
SNP	Single nucleotide polymorphism
SSU	Small subunit
TCA	Trichloroacetic acid
TCA (cycle)	Tricarboxylic acid
TOM	Translocase of the outer membrane
UTR	Untranslated region
VDAC	Voltage dependent ion channels
WES	Whole exome sequencing
WGS	Whole genome sequencing
WT	Wild-type
µg	Microgram
µL	Microlitre

Chapter 1 : Introduction

1.1 Mitochondria: The organelle

Mitochondria are dynamic double membrane bound organelles present in, and essential to, all nucleated human cells. Mitochondria are the product of an endosymbiotic event some 1.5 billion years ago, in which the common cellular ancestor of all eukaryotes endocytosed an α-proteobacterium with anaerobic respiratory capability (Gray, Burger and Lang, 1999). As such, mitochondria possess a genome containing retained genes of bacterial origin. However, the evolution of this genome varied vastly between both animal and non-animal species (Gray, 2012). From this point forward this thesis will focus on human mitochondria, unless otherwise specified.

A primary function of mitochondria is the generation of chemical cellular energy, in the form of adenosine triphosphate (ATP), through a process known as oxidative phosphorylation (OXPHOS). Several other vital cellular processes are mediated by the mitochondria, including iron sulphur cluster and haem biosynthesis, calcium homeostasis and apoptosis (Osellame, Blacker and Duchen, 2012). Many features of human mitochondrial biology that are seen today, such as the unique circular genome, distinct translation machinery, double membrane bound structure and dynamic fission and fusion capabilities are reminiscent of their ancestry as a once independent bacterium (Roger, Munoz-Gomez and Kamikawa, 2017).

1.1.1 Mitochondrial structure

The composition of the outer mitochondrial membrane (OMM) and the inner mitochondrial membrane (IMM) differ from each other to reflect their roles within mitochondrial structure and function. The OMM forms a smooth lipid bilayer, most similar to the plasma membranes of eukaryotes, containing voltage dependent anion channels (VDAC) and translocase of the outer membrane (TOM) complexes to mediate the movement of small molecules and ions between the cytosol and the

intermembrane space (IMS) (Ponnalagu and Singh, 2017). The IMM is less permeable and more selective than the OMM, a property which is of significant importance in the maintenance of the proton gradient that drives ATP synthesis during oxidative phosphorylation. The architecture of the IMM is highly convoluted with many invaginations, termed cristae **(Figure 1.1)** (Gohil and Greenberg, 2009). The cristae provide a large surface area, allowing mitochondria to house and abundance of membrane proteins (Kondadi, Anand and Reichert, 2019). The central cavity of mitochondria, named the matrix, sits within the IMM.

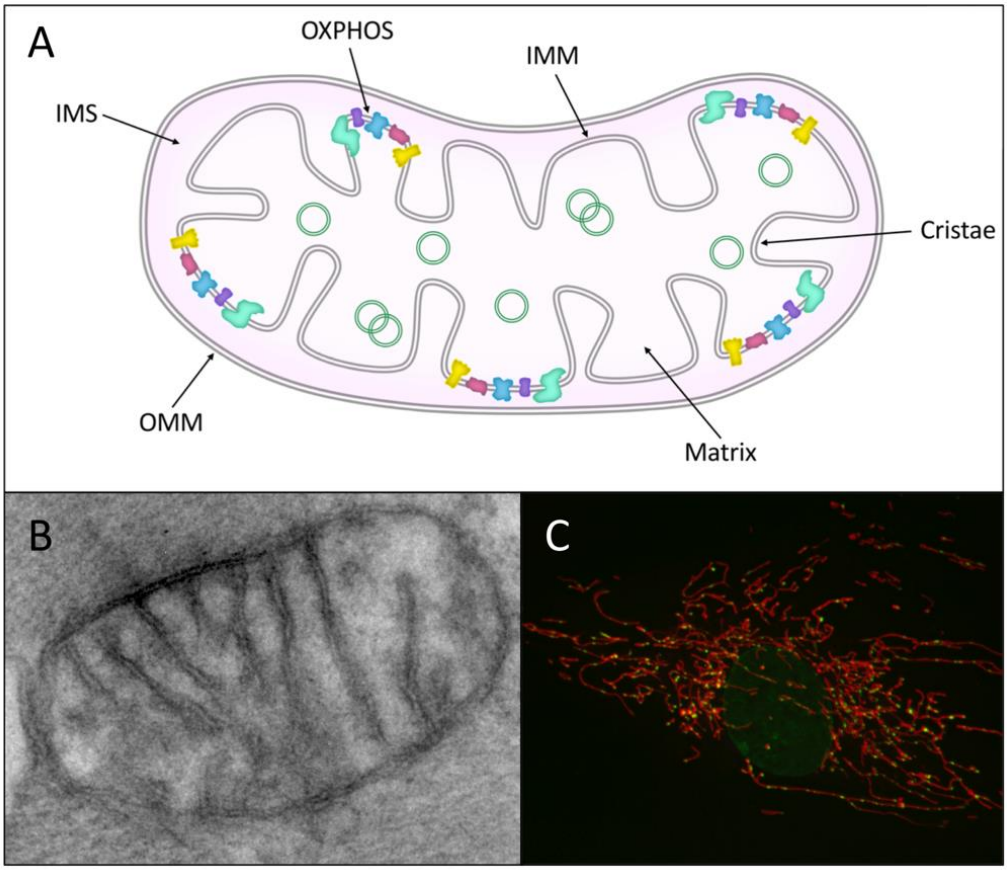

Figure 1.1 Mitochondrial ultrastructure and network organisation. A schematic **(A)** and an electron micrograph **(B)** image of a single mitochondrion, highlighting the key structural features and compartments formed by the outer mitochondrial membrane (OMM), the inner mitochondrial membrane (IMM), the intermembrane space (IMS), cristae and matrix. A confocal image of a single cell stained with TMRM, illustrating the reticular nature of mitochondrial networks **(C)**.

1.1.2 Mitochondrial dynamics

Though commonly depicted diagrammatically as static organelles around 2μm in length, the mitochondria of healthy cells are typically part of a dynamic reticular network, allowing mitochondria to travel between different cellular regions in response to energy requirements (Chan, 2012) **(Figure 1.1)**. These changes in network shape and mitochondrial morphology are primarily driven by fission and fusion events.

Mitochondrial fission is the process by which both the OMM and IMM divide, to produce two separate daughter mitochondria. For this to occur, the protein dynamin-related protein 1 (DRP1), a large GTPase, is recruited from the cytosol to the OMM by four key proteins; mitochondrial fission protein 1 (Fis1), mitochondrial fission factor (Mff), and mitochondrial dynamics proteins 49 and 51 (Mid49 and Mid51) (Loson *et al.*, 2013). Once positioned at the OMM, DRP1 forms oligomeric ring-like structures at ER-mitochondria contact sites, where GTP-driven hydrolysis drives constriction of mitochondria. The final stage of mitochondrial fission is the scission of the constricted area, carried out by the Dynamin-2 (Dnm2) protein, to produce two daughter mitochondria (Kraus and Ryan, 2017).

Fusion of mitochondria is initiated upon the docking of mitofusin GTPases Mfn1 and Mfn2 at adjacent outer mitochondrial membranes of two proximal mitochondria. Conformational changes in mitofusins cause an increase in membrane contact sites, followed by GTPase dependent fusion of the OMM (Song *et al.*, 2009). Mitochondrial dynamin-like protein OPA1, a large GTPase, interacts with IMM phospholipid content to drive subsequent fusion of the IMM (Ban *et al.*, 2017).

1.1.3 The mitochondrial genome

In the matrix of mitochondria there are approximately 1-15 mtDNA molecules, however this number is dynamic and responsive to cell-type specific mechanisms of copy number control (Clay Montier, Deng and Bai, 2009; Satoh and Kuroiwa, 1991). At 16,569bp in size, the circular double stranded mitochondrial genome encodes 37

genes **(Figure 1.2)** (Anderson *et al.*, 1981). Of these genes, 13 encode polypeptides, all of which are core subunits of one of the OXPHOS complexes I, III, IV and V. The remaining genes encode 22 transfer RNAs (tRNAs) and two ribosomal RNAs (rRNAs), *16S* and *12S*, that are integral parts of the large and small mitoribosomal subunits respectively.

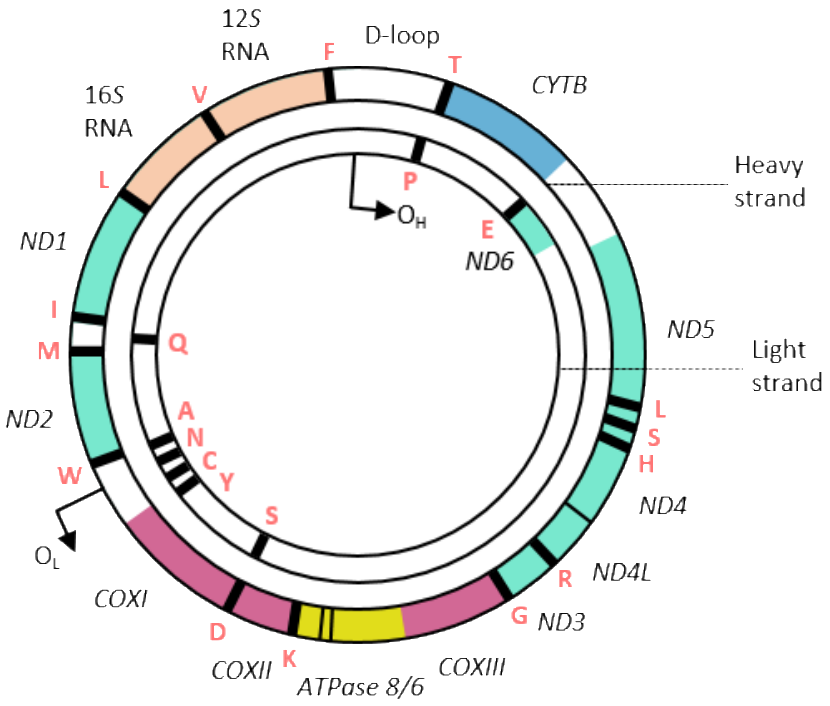

Figure 1.2 The human mitochondrial genome. Diagram of the 16,569 bp human mtDNA molecule with protein coding regions in turquoise (complex I), blue (complex III), pink (complex IV) and yellow (complex V). Ribosomal RNAs are orange and tRNAs are in black. O_H and O_L depict the origins of replication for the heavy and light strand respectively, with arrows pointing in the direction of replication. Mitochondrial tRNA genes in black are labelled with their single letter abbreviations in red.

The two strands of mtDNA are termed the heavy strand (H strand) and light strand (L strand) and differ in their guanine content. The H strand is particularly guanine rich and encodes the majority of mitochondrial transcripts, whilst the L strand generates the *MT-ND6* transcript and eight of the tRNAs **(Figure 1.2)**. The amount of non-coding DNA within mtDNA is very low in comparison to the nuclear genome, with no intronic regions and just one main non-coding region (NCR) within which the displacement loop (D-loop) is found. The D-loop region is a section of the mitochondrial genome approximately 1.1 kb in length, in which the H strand has been displaced by the binding

of an additional linear DNA strand, termed *7S* DNA, to the L strand. The NCR contains both heavy (HSP) and light (LSP) strand promoters and other regulatory elements involved in the control of mtDNA replication and transcription (Walberg and Clayton, 1981).

1.1.3.1 Maternal inheritance

Unlike the mendelian pattern of inheritance displayed by genes of diploid nuclear DNA, mtDNA is widely accepted to be inherited solely through the maternal lineage (Giles *et al.*, 1980). An unfertilised egg contains up to 600,000 copies of mtDNA which vastly outnumbers the ~100 copies carried within each sperm cell (Shoubridge and Wai, 2007; Wai *et al.*, 2010). In mice, during the early stages of fertilisation, the mitochondria of sperm cells were demonstrated to be ubiquitinated within the oocyte cytoplasm, marking them for subsequent autophagic proteolytic degradation (Sutovsky *et al.*, 2004). However, in later studies the role of autophagy in the degradation of sperm mitochondria was questioned when it was shown that the association of autophagic proteins occurring only transiently and significantly earlier than the elimination of paternal mitochondria (Luo *et al.*, 2013). A single case of paternal inheritance of a rare mtDNA disease variant isolated to patient muscle has been previously reported (Schwartz and Vissing, 2002), igniting debate surrounding the possibility and prevalence of paternal mtDNA 'leakage'. A subsequent study of a cohort of 35 mitochondrial myopathy patients detected no evidence of paternal mtDNA inheritance, suggesting that the phenomenon does not frequently occur (Taylor *et al.*, 2003). More recently the publication of data indicating the existence of high heteroplasmy and two individual haplotypes resulting from biparental mtDNA inheritance within three unrelated families (Luo *et al.*, 2018) has renewed academic interest and debate around this topic, though whether paternal mtDNA inheritance exists remains a contentious question (Lutz-Bonengel and Parson, 2019; McWilliams and Suomalainen, 2019).

In 2019, it was hypothesised that the second mtDNA haplotypes detected by Luo et al., could be assigned to multi-copy mtDNA concatemers within the nuclear genome, rather than circular mtDNA inherited paternally (Balciuniene and Balciunas, 2019). It has since been demonstrated experimentally, through the application of WGS in a cohort of 11,03 trios, rare instances of heteroplasmic haplotypes can be attributed to nuclear-encoded mitochondrial segments (NUMTs) that create the impression of paternally inherited mtDNA (Wei *et al.*, 2020).

1.1.4 Bi-genomic control of mitochondria

An estimated 1,158 proteins are present within mitochondria to maintain regular function, of which only 13 are encoded by mtDNA (Calvo, Clauser and Mootha, 2016). During mitochondrial evolution there was vast gene transfer from ancestral endosymbiont genome to the nuclear genome (Adams and Palmer, 2003) These proteins are synthesised in the cytosol, prior their import into mitochondria. A complex system of protein import machinery is required for the appropriate transport of nuclear encoded mitochondrial proteins across the OMM and IMM, essential to the maintenance of mitochondrial function.

1.1.5 Mitochondrial protein import

Transport of proteins into mitochondria is facilitated by dedicated protein translocases. The exact route taken for translocation and assembly is dependent on the type of precursor protein being imported and the targeting sequence it carries. Five distinct mitochondrial protein import pathways have been described to date (Wiedemann and Pfanner, 2017) **(Figure 1.3)**.

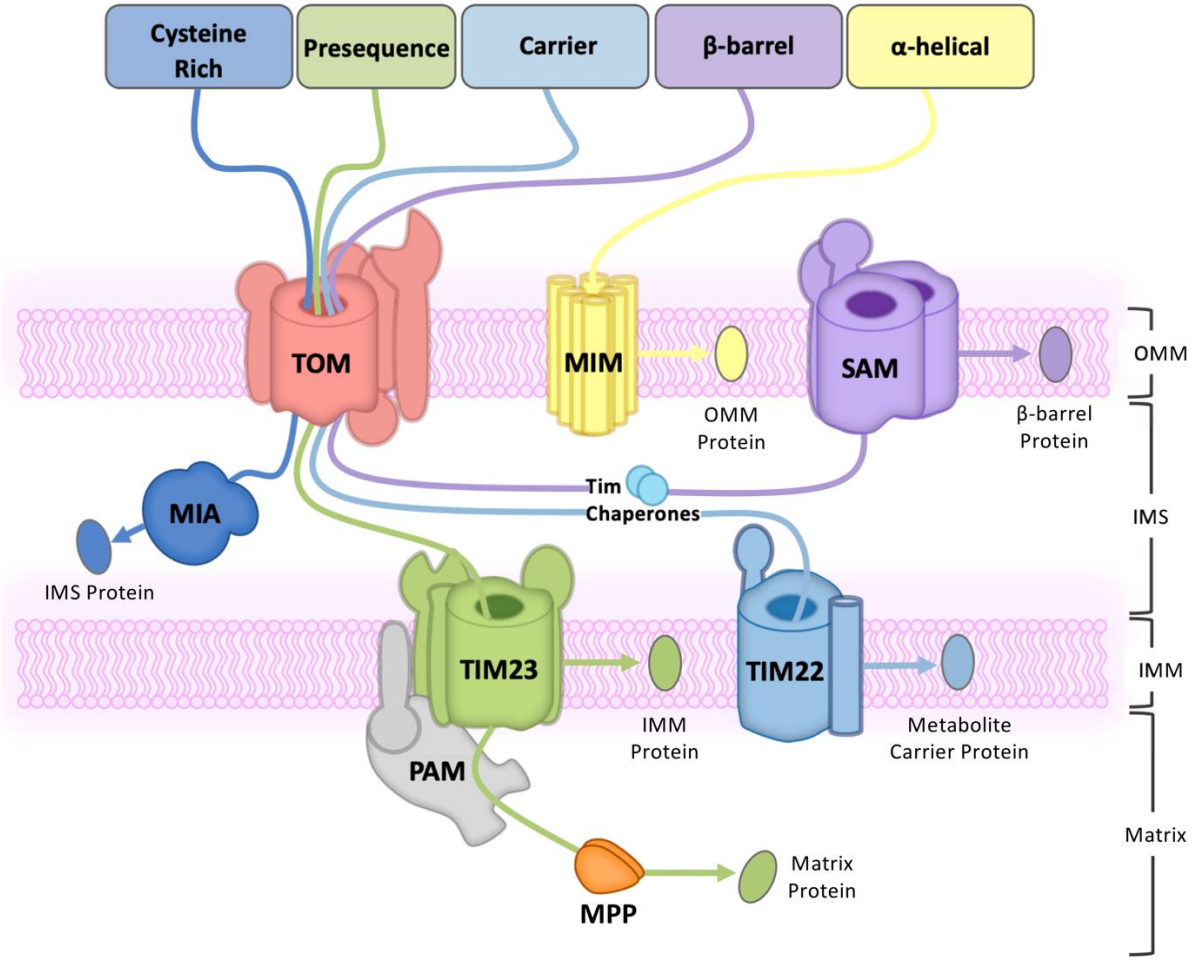

Figure 1.3 Mitochondrial protein import pathways. Schematic overview of the five major mitochondrial protein import pathways. Cysteine rich proteins cross the OMM through translocase of the outer membrane (TOM) and are then undergo folding and assembly directed by the mitochondrial import and assembly (MIA) pathway. Proteins with an N-terminal pre-sequence are imported through TOM and then translocase of the inner membrane 23 (TIM23) driven by the presequence translocase associated motor (PAM). IMM carrier proteins cross the OMM through TOM and are then directed to translocase of the inner membrane 22 (TIM22) by Tim chaperone proteins. Mitochondrial β-barrel proteins also cross the OMM through TOM and interact with Tim chaperone proteins as they are directed to the OMM sorting and assembling machinery (SAM). OMM α- helical proteins are imported and inserted into the membrane by the mitochondrial import complex MIM.

1.1.5.1 Import pathway for N-terminal presequence proteins

The first import pathway to be described, often termed the ‘classical import pathway’, is responsible for the translocation of mitochondrial precursor proteins that carry N-terminal presequences as mitochondrial targeting signals. Translocase of the outer membrane (TOM) and translocase of the inner membrane (TIM23) transport these precursor proteins through the outer and inner mitochondrial membranes respectively

(Abe *et al.*, 2000; Dayan *et al.*, 2019). Presequence translocase-associated motor (PAM) is the driving force behind import through TIM23 and into the matrix (Schiller, 2009). N-terminal presequences are subsequently cleaved off by the mitochondrial processing peptidase (MPP) (Hawlitschek *et al.*, 1988).

1.1.5.2 Import pathway for cysteine rich proteins

The TOM complex also acts as the common OMM entry gate for proteins that do not possess cleavable mitochondrial targeting sequences (MTS). These proteins are imported according to a range of different internal targeting sequences (Backes *et al.*, 2018). Proteins targeted to the IMS commonly have mitochondrial IMS sorting signals (MISS) residing next to a number of cysteine residues that, once in the IMS, direct them into the mitochondrial import and assembly (MIA) pathway (Sideris *et al.*, 2009). Components of the MIA machinery interact with imported precursor IMS proteins through transiently formed disulphide bonds using specific cysteine residues to facilitate proper folding and assembly (Banci *et al.*, 2009).

1.1.5.3 Import pathway for metabolite carrier proteins

The translocation and assembly of IMM metabolite carrier protein precursors represent a third unique import mechanism, known as the carrier pathway. Following their TOM mediated import into the IMS, carrier precursors are bound by a complex of small Tim chaperones Tim9-Tim10 and Tim12 (Ivanova, Jowitt and Lu, 2008; Gebert *et al.*, 2008). These chaperone proteins direct the carrier precursors to the carrier translocase of the inner membrane (TIM22) for insertion and assembly within the IMM (Koehler *et al.*, 1998).

1.1.5.4 Import pathways for OMM proteins

Mitochondrial β-barrel proteins of the OMM also rely on the small Tim chaperone complexes of the IMS, through which they are directed to the sorting and assembly

machinery (SAM), embedded within the OMM (Wiedemann *et al.*, 2003). Conformational changes within the SAM complex mediate the folding of β-barrel substrates and their release into the lipid bilayer of the OMM (Becker *et al.*, 2008). Another group of OMM proteins, containing α- helical transmembrane segments, are thought to be the only class of mitochondrial proteins not to rely on TOM for import. Instead, the mitochondrial import (MIM) complex promotes the insertion of these proteins into the outer membrane (Dimmer *et al.*, 2012).

1.2 Mitochondrial DNA replication

A faithful system of mtDNA replication is essential to the maintenance of the mitochondrial genome and the expression of its 13 encoded genes. Two main origins of replication have been described: the origin of H-strand replication (O_H), which lies within the NCR, and the origin of L-strand replication (O_L), which lies within a cluster of tRNAs downstream from O_H. The RNA primers necessary for mtDNA replication are synthesised by the mitochondrial RNA polymerase (POLRMT) (Fusté *et al.*, 2010; Kuhl *et al.*, 2016). DNA synthesis is driven by the mitochondria-specific DNA polymerase γ (Pol γ), a heterotrimer composed of one catalytic subunit encoded by *POLG* and a homodimeric accessory subunit, encoded by *POLG2*, which confers processivity to Pol γ by increasing its affinity to DNA (Lee, Kennedy and Yin, 2009).

In order for Pol γ to proceed the two mtDNA strands must be unwound at the replication fork, a role carried out by a hexamer of the mtDNA helicase Twinkle (TWNK) through disruption of the hydrogen bonds between strands (Milenkovic *et al.*, 2013). The mitochondrial single strand binding protein (mtSSB) additionally enhances the activity of both Pol γ and Twinkle (Oliveira and Kaguni, 2010). In addition to these mitochondria-specific proteins, several other proteins with dual nuclear and mitochondrial functions are involved in mtDNA replication, including DNA ligase III, ribonuclease H1 (RNase H1) (Cerritelli *et al.*, 2003), flap structure-specific endonuclease 1 (FEN1) and topoisomerase 3 alpha (TOP3α) (Ruhanen, Ushakov and Yasukawa, 2011; Nicholls *et al.*, 2018). The termination of replication requires several factors with nuclease activity for primer removal, processing and re-ligation. The processing of RNA primers can take place in a number of ways, usually involving the partial degradation of annealed primers by RNase H1 and subsequent displacement of remaining nucleotides by Pol γ to generate a 'flap' of varying length. This flap can then be cleaved and cleared by FEN1, DNA2 or MGME1 (Uhler and Falkenberg, 2015).

To complete each replication event, separation of the two newly synthesised mtDNA molecules must take place. It has been demonstrated recently that the protein topoisomerase 3α (TOP3α) carries out decatenation of interlinked mtDNA, releasing

each mtDNA molecule to form their final compact nucleoid structure (Nicholls *et al.*, 2018).

Mitochondria maintain continuous cycles of DNA replication, running independently of the broader cell cycle in both actively proliferating and post-mitotic cells (Korr *et al.*, 1998; Magnusson *et al.*, 2003). Different models for mtDNA replication have been proposed, with the main points of contention being whether replication proceeds in a strand-synchronous or strand-asynchronous manner and whether the lagging-strand template is coated with protein or RNA (Robberson, Kasamatsu and Vinograd, 1972; Clayton, 1982; Falkenberg, 2018) **(Figure 1.4)**.

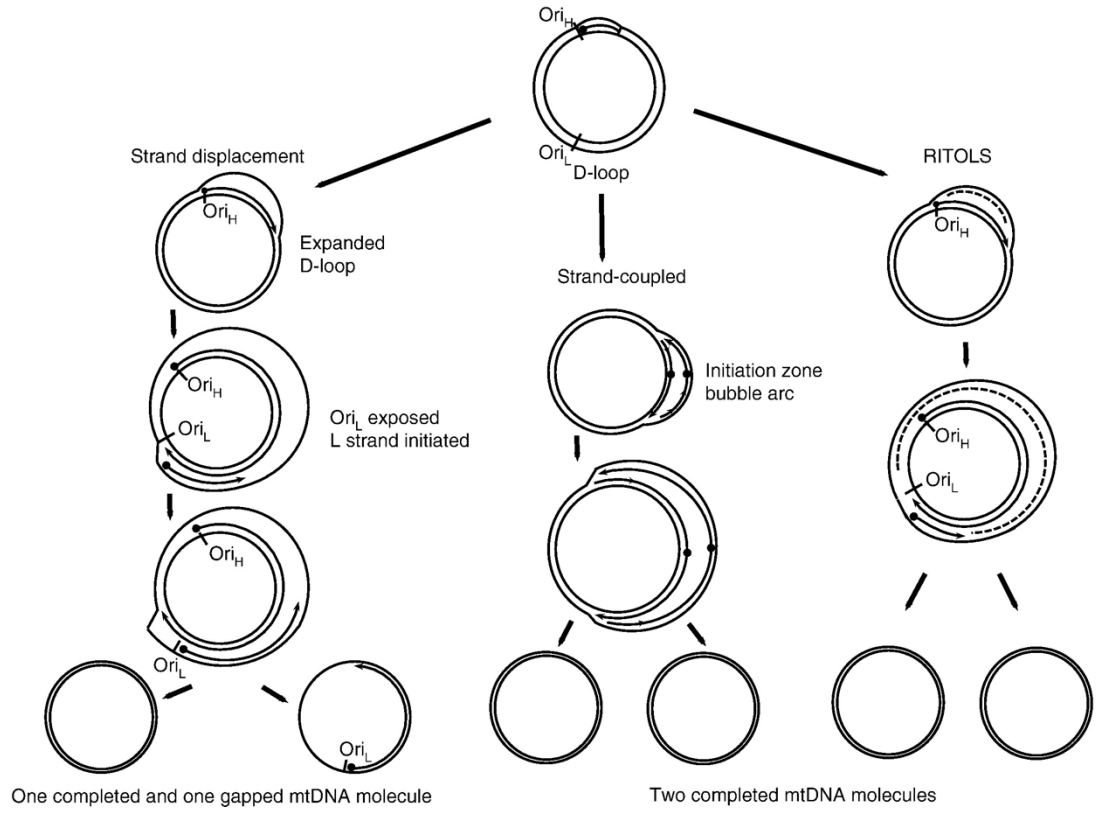

Figure 1.4 The three models of mtDNA replication. Left to right: The strand displacement model (asynchronous), the strand coupled model and the RITOLS model. Figure adopted from (Kasiviswanathan, Collins and Copeland, 2012)

1.2.1 'Strand displacement' model of mtDNA replication

The model of asynchronous strand-displacement, first described in 1972, suggests that replication begins at the O_H within the NCR (Robberson, Kasamatsu and Vinograd, 1972). Unidirectional replication of the H-strand alone then proceeds, either stalling at a termination associated sequence (TAS) ~700 nucleotides after the O_H, or continuing fully around the genome. The displaced lagging-strand template is coated and protected by mtSSB until L-strand synthesis is initiated (Miralles Fusté *et al.*, 2014). Once the replisome has passed O_L, a stem-loop structure becomes exposed, allowing POLRMT to form a primer for L-strand replication to begin in the opposite direction(Shadel and Clayton, 1997; Clayton, 1982).

1.2.2 'Synchronous' model of mtDNA replication

An alternative model of mtDNA replication postulates that conventional strand-coupled DNA synthesis, resulting from bidirectional replication initiation, occurs in mitochondria. This theory is predominantly based upon the observation of fully duplex replication intermediates using 2-dimensional agarose gel electrophoresis (Holt, Lorimer and Jacobs, 2000), and implies the presence of multiple short Okazaki fragments during lagging-strand synthesis. However, their role within the mtDNA replication system has yet to be demonstrated experimentally (Holt, 2009; Wanrooij and Falkenberg, 2010).

1.2.3 'Ribonucleotide Incorporation Throughout Lagging Strand (RITOLS)' model of mtDNA replication

The third, most recently proposed model of mtDNA replication is RITOLS. The model postulates that RNA (rather than mtSSB) is hybridised to the displaced H strand during leading-strand replication, providing stability and protection to the exposed ssDNA as replication advances. This RNA was more recently suggested to derive from processed RNA transcripts, and is referred to as the 'bootlace model' due to its emphasis on RNA 'threading' (Reyes *et al.*, 2013). An enzymatic machinery responsible for this process has not been identified.

1.2.4 Maintenance of the dNTP pool

The replication and repair of both the nuclear and mitochondrial genomes requires a steadily available pool of deoxyribonucleoside triphosphates (dNTPs). The two major pathways that regulate dNTP supply to mitochondria are the salvage and the *de novo* synthesis pathways. The latter operates in the cytosol where the key regulatory enzymes involved in dNTP synthesis are ribonucleotide reductase (RNR) and thymidylate synthase (TS). RNR is responsible for the reduction of ribonucleotides to deoxyribonucleotides (Penque *et al.*, 2018; Pontarin *et al.*, 2008). Specific mitochondrial carriers, such as MPV17, then facilitate the transport of cytosolic dNTPs into the matrix, as mitochondria do not possess *de novo* nucleotide synthesis pathways, nor can such molecules permeate the inner mitochondrial membrane (IMM) due to their charge (Dahout-Gonzalez, 2006).

The unique mitochondrial dNTP salvage pathway constantly converts former deoxynucleosides, already within the mitochondrial matrix as a result of DNA turnover, into dNTPs (D'Souza and Minczuk, 2018). Mitochondrial thymidine kinase 2 (TK2) is a key driver of the pyrimidine nucleotide salvage pathway as it carries out the initial phosphorylation of pyrimidine precursors (Johansson and Karlsson, 1997). Similarly, the primary phosphorylation step in purine nucleotide salvage is carried out by mitochondrial deoxyguanosine kinase (DGK) (Johansson and Karlsson, 1996). Two additional phosphorylation steps follow, performed sequentially by nucleotide monophosphate kinase (NMPK) and nucleotide diphosphate kinase (NDPK), resulting in the conversion of each of the deoxyribonucleoside monophosphates (dNMPs) into dNTPs (Wang, 2016). For NMPK to execute the final phosphorylation of each nucleotide it must form a complex with succinyl CoA ligase (SUCL) and 4-aminobutyrate transaminase (ABAT) (Besse *et al.*, 2015; Kowluru, Tannous and Chen, 2002).

1.3 Mitochondrial transcription

Within the D-loop of the mitochondrial genome are the sites of transcription initiation for both the H and L strands. Early studies of mitochondrial transcription identified two heavy-strand promoters, named HSP1 and HSP2, while the initiation of light strand transcription was attributed to a single LSP site. Transcription originating from HSP1 was proposed to run from the 5' end of the mitochondrial (mt)-tRNA^{Phe} gene through to the 3' end of the *16S* gene, thus transcribing two mt-tRNA genes (encoding mt-tRNA^{Phe} and mt-tRNA^{Val}) and the two mt-rRNA genes (*12S* and *16S*). Transcription originating from HSP2, 100bp downstream of HSP1, begins at the boundary between the gene encoding mt-tRNA^{Phe} and the *12S* gene and proceeds along the entirety of the H strand to produce a long polycistronic transcript containing all of the mt-tRNAs, mt-rRNAs and mt-mRNAs encoded within the H strand (Montoya *et al.*, 1982). Similarly, transcription originating at the LSP continues along the full strand to produce a polycistronic transcript of all genes encoded within the L strand. However, difficulties in faithfully reconstituting transcription initiation from HSP2 *in vitro* (Litonin *et al.*, 2010), as well as the finding that the proposed HSP transcription termination protein MTERF1 appears to terminate transcription from LSP rather than HSP (Terzioglu *et al.*, 2013), have led many to question the existence of HSP2 as a functional promoter, and there is currently little consensus.

The mitochondrial transcription machinery is entirely nuclear encoded and it is well demonstrated that mitochondrial transcription can be reconstituted in vitro in the presence of just three proteins: mitochondrial RNA polymerase (POLRMT), mitochondrial transcription factor A (TFAM) and mitochondrial transcription factor B2 (TFB2M) (Posse *et al.*, 2015; Falkenberg *et al.*, 2002). POLRMT, a single subunit RNA polymerase that is related to the bacteriophage T7 RNA polymerase (T7 RNAP) is the driver of mitochondrial transcription. The transcription activity of POLRMT is exclusive to the mitochondrial genome. POLRMT requires the two additional cofactors TFAM and TFB2M for promoter recognition and melting during transcription initiation (Hillen, Temiakov and Cramer, 2018).

1.3.1 Transcription initiation

TFAM has the ability to bind to high affinity binding sites ~10-15bp upstream of the promoter sites and introduce a 180° bend in the bound mtDNA. TFAM binding and the subsequent conformational change allows for the recruitment of POLRMT to promoter DNA to form the pre-initiation complex (Hillen, Temiakov and Cramer, 2018). Finally, the recruitment of TFB2M to the pre-initiation complex introduces structural changes in POLRMT that drive promoter melting and allow the entry of the initiating nucleotide into the catalytic site of POLRMT; thus completing initiation and allowing elongation to commence **(Figure 1.5)**.

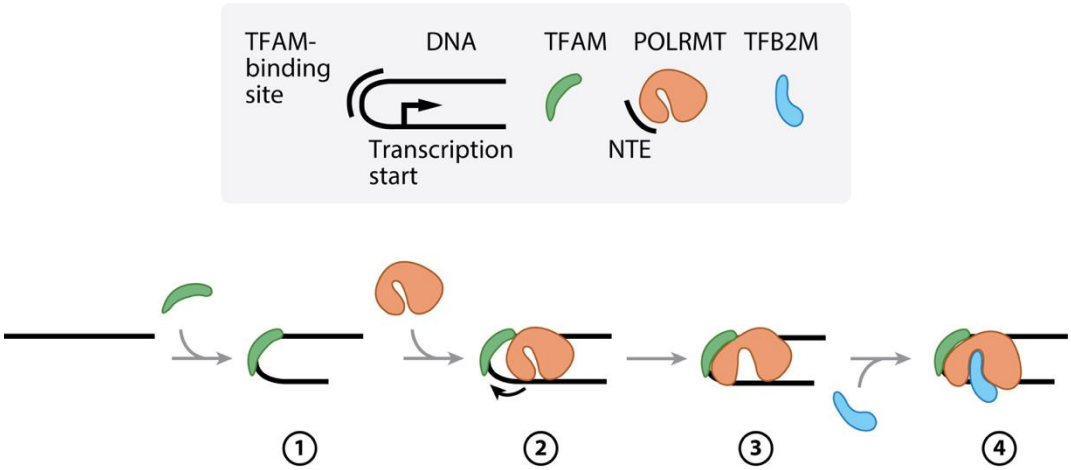

Figure 1.5 Mitochondrial transcription initiation. A four-step model of transcription initiation. **1.** TFAM binds mtDNA upstream of the transcription start site, introducing a 180° bend. **2.** TFAM recruits POLRMT, which interacts with a DNA region upstream of the TFAM binding site. **3.** POLRMT undergoes a conformational change. **4.** This conformational change allows the binding of TFB2M, the final step in the formation of a complete transcription initiation complex. Figure adopted from (Gustafsson, Falkenberg and Larsson, 2016).

1.3.2 Transcription elongation

During the transition from initiation to elongation, TFB2M dissociates and a new combination of proteins, the elongation complex, assembles. The mitochondrial transcription elongation factor TEFM forms a dimer, binding the POLRMT site previously occupied by TFB2M, thus promoting the formation of a sliding clamp structure (Hillen *et al.*, 2017). TEFM drives elongation by increasing POLRMT-DNA

interactions, greatly enhancing POLRMT processivity along the mtDNA strand and preventing premature termination or stalling (Posse *et al.*, 2015; Posse *et al.*, 2014).

1.3.3 Transcription termination

The exact mechanism by which mitochondrial transcription is terminated remains somewhat unresolved. One protein known to play a key role in the termination of transcription is MTERF1 (Terzioglu *et al.*, 2013). As a member of a family of proteins with nucleic acid binding properties, MTERF1 binds along the major groove of mtDNA at the 3' end of the 16S rRNA gene and induces a bend, partial unwinding of the double helix and the eversion of three nucleotides to stabilise this interaction (Asin-Cayuela *et al.*, 2005). MTERF1 exhibits polar transcription termination activity consistent with a role in terminating transcription originating only from LSP (Terzioglu *et al.*, 2013). Equivalent proteins involved in the termination of transcription originating from HSP are yet to be identified. As previously described, mitochondrial transcription, from either HSP or LSP, produces long polycistronic messages that must undergo essential post-transcriptional processing and modification steps prior to mitochondrial translation.

1.3.4 Transcript processing

The majority of protein coding mtDNA genes, along with both mt-rRNA genes, are separated by individual mt-tRNA genes. The mt-tRNAs act as guides for endonucleolytic excision and thus the release of each flanking mRNA and rRNA transcript in a system termed the 'tRNA punctuation model' (Ojala, Montoya and Attardi, 1981). Cleavage of each tRNA is carried out by ribonuclease P (RNaseP) and ribonuclease Z (RNase Z) at the 5' and 3' ends respectively. In human mitochondria the RNAseP is a complex of 3 proteins, MRPP1, MRPP2 and MRPP3 whereas the RNaseZ activity is carried out by a single protein, ElaC ribonuclease Z (ELAC2). Though this model can account for the release of the majority of individual transcripts, there are some protein-coding genes not flanked by tRNAs on either side. It has been suggested that the remaining 3 precursors that are not flanked by tRNAs require one of two proteins for their processing, GRSF1 or PTCD2. GRSF1 is crucial for the

processing of the *MTND6-ncRNA* and *RNA14-MT-CO3* precursors (Jourdain *et al.*, 2013; Antonicka *et al.*, 2013) while PTCD2, a pentatricopeptide repeat (PPR) RNA-binding protein that is involved in the processing of the *MT-ND5-MT*-CYB transcript (Xu *et al.*, 2008).

1.3.5 mt-mRNA maturation

Following the nucleolytic processing of each polycistronic message, all but one of the mt-mRNA transcripts undergo adenylation on their 3' ends. The majority of mt-mRNAs are polyadenylated with poly(A) tails (~45-55 nucleotides in length) with the exception of the *MT-ND6* transcript. In addition, the poly(A) tails detected on the *MT-ND5* transcript are much shorter in length (between 0-10 nucleotides) than the majority of other mt-mRNAs (Temperley *et al.*, 2010). Poly(A) tail synthesis is carried out by the poly(A) polymerase (mtPAP) that is localised to the mitochondrial RNA granules and is capable of using each of the four NTPs in its polymerase activity, despite showing an ATP substrate preference (Bai *et al.*, 2011). An essential function of poly(A) tails is to provide mt-mRNA transcripts with a complete 'stop' codon. Seven of the thirteen mitochondrial open reading frames have incomplete stop codons ('U' or 'UA') that, without poly- or oligo-adenylation to form 'UAA', would not cause termination of mitochondrial translation (Temperley *et al.*, 2010). The impact of polyadenylation upon mt-mRNA stability varies between transcripts. Some mt-mRNAs, such as *MT-ATP6/8*, *MT-CO1*, *MT-CO2* and *MT-CO3* appear to be destabilised upon addition of poly(A) tails, whereas *MT-CYTB*, *MT-ND3*, *MT-ND4/4L* and *MT-ND5* all show increased stability in their polyadenylated state (Temperley *et al.*, 2010). The mechanism and function behind this transcript-specific response to polyadenylation remains unclear

1.3.6 mt-mRNA turnover

An important regulator of mtDNA gene expression is the 'mitochondrial degradosome' dedicated to the turnover of RNAs within the matrix. The RNA degradosome apparatus consists of a mitochondria-specific helicase hSuv3p that can unwind double stranded DNA (dsDNA), double stranded RNA (dsRNA) and DNA-RNA hybrids (Minczuk *et al.*,

2002) and polynucleotide phosphorylase (PNPase), encoded by the *PNPT1* gene, that has poly(A) polymerase (PAP) and 3'-5' exoribonuclease activities. It has been demonstrated that hSuv3p and PNPase form a stable complex that is believed to play a role in the removal of RNA transcripts that are antisense, aberrant or have undergone damage as well as normally processed mature transcripts in the mitochondrial matrix (Borowski *et al.*, 2013; Szczesny *et al.*, 2010). A third protein with a proposed role in mitochondrial RNA degradation is RNA exonuclease 2 (REXO2). Showing localisation to the matrix and the IMS, as well as the cytosol, REXO2 is an exonuclease that degrades oligonucleotides in the 3' to 5' direction. The substrates of REXO2 are likely to be short ribonucleotides generated during the degradation of RNA transcripts by hSuv3p-PNPase or by other nucleases (Bruni *et al.*, 2013).

The leucine rich PPR (pentatricopeptide repeat)-containing protein (LRPPRC) and stem-loop interacting RNA binding protein (SLIRP) are both mitochondrial RNA binding proteins involved in the regulation of mt-mRNA stability. It has been demonstrated that the LRPPRC-SLIRP complex conveys stability to mt-mRNAs by blocking PNPase access and aiding in the polyadenylation of the 3' terminus of bound mRNAs (Chujo *et al.*, 2012).

1.3.7 mt-tRNA maturation

Following their release from primary polycistronic transcripts, mt-tRNAs are subject to a broad range of different post-transcriptional maturation and modification steps, necessary for the formation of stable and fully functioning tRNA structures (Salinas-Giege, Giege and Giege, 2015; Suzuki and Suzuki, 2014). A number of different nuclear encoded tRNA modifying enzymes are responsible for the chemical modifications of different sites of each mitochondrial tRNAs, some of which also modify nuclear tRNAs (Suzuki, Nagao and Suzuki, 2011). The final maturation step that involves the addition of CCA nucleotides to the 3' terminus of mt-tRNAs is followed by aminoacylation by the correct mitochondrial aminoacyl-tRNA synthetase (aa-RS). Nineteen unique aa-RSs are required for mitochondrial translation (Sissler, Gonzalez-Serrano and Westhof, 2017). The aa-RSs that produce aminoacyl-tRNA conjugates in the cytosol and in mitochondria are generally encoded by two distinct genes. However, two aa-RSs, glycyl-ARS aa-RS (GARS) and lysyl-ARS aa-RS (LARS), act within both

the cytosolic and mitochondrial systems, which is achieved via the inclusion or exclusion of a mitochondrial targeting sequence as a result of alternative initiation sites or splicing (Tolkunova *et al.*, 2000; Echevarria *et al.*, 2014).

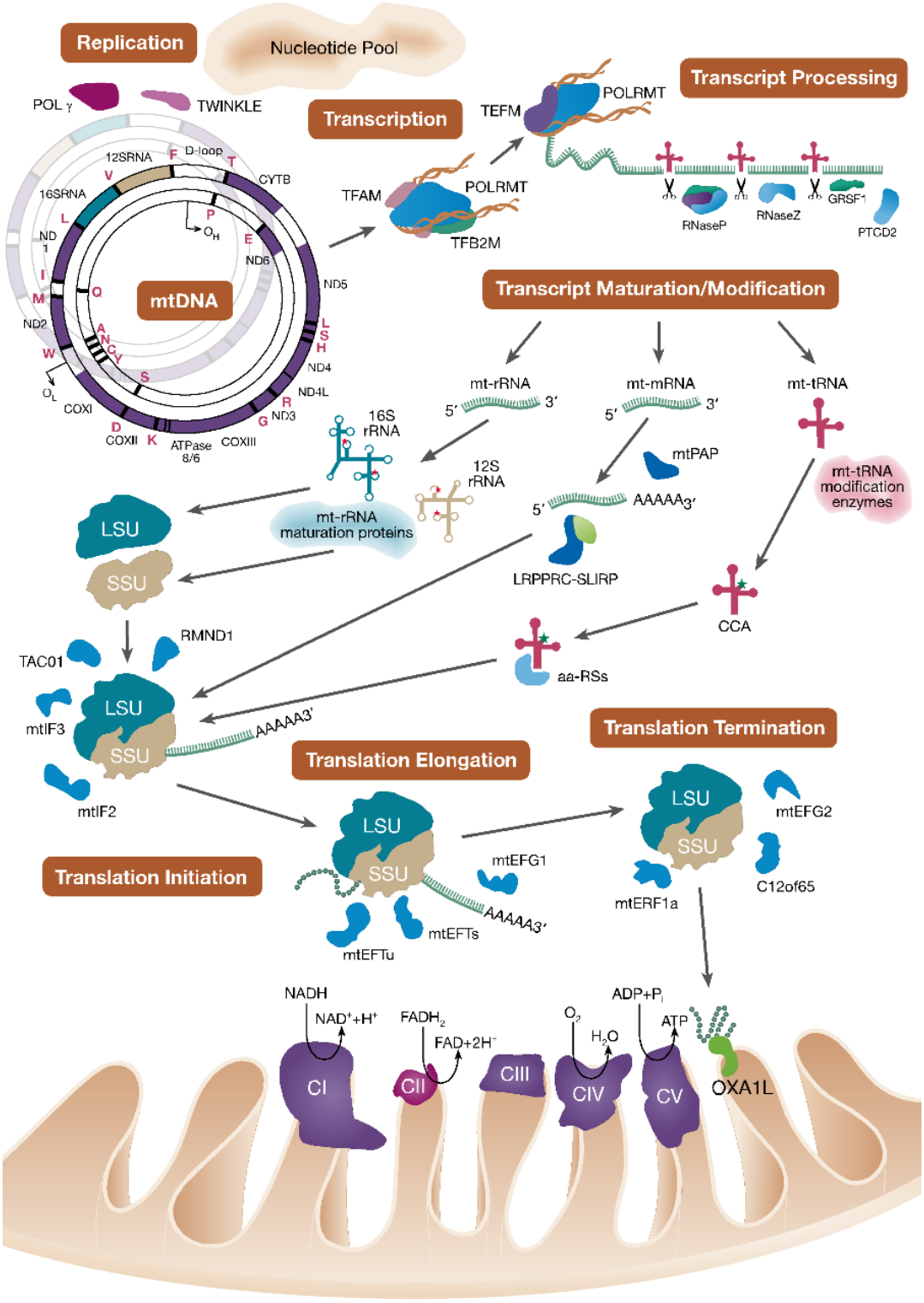

Figure 1.6 Schematic of mtDNA gene expression. Replication and transcription of the mitochondrial genome depends on a pool of available nucleotides. Following transcription and processing, mt-rRNAs (beige and turquoise), mt- mRNAs (light green) and mt-tRNAs (pink) undergo a number of post-transcriptional modification steps facilitated by numerous maturation and modification enzymes. The mitoribosomal LSU (turquoise) and SSU (beige) assemble to synthesise each of the 13 mitochondrial-encoded OXPHOS polypeptides, followed by their insertion into the IMM as constituents of complexes I, III, IV and V (purple).

1.3.8 mt-rRNA maturation

Like mt-tRNAs, both the 12S and 16S mt-rRNAs undergo a number of nucleotide modifications believed to convey stability and promote mitoribosome biogenesis. The 12S mt-rRNA is subject to methylation of a cytidine at position 841 and dimethylation of neighbouring adenines at positions 936 and 937 by the methyltransferase NSUN4 and dimethyltransferase TFB1M proteins respectively (Metodiev *et al.*, 2014; Metodiev *et al.*, 2009). The recently identified METTL15 protein introduces an N-4 methylcytedine at position 839 of the 12S mt-rRNA believed to stabilise folding (Haute *et al.*, 2019).

The 16S mt-rRNA undergoes one pseudouridinylation, carried out by the pseudouridine synthase RPUSD4 at position 1397 (Zaganelli *et al.*, 2017). There are also several methylation sites on the 16S mt-rRNA. The protein TRMT61B, a known tRNA modifying enzyme, has been shown to introduce a methyladenosine at position 947 of the 16S mt-rRNA. Structurally this modification sits at the interface of the mitochondrial large (mt-LSU) and small subunit (mt-SSU) and may be required to maintain mitoribosomal structure and function (Bar-Yaacov *et al.*, 2016). The three proteins MRM1, MRM2 and MRM3 are a group of 2'-O-ribose methyltransferases, each believed to modify specific bases (Gm1145, Um1369, and Gm1370) within the peptidyl transferase centre of the 16S mt-rRNA (Rorbach *et al.*, 2014; Lee and Bogenhagen, 2014; Lee *et al.*, 2013).

1.4 Mitochondrial translation

Reflective of their alphaproteobacterial ancestral origins, the mechanism of translation employed by mitochondria is more akin to prokaryotic protein synthesis systems than to the cytosolic translation of eukaryotes (Smits, Smeitink and van den Heuvel, 2010). Unlike transcription, mitochondrial translation is yet to be successfully reconstituted *in vitro* and as such is not as well characterised as eubacterial or eukaryotic cytosolic translation.

1.4.1 The mammalian mitoribosome

The core driver of mitochondrial translation is the mitoribosome. Consisting of a small (28S) subunit (SSU) and large (39S) subunit (LSU), the human mitoribosome contains ~80 nuclear encoded proteins, two mt-rRNAs (12S and 16S) and a mt-tRNA^{Val} that assemble to form the 55S monosome (Chrzanowska-Lightowlers, Rorbach and Minczuk, 2017; Amunts *et al.*, 2015). Mammalian mitoribosomes have undergone evolutionary changes leading to mitochondria specific features that differ to those of bacterial ribosomes. One of the most striking discrepancies is the proportion of RNA to protein content. Bacterial ribosomes are comprised of ~70% RNA and 30% protein. This ratio has been reversed in mammalian mitoribosomes, which are 70% protein content and just 30% RNA (Brown *et al.*, 2014), resulting from an evolutionary loss of rRNA domains combined with extension of conserved proteins and gain of mitochondria specific proteins (Mai, Chrzanowska-Lightowlers and Lightowlers, 2017). Many of the more recently obtained mitochondria specific proteins are located on the periphery of the mitoribosome. Once believed to simply fill the structural gaps left behind by lost RNA components, it has since been demonstrated that these additional mitoribosomal proteins also convey a number of different functionalities including membrane association and mRNA recruitment (Greber and Ban, 2016).

It has been proposed that these additional proteins could function in part as a protective layer, shielding the ribosomal RNA from the damaging levels of ROS present within mitochondria (Mai, Chrzanowska-Lightowlers and Lightowlers, 2017). The process of

mitochondrial translation can, therefore, be divided into three major stages: initiation, elongation and termination **(Figure 1.7)**.

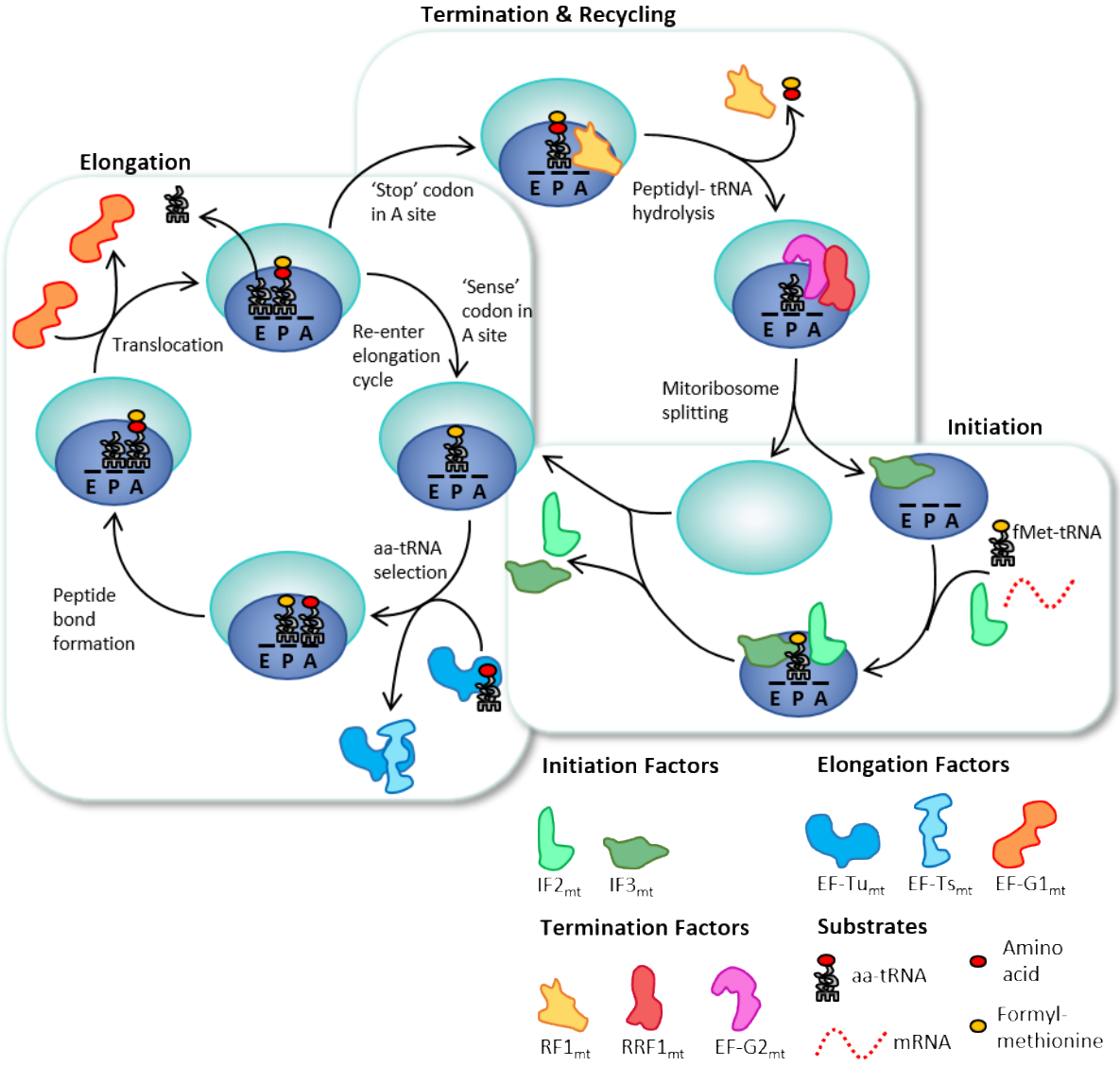

Figure 1.7 Mitochondrial translation. Diagram depicting the cyclical nature of the three stages of mitochondrial translation; Initiation, Elongation and Termination/Recycling. A = acceptor site. P = peptidyl tRNA site. E = polypeptide exit site

1.4.2 Translation initiation

Initiation of mitochondrial translation requires the recruitment of a mitochondrial mRNA transcript to the SSU of the mitoribosome. When not active in translation, the SSU is bound by mitochondrial initiation factor 3 (mtIF3) which blocks its association with the

LSU preventing 55S formation (Christian and Spremulli, 2009). Binding of an mRNA transcript at the mRNA entry channel of the SSU may be facilitated by the PPR-containing mS39 protein with mRNA binding properties (Greber *et al.*, 2015). In addition to the 'universal' AUG initiating codon, the mitochondrial translation system also recognises AUA and AUU as 'start' codons (Jukes, 1983). Upon the entry of an initiating codon of an mt-mRNA into the SSU entry site, formylated $tRNA^{Met}$ ($tRNA^{fMet}$) is recruited by mitochondrial initiation factor 2 in its GTP bound state (mtIF2:GTP) to form an initiation complex with the SSU (Christian and Spremulli, 2010). Binding of $tRNA^{fMet}$ through a codon:anticodon interaction triggers the recruitment of the LSU to form the monosome, and the subsequent hydrolysis of mtIF2:GTP to mtIF2:GDP results in the release of both mtIF2 and mtIF3 from the SSU. The monosome can then enter the elongation phase of mitochondrial translation.

1.4.3 Translation elongation

The formation of a ternary complex of elongation factors, along with an aminoacylated tRNA (aa-tRNA) binding at the acceptor site (A-site) of the mitoribosome, is required for elongation of nascent polypeptides. The elongation phase begins with the binding of GTP-bound mitochondrial elongation factor Tu (mtEFTu:GTP) to an aa-tRNA which directs the aa-tRNA into the A-site of the mitoribosome. The formation of a correctly-matched codon:anticodon between the bound mt-mRNA transcript and the aa-tRNA in the A-site, triggers hydrolysis of the mtEFTu:GTP to mtEFTu:GDP that is then released from the mitoribosome (Cai *et al.*, 2000). This GTP hydrolysis catalyses the formation of a peptide bond at the peptidyl transferase centre (PTC) between the aa-tRNA within the A-site and the amino acid sitting at the adjacent peptidyl tRNA site (P-site). The tRNA occupying the P-site becomes deacylated as a result and is then displaced by the translocation of the bi-peptidyl tRNA from the A-site to the P-site driven by the hydrolysis of a second elongation factor, mitochondrial elongation factor (G1), from mtEFG1:GTP to mtEFG1:GDP. Regeneration of mtEFTu:GDP back to mtEFTu:GDP is carried out by mitochondrial elongation factor Ts (mtEFTS) which allows this process to cycle and the peptide chain to grow (Mai, Chrzanowska-Lightowlers and Lightowlers, 2017).

1.4.4 Translation termination and ribosome recycling

Upon entry of a ‘stop’ codon UAA or UAG into the A-site of the mitoribosome, mitochondrial translation release factor A (mtRF1a) is recruited (Christian and Spremulli, 2012). mtRF1a catalyses the hydrolysis of the ester bond between the peptidyl-tRNA occupying the A-site and the terminal amino acid of the complete nascent polypeptide. This GTP-dependent cleavage results in the release of the full length polypeptide through the exit tunnel of the LSU (Lightowlers and Chrzanowska-Lightowlers, 2010). Following this release, the mitoribosome must undergo a recycling process to return to independent large and small subunits available for the initiation of a new translation event, also releasing the mRNA template and final terminating tRNA. Two proteins, mitochondrial ribosome release factor (mtRRF) and mitochondrial elongation factor G2 (mtEFG2), promote the dissociation of the mitoribosomal subunits in a GTP dependent manner (Tsuboi *et al.*, 2009). A ribosome-dependent peptidyl-tRNA hydrolase, ICT1, thought to be a structural component of the LSU, and C12orf65 are believed to facilitate the hydrolysis and release of prematurely terminated peptidyl chains from any stalled mitoribosomes (Richter *et al.*, 2010).

1.4.5 IMM insertion

Following their synthesis by the mitoribosome, the 13 mtDNA encoded OXPHOS proteins are inserted into the IMM. Correct insertion of nascent polypeptides into the IMM is believed to be aided by a family of insertases. A major candidate for a human insertase that carries out this role, OXA1L, has been shown to directly interact with at least nine of 13 mtDNA encoded polypeptides and other nuclear encoded accessory subunits of OXPHOS complexes to aid insertion of newly synthesised proteins into IMM (Haque, Spremulli and Fecko, 2010; Thompson *et al.*, 2018).

1.5 Functions of mitochondria

Though best known as the main generators of cellular energy through OXPHOS, mitochondria are responsible for a number of different molecular mechanisms essential to normal cellular function (Osellame, Blacker and Duchen, 2012).

Mitochondria are essential mediators of cellular calcium ion homeostasis, through their dynamic sequestration and release of calcium ions (Ca^{2+}) which act as versatile intracellular signalling molecules with regulatory roles in a multitude of biochemical pathways. Uptake and release of Ca^{2+} by mitochondria is mediated by the highly selective mitochondrial calcium uniporter (MCU) and the electrogenic Na^{2+}-Ca^{2+} exchanger respectively (Samanta, Mirams and Parekh, 2018). The TCA cycle and ATP synthesis are two mitochondrial processes regulated by Ca^{2+}, while influx of calcium ions into mitochondria is an important step in apoptosis (Giorgi, Marchi and Pinton, 2018).

Apoptosis, the process of programmed cell death, is driven by a number of sequential mitochondrial events. The Bcl-2 family of proteins regulate apoptosis through dynamic interactions of pro- and anti-apoptotic family members with the IMM (Cory and Adams, 2002). The activation of pro-apoptotic Bak or Bax proteins, or the inhibition of anti-apoptotic Bcl-2, permeabilises the OMM and triggers the cytosolic release of cytochrome *c* from the IMS (Kluck *et al.*, 1997). This in turn activates a caspase cascade essential for proteolytic degradation of proteins during apoptosis (Salvesen and Dixit, 1997).

The process of iron-sulphur (Fe-S) cluster biogenesis also takes place within the mitochondrial matrix. Fe-S clusters are essential inorganic co-factors found in abundance within mitochondria and the cytosol (Beinert, Holm and Munck, 1997). Fe^{2+} ions are transported into the matrix of mitochondria by mitoferrin carriers (Richardson *et al.*, 2010), while sulphide ions are released from cysteine by the cysteine desulphurase Nfs1 (Kispal *et al.*, 1999). A backbone for cluster synthesis and formation is provided by the iron sulphur cluster assembly enzyme ISCU (Marinoni *et al.*, 2012). Fe-S clusters are present within respiratory chain complexes I-IV, where they mediate

electron transfer through a chain of reactions and are therefore fundamental to oxidative phosphorylation (Brzoska, Meczynska and Kruszewski, 2006).

1.6 ATP production through oxidative phosphorylation

The production of ATP through OXPHOS is a multi-step process that relies on a number of upstream metabolic reactions. Glycolysis, taking place in the cytosol, is a series of catabolic reactions resulting in the breakdown of glucose into two molecules of pyruvate. These pyruvate molecules can be imported into the mitochondrial matrix to feed into the tricarboxylic acid (TCA) cycle, the products of which - 3 molecules of NADH and 2 molecules of $FADH_2$ - enter through complex I and complex II respectively and are utilised as substrates during oxidative phosphorylation (Wilson, 2017; Yellen, 2018).

The process of oxidative phosphorylation is achieved by a system of five multi-subunit complexes embedded within the IMM. Complexes I-IV make up a set of four respiratory chain (RC) complexes forming the electron transport chain (ETC). The oxidation of NADH and $FADH_2$ to NAD/FAD provides electrons that are transferred to the OXPHOS cofactor uniquinone (Q). Transport of electrons down the ETC is coupled with the translocation of protons from the matrix into the IMS, producing a proton gradient across the IMM. This electrochemical force is used by complex V, coupling the flow of protons back into the matrix with the synthesis of ATP (Mitchell, 1961) **(Figure 1.8)**.

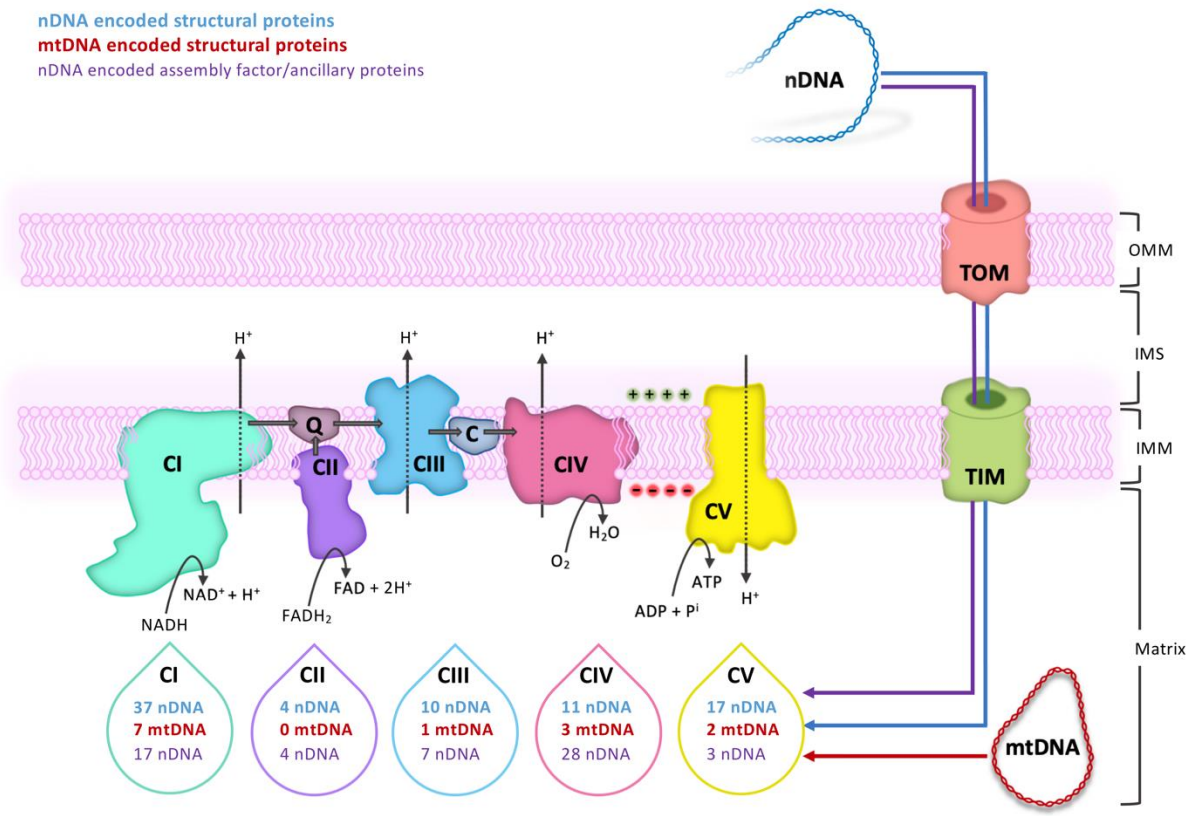

Figure 1.8 Schematic and of OXPHOS complexes and their dual genetic origin. Five multimeric complexes are embedded within the inner mitochondrial membrane (IMM). Complexes I-IV form the electron transport chain, with cofactors ubiquinone (Q) and cytochrome *c* (cyt *c*) acting as mobile electron carriers. The transfer of electrons is coupled to the pumping of protons (H^+) into the intermembrane space (IMS), generating an electrochemical gradient across the IMM. Complex V utilises this proton motive force to synthesise ATP. Each complex, with the exception of complex II, is comprised of a combination of mtDNA and nDNA encoded structural subunits and assembly factors. Complex II is entirely nuclear-encoded.

1.6.1 Complex I

Complex I (CI), NADH:ubiquinone oxidoreductase, is the first entry point for the ETC. A multiprotein structure containing 44 subunits and ~1,000 kDa in size, Complex I is the largest of the respiratory chain complexes. Seven of the 14 CI core subunits are encoded within the mtDNA, while the remainder of the core subunits, along with all accessory components, are nDNA encoded (Zickermann *et al.*, 2015; Carroll *et al.*, 2006). The subunits of complex I assemble to form an 'L shaped' structure, with a hydrophobic arm embedded within the IMM and a hydrophilic arm extending into the matrix **(Figure 1.9)**. This configuration can be divided into three functionally distinct modules; the N module, the Q module and the P module (Zickermann *et al.*, 2015). The role of the N module is to bind and oxidise NADH, made available by the TCA

cycle. The released electrons are transferred onto a flavin mononucleotide (FMN) molecule, forming $FMNH_2$ (Efremov and Sazanov, 2011). A chain of Fe-S clusters then form an electron transport cascade, transporting electrons down the Q module, ultimately reaching and reducing Q to ubiquinol (QH_2). This transfer of electrons results in conformational changes in both the IMM and matrix arms to open a channel within the P module proton pump, allowing the movement of four protons into the IMS for every NADH molecule oxidised (Galkin and Moncada, 2017).

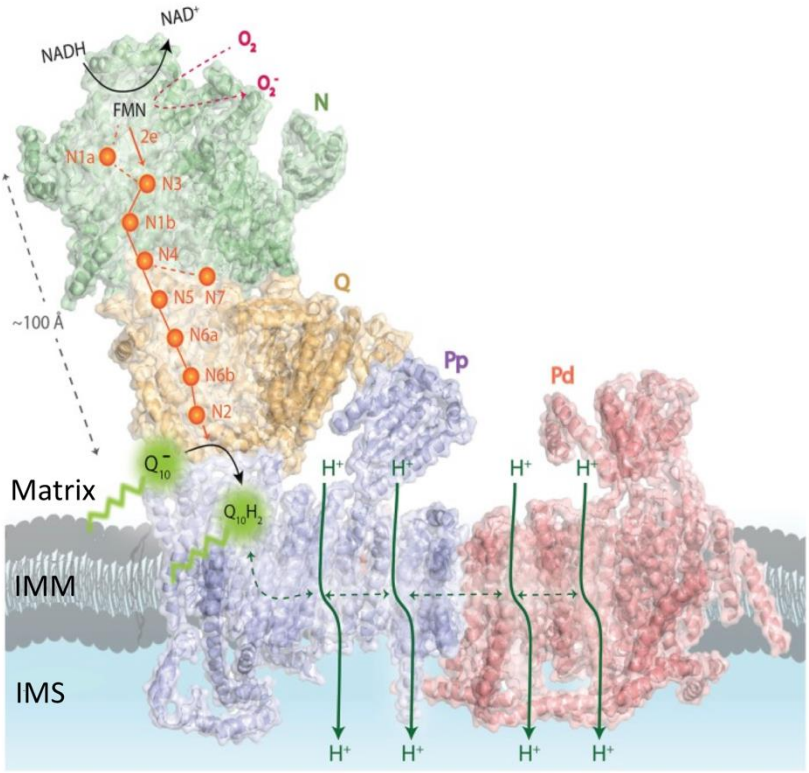

Figure 1.9 Structure and functional domains of complex I. The oxidation of $NADH_2$ takes place within the N module (green) releases two electrons that are shuttled into the Q module (yellow) via a chain of iron-sulphur clusters (orange). Here, the electrons reduce ubiquinone to ubiquinol (bright green) inducing a conformational change in the P-proximal (Pp - purple) and P-distal domains (Pd - red) and resulting in the pumping of four protons into the IMS. Figure adapted from (Giachin *et al.*, 2016).

1.6.2 Complex II

Complex II (CII), or succinate:ubiquinone oxidoreductase, is the only complex within the OXPHOS system to be composed of subunits entirely encoded within the nuclear genome. With only four nuclear encoded structural subunits, SDHA, SDHB, SDHC and SDHD, succinate dehydrogenase is the smallest of the five complexes. SDHA and SDHB are hydrophilic proteins that project into the mitochondrial matrix to form the catalytic core while SDHC and SDHD form an anchor embedded firmly within the IMM to hold the complex in place and confer upon complex II the ability to transfer electrons (Sun *et al.*, 2005) **(Figure 1.10)**. The SDHA subunit harbours a covalently bound prosthetic flavin adenine dinucleotide (FAD) group which receives electrons for its upon oxidation of succinate to fumarate by SDHA. The released electrons are passed from FAD through three Fe-S clusters within SDHB. The SDHC/SDHD subunits then transfer these electrons to ubiquinone, reducing it to QH_2.

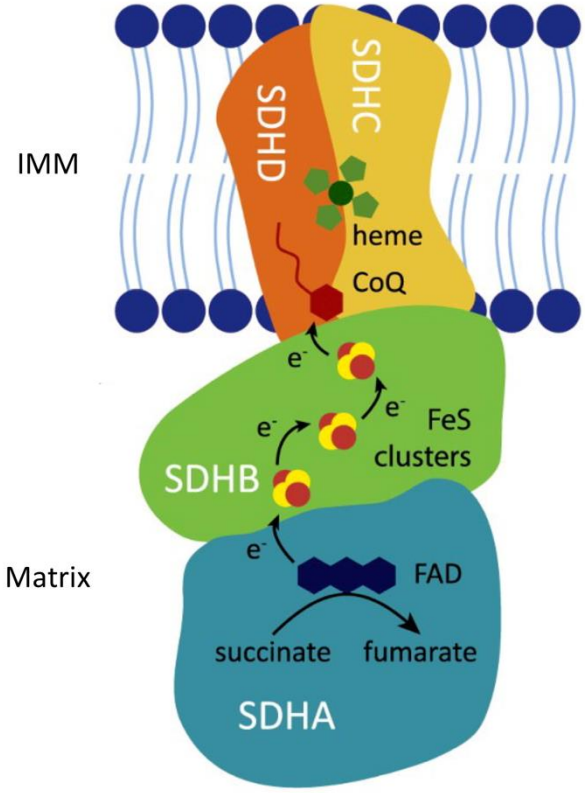

Figure 1.10 Structure of complex II. SDHA (blue) and SDHA (green) extend into the mitochondrial matrix, anchored to the IMM by membrane bound SDHC (yellow) SDHD (orange). Electrons gained from the oxidation of succinate to fumarate at SDHA are passed along three Fe-S clusters in SDHB too ubiquinone at the Q binding site between SDHB, SDHC and SDHD. Figure adapted from (Hadrava Vanova *et al.*, 2020).

1.6.3 Complex III

Also known as ubiquinol:cytochrome *c* oxidoreductase, complex III (CIII) contains one mtDNA encoded subunit (cytochrome *b*) and 10 nDNA encoded subunits, forming a structure approximately 480 kDa in size (Benit, Lebon and Rustin, 2009) **(Figure 1.11)**. Complex III functions as a symmetrical homodimer, with a catalytic core of cytochrome b and c subunits together with a Rieske Fe-S cluster protein (UQCRFS1) responsible for the transfer of electrons from QH_2 to cytochrome b and cytochrome c (Fernandez-Vizarra and Zeviani, 2018). This process is termed the Q cycle, and is coupled with the transport of two protons in to the IMS for every electron passed through CIII (Cramer, Hasan and Yamashita, 2011).

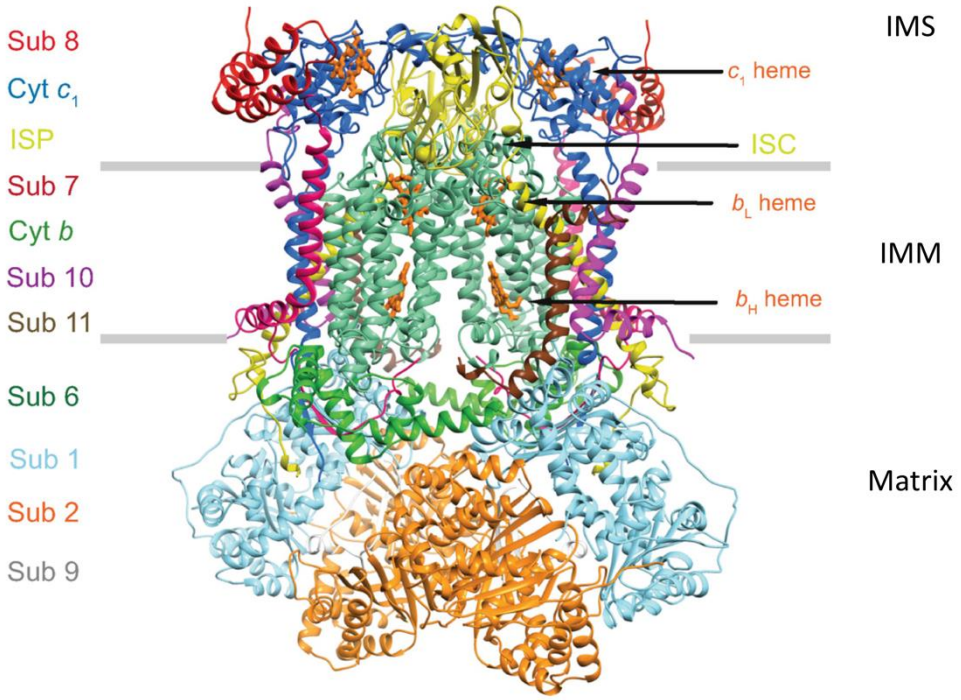

Figure 1.11 Crystal structure of dimeric complex III. Each of the 11 structural subunits of mammalian complex III are presented as colour coded ribbons and labelled with subunit designation of the left. Figure adapted from (Xia *et al.*, 2018).

1.6.4 Complex IV

Complex IV (CIV), termed cytochrome *c* oxidase (COX) acts as the terminal oxidase in the ETC. At ~200 kDa in size, monomeric CIV is composed of 14 subunits, three of which (COXI, COXII and COXIII) are mtDNA encoded (Zong *et al.*, 2018) **(Figure 1.12)**. Electrons accepted from reduced cytochrome *c* are transported through haem groups and copper centres of CIV and used to reduce O_2 to H_2O. The reduction of each O_2 molecule is coupled to the transport of four protons into the IMS (Faxen *et al.*, 2005).

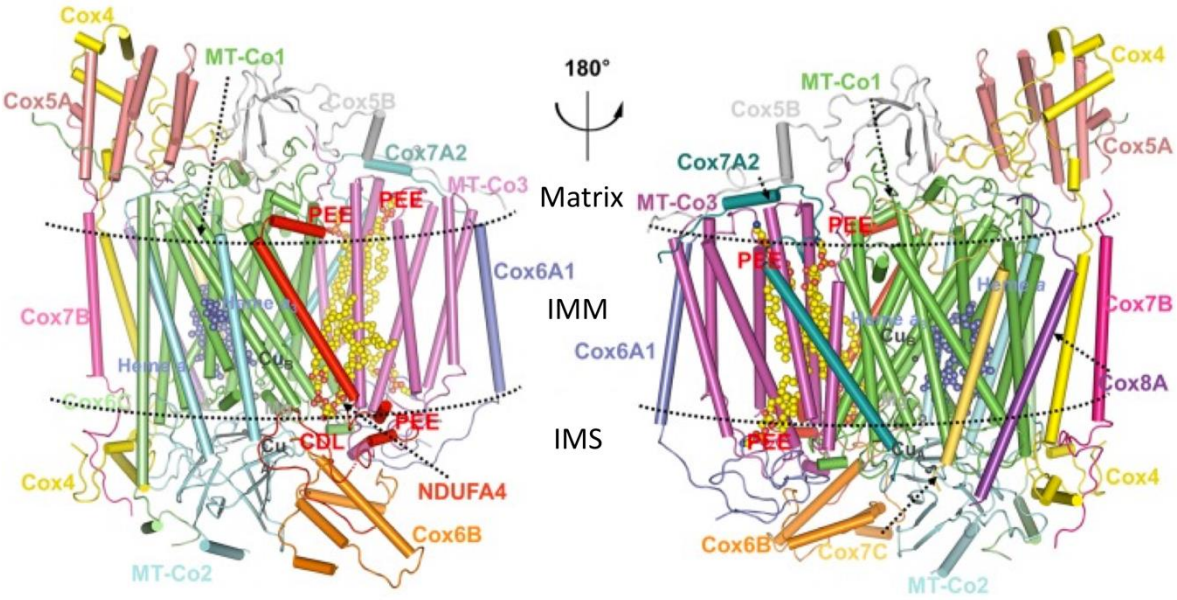

Figure 1.12 Crystal structure of complex IV. Subunits are coloured and labelled with text in the same colours. The two dashed lines indicate the transmembrane region. Figure adapted from (Zong *et al.*, 2018).

1.6.5 Complex V

As the final complex within the OXPHOS system, complex V (CV) is an ATP synthase made up 19 subunits, two of which (ATP6 and ATP8) are mtDNA encoded, assembled as two functional domains – F_0 and F_1. The F_0 domain forms a ring-like structure spanning the IMM, while the F_1 module extends into the matrix **(Figure 1.13)** (Von Ballmoos, Wiedenmann and Dimroth, 2009). The pore formed by the F_0 domain acts as a proton channel, allowing the flow of protons from the IMS back into the matrix, driven by electrochemical gradient generated by the ETC. This movement of protons drives rotary movement of the catalytic F_1 module, resulting in its synthesis of ATP from ADP and P_i. One ATP molecule is synthesised for every 2.7 protons translocated through the proton channel of complex V (Jonckheere, Smeitink and Rodenburg, 2012).

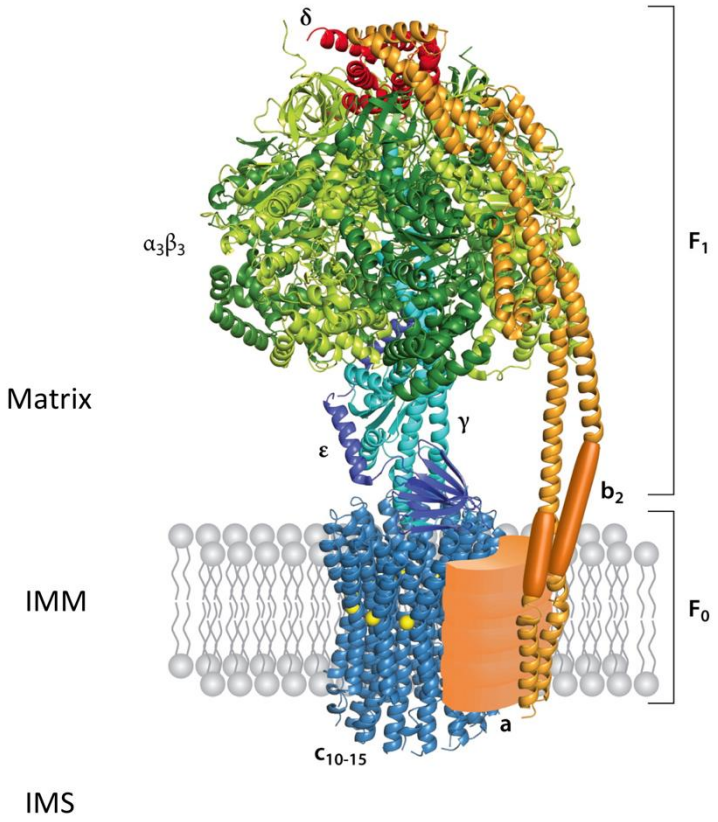

Figure 1.13 Structure of complex V (ATP synthase). Schematic of the known crystal structure of complex V F1 subunits δ (red), α/β (green), γ (turquoise) and ε (purple) and F0 subunits b (orange) c (blue). F0 subunit a is depicted in cartoon form (peach). Figure adapted from (Von Ballmoos, Wiedenmann and Dimroth, 2009).

1.6.6 Supercomplex formation

While often depicted as a chain of single, free-moving complexes, it is well demonstrated that individual respiratory chain enzymes are able to assemble into higher order structures of varying compositions. Blue-native polyacrylamide gel electrophoresis (BN-PAGE) experiments using mildly solubilised mitochondrial membranes allows the separation and visualisation of intact respiratory complexes and supercomplexes (Schagger and Pfeiffer, 2000). Structural evidence for the supramolecular organisation of OXPHOS complexes has been obtained through electron microscopy (Schafer *et al.*, 2006). Complexes I, III and IV can assemble into three distinct arrangements; $I+III_2$, III_2+IV_{1-2} or $I+III_2+IV_{1-4}$ (known as the respirasome). ATP-synthase forms dimeric structures, while complex II appears to remain isolated with no higher order interactions. The most prevalent supercomplex in mammalian mitochondria is the respirasome (Chaban, Boekema and Dudkina, 2014).

1.7 Mitochondrial disease

Mitochondrial disease is used as an umbrella term for the many different genetic disorders resulting from dysfunctional oxidative phosphorylation. With a prevalence estimated at 12.5 per 100,000 adults and 4.7 per 100,000 children, mitochondrial diseases are the most common group of inherited metabolic disorders (Gorman *et al.*, 2015; Skladal, Halliday and Thorburn, 2003).

The clinical features associated with mitochondrial disorders are diverse. The spectrum of clinical disease includes multi-system and isolated organ dysfunction, resulting in a range of 'syndromic' presentations. However, many patients do not fit these classic syndromic archetypes, presenting at various stages of life, with markedly different disease severity and outcome (Gorman *et al.*, 2016). Tissues with high energy demands are considered the most sensitive to defects in ATP synthesis and consequently heart, brain and skeletal muscle are the most commonly affected tissues (Frazier, Thorburn and Compton, 2019) while neurological deficits are the most commonly reported category of symptoms reported in mitochondrial disease patients (Parikh, 2010). However, patients carrying identical pathogenic variants in the same gene can present with quite different pathology, while those with similar clinical features may have distinct genetic aetiologies. For example, mutations in the nuclear gene *POLG* are reported in disorders with a broad phenotypic spectrum. The age of onset of *POLG* related disease ranges from infancy through to late adulthood, causing a number of distinct but phenotypically overlapping disorders (Rahman and Copeland, 2019). Conversely, paediatric presentation of Leigh syndrome, characterised by neurodevelopmental delay and regression, axial hypotonia, failure to thrive, lactic acidosis and typical neuroimaging with bilateral symmetrical involvement of brainstem and basal ganglia. has been reported in patients with over 75 different monogenic causes to date (Schubert Baldo and Vilarinho, 2020). This extensive clinical and genetic heterogeneity makes the identification, characterisation and diagnosis of mitochondrial disease challenging. Further complicating matters, the clinical features of mitochondrial disease often overlap with other neurological or systemic diseases (Martikainen and Chinnery, 2015) **(Figure 1.14)**.

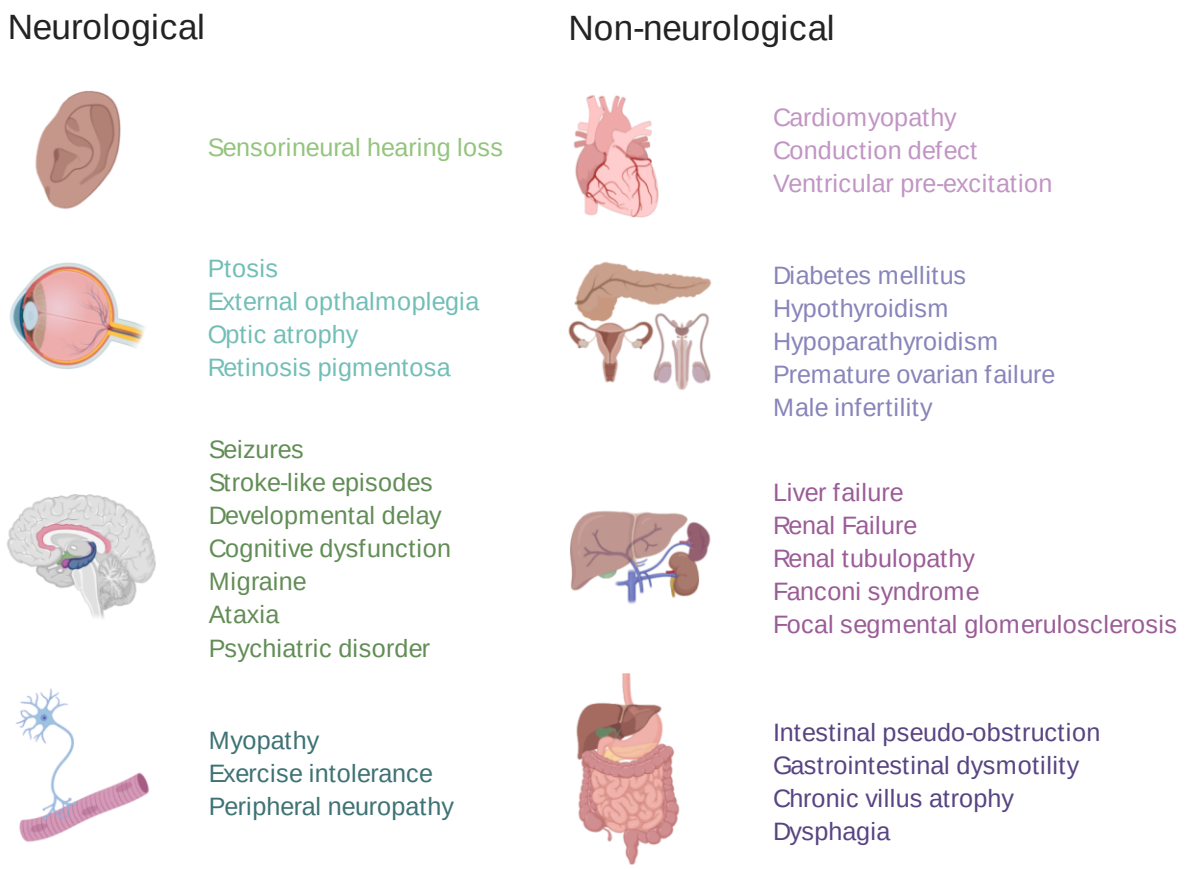

Figure 1.14 Clinical presentations of mitochondrial disease. The clinical features of mitochondrial can be classified into two groups; those with a neurological or those with non-neurological origins. Mitochondrial diseases are clinically heterogeneous and commonly present with dysfunction in a number of different organs or tissues

1.7.1 mtDNA disease

The mutation rate of mtDNA is 10-20 times higher than that of nuclear DNA (Brown, 1980). One factor thought to play a part in the accumulation of polymorphisms in mtDNA is its proximity to DNA-damage inducing reactive oxygen species (ROS) that are produced through electron leaking during their movement along the ETC, along with a lack of histone protection on molecules of mtDNA (Yakes and Van Houten, 1997).

The mitochondrial genome undergoes continuous cycles of replication, independently of the broader cell cycle. While pol γ possesses proofreading capability, mitochondria have fewer DNA repair mechanisms than those that function within the nucleus. Together this gives rise to a much greater frequency of copying errors and the

introduction of mtDNA polymorphisms (Hahn and Zuryn, 2019). Mutations in mtDNA can occur in the form of single nucleotide substitutions within the mRNA, tRNA or rRNA genes, or single, large-scale rearrangements (Taylor and Turnbull, 2005).

1.7.1.1 Heteroplasmy and homoplasmy

Mutations in mtDNA can result in the co-existence of two variant mtDNA populations within a single cell, a concept named heteroplasmy. If all copies of mtDNA within a cell are identical, cells are described as homoplasmic. The concepts of heteroplasmy and homoplasmy become extremely pertinent in instances of mutations that give rise to dysfunctional mitochondria and disease (Taylor and Turnbull, 2005).

If cells contain a combination of wild-type (WT) and pathogenic mutated DNA, the level of heteroplasmy, sometimes referred to as the mutation load, can vary significantly. The mutation load of mutant mtDNA has positive correlation with both the chances of presenting a disease phenotype and the severity of any clinical presentations. This phenomenon is recognised as a ‘threshold effect’ whereby an OXPHOS dysfunction will not occur until the mutation load has reached a minimum percentage within a cell. This threshold typically lies between 60-80% mutant mtDNA, though varies between cell and tissue type, at which point the remaining WT mtDNA cannot achieve adequate compensation of the resulting metabolic dysfunction (Stewart and Chinnery, 2015) **(Figure 1.15)**.

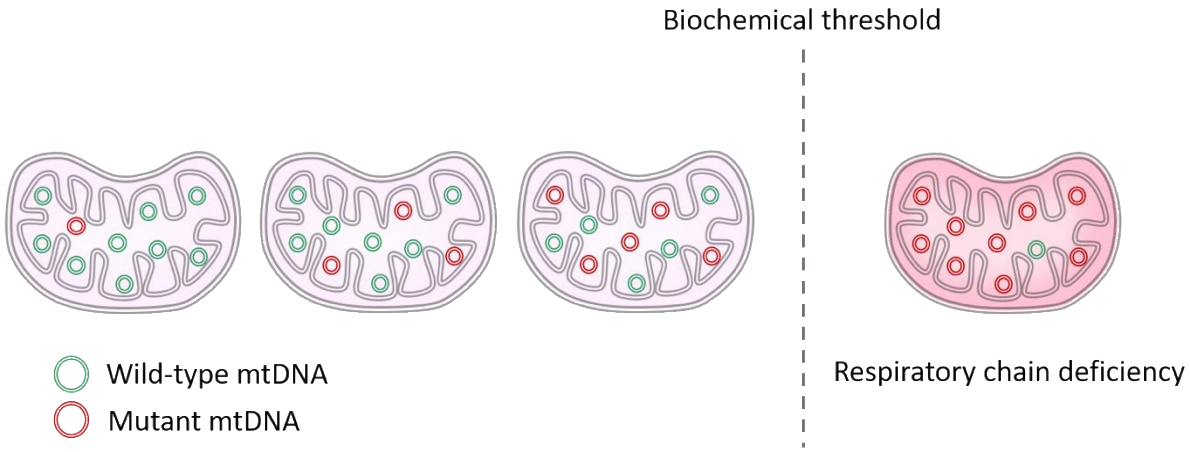

Figure 1.15 Heteroplasmy and the threshold effect. Mitochondria can harbour two versions (wild-type and mutant) of mtDNA. The proportion of mutant mtDNA within a mitochondrion is known as heteroplasmy, which can lie anywhere between 0-100%. Mitochondria can usually tolerate lower levels of heteroplasmy while remaining biochemically normal. If heteroplasmy reaches a particular biochemical threshold, usually somewhere between 60-80%, mitochondria demonstrate a biochemical defect manifesting in a respiratory chain deficiency.

1.7.1.2 mtDNA point mutations

Point mutations in mtDNA have an estimated population prevalence of one in every 5,000 people (Gorman *et al.*, 2015). It has been reported that approximately 75% of mtDNA point mutations are inherited, while the remaining 25% occur as sporadic *de novo* mutations (Sallevelt *et al.*, 2017). Disease causing mutations have been identified in all genes of the mitochondrial genome, of which mutations in tRNA genes are the most common (Lott *et al.*, 2013; Elson *et al.*, 2009). The most prevalent, and as such the more thoroughly characterised, mtDNA point mutation is m.3243A>G in the *MT-TL1* gene encoding mitochondrial $tRNA^{Leu(UUR)}$. This mutation is responsible for 80% of mitochondrial encephalopathy, lactic acidosis and stroke-like episodes (MELAS), though only 15% of m.3243A>G patients have MELAS. Other syndromes commonly associated with this point mutation are maternally inherited deafness and diabetes (MIDD) and progressive external ophthalmoplegia (PEO) (Boggan *et al.*, 2019).

1.7.1.3 Single, large-scale mtDNA deletions

With an estimated prevalence of 1.5 in 100,000, single, large-scale mtDNA deletions can range from 1.3-10kb in size, with the most common deletion spanning 4,977bp (Gorman *et al.*, 2015). These deletions characteristically occur sporadically during embryonic development, meaning that the recurrence risk in future pregnancies is low (Chinnery *et al.*, 2004). The three main clinical presentations associated with large scale mtDNA deletions are CPEO, Kearns-Sayre syndrome (KSS) and Pearson's syndrome, all three of which share significant overlapping features such as PEO (Grady *et al.*, 2014).eo

1.7.2 Nuclear mitochondrial disease

A mutation in any one of the estimated 1145 nuclear encoded mitochondrial proteins (Calvo, Clauser and Mootha, 2016) theoretically has the potential to result in mitochondrial dysfunction. As such, an ever-expanding number of nuclear genetic mutations are implicated in the causation of mitochondrial disease. These pathogenic variants are subject to Mendelian patterns of inheritance and therefore autosomal dominant, autosomal recessive, X linked and *de novo* mutations have all been identified. The first mitochondrial disease-causing mutation in a nuclear gene was identified in the *SDHA* gene in 1995, causing Leigh syndrome in two siblings (Bourgeron *et al.*, 1995). Since 2012, an average of 22 novel nuclear disease genes have been implicated in mitochondrial disease each year (Frazier, Thorburn and Compton, 2019) almost entirely due to the availability and implementation of next generation sequencing technologies in diagnostic and research laboratories.

1.7.2.1 Nuclear disorders of mtDNA maintenance

The integrity of the mitochondrial genome can be affected as a result of defects in nuclear encoded proteins with roles in mtDNA replication, maintenance and transcription, resulting in secondary mtDNA depletions or large-scale deletions.

Pathogenic variants in *POLG*, the gene encoding the catalytic subunit of pol γ, are the most common single gene causes of inherited mitochondrial disorders (Hikmat *et al.*, 2017). In one Australian cohort, *POLG* mutations accounted for 10% of adult cases (Woodbridge *et al.*, 2013). At present, over 300 different pathogenic *POLG* variants have been deposited into the Human DNA Polymerase Gamma Mutation Database (https://tools.niehs.nih.gov/polg/). These mutations span the entirety of the amino acid sequence of POLG, some with autosomal recessive and others with autosomal dominant inheritance patterns. Functionally these *POLG* defects can cause decreased activity of Pol γ and stalling at the replication fork. The result of this mtDNA synthesis defect can be mtDNA depletion, mtDNA multiple deletion or a combination of both (El-Hattab, Craigen and Scaglia, 2017).

As with POLG defects, biallelic mutations in *TWNK*, the gene encoding the mtDNA helicase Twinkle, result in the stalling of replication and can cause qualitative defects in the form of mtDNA deletions or quantitative mtDNA depletion defects (Hebbar *et al.*, 2017).

Autosomal recessive mutations (homozygous nonsense and homozygous missense variants) in the *MGME1* gene have been reported in three families, resulting in both mtDNA depletion and multiple deletions. The mtDNA rearrangements identified in all affected patients are significantly larger than deletions characteristic of *POLG*-related mtDNA maintenance defects and include numerous duplications (Nicholls *et al.*, 2014).

1.7.3 Diagnosing mitochondrial disease

Due to the complex nature of mitochondrial genetics, vast heterogeneity and broad clinical spectrum implicated in mitochondrial disease, a collaborative and multidisciplinary approach is most effective when seeking genetic diagnosis. Histopathological and biochemical investigation of patient muscle tissue has traditionally been, and remains, an important aspect of diagnostic investigation. Owing to its strong energy dependence, muscle is one of the most commonly affected tissues in both isolated organ and multi-system mitochondrial disease, rendering patient

muscle biopsies a very valuable diagnostic resource (Taylor *et al.*, 2004). Immunofluorescent techniques developed in recent years can also utilise patient tissues to assess the abundance of a number of mitochondrial OXPHOS proteins simultaneously (Rocha *et al.*, 2015). Alongside these tissue-based investigative techniques a range of molecular genetic tools are employed in the diagnosis of mitochondrial disease. The preferred genetic investigation undertaken in each case is determined by a number of factors including clinical characterisation, familial inheritance patterns and the results of any prior histopathological and biochemical studies (Thompson *et al.*, 2019).

1.7.3.1 Histopathology and biochemistry

The basic morphology of patient muscle can be investigated through the application of stains such as haematoxylin and eosin (H&E) and modified Gomori trichrome. H&E staining will reveal the presence of a number of abnormalities to fibre shape and size. Modified Gomori trichrome is applied to visualise mitochondrial and endoplasmic reticulum membranes. The presence of 'ragged red fibres' (RRF) signifies the accumulation of mitochondria along the sarcolemma of myofibres, suggestive of mitochondrial proliferation in response to a respiratory chain defect (Joyce, Oskarsson and Jin, 2012).

A sequential cytochrome *c* oxidase/succinate dehydrogenase (COX/SDH) histochemical assay is regularly performed to provide a histopathological read out of respiratory chain function. The activities of complex II, which is entirely nuclear encoded, and complex IV, which is encoded by genes of both mtDNA and nDNA, are visualised. A mosaic pattern of COX-deficient fibres in the presence of normal SDH (CII) activity is can be indicative of a heteroplasmic mtDNA disease mechanism. Each muscle fibre harbours differing mutation loads that will only manifest as COX-deficient if above the mutation threshold. Widespread and generalised loss of COX reactivity is highly suggestive of respiratory chain dysfunction resulting from nuclear DNA mutations or pathogenic homoplasmic mtDNA variants (Taylor *et al.*, 2004).

The *In vitro* biochemical measurement of individual respiratory chain enzyme activities in both muscle and fibroblasts is another widely used diagnostic technique. The activity of each complex (I-IV) can be investigated through spectrophotometry measured, against the citrate synthase enzyme as a matrix marker, to identify any defects in enzymatic activity (Frazier *et al.*, 2020).

1.7.3.2 Immunohistochemical assessments

The aforementioned histopathology based techniques do not assess the activity of complex I, despite complex I being one of the most commonly affected enzymes in isolated and combined OXPHOS deficiencies (Loeffen *et al.*, 2000; Mayr *et al.*, 2015). A more recently developed technique, named the quadruple immunofluorescent assay, targets NDUFB8 of complex I and COXI of complex IV along with porin (mitochondrial mass marker) and laminin (marker of myofibre boundaries) in single muscle fibres. This assay is able to give precise and reproducible protein quantification in large numbers of individual muscle fibres in mitochondrial disease patients with a range of genetic defects (Rocha *et al.*, 2015).

1.7.4 Application of whole exome sequencing in mitochondrial disease

The earliest approaches to the identification of novel human disease genes relied on the use of linkage analysis across a number of affected and unaffected individuals. This method works to identify specific loci on individual chromosomes that are co-inherited with disease, relying on the high probability that proximally close regions of chromosomes remain close following homologous recombination during meiosis (Pulst, 1999). While this approach remains in use, it is most powerful when utilised in large families/cohorts but is of limited value in individual cases of rare disease (Smith *et al.*, 2011). The traditional approach to DNA sequencing, developed by Fred Sanger in 1977, utilised radioactively labelled chain-terminating nucleotides to generate libraries of products of random sizes that could then be visualised using autoradiography of polyacrylamide gels (Sanger, Nicklen and Coulson, 1977). The development of methods that allowed Sanger sequencing to be carried out in parallel

using capillary sensors marked the beginning of a rapid development and advancement of new massively parallel sequencing techniques, also termed ‘next generation sequencing’ (NGS) (Luckey *et al.*, 1990).

A number of different NGS platforms exist, with provider developing different technologies specific to the type of sequencing that will be carried out (gene targeted/panel/exome/genome) (Meera Krishna, Khan and Khan, 2019). Increased implementation of NGS to diagnostic pathways has resulted in the widespread application of whole exome (WES) **(Figure 1.16)** and whole genome sequencing (WGS) in rare disease. The human exome represents less than 2% of the total human genome, making WES a cost-effective method in the investigation of mendelian disease (Rabbani, Tekin and Mahdieh, 2014). Where candidate or targeted gene panel approaches to genetic diagnosis rely on neat phenotype-genotype correlations, WES/WGS are unbiased sequencing tools, that when used in conjunction with bioinformatic filtering pipelines, have proven to be extremely effective in the diagnosis of such a complex phenotypic spectrum. WES has been incorporated into routine mitochondrial diagnostic pathways across the world, with some centres achieving successful diagnosis in approximately 60% of cases (Pronicka *et al.*, 2016; Taylor *et al.*, 2014).

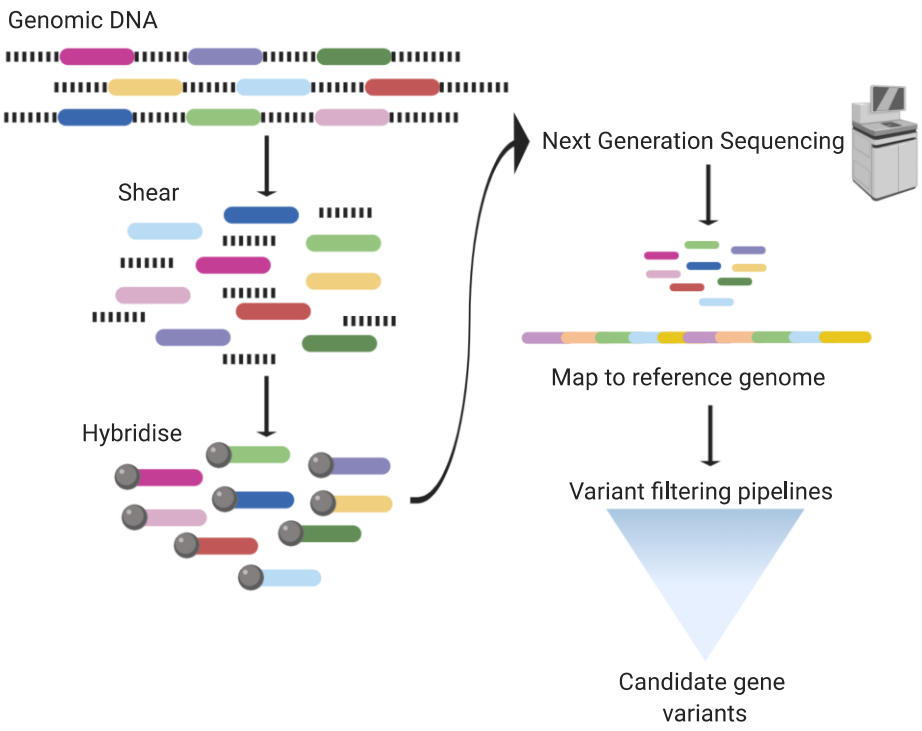

Figure 1.16 Whole exome sequencing. Genomic DNA is sheared before being enriched for sequences corresponding to exons (coloured sections) which are then hybridised to biotinylated DNA baits (grey beads). DNA captured is amplified, then sequenced massively in parallel. Output sequences are mapped, aligned to a reference genome and then subject to calling of candidate causal variants.

1.7.5 Functional validation of putative pathogenic variants

One possible outcome of WES or WGS is the identification of a previously reported variant in a known disease gene. In such cases, a genetic diagnosis can be confirmed with confidence. However, WES/WGS have several other possible outcomes. Novel variants may be identified in a known disease gene, in a gene of known function that has not been previously reported in association with mitochondrial disease or in a gene with unknown function. In each of these cases further functional characterisation of candidate variants is required in order to assign pathogenicity. The precise nature of each validation study is influenced by the information available pertaining to the candidate gene and identified variants, the mitochondrial processes that would be most likely affected in the presence of a defect, along with the availability of cells, tissues and genetic models **(Figure 1.17)**.

As the term ‘mitochondrial disease’ refers specifically to disorders of energy production, the assessment of steady-state levels of various OXPHOS subunit proteins and complexes through SDS- and BN-PAGE with immunoblotting is a standard experiment utilised in the functional characterisation of patient cells and tissues. Immunoblotting with an antibody targeting a candidate protein is also rapid way of validating destabilising or loss of protein mutations. Other protein-based validation studies utilised in patient cells and/or tissues are complexome profiling to assess complex assembly (Alston *et al.*, 2016) and [^{35}S] metabolic labelling to interrogate mitochondrial translation (Bugiardini *et al.*, 2019). Imaging-based studies, such as transmission electron microscopy and high-resolution confocal imaging, are useful when investigating disorders affecting mitochondrial morphology and dynamics (Janer *et al.*, 2016).

Lentiviral studies can be used to confirm the pathogenicity of novel variants in patient cell lines that exhibit clear functional consequences, such as OXPHOS deficiencies or translation defects. Rescue of these defects upon the introduction of WT copies of the candidate gene is seen as the ‘gold-standard’ technique for assignment of variant pathogenicity (Metodiev *et al.*, 2016) however, this is not an option if patient cell lines do not exhibit a biochemical defect. The generation of genetic models as an aid in the delineation of molecular mechanisms underlying disease variants can be extremely informative, particularly when patient cells/tissues are unavailable or biochemical defects are only present in a specific tissue. Suitable model systems can obtained through both cell line-based studies, including CRISPR/Cas9 knock-outs, or the genetic manipulation of whole organisms.

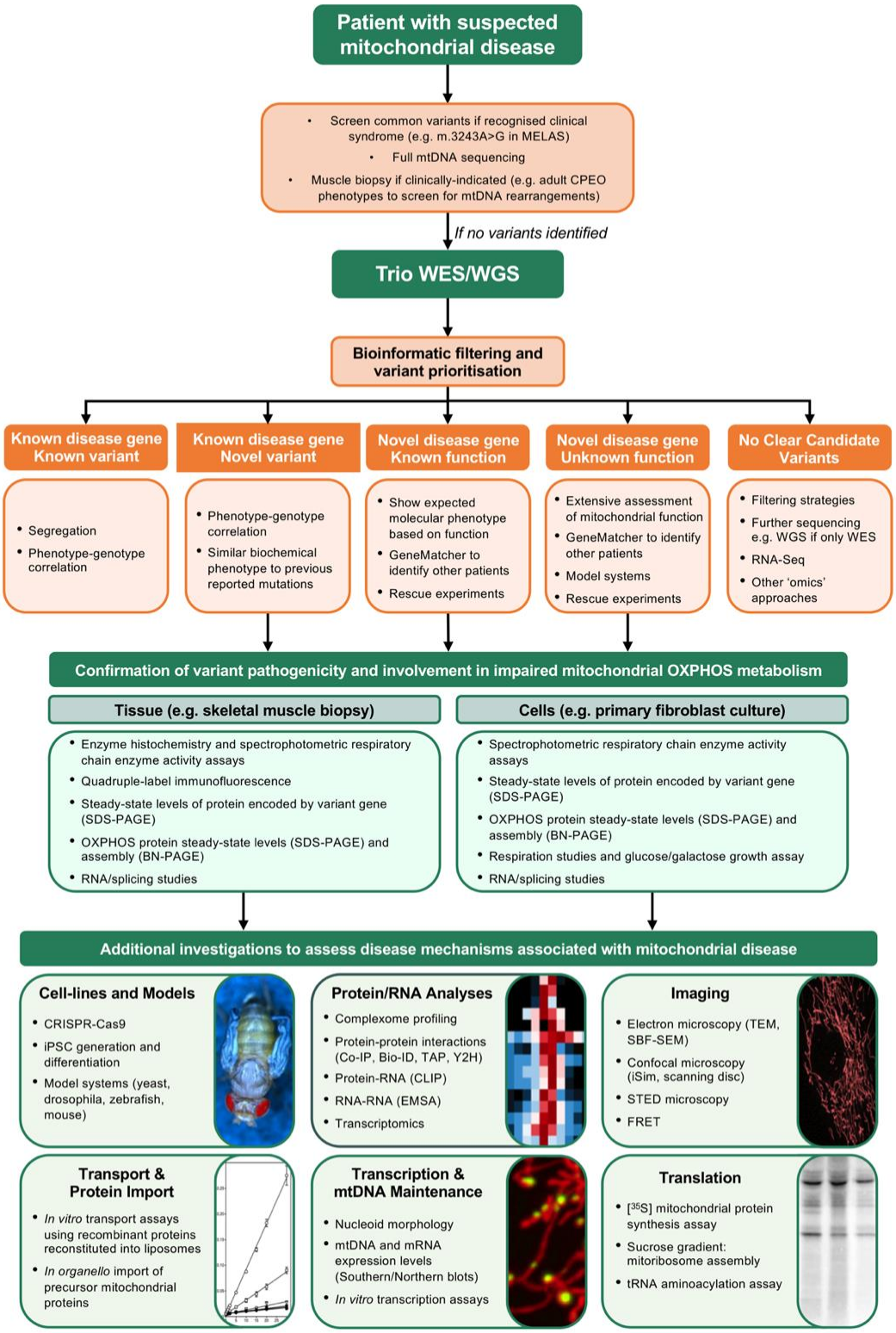

Figure 1.17 Workflow for the identification and validation of mitochondrial disease variants. The choice of appropriate genetic testing is directly influenced by the clinical information that is available. Full mtDNA sequencing is often carried out in patients with clinical features that strongly suggest a mitochondrial aetiology. If no mtDNA or syndrome-associated nuclear variants are identified, patients are candidates for trio WES or WGS. The five possible

outcomes of WES range from the identification of previously reported variant in a known disease gene to no clear candidate variants identified. The identification of a novel variant in a known disease gene, a novel disease gene or a disease gene of unknown function all require further functional work to varying extents. The approaches taken to confirm variant pathogenicity depend on the availability of patient tissues and/or cell lines. Segregation studies, respiratory chain enzyme activity assays and investigation into steady-state levels of OXPHOS proteins/the protein of interest are first line approaches in the assignment of pathogenicity. Any additional investigation into unique pathomechanisms of disease are chosen based on the function of proteins encoded by the identified disease gene. Abbreviations: Co-IP (co-immunoprecipitation); EMSA (electrophoretic mobility shift assay); FRET (fluorescence resonance energy transfer); iPSC (induced pluripotent stem cells); MELAS (mitochondrial encephalomyopathy, lactic acidosis, and stroke-like episodes); MIDD (maternally inherited diabetes and deafness); OXPHOS (oxidative phosphorylation); SBF-SEM (serial block-face scanning electron microscopy); STED (stimulated emission depletion); TAP (transporter associated with antigen processing); TEM (transmission electron microscopy); WES (whole-exome sequencing); WGS (whole-genome sequencing); Y2H (yeast two-hybrid). Figure adapted from (Thompson *et al.*, 2019).

1.8 Disorders of mitochondrial translation

Over one third of reported mitochondrial disease-causing nuclear defects are in genes encoding proteins with a role in mtDNA gene expression, encompassing mtDNA maintenance and replication through to mitochondrial transcription and translation (Thompson *et al.*, 2019). Defects of mtDNA expression, specifically those affecting mitochondrial translation, will be the focus of this thesis.

Mutations in a whole host of genes with roles in processes ranging from tRNA modification through to individual translation factors can compromise mitochondrial translation. Defects of mitochondrial translation represent a growing group of disorders causing both childhood- and adult-onset mitochondrial disease with a broad range of clinical presentations. Groups of disorders, such as those affecting mitochondrial aminoacyl tRNA synthetases (mt-tRNA aa-RS) and mitoribosomal subunits, show some commonalities in disease presentation but also help to highlight the clinical heterogeneity seen in defects of mitochondrial translation

Function	Genes
mtRNA maturation/ modification	*ELAC2, ERAL1, DHX30, FASTKD, GTPBP3, HSD17B10, LRPPRC, MTO1, MTPAP, MRM2, MTFMT, NSUN3, PRORP, PNPT1, PUS1, TRMT10C, TRIT1, TRMU, TRMT5, TRNT1*
Mitochondrial aa-RS	*AARS2, CARS2, DARS2, EARS2, FARS2, GARS, GATB, GATC, HARS2, IARS2, KARS, LARS2, MARS2, NARS2, PARS2, QRSL1, RARS2, SARS2, TARS2, VARS2, WARS2, YARS2*
Mitoribosomal subunits	*MRPS2, MRPS7, MRPS14, MRPS16, MRPS22, MRPS23, MRPS25, MRPS28, MRPS34, MRPS39, MRPL3, MRPL12, MRPL24, MRPL44*
Mitochondrial Translation	*C12orf65, C12orf62, COA3, GFM1, GFM2, GUF1, OXA1L, RMND1, TACO1, TSFM, TUFM*

Table 1.1 Nuclear encoded genes implicated in disorders of mitochondrial translation. Genes with reported pathogenic variants resulting in defects of mitochondrial translation are categorised according to function. This list was compiled through comprehensive searches of the literature using the following key words and phrases: 'mitochondrial translation' 'mitochondrial protein synthesis' 'mitochondrial disease' and is accurate as of June 2020.

Pathologies caused by mutations in all 19 mt-tRNA aa-RS have now been described. These disorders are often hallmarked by features of central nervous system (CNS) involvement such as leukodystrophy (*AARS2*, *DARS2*, *EARS2, MARS2*), encephalopathy (*RARS2, NARS2, CARS2, IARS2, FARS2, PARS2, TARS2, VARS2*), deafness or hearing loss (*NARS2, PARS2, MARS2*) (Webb *et al.*, 2015; Mizuguchi *et al.*, 2017) or Perrault syndrome (*HARS2, LARS2*) (Sissler, Gonzalez-Serrano and Westhof, 2017). However, non-CNS and isolated pathologies also occur in mt-tRNA aa-RS disease. Cardiomyopathy has been reported in patients with pathogenic variants in *GARS, KARS, YARS2 and AARS2* (McMillan *et al.*, 2014; Verrigni *et al.*, 2017; Riley *et al.*, 2013; Sommerville *et al.*, 2018), while two distinct syndromes, MLASA (mitochondrial Myopathy, Lactic acidosis and Sideroblastic Anaemia) and HUPRA (Hyperuricemia, Pulmonary hypertension, Renal failure in infancy and

Alkalosis), can be caused by mutations in the *YARS2* and *SARS2* genes respectively (Nakajima *et al.*, 2014; Belostotsky *et al.*, 2011). Along with the clinical heterogeneity between different mt-tRNA aa-RS disease genes, vast variability in disease presentation also exists within disorders of single aa-RS genes, such as *AARS2*. Through WES, pathogenic mutations in the *AARS2* gene were first reported in an infant with fatal hypertrophic cardiomyopathy (Gotz *et al.*, 2011) and then in two further families with cardiomyopathic clinical presentation in infancy (Sommerville *et al.*, 2018), consistent with the original report of *AARS2* disease. However, a second distinct disease phenotype is seen in patients with *AARS2* mutations, characterised by leukoencephalopathy with, in female patients, premature ovarian failure (Dallabona *et al.*, 2014). The mutations reported across all 19 mt-tRNA aa-RS enzymes do not appear to follow any general trends in regard to the location of variants within core domains or at evolutionarily conserved residues. This, together with the variability in clinical presentation, both within and between the mt-tRNA aa-RS groups, suggests a number of different pathomechanisms underlying this broad group of diseases (Sissler, Gonzalez-Serrano and Westhof, 2017).

The first disorder of mitochondrial translation caused by a mitoribosomal defect was identified in a patient with a nonsense mutation in the *MRPS16* gene. The patient presented with neonatal lactic acidosis, agenesis of the corpus callosum and dysmorphism. Patient fibroblasts exhibited a severe mitochondrial translation defect and a combined OXPHOS deficiency, the latter also observed in patient muscle and liver homogenates (Miller *et al.*, 2004). In the past 15 years, disease causing variants have been reported in genes for a further nine proteins of the mitoribosomal SSU: MRPS2, MRPS7, MRPS14, MRPS22, MRPS23, MRPS25, MRPS28 MRPS34 and MRPS39 (also known as PTCD3) (Gardeitchik *et al.*, 2018; Menezes *et al.*, 2015; Jackson *et al.*, 2019; Saada *et al.*, 2007; Kohda *et al.*, 2016; Lake *et al.*, 2017; Borna *et al.*, 2019; Bugiardini *et al.*, 2019; Pulman *et al.*, 2019); and four of the LSU: MRPL3, MRPL12, MRPL24, MRPL44 (Galmiche *et al.*, 2011; Serre *et al.*, 2013; Carroll *et al.*, 2013; Di Nottia *et al.*, 2020), taking the total number of reported MRP disease genes to 14. Although there is significant variation in clinical presentation, some common features are seen across the MRP cases. Disease-onset consistently occurs very early in life (neonatal or infantile) and almost all patients exhibit mild to severe/fatal lactic acidosis (Jackson *et al.*, 2019; Gardeitchik *et al.*, 2018). Many MRP defects result in

death early in life and the poor survival associated with these disorders may explain the small number of patients carrying pathogenic variants from the 80 mitoribosomal proteins that have been identified to date.

1.8.1 Mutations in mitochondrial translation factors

Alongside mitoribosomal mutations, affecting the core translation machinery, defects of individual mitochondrial translation factors have also been implicated in mitochondrial disease. The first nuclear disease gene to be identified associated with defective mitochondrial translation (Coenen *et al.*, 2004), *GFM1* encodes the elongation factor mtEFG1. Recessive variants in GFM1 have been reported in a total of 17 patients with early onset mitochondrial disease. Many of the early cases of *GFM1* disease were rapidly progressive and fatal before the age of two and a half years (Smits *et al.*, 2011a; Balasubramaniam *et al.*, 2012; Galmiche *et al.*, 2012; Coenen *et al.*, 2004; Antonicka *et al.*, 2006; Valente *et al.*, 2007). The brain imaging typically showed hypoplasia of corpus callosum, symmetrical cystic lesions in the white matter and involvement of basal ganglia. However, more recent cases of *GFM1* disease demonstrate long term survival further into childhood, with a less severe clinical disease presentation (Brito *et al.*, 2015; Simon *et al.*, 2017). The loss of function mutations described in *GFM1* result in generalised defects of mitochondrial translation, causing combined OXPHOS deficiencies. The severity of OXPHOS deficiency in each case appears to correlate with the residual amount of expressed mtEFG1. Patients with a higher residual steady-state level of mtEFG1 tend to exhibit a less severe OXPHOS defect (Brito *et al.*, 2015). Recessive mutations in the TSFM gene encoding another elongation factor, mtEF-Ts, have been described in a number of cases of early onset mitochondrial disease resulting in death in early infancy, or a more slowly progressing childhood onset cardiomyopathy with ataxia and a neurological phenotype (Smeitink *et al.*, 2006b; Vedrenne *et al.*, 2012; Calvo *et al.*, 2012; Emperador *et al.*, 2017).

In addition to defects of translation elongation, pathogenic variants in initiation factors have also been identified. The protein methionyl tRNA formyltransferase (MTFMT), encoded by the *MTFMT* gene, carries out formylation of a tightly regulated proportion

of the general Met-tRNA^{Met} pool to provide Met-tRNAs for both mitochondrial translation initiation and elongation (Takeuchi *et al.*, 1998). Autosomal recessive variants in the *MTFMT* gene were first identified as pathogenic in two cases of Leigh syndrome (Tucker *et al.*, 2011), but have since been implicated in a range of Leigh-like encephalomyopathic presentations, along with one case of relapsing-remitting attacks of neurological dysfunction more reminiscent of a de-myelinating disease (Haack *et al.*, 2014; Pena *et al.*, 2016).

Initiation factor RMND1 is responsible for the anchoring and stabilisation of the mitoribosome in close proximity to sites of mt-mRNA maturation. Combined and isolated OXPHOS defects have both been observed in *RMND1* disease patients, along with decreased steady-state levels of mitoribosomal proteins and defects of mitochondrial translation (Janer *et al.*, 2015; Ng *et al.*, 2016). The clinical disease spectrum of *RMND1* variants ranges from fatal encephalomyopathy with lactic acidosis to developmental delay, sensorineural deafness, hypotonia and renal disease (Garcia-Diaz *et al.*, 2012; Janer *et al.*, 2015; Ng *et al.*, 2016). The disease onset varies from severe infantile encephalomyopathy culminating in death to, childhood-onset nephropathy with longer survival (Garcia-Diaz *et al.*, 2012; Janer *et al.*, 2015).

1.9 Aims and Objectives

This PhD was funded by The Lily Foundation as part of their WES project; A UK wide recruitment of patients for whole exome sequencing through three highly specialised mitochondrial diagnostic and research centres in Newcastle, Oxford and London. As part of this wider project, The Lily foundation fund a number of PhD studentships and postdoctoral scientists to work on WES, bioinformatic analysis and functional characterisation of novel mitochondrial disease genes. Within the WES Project, 202 families have been screened to date with a diagnostic yield of 73%. Although my work has been funded as part of the UK based Lily WES project, it is collaborative relationships between clinicians and researchers from across the globe that underpin WES gene discovery. A large proportion of the patient investigations presented throughout the following chapters have been the result of collaborations with international diagnostic and research centres.

While seeking to expand current knowledge of molecular genetic mechanisms underlying mitochondrial disease, this work is also of significant diagnostic value. Assigning pathogenicity to novel genes/variants in mitochondrial disease provides affected patients with firm genetic diagnoses and can expand reproductive options for families considering future pregnancies.

My interest in defects of mitochondrial translation began with the investigation of patients carrying novel variants in known disease genes encoding mitochondrial translation factors. As my PhD progressed the scope of this research broadened to include disorders of mitoribosomal proteins upon the identification of variants in novel mitoribosomal LSU disease genes. The objective of the research presented within this thesis is to functionally validate candidate mitochondrial disease gene variants identified through whole exome sequencing, with a focus on disorders of mitochondrial translation, thus contributing to the ever-growing signature of nuclear genetic mechanisms causing mitochondrial disease.

Chapter 2 : Materials and methods

2.1 Materials

2.1.1 Equipment

Analogue Tube Roller	ThermoScientific
Aspiration System Vacusafe	Integra
Benchtop Centrifuge 5417R (Refrigerated)	Eppendorf
Benchtop Centrifuge 5418	Eppendorf
Benchtop Centrifuge, Universal 32	Hettich
Benchtop Electrophoresis Digital Slab Gel Dryer	Savant
Cellometer Auto 1000 Bright Field Cell Counter	Nexcelom
Class II Microbiological Safety Cabinet, BH-EN-2004	Faster
CO_2 Cell Culture Incubator, MCO-18AIC	Panasonic
CoolCell Cell Freezing Container	Biocision
Dry Heat Block	Techne
Electrophoresis Unit, HU10 Mini-Plus Horizontal Unit	Scie-Plas
Falcon Cell Strainer	FisherScientific
Falcon Round-Bottom FACS Tubes	FisherScientific
Genetic Analyser, ABI 3130*xl*	Applied Biosystems
Imaging System, ChemiDoc MP	Bio-Rad

LED Microscope, Leica DM IL	Leica
Microcentrifuge, Technicomini	Griffin Education
Mighty Small SDS-PAGE System	Hoefer
Mini-Protean Tetra Cell system	Bio-Rad
MoFlo Astrios Cell Sorter	Beckman Coulter
NanoDrop Spectrophotometer, ND-1000	ThermoScientific
Nucleofector 2b Device	Lonza
OptimaTM TLX Ultracentrifuge	Beckman Coulter
Orbital Shaker, SSL1	Stuart
Pestle and Mortar	CoorsTek
pH Meter 3510	Jenway
Plate Reader, SpectraMax M5e Multimode	Molecular Devices
Stirrer, Ceramic Plate U151	Stuart
Thermal Cycler, Veriti 96 Well	Applied Biosystems
Ultra-Turrax homogeniser (IKA)	IKA
UVP PCR Cabinet	FisherScientific

2.1.2 Consumables

96-Well PCR Plate, Semi-Skirted, Clear	StarLab
Cell Line Nucleofector Kit V	Lonza
Cellstar Disposable Tubes (5 mL, 10 mL, 25 mL)	Greiner Bio-One
Cellstar Falcon Tubes (50 mL)	Greiner Bio-One
Cellstar Tissue Culture Flasks (25cm^2, 75cm^2)	Greiner Bio-One
Chromatography Paper, 3mm	Whatman
DNeasy Cell and Tissue Kit	Qiagen
Flat-bottom 6 Well Plates	TPP
Flat-bottom 96 Well Plate	TTP
Immobilon-P PVDF membrane (0.45 µm)	Merck
Nunc-Cryotube Vials	Thermo-Scientific
PCR tubes (200 µL)	StarLab
Plasmid Miniprep Kit	Monarch
RNeasy Mini Kit	Qiagen
Sarogold Pro Food Wrap	Sarogold
Scalpel	Swan-Morton
Stericup-GP, 0.22µm, Polyethersulfone, 500 mL	Merick-Millipore
Ultracentrifuge Tubes	Beckman Coulter
Universal tubes, 20 mL	Starlab

2.1.3 Chemicals and reagents

2.1.3.1 General reagents

Dulbecco's Phosphate buffered saline X1 (DPBS)	Gibco
EDTA	Sigma-Aldrich
Emetine Dihydrochloride	Sigma-Aldrich
Glycerol	Sigma-Aldrich
Phenylmethylsulphonyl Fluoride (PMSF)	Roche
Pierce Protease Inhibitor Cocktail Tablet	ThermoFisher
Proteinase K	ThermoFisher

2.1.3.2 Tissue culture

DMSO	Sigma-Aldrich
Dulbecco's Modified Eagle Medium	Gibco
Foetal Bovine Serum (FBS)	Gibco
Lipofectamine RNAiMAX	ThermoFisher
MEM Non-essential Amino Acid Solution (100X)	Sigma-Aldrich
MEM Vitamins	Gibco
Minimum Essential Media	Gibco
Opti-MEM Reduced Serum Media	Gibco
Penicillin and Streptomycin Solution	Gibco
siGENOME siRNA	Horizon
Sodium pyruvate	Gibco
TrypLE Express	Gibco
Uridine	Sigma-Aldrich

2.1.3.3 SDS-PAGE and western Blot

Acrylamide/Bis-acrylamide, 30%, 29:1	Bio-Rad
Amersham ECL Prime	GE Healthcare
Blue Wide Range Protein Ladder	Cleaver Scientific
Dried Skimmed Milk Powder	Marvel
Glycine	Sigma-Aldrich
N, N, N', N'- Tetramethylethylenediamine (TEMED)	Sigma-Aldrich
Polysorbate 20 (Tween-20)	Acros Organics
Protein Assay Dye Reagent Concentrate	Bio-Rad
Sodium Dodecyl Sulphate (SDS)	Sigma-Aldrich
Trisma Base	Sigma-Aldrich

2.1.3.4 [^{35}S] Metabolic labelling

Easy Tag Express Protein Labelling Mix (73% L-met, 22% L-cys)	Perkin-Elmer
L-Methionine	Sigma-Aldrich
Met/Cyst Free DMEM	ThermoFisher

2.1.3.5 Sucrose gradient

Chloramphenicol	Duchefa Biochemie
KCl	Sigma-Aldrich
Magnesium Acetate	Sigma-Aldrich
NH_4Cl	Sigma-Aldrich
Sucrose	Sigma-Aldrich
Trichloroacetic Acid (TCA)	Sigma-Aldrich

2.1.3.6 Polymerase chain Reaction

Ambion™ Nuclease-free water	Invitrogen
Colourless GoTaq Reacting Buffer, 5X	Promega
Deoxyribonucleotide Triphosphate (dNTP) Mix, 2mM	Bioline
GoTaq G2 DNA Polymerase, 5U µl-1	Promega
Orange G powder	Sigma-Aldrich

2.1.3.7 Gel electrophoresis

Agarose (Molecular Grade)	Bioline
GeneRuler 100bp Plus DNA Ladder	ThermoFisher
GeneRuler 1kb Plus DNA Ladder	ThermoFisher
SYBR Safe DNA Gel Stain, 10,000X	Invitrogen
Tris-Acetate-EDTA (TAE) Buffer	Formedium

2.1.3.8 Sanger sequencing

Big Dye Terminator v3.1 Cycle Sequencing Kit	Applied Biosystems
Exonuclease I, 20U μL^{-1}	Thermo Scientific
FastAP, thermosensitive Alkaline Phosphatase, 1U μl^{-1}	Thermo Scientific
Hi-Di formamide	Applied Biosystems

2.1.3.9 Plasmid cloning and transfection

10x Buffer 2.1	NEB
10x PNK Buffer	NEB
2x T7 Ligase Buffer	NEB
Alkaline Phosphatase	ThermoFisher
Ampicillin	Sigma-Aldrich
ATP	ThermoFisher
BBsI	NEB
EcoRI	NEB
Glycerol	Sigma-Aldrich
LB Broth	Miller
LB Broth with Agar	Miller
pSpCas9(BB)-2A-GFP (PX458)	Addgene
SOC Media	Sigma-Aldrich
Subcloning Efficiency DH5α Chemically Competent Cells	NEB
T4 PNK Enzyme	NEB
T7 Ligase	NEB

2.1.3.10 cDNA studies

5x Reaction Buffer	Promega
Hotstart GoTaq G2 polymerase	Promega
M-MLV Reverse Transcriptase	Promega
M-MLV Reverse Transcriptase Buffer	Promega
$MgCl_2$	Promega
Random Hexamers	Promega
RNasin	Promega

2.1.4 Solutions

2.1.4.1 Growth media

Reagent	Final Concentration
Dulbecco's Modified Eagle Media (DMEM) High Glucose	-
Foetal Bovine Serum (FBS)	10%
Non-Essential Amino Acids	1x
Penicillin/Streptomycin	1%
Uridine	50 µg/mL

2.1.4.2 Cell lysis buffer

Reagent	Final Concentration
Tris-HCl pH7.4	50 mM
NaCl	130 mM
$MgCl_2$	2 mM
Nonidet P-40	1%
Protease Inhibitor Tablet	1x
PMSF	1 mM

2.1.4.3 RIPA buffer

Reagent	Final Concentration
Tric-Hcl pH 8.0	10 mM
EDTA	1 mM
Triton-X	1%
EGTA	0.5 mM
Sodium Deoxycholate	0.1%
SDS	0.1%
NaCl	140 mM
PMSF (added just before use)	1 mM

2.1.4.4 Sample dissociation buffer

Reagent	Final Concentration
Tris-HCl pH 6.8	6.25 mM
SDS	2%
Glycerol	10%
DDT	100 mM
Bromophenol Blue	0.01%

2.1.4.5 12% Resolving gel

Reagent	Final Concentration
Tris-HCl pH 8.5	380 mM
Acrylamide/Bis-acrylamide, 30%, 29:1	12%
SDS	0.1%
APS	0.1%
TEMED	0.1%

2.1.4.6 3.75% Stacking gel

Reagent	Final Concentration
Tric-HCl pH 6.8	125 mM
Acrylamide/Bis-acrylamide, 30%, 29:1	3.75%
SDS	0.1%
APS	0.1%
TEMED	0.1%

2.1.4.7 1x Running buffer

Reagent	Final Concentration
Trisma Base	25mM
Glycine	192 mM
SDS	0.1%

2.1.4.8 1x Transfer Buffer

Reagent	Final Concentration
Trisma Base	25mM
Glycine	192 mM
SDS	0.02%
Methanol	15%

2.1.4.9 TBS-T

Reagent	Final Concentration
Tris-Buffered Saline	1x
Tween-20	0.1%

2.1.4.10 Sucrose gradient buffer

Reagent	Final Concentration
Tris-HCl pH 7.2	50 mM
Magnesium Acetate	10 mM
NH_4Cl	40 mM
KCl	100 mM
PMSF	1 mM
Chloramphenicol	50 µg/mL

2.1.4.11 DNA isolation reagent

For 20 samples:

Reagent	Volume
DirectPCR Lysis Reagent	1 mL
Proteinase K	40 µL

2.1.4.12 PCR master mix

Reagent	Final Concentration
GoTaq Reaction Buffer	1x
dNTPs	200 µM
GoTaq G2 Polymerase	1.25u
Fwd/Rev Primer Mix	1.25 µM
Nuclease-Free H_2O (up to final volume)	

2.1.5 Software

Program	Developer
ImageLab (Version 6.1)	Bio-Rad
ImageJ (Version 1.48)	Open Source
FinchTV (Version 1.4.0)	Geospiza Incorporated
Seaview (Version 4.5.3)	PRABI-Doua Pôle Rhône-Alpes de Bioinformatique Site Doua

2.1.6 Online web tools

Tool	Access Link
Align GVGD	http://agvgd.hci.utah.edu/
Combined Annotation Dependent Depletion (CADD)	https://cadd.gs.washington.edu/snv
Mutation Taster	http://www.mutationtaster.org/
Polymorphism Phenotyping v2 (Polyphen2)	http://genetics.bwh.harvard.edu/pph2/
Sorting Intolerant From Tolerant (SIFT)	https://sift.bii.a-star.edu.sg/www/SIFT_aligned_seqs_submit.html
Alternative Splice Site Predictor (ASSP)	http://wangcomputing.com/assp/
Splice Site Prediction by Neural Network	https://www.fruitfly.org/seq_tools/splice.html
Benchling	https://www.benchling.com/

Tool	Access Link
ZiFiT Targeter	http://zifit.partners.org/ZiFiT/
CRISPR.MIT	http://crispr.mit.edu/
Primer3Plus	https://primer3plus.com/
SNPCheck3	https://genetools.org/SNPCheck/snpcheck.htm

2.2 Methods

2.2.1 Patient recruitment and ethical guidelines

Patients were recruited via the NHS Highly Specialised Service for Rare Mitochondrial Disorders and the NHS Highly Specialised Mitochondrial Diagnostic Service in Newcastle upon Tyne. Patient and control tissue samples were stored within the Newcastle Mitochondrial Research BioBank (REC reference: 16/NE/0267) and obtained from the Diagnostic laboratory via a tissue and DNA request form. In agreement with the Declaration of Helsinki, all individuals or their guardians provided written informed consent before undergoing clinical evaluation and diagnostic genetic testing.

Appropriate age-matched control skin fibroblast cell lines, control cardiac tissue samples and control skeletal muscle samples were obtained from the NHS Highly Specialised Service for Rare Mitochondrial Disorders.

Patient	Referring Centre	Year of Recruitment
GFM2 Patient 1	Royal Manchester Children's Hospital, UK	2015
GFM2 Patient 2	University Medical Centre, Hamburg-Eppendorf, Germany	2015
TSFM Patient 1	Sapienza University, Rome, Italy	2016
MRPL47 Patient 1	King Saud university , Riyadh, Saudi Arabia	2017
MRPL47 Patient 2	King Saud university , Riyadh, Saudi Arabia	2017
MRPL47 Patient 3	Helmhotz Centre, Munich, Germany	2018
MRPL65 Patient 1	American University of Beirut Medical Centre, Lebanon	2018
MRPL65 Patient 2	Children's Hospital of Michigan, USA	2019

Table 2.1 Details of Individual Patient Referral and Recruitment

2.2.2 Maintenance of human cell lines

Patient skin fibroblasts, age-matched control skin fibroblasts, HEK293 and U2OS cell lines were cultured in vented T75 or T25 flasks (unless otherwise stated) with Growth Media at 37°C in 5% CO_2. Cells were monitored regularly with a benchtop LED Microscope. When cell confluency reached ~80%, cells were trypsinised with 1x TrypLE Express, resuspended in an equal volume of growth media and pelleted in a universal tube via centrifugation at 1,200 rpm. The supernatant was subsequently disposed of, and the pellet was resuspended in 1 mL of growth media. The 1 mL cell suspension was then split evenly between 2-3 flasks for subculture.

HEK293 Flp-In™ TREx™ is a commercially available human embryonic kidney cell line (Life Technologies). These cells will be referred to as HEK293 cells throughout this text.

U2OS Flp-In™ TREx™ is an osteosarcoma derived cell line. Cells from this line will be referred to as U2OS cells throughout this text.

2.2.2.1 Harvesting of cells

To harvest cells for subsequent lysis, 1 mL of cell suspension, as described in **2.2.2**, was aliquoted into a single 1.5 mL eppendorf tube and centrifuged at 3,000 rpm in a benchtop centrifuge (Eppendorf 5418) or 3 minutes at room temperature. The resulting supernatant was disposed of and the pellet was snap frozen in liquid nitrogen then stored at -80°C.

2.2.2.2 Freezing and storage of cells

For long-term storage, cell pellets obtained following the centrifugation step in **2.2.2.1** were resuspended in 0.5 mL of FBS with 10% DMSO, then aliquoted into a cryostorage vial and placed in a CoolCell Cell Freezing Container. The CoolCell was placed in a -80°C freezer for a minimum of 24 hours before tubes were transferred into a liquid nitrogen storage vessel.

2.2.2.3 siRNA transfection

Cells were transfected with siRNA in 6 well plates for 6 days. A prewarmed mixture of 250 µL of Opti-MEM, 2.5 µL of 20 µM siRNA and 2 µL of Lipofectamine was prepared for each well and left at room temperature for 15 minutes. Cells were harvested and counted using a Cellometer Auto 1000 Bright Field Cell Counter, then diluted into 1.25 mL aliquots containing 80,000 (U2OS) or 100,000 (fibroblast) cells for seeding into each individual well. 6 well plates were placed at 37°C with 5% CO_2. After 3 days, a second mixture of 250 µL of Opti-MEM, 2.5 µL of 20 µM siRNA and 2 µL of Lipofectamine was prepared for each well and left at room temperature for 15 minutes. Each mixture was combined with 1.25 mL of pre-warmed Opti-MEM. All media was removed from growing cells, avoiding cell disturbance or detachment. A 1.544 mL Opti-MEM/siRNA/Lipofectamine mixture was added to each well for forward transfection. Cells were cultured for a further 3 days then harvested for analysis.

2.2.3 Protein manipulation

2.2.3.1 Preparation of human cell lysate

Cell pellets were resuspended in approximately 50 µl of cell lysis buffer per 10 mg of cell pellet. Samples were vortexed for 30 seconds and centrifuged at 1000*g* for 3 minutes to pellet nuclei and any unbroken cells. The supernatant was then transferred to a fresh 1.5 mL Eppendorf tube, snap frozen in liquid nitrogen and stored at -80°C.

2.2.3.2 Preparation of human muscle lysate

Approximately 10-20 mg of frozen (in liquid nitrogen) muscle was powdered in a pestle and mortar, suspended in 1 mL RIPA buffer and transferred to a 1.5 mL microcentrifuge tube. The muscle homogenate was then vortexed 5 times for 15 seconds with 15 second intervals on ice followed by a 45 minute incubation on ice. The homogenate then underwent two 5 second homogenisation steps using an Ultra-Turrax tissue homogeniser. The final muscle lysates were prepared by centrifugation at 14,000*g* for 10 minutes at 4 °C, retaining the supernatant before snap freezing in liquid nitrogen.

2.2.3.3 Bradford assay

Measurement of protein concentration was carried out using the Bradford assay. 1 and 2 µL of cell or tissue lysates alongside standard curve standard curve (0, 2, 5, 10, 15 and 20 µL) volumes of BSA were added to a final volume of 800 µL of dH_2O. 200 µL of protein assay dye reagent was added to both the lysate and BSA standard curve mixtures. The samples were vortexed for a few seconds, then incubated for 5 minutes at room temperature. 200 µL aliquots of each sample were added to a 96 well plate. The absorbance at 595nm of samples was measured on an ELx800 microplate reader. The optical density of samples relative to the BSA standard curve were used to calculate the average protein concentration in the test samples.

2.2.3.4 TCA precipitation

Precipitation of proteins was carried out through the addition of an equal volume of 20% trichloroacetic acid (TCA) followed by a 30 minute incubation on ice. The samples were then centrifuged at 15,700*g* for 15 minutes at 4°C. The resulting pellets underwent 3 washes with 200 µL of cold acetone. The final pellets were air dried then resuspended in 1x sample dissociation buffer.

2.2.3.5 SDS-PAGE

Casting and running of polyacrylamide gels was performed using the Bio-Rad Mini-Protean® Tetra Cell system, unless otherwise specified. Gels were cast with resolving phases of 12% polyacrylamide. Addition of isopropanol on top of the resolving matrix as it was setting allowed a flat and even gel surface to form. Isopropanol was removed after polymerisation had occurred and washed 3 times with water before the addition of a 3.75% stacking gel on top. Lysates used for SDS-PAGE were incubated with 5x sample dissociation buffer for 15-20 minutes at 37°C to denature and introduce a negative charge to proteins prior to loading. SDS-PAGE was performed in 1x running buffer at a stable 200V.

2.2.3.6 Western blotting and immunodetection

Proteins separated by SDS-PAGE were transferred onto a PVDF membrane using the Mini Trans-Blot module Bio-Rad system. PVDF membrane was submerged in 100% methanol for 15 seconds to activate and then left to equilibrate in transfer buffer for ~1 minute. The SDS-PAGE gel and activated membrane were then sandwiched between double layers of 3 mm Whatman filter papers and sponges within a cassette, prior to being placed into the transfer tank containing 1x transfer buffer. Transfer was performed at a stable 100V for 1 hour at 4°C.

Following transfer, the PVDF membrane was blocked with 5% milk/TBS-T for 1 hour at room temperature before incubation with primary antibodies. Dilution of primary antibodies in 5% milk/TBS-T was carried out, as described in **Table 2.2**, for overnight incubation at 4°C with membrane agitation. The following morning, 3 x 10 minute washes of the membrane in TBS-T were carried out, prior to incubation with the appropriate secondary antibody for 1 hour at room temperature with membrane agitation. The membrane was then subjected to 3 further 10 minute TBS-T washes, before the application of ECL prime reagent (GE healthcare) incubated for a minimum of 5 minutes. The resulting chemiluminescent signals were visualised using the ChemiDocTM MP system (Bio-Rad).

Antibody	**Dilution**	**Predicted Size (kDa)**	**Host Species**	**Clonality**
NDUFB8 (ab110242, Abcam)	1:1,000	17	Mouse	Monoclonal
SDHA (ab14715, Abcam)	1:1,000	73	Mouse	Monoclonal
CORE2 (ab14745, Abcam)	1:1,000	48	Mouse	Monoclonal
COXI (ab14705, Abcam)	1:1,000	40	Mouse	Monoclonal
COXII (ab110258, Abcam)	1:1,000	21	Mouse	Monoclonal

Antibody	Dilution	Predicted Size (kDa)	Host Species	Clonality
ATP5A (ab14748, Abcam)	1:2,000	53	Mouse	Monoclonal
ATP5B (ab14730, Abcam)	1:1,000	52	Mouse	Monoclonal
VDAC1 (ab14734, Abcam)	1:10,000	39	Mouse	Monoclonal
Beta Actin (CAB340Hu22, CloudClone)	1:10,000	42	Mouse	Monoclonal
MRPL47 (PA5-101365, Invitrogen)	1:1,000	29	Rabbit	Polyclonal
MRPL65 (MRPS30 - HPA021149 Sigma-Aldrich)	1:1,000	55	Rabbit	Polyclonal
MRPL45 (15682-1-AP, Proteintech)	1:1,000	35	Rabbit	Polyclonal
DAP3 (ab11928, Abcam)	1:1,000	43	Mouse	Monoclonal

Table 2.2 Primary antibodies used for immunoblotting.

Antibody	Dilution	Host Species	Clonality
Anti-Mouse Secondary (P0260, Dako)	1:2,000	Rabbit	Polyclonal
Anti-Rabbit Secondary (P0399, Dako)	1:3,000	Swine	Polyclonal

Table 2.3 Secondary antibodies used for immunoblotting.

2.2.3.7 Sucrose gradient

To generate a linear 10-30% sucrose gradient, 10% and 30% mixtures of sucrose in sucrose gradient buffer were made up in individual falcon tubes. A syringe was used to add 0.5 mL of 10% sucrose solution into the bottom of an ultracentrifuge tube. A second syringe was used to add 0.5 mL of 30% sucrose solution into the tube, below the first 10% sucrose layer. A gradient was generated using the 107 Gradient Master Ip (BioComp) set to 'TLS55, short sucrose 10%-30%, 55 seconds'. The gradient was then placed at 4°C for 60 minutes.

Once gradients had been prepared, 100 µL of cell lysate containing 700 µg of protein was carefully added to the top of the gradient. The tube was then centrifuged using the OptimaTM TLX Ultracentrifuge (rotor TLS 55) at 39,000 rpm (100,000*g*) for 2 hours and 15 minutes at 4°C. Following ultracentrifugation, eleven 100 µL fractions were collected, each taken from the top of the gradient. Fractions were stored at -20°C for subsequent SDS-PAGE and western blot analysis.

2.2.4 [^{35}S] Metabolic labelling

Using cells that had reached a confluency of 80%, growth media was replaced with DMEM free of methionine and cysteine and incubated at 37°C for 10 minutes. This was repeated twice, before the media was replaced with methionine/cysteine free DMEM supplemented with 10% dialysed FBS and 100 µg/mL emetine dihydrochloride (to inhibit cytosolic translation) and incubated at 37°C for a further 10 minutes. 20 µL/mL of [^{35}S]-methionine/cysteine mix (Perkin-Elmer Easy Tag Express protein labelling mix NEG-772, 73% L-met, 22% L-cys) was then added to each flask and cells were left to incubate at 37°C for 1 hour. Cells were washed in standard growth medium supplemented with methionine and then harvested in TrypLE Express, pelleted and re-suspended in PBS (plus protease inhibitor and 1mM PMSF). The protein concentration of each sample was determined using a standard Bradford assay **(2.2.3.3).** 20-50 µg of each radiolabelled sample was loaded onto a 15% SDS-PAGE gel and electrophoresed at 20mA for 2 hours. The gel was fixed overnight (3% glycerol, 10% glacial acetic acid, 20% methanol), stained with Coomassie brilliant blue for an indication of loading, and then dried under a vacuum at 70°C for 2 hours, prior to signal detection using Typhoon FLA9500 Phosphorimager and ImageJ software.

2.2.5 DNA manipulation

2.2.5.1 DNA extraction from human cells

DNA was extracted from growing 96 well cell culture plate clonal populations by first trypsinising cells with 200 µL of 1x TrypLE Express. 50 µl of trypsinised cell suspension was used to re-seed and continue cell culture, while the remaining 150 µl was transferred into a 96 well PCR plate and centrifuged at 12,000 rpm to pellet cells. The supernatant was removed and 50 µL of DNA isolation reagent solution was added to each well, disturbing the pellet. The plate was incubated at 56°C for 16 hours shaking at 300rpm. The plate was then incubated at 95°C for 10 minutes and end samples were stored at -20°C.

For extraction of DNA from T75 cell culture flasks for SNP analysis, a Qiagen DNeasy Blood & Tissue Kit (cat no. 69504) was used following the manufacturer's spin column quick-start protocol.

2.2.5.2 Primer design

Custom-designed forward and reverse primers were generated using Primer3Plus The generated primer sequences were checked for common single nucleotide polymorphisms (SNPs) using SNPCheck3.

Target	Forward	Reverse
GFM2 Exon 8	GCACACTCCCCTTCACACTT	TGGAATCATCAAGAAGCCACT
GFM2 Exon 9	GCGTTAAGGAGAATAAAGTGAGTTAAA	GAAAACTACAATGATGACAAGTCTTT
MRPL65 Exon 1	AGACTGGCTCAGATTCCGCT	GCATTCAGCGCGAAGGTCT
MRPL65 Exons 1-2 (A)	CCTCTGGGTCCGGAATCG	AATTTCTTCACCACGCACCC
MRPL65 Exons 1-2 (B)	GCGAGGTCATATCTTTGCCC	AATTTCTTCACCACGCACCC
MRPL65 Exons 1-4	CCTCTGGGTCCGGAATCG	GTGTGACCGTAACAGCAAGG
PX458 Vector	GACTATCATATGCTTACCGT	GGAAAGTCCCTATTGGCGTTA

Table 2.4 Custom primers used for PCR and Sanger sequencing.

2.2.5.3 DNA amplification by PCR

PCR amplification of target DNA was performed by adding 1.0 µl of sample DNA to 24.0µl of Go Taq PCR master mix and subjecting samples to the following PCR programme:

1 cycle	94ºC	4 minutes
30 cycles	94ºC	45 seconds
	62ºC	45 seconds
	72ºC	45 seconds
1 cycle	72 ºC	5 minutes
Hold	4ºC	∞

2.2.5.4 DNA gel electrophoresis

For gel electrophoresis of PCR products, either 1.0 g (1% gel) or 3.0 g (3% gel) of agarose was dissolved in 100 mL of 1x TAE buffer. 4 µL of SYBR Safe was added to the solution which was then poured into a casting cassette and comb. The gel was left to solidify and then submerged in 1x TAE buffer prior to loading. An appropriate ladder marker was loaded alongside DNA samples containing a 1:1 mixture of PCR products and loading dye. The agarose gel was typically electrophoresed at 80V for 30-50 minutes prior to visualisation on the ChemiDocTM MP system (Bio-Rad) using the UV transilluminator setting.

2.2.5.5 Sanger sequencing

PCR products were treated with ExoFAP for clean up prior to cycle sequencing. Duplicates of 5 µL of PCR product were added to 1.5 µL of ExoFAP. The samples were mixed and briefly spun down. The mixture was heated according to the following programme: 37°C for 15 minutes then 80°C for 15 minutes, finishing with a hold at 4°C. Sanger sequencing of amplified gene products was subsequently carried out in accordance with BigDye® Terminator v3.1 Cycle Sequencing Kit (cat no. 4337455) manufacturing protocol with the following program:

1 cycle	96 ºC	1 minutes
35 cycles	96 ºC	10 seconds
	50 ºC	5 seconds
	60 ºC	4 minutes
Hold	4ºC	∞

2.2.6 RNA manipulation

2.2.6.1 RNA extraction from human cells

RNA was extracted from fibroblasts grown to 80% confluency in a T75 flask, using the Qiagen RNeasy Mini Kit (cat no. 74104) , following the manufacturer's quick-start protocol.

2.2.6.2 Reverse transcription

For synthesis of cDNA, 1 µg of RNA, 1 µl of random hexamers (250 µg/mL) and nuclease free H_2O were combined up to a final volume of 15 µl. This mixture was incubated at 70ºC for 5 minutes and then placed immediately on ice for 1 minute. A second mixture containing 5 µl of M-MLV reverse transcriptase buffer, 2.5 µl of 20 mM dNTPs, 0.5 µl of RNasin, 1 µl of M-MLV reverse transcriptase and 1 µl of RNAse free H_2O was added and the total mixture incubated at 37ºC for 60 minutes. This sample was kept at -80ºC, for long-term storage.

2.2.6.3 Second strand synthesis

For second strand synthesis of reverse transcription generated cDNA, 1 µl of cDNA was added to a master mix containing 5 µl of 5x Promega reaction buffer, 2.5 µl of 2 mM dNTPs, 2 µl of 25 mM $MgCl_2$, 2.5 µl of 10 µM primer mix, and 0.2 µl of 5 U/µl Hotstart GoTaq G2 polymerase. The mixture was made up to 25 µl with nuclease free H_2O. The final mixture was subject to the following PCR cycling program:

1 cycle	95 ºC	2 minutes
30 cycles	95 ºC	1 minute
	62 ºC	1 minute
	72 ºC	1 minute
1 cycle	72 ºC	10 minutes

2.3 CRISPR/Cas9 gene editing

2.3.1 sgRNA oligo design

Three freely available web tools, Benchling, ZiFit Targeter and CRISPR.MIT were used for the design of four sgRNA oligos **(**Error! Reference source not found.**)**. These online resources identified suitable 20 nucleotide regions located directly adjacent to PAM sites and ranked the guide sequences based on predictions of high target specificity with low off-target binding.

	Forward	**Reverse**
MRPL65 sgRNA 1	CACCGAGGCTTTCATTGCACACCG	AAACCGGTGTGCAATGAAAGCCTC
MRPL65 sgRNA 2	AAACTCGCGCGGTACCCGCCGATTC	CACCGAATCGGCGGGTACCGCGCGA
MRPL65 sgRNA 3	AAACTTGCTACGCGGTCCGAGGCTC	CACCGAGCCTCGGACCGCGTAGCAA
MRPL65 sgRNA 4	AAACGCCAAGACGTCGCGGCGACC	CACCGGTCGCCGCGACGTCTTGGC

Table 2.5 Custom sgRNA Oligos for use in CRISPR/Cas9 Studies

2.3.2 Plasmid vector manipulation

2.3.2.1 sgRNA oligo annealing

For the annealing of short guide RNA oligos, 1 µl of forward oligo and 1 µl of reverse oligo (both at 100 µM) were mixed with 1 µl of 10x PNK buffer, 1 µl of ATP, 1 µl of T4 PNK enzyme and made up to 10 µl with ddH_2O. This mixture was treated to the following heating program: 37°C for 30 minutes then 95°C for 5 minutes then placed in a boiling water bath and allowed to cool for 45 minutes to room temperature. The final sample is stored at -20°C.

2.3.2.2 Backbone cutting

In order to cut the Px458 vector at the multiple cloning site, 1 µl of *BbsI* restriction enzyme and 2 µl of 10x Buffer 2.1 was added to 1 µg of PX458 plasmid, then the total volume was made up to 20 µl with ddH_2O. This mixture was incubated for 1 hour at 37 °C.

The total 20 µl mixture was combined with 3.5 µl of 1M Tris-HCl pH 9.0, 1 µl of 10% SDS and 1 µl of alkaline phosphatase. This mixture was incubated at 37 °C for 30 minutes followed by a 50°C incubation for a further 30 minutes. 1 µl of 0.5 M EDTA was then added and the treated plasmid was gel purified.

2.3.2.3 Ligation

For the ligation of the plasmid vector with sgRNA molecules, 50 ng of *BbsI* digested PX458 plasmid (from section **Error! Reference source not found.**) was added to a ligation mixture containing 2 µl of annealed oligo duplex (from section Error! Reference source not found. and diluted 1:200 in ddH_2O), 5 µl of 2x T7 Ligase

Buffer, 1 µl of T7 Ligase and made up with ddH_2O to a total volume of 11 µl. This reaction was incubated for 30 minutes at room temperature.

2.3.2.4 Restriction endonuclease DNA digestion

Double digests of PX458 were carried out using 500 ng of plasmid DNA obtained from bacterial minipreps **(**Error! Reference source not found.**)**, added to a mixture containing 0.5 µl of *BbsI* restriction enzyme, 0.5 µl of *EcoRI* restriction enzyme, 2 µl of 10x Buffer 2.1 and made up to 10 µl with ddH_2O. This reaction was incubated at 37 °C for 2 hours and then run on a 1% agarose gel to check digestion product sizes.

2.3.3 Plasmid transfection

For transfection of cells with a pSpCas9(BB)-2A-GFP (PX458) plasmid, an Amaxa® Cell Line Nucleofector® Kit V (cat no. VVCA-2003) was used. U2OS cells were grown an 80% confluency, trypsinised, counted and diluted into 100µL aliquots of Cell Line Nucleofector® solution containing 1 million cells. 2 µg plasmid DNA or 2 µg pmaxGFP® Vector (control) was added to the solution and cells were transferred into a kit-provided cuvette. Cuvettes were inserted into the Nucleofector® device and subject to program X-001. 500 µL of growth media was then added to the cuvette and the entire contents transferred into a 6 well plate and allowed to recover for 24-48 hours.

2.3.4 Single cell sorting

Following recovery of post-transfection cells, each population was at ~2-3 million cells. Cell populations were trypsinised and resuspended in 500-600µl of PBS (+ 1-2% FBS) in individual FACS tubes to the Core Flow Cytometry Facility. Cells were strained through 40µm filters to prevent clumping and were then stained with DAPI (0.1µg/mL-

10µg/mL) before sorting with a MoFlo Astrios EQ Cell Sorter. The Astrios machine sorted cells into single cell wells of a 96 well plate based on positive DAPI signal and GFP signal indicating live cells with successful nucleofection. Two 96 well plates were sorted for each of the sgRNA plasmids alongside single plates of pmaxGFP® Vector cell and no-cell controls. The single cells were then left to proliferate into clonal populations in high glucose growth media.

2.3.5 Bacterial culture

2.3.5.1 Propagation and storage

Subcloning efficiency DH5α chemically competent cells were used in cloning experiments. Competent cells were grown at 37°C in plates of 4% LB broth with agar that had been autoclaved prior to pouring.

Transformed strains were stored in 18% glycerol 4% LB stocks and then kept at -80°C for future use. For defrosting and propagation a small amount of glycerol stock was scraped on a 4% LB broth agar plate and left to grow at 37°C overnight.

2.3.5.2 Transformation

Heat shock was used for the transformation of DH5α cells. 4 µl of ligation reaction from section **Error! Reference source not found.** was added to 40 µl of subcloning efficiency DH5α cells. This mixture was left on ice for 30 minutes and then treated to heat shock at 42°C for 45 seconds. Following heat shock, the mixture was placed back on ice for 2 minutes. 950 µl of pre-warmed SOC media was added prior to incubation for 1 hour at 37°C in a shaking incubator. The mixture was centrifuged at 15,000*g* for one minute and the pellet was resuspended in 200 µl of SOC media. This suspension was spread out onto LB agar plates supplemented with 100 µg/mL ampicillin and incubated at 37°C overnight.

2.3.5.3 Colony screening

Individual transformed clones were picked and spread onto fresh LB+ampicillin plates then incubated overnight at 37°C. Half of each colony was resuspended in 40 µl of 10% Triton-X and frozen at -80°C for 30 minutes. The suspension was then defrosted

and centrifuged at 15,000*g* for 5 minutes at 4°C. The supernatant was kept and used to set up PCR using sgRNA forward primer with PX458 plasmid reverse primer. The presence of an insert was checked by electrophoresis of PCR product on 1% agarose gel.

2.3.5.4 Isolation of plasmid DNA

Plasmid positive cells were propagated on LB+Ampicillin agar plates overnight at 37°C. Single colonies were picked and propagated overnight in 5-7 mL of 2.5% LB broth supplemented with 100 µg/ml ampicillin at 37°C. Cells were pelleted through centrifugation for 2 minutes at 16,000*g* and plasmid was isolated using the Monarch® Plasmid Miniprep Kit (cat no. T1010S) following manufacturer's guidelines.

Chapter 3 : Defects of mitochondrial translation factors in mitochondrial disease

3.1 Introduction

The complex process of mitochondrial translation requires a multitude of different proteins, along with 22 mt-tRNAs and two ribosomal RNAs, that must all function in concert. As discussed in **1.8**, disorders of mitochondrial translation can result from mutations within a wide range of different genes in both the mitochondrial and nuclear genomes. A growing number of genes encoding mitoribosomal proteins are implicated in early-onset mitochondrial disease presentations (Pulman *et al.*, 2019). Mitochondrial translation factors, those proteins directly involved in the initiation, elongation and termination stages of mitochondrial translation, are another well documented group of genes with the potential to cause disorders of mitochondrial translation when mutated. Genetic variants affecting mitochondrial translation factors characteristically result in combined OXPHOS deficiencies due mtDNA origin of some subunits of OXPHOS complexes I, III, IV and V, while the spectrum of resulting clinical phenotypes is broad (Pearce, Nezich and Spinazzola, 2013). In 2006 the elongation factor mtEF-G1, encoded by the *GFM1* gene, was the first mitochondrial translation factor to be implicated in disease (Antonicka *et al.*, 2006). In the years following, in part due to the application of next generation sequencing techniques within the rare disease field, novel pathogenic variants have been described in a number of genes encoding mitochondrial translation factors including the mitoribosome recycling factor *GFM2,* elongation factors *TSFM* and *TUFM* and the termination factor *C12orf65 (Fukumura et al., 2015; Glasgow et al., 2017; Shamseldin et al., 2012; Valente et al., 2009; Shimazaki et al., 2012; Antonicka et al., 2010)*. This chapter will focus on the investigation of novel variants in genes encoding two of these mitochondrial translation factors, *GFM2* and *TSFM.*

3.1.1 mtEF-G2: a mitochondrial translation factor

The human genes *GFM1* and *GFM2* encode the proteins mtEF-G1 and mtEF-G2 respectively. These genes are homologs of the highly conserved bacterial translation elongation factor G (EF-G) (Hammarsund *et al.*, 2001). In prokaryotes, EF-G catalyses the translocation tRNAs sitting in the A- and P-sites of the ribosome into the P and E sites, facilitating translation elongation (Wintermeyer and Rodnina, 2000; Rodnina *et al.*, 2000). Bacterial EF-G also works alongside ribosome recycling factor (RRF) to play a crucial role in the dissociation of the post-termination ribosome complex (PoTC) and the recycling of the ribosome at the end of each translation event (Hirokawa *et al.*, 2006). The EF-G equivalent in eukaryotic cytosolic translation is EF-2 (Rapp *et al.*, 1989), while the mitochondrial translation system possesses both mtEF-G1 and mtEF-G2 as functional counterparts of prokaryotic EF-G (Hammarsund *et al.*, 2001).

Prokaryotic EF-G and the eukaryotic cytosolic protein EF-2 possess both elongation and ribosome recycling properties. However, it has been demonstrated that these roles are split between the two mitochondrial translation homologs mtEF-G1 and mtEF-G2. Mitochondrial mtEF-G1 requires GTP for its translocation function during the elongation stage of translation, whereas mtEF-G2 is not active during translation elongation. Instead, mtEF-G2 interacts with RRF to enable mitoribosome recycling (Tsuboi *et al.*, 2009). In light of these findings, it was proposed that the translation factor be renamed RRF2, reflective of its ribosome recycling activity (Christian, Haque and Spremulli, 2009). Unlike bacterial EF-G, mtEF-G2 does not require GTP hydrolysis in order to disassemble the monosome. Instead, GTP hydrolysis is required for the release of mtEF-G2 itself from the newly disassembled LSU (Tsuboi *et al.*, 2009).

3.1.2 *GFM2* in mitochondrial disease

Prior to the work presented here, two sets of sibling pairs with pathogenic variants in the *GFM2* gene had been identified through WES and reported in the literature. The

clinical presentations of these patients included microcephaly, simplified brain gyral pattern with insulin dependent diabetes in the first family and Leigh syndrome complicated by arthrogryposis multiplex congenita in the second (Fukumura *et al.*, 2015; Dixon-Salazar *et al.*, 2012). The functional characterisation of the molecular mechanisms underlying disease in these patients was limited to the demonstration of nonsense mediated mRNA decay of *GFM2* transcripts the first patients identified (Fukumura *et al.*, 2015).

3.1.3 mtEF-Ts: a mitochondrial translation elongation factor

The mitochondrial elongation factor mtEF-Ts, encoded by the nuclear *TSFM* gene, acts as a guanine nucleotide exchange factor for EF-Tu promoting the formation of EF-Tu/GTP from EF-Tu/GDP. This exchange allows EF-Tu/GTP to form a ternary complex with aminoacylated mt-tRNAs, for their transport to the mitoribosomal A-site. In the A-site, a correct codon-anticodon interaction results in the hydrolysis of GTP and the release of EF-Tu/GDP to begin a new cycle (Chiron, Suleau and Bonnefoy, 2005).

3.1.4 *TSFM* in mitochondrial disease

Pathogenic variants in the *TSFM* gene were first identified in 2012 in two unrelated paediatric patients with the same homozygous c.997C>T, p.(Arg333Trp) mutation. Despite harbouring an identical *TSFM* variant, each patient presented with a distinct clinical phenotype. Smeitink *et al.* reported that their first patient experienced fatal mitochondrial encephalopathy, alongside muscle weakness, hypotonia, rhabdomyolysis and epilepsy, while a second patient presented with hypertrophic cardiomyopathy with general hypotonia without any further neurological involvement (Smeitink *et al.*, 2006b).

A further thirteen patients with disease-causing *TSFM* variants have been reported in the years following these two initial cases. There is significant heterogeneity in the

clinical presentation of *TSFM* related disease, though patients can be sub-categorised into two clear groups, based on age of onset and disease severity. Disease onset in the first seven cases to be reported was extremely early, with presentation of severe symptoms in the congenital or neonatal period. Despite each patient displaying an individual combination of symptoms, some of the more common clinical features included hypotonia, respiratory failure and hypertrophic cardiomyopathy. All seven of these patients died within their first weeks/months of life (Smits *et al.*, 2011a; Calvo *et al.*, 2012; Shamseldin *et al.*, 2012; Vedrenne *et al.*, 2012; Smeitink *et al.*, 2006b).

The following six patients to be reported with pathogenic variants in the *TSFM* gene were adults surviving into their late teens, twenties and thirties. These patients presented with milder phenotypes in infancy or childhood. Similar to the early onset cluster of patients, the clinical features of each adult patient vary significantly, though optic atrophy, ataxia and hypertrophic cardiomyopathy are common to most cases (Ahola *et al.*, 2014; Emperador *et al.*, 2017; Perli *et al.*, 2019; Traschutz *et al.*, 2019).

Most recently, Scala *et al*. identified a five-year-old boy with encephalocardiomyopathy, sensorineural hearing loss and spontaneously regressing lesions on brain MRI. The hypertrophic cardiomyopathy symptoms in this patient remain relatively stable with little progression or worsening over time (Scala *et al.*, 2019).

The data presented here describes the clinical and biochemical profiles of two paediatric patients with novel variants in the *GFM2* gene, and one adult patient with novel compound heterozygous variants in the *TSFM* gene, in order to assign pathogenicity and broaden the clinical manifestations associated with variants in each gene. As discussed in **1.9**, confirming pathogenicity in such cases is of vast diagnostic value to patients and their families, while also providing insight into the molecular mechanisms underlying these extremely rare disorders.

3.2 Patient reports

3.2.1 *GFM2* Patient 1

Patient 1, a 13-year-old male, is the first child of healthy non-consanguineous parents and has a healthy younger brother. Pregnancy was complicated by intrauterine growth restriction and he was born at term by normal vaginal delivery weighing 2.0 kg. He had asymptomatic hypoglycaemia in the neonatal period and mild jaundice and was tube fed initially. He subsequently had a urinary tract infection and required orchidopexy for an undescended right testis.

Developmental delay was first noted at 2.5 years in relation to language and communication skills; he had acquired his first words at 12–18 months, but did not put words together until aged 3 years. From 5 years onwards, he has become increasingly dysarthric. He has used a knife and fork from 3 years of age but has never been able to write. He started walking at 14 months and could run at 4 years, but he subsequently developed a dystonic posture of his right foot and spasticity in both legs, leading to toe walking and loss of ambulation at 8 years; he currently mobilises by crawling. He has been continent since 2 years of age. He has a normal head circumference, normal vision and hearing and no involuntary movements or seizures and continues to make slow academic progress.

Cranial MRI showed symmetrical bilateral high signal on T2-weighted images in the caudate, putamen and cerebellar dentate nucleus. There were also abnormalities in the corpus callosum and the subcortical white matter of the cerebral and, particularly, the cerebellar hemispheres, with further abnormal areas in the deep white matter **(Figure 3.1)**. CSF lactate was elevated on two occasions at 3.2 and 3.4 mmol/L (normal range, 0.7–2.1 mmol/L). Sequencing of the mitochondrial genome and the *NFU1* gene both failed to detect pathogenic variants. This patient was referred by Dr.Andrew Morris, Alder Hey Children's Hospital NHS Foundation Trust.

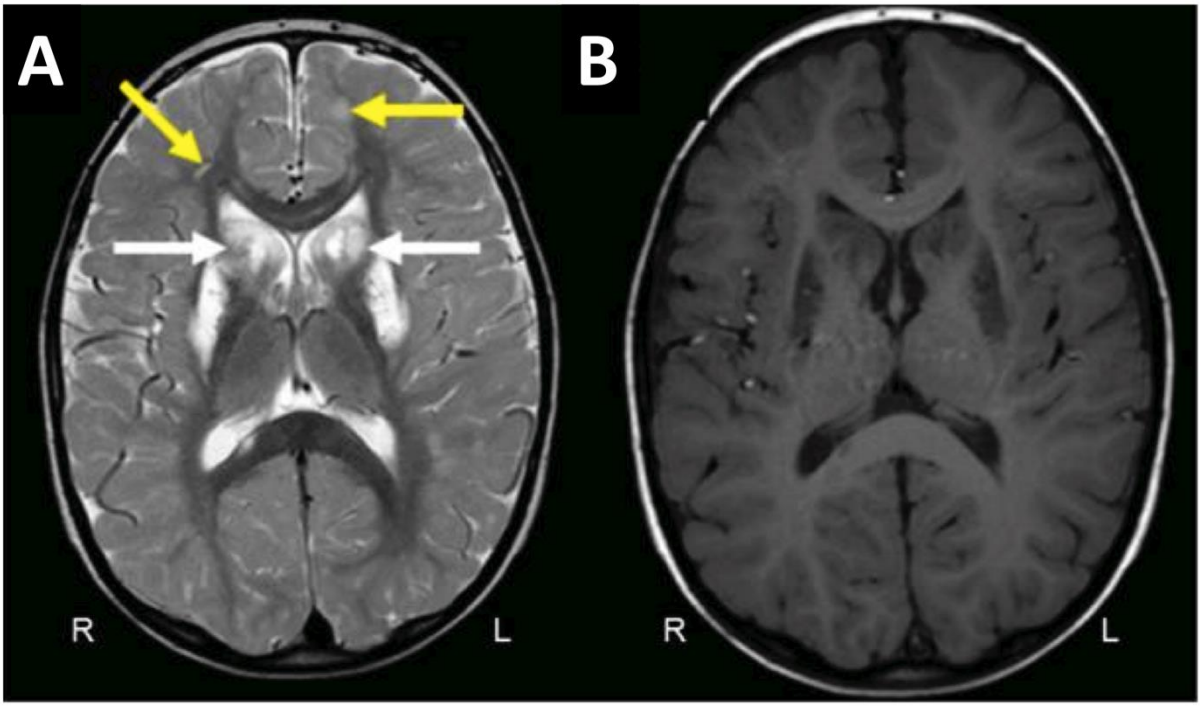

Figure 3.1 MRI of Patient 1. MRI demonstrates bilateral T2 hyperintensities involving supratentorial white matter (yellow arrows), head of caudate nucleus (white arrows), putamen and genu and splenium of the corpus callosum (A) characterised by low T1 signal suggesting irreversible tissue damage (B). Right (R) and left (L) are indicated.

3.2.2 *GFM2* Patient 2

Patient 2, a 9-year-old female, is the second child of consanguineous parents originating from Syria. Born following an uneventful pregnancy at full term, development was unremarkable in the first 2 years of life. At the age of 2 years and 2 months, involuntary movements of the left hand were reported and within a few months, these had extended to involve all four limbs. Muscle strength and mass deteriorated and she lost the ability to walk at 4 years, to sit at 5 years and subsequently lost the ability to speak. At the age of 6 years, she presented with her first seizure and has subsequently developed a severe epilepsy disorder. Clinical assessment reveals severe global developmental delay, myopathic facies with an open mouth appearance and drooling, severe axial hypotonia with hypertonic limbs and dystonic involuntary movements. Communication was restricted to phonetic reading. This Patient was referred by Dr.Maja Hempel, University Medical Center Hamburg-Eppendorf.

Lactate was repeatedly elevated in both serum, to 4.1 mmol/L, and CSF, to 3.1 mmol/L, (normal <2.5mmol/L). Cranial MRI showed diffuse hyperintensities on T2-weighted imaging of the periventricular and central white matter with associated volume loss and atrophy of corpus callosum as well as T2 hyperintense defects of bilateral putamen and head of caudate nucleus **(Figure 3.2)**. EEG revealed multifocal seizure activity.

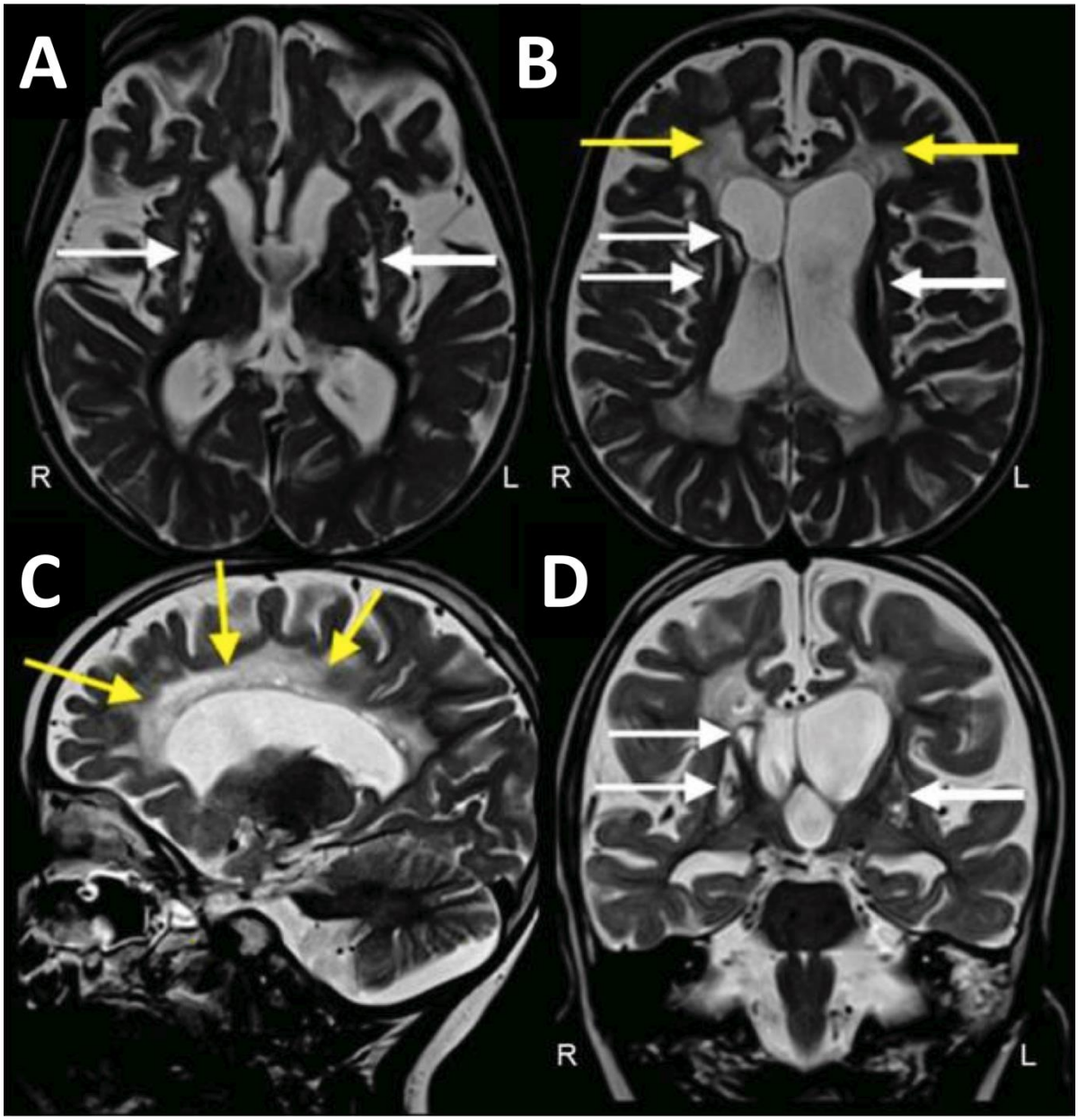

Figure 3.2 MRI of Patient 2. MRI demonstrates extensive T2 hyperintensities associated with volume loss involving bilateral periventricular and central white matter (**A**, **B**, yellow arrows) and defects involving both putamina and the head of caudate nucleus on the right (**A**, **B**, **D**, white arrows). Right (R) and left (L) are indicated.

3.2.3 *TSFM* Patient

This 36-year-old female patient was born at term to non-consanguineous healthy parents. Early psychomotor development was normal, however gross-and fine-motor clumsiness with frequent falls were observed in infancy. This was followed by mild muscle weakness and reduced limb coordination. Genetic screening for spinocerebellar and Friedreich's ataxias was negative. These symptoms remained stable until the patient reached the age of 27 when she experienced worsening fatigue and dyspnoea and was referred to the Cardiomyopathies Unit of San Camillo-Forlanini Hospital, Rome. Echocardiography revealed a mildly dilated left ventricle (LV), LV end-diastolic diameter (LVDD) of 51 mm and ejection fraction (EF) of 21%, consistent with dilated cardiomyopathy. Serum lactate levels were slightly increased (3.70 mmol/L; control <2.2 mmol/L). LV function progressively decreased, despite therapeutic intervention. At the age of 33 years, echocardiography showed a hypokinetic and dilated LV, LVDD of 54 mm, ventricular septum thickness of 10 mm and EF of 15%. The patient underwent cardiac transplant a few months later. This patient was referred by Dr.Giulia d'Amati and Dr.Carla Giordano, Department of Molecular Medicine, Sapienza University.

3.3 Results: *GFM2*

3.3.1 Histopathological and biochemical studies

Due to the presentation of muscle related clinical features in Patient 1, a skeletal muscle biopsy was obtained for histopathological and biochemical investigations. No marked structural abnormalities were identified upon H&E staining of skeletal muscle from Patient 1 **(Figure 3.3A)**. Oxidative enzyme histochemistry showed intense SDH activity and a generalised decrease in cytochrome *c* oxidase activity throughout the muscle section **(Figure 3.3B-C)**. Sequential COX-SDH histochemistry confirmed a widespread COX deficiency in the presence of normal SDH activity **(Figure 3.3D)**.

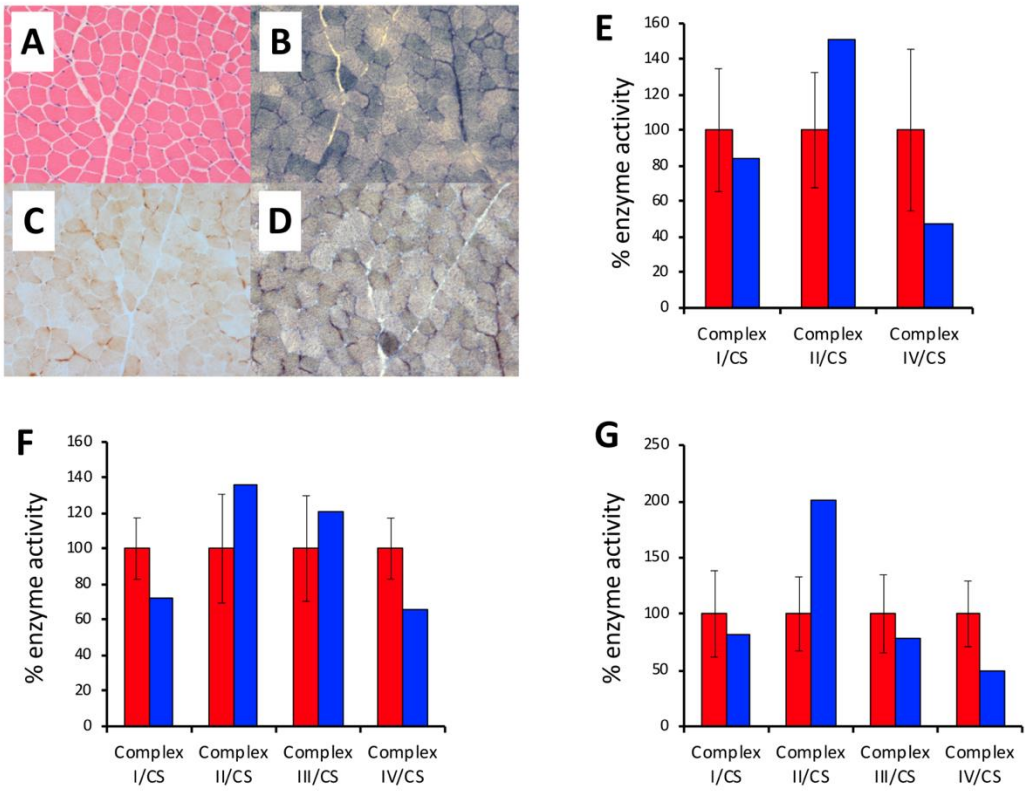

Figure 3.3 Histochemical investigation of patient skeletal muscle and biochemical analysis of skeletal muscle and fibroblasts. (A) Haematoxylin and eosin stain. Succinate dehydrogenase (SDH) (B), cytochrome c oxidase (COX) (C) and COX-SDH histochemistry (D). Respiratory chain enzyme activity measurements in the skeletal muscle of Patient 1 (E), the fibroblasts of Patient 1 (F) and the fibroblasts of Patient 2 (G) normalised to citrate synthase. (red: controls, blue: patient). Control datasets for skeletal muscle and fibroblast biochemistry are based on n=25 normal samples, normalised and set to 100% with error bars to represent standard deviation. These

data were generated by Langping He and Gavin Falkous. Figure adopted and amended from (Glasgow *et al.*, 2017).

The assessment of respiratory chain enzyme activities in the muscle of Patient 1 revealed impaired complex IV activity, while the activities of complexes I and II were both within the limits of the standard deviation of control values **(Figure 3.3E)**. Fibroblast cells from Patient 1 appear to express a mild combined OXPHOS defect affecting complexes I and IV, with residual enzyme activities approximately 60% of the average of control fibroblasts **(Figure 3.3F)**. Complex activity measurements in the fibroblasts of Patient 2 revealed a severe complex IV deficiency, while activity of complex II is two-fold higher than controls. Complex I and III activities are within the control range **(Figure 3.3G)**.

3.3.2 Variant identification, confirmation and segregation studies

WES of Patient 1 identified compound heterozygous variants in the *GFM2* gene, a c.569G>A single nucleotide substitution in exon 8 resulting in an arginine to glutamine missense change at residue 190 (p.(Arg190Gln)) and a c.636delA single nucleotide deletion in exon 9 producing a frameshift mutation and premature termination codon (p.(Glu213Argfs*3)). WES of Patient 2 revealed a homozygous c.275A>C variant in exon 5 of *GFM2*, predicted to cause a tyrosine to serine missense change at residue 92 (p.(Tyr92Ser)). Sanger sequencing of the probands plus their respective parents confirmed the segregation of the bi-allelic *GFM2* variants with disease in both families **(Figure 3.4)**.

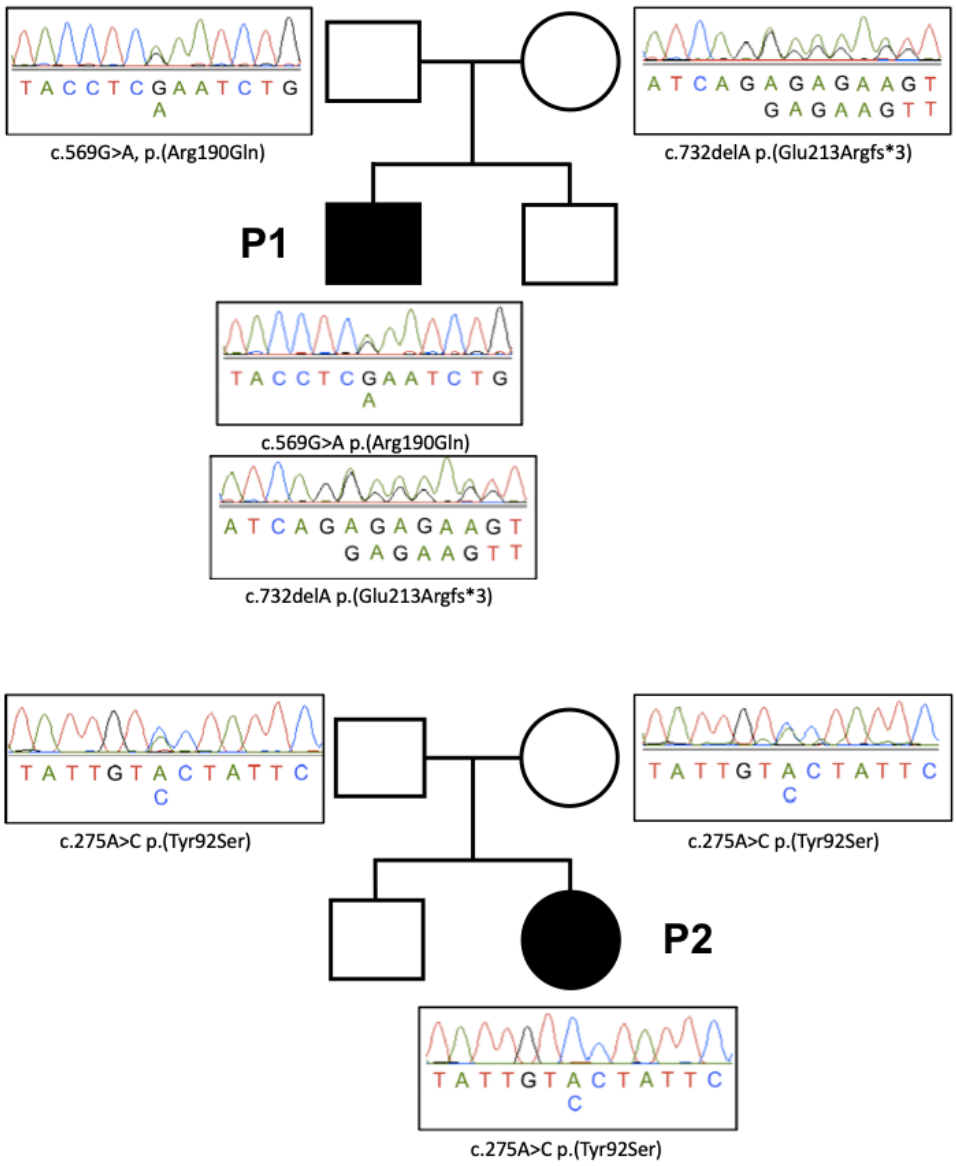

Figure 3.4 Segregation of recessive GFM2 variants. Familial pedigrees and Sanger sequence data demonstrating recessive inheritance of GFM2 variants in Patients 1 (top) and 2 (bottom) from heterozygous parents. Figure adopted and amended from (Glasgow *et al.*, 2017).

3.3.3 Missense residue conservation and *in silico* pathogenicity predictions

Conservation and *in silico* pathogenicity predications were carried out in order to assess the possible structural and functional importance of amino acids affected by missense mutations. Multiple sequence alignment and assessment of the evolutionary conservation of each missense variant demonstrates that the Arg190 residue is conserved in mammals, and amphibians, but is less so in more distant species such

as *Danio rerio* and *Caenorhabditis elegans*. The region flanking the p.(Arg190Gln) change is similarly conserved throughout most higher order species **(Figure 3.5)**. The residue affected by the homozygous p.(Tyr92Ser) variant in Patient 2 is conserved from humans through to *Caenorhabditis elegans* with only *Drosophila melanogaster* varying from the conserved tyrosine to phenylalanine. The surrounding region is extremely well conserved **(Figure 3.5)**.

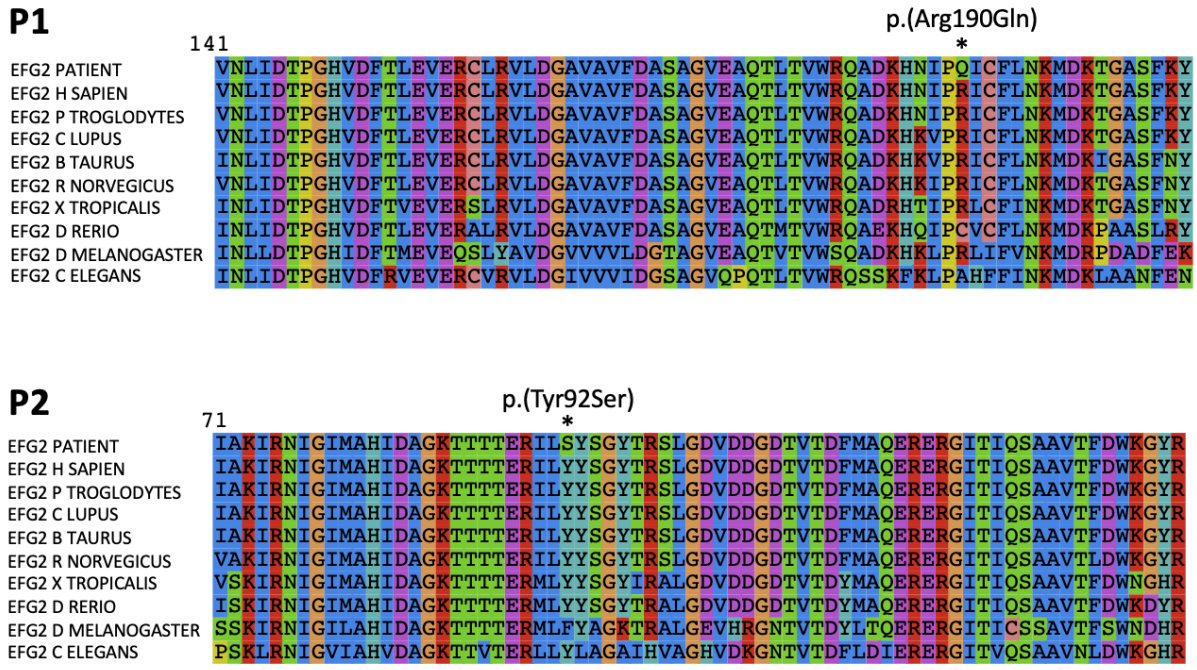

Figure 3.5 Multiple sequence alignment of mtEF-G2 regions surrounding each missense variant. Mutant and Wildtype human mtEF-G2 sequence aligned alongside orthologs from 8 further species to visualise evolutionary conservation of each affected residue and surrounding sequence.

All three *GFM2* variants are extremely rare; the c.564A>G, p.(Arg190Gln) allele, harboured by Patient 1, is present in 5/276,072 alleles on gnomAD (MAF = 0.00002) but never in a homozygous state, while the other c.636delA, p.(Glu213Argfs*3) variant found in Patient 1 and the c.275A>C, p.(Tyr92Ser) variant present in Patient 2 are unreported in the database (https://gnomad.broadinstitute.org/).

In silico pathogenicity prediction tools generated consistent results for the p.(Tyr92Ser) missense variant belonging to Patient 2, this change was classified as

likely to affect protein function according to all *in silico* prediction tools used. SIFT and aGVFD classified the p.(Arg190Gln) change in Patient 1 as unlikely to interfere with protein function while Mutation Taster, PolyPhen and CADD scores were supportive of a deleterious effect **(Table 3.1)**. CADD scores of 32 for c.569G>A and 27.2 for c.275A>C, predict that these variants are in the top 0.01 and 0.1% of deleterious single nucleotide variants of the reference genome, respectively.

	Mutation Taster	Align GVGD	SIFT	Polyphen	CADD
R190Q	'disease causing'	Class C0	'tolerated'	'probably damaging'	32
Y92S	'disease causing'	Class C55	'affect protein function'	'probably damaging'	27.2

Table 3.1 Assessment of missense *GFM2* variants using a panel of *in silico* pathogenicity prediction tools. Output of each *in silico* pathogenicity prediction tool when assessing missense changes p.(Arg190Gln) (Patient 1 – first row)) and p.(Tyr92Ser) (Patient 2 – second row). Deleterious predictions are shaded in red, tolerated predictions are shaded in green. Align GVGD uses Grantham scores of evolutionary distance alongside sequence conservation to categorise missense changes into one of six classes. Class C0 = class containing variants least likely to interfere with protein function, Class C55 = class containing variants second most likely to interfere with protein function. Combined annotation dependent depletion (CADD) scores are calculated using an array of different tools assessing variants and simulated mutations. A CADD score of 20 classifies a variant as within the top 1% of most deleterious SNVs in the genome. A CADD score of 30 classifies a variant as within the top 0.1% of most deleterious SNVs in the genome. All web-based tools are freely available - see Materials and Methods section **2.1.6**.

3.3.4 Western blot analysis of patient fibroblasts and skeletal muscle

In order to assess the impact of the *GFM2* variants on OXPHOS complex stability, investigation into the steady-state levels of individual OXPHOS complex subunits in fibroblasts were carried out, revealing patient-specific differences. There was an extremely mild decease in the abundance of OXPHOS proteins in the fibroblasts of Patient 1, primarily affecting subunits of complexes I (NDUFB8) and IV (COXI and COXII) **(Figure 3.6A)**, while the fibroblasts of Patient 2 exhibited a clear decrease in

the steady-state levels of subunits of complex I (NDUFB8), complex III (CYTB and CORE2) and complex IV (COXI and COXII) **(Figure 3.6A)**. Skeletal muscle sample from Patient 1 was obtained, however no tissue samples from Patient 2 were available. Skeletal muscle lysates from Patient 1 exhibited a marked decrease in steady-state levels of complex IV components COXI and COXII, with subunits of each of the other OXPHOS complexes relatively unchanged compared to controls **(Figure 3.6B)**.

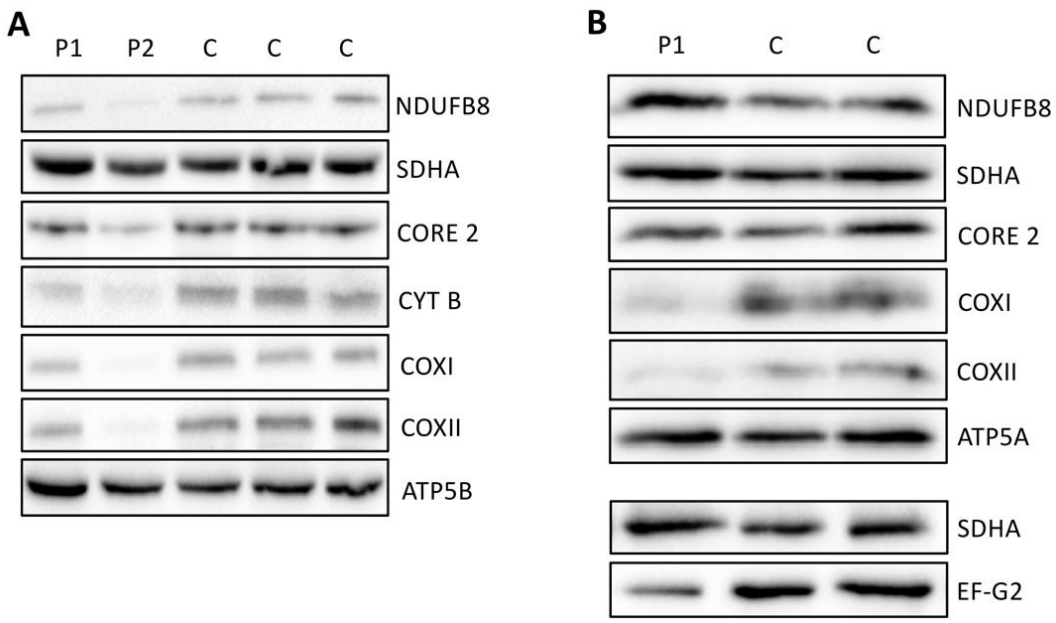

Figure 3.6 Western blot analysis in fibroblasts and skeletal muscle. Whole cell lysates from fibroblasts of Patient 1 and Patient 2 subjected to SDS-PAGE and western blotting using with antibodies against NDUFB8, SDHA (loading control), CORE2, CYT B, COXI, COXII and ATP5B **(A)**. Skeletal muscle lysate from Patient 1 subjected to SDS-PAGE and western blotting using antibodies against NDUFB8, SDHA (loading, CORE2, COXI, COXII, ATP5A and SDHA (loading) and mtEF-G2 **(B)**. Figure adopted and amended from (Glasgow *et al.*, 2017). Data shown is representative of three independent repeats.

Attempts at detecting mtEF-G2 signal in fibroblasts using a commercial antibody repeatedly resulted in the presence of non-specific bands. Consequently, investigation into the steady-state level of mtEF-G2 was only possible in the skeletal muscle of Patient 1, which produced clear signal. The abundance of mtEF-G2 protein in patient skeletal muscle lysate was decreased to approximately 50% of the controls (measured using an ImageLab densitometry tool) **(Figure 3.6B)**.

3.3.5 [^{35}S] translation assay in growing fibroblasts

Due to the defects on OXPHOS subunits identified in patient fibroblasts **(Figure 3.6A)**, and the role of mtEF-G2 as a mitoribosomal recycling factor, it was important to assess mitochondrial translation in patient cell lines. A [^{35}S] metabolic labelling assay was performed in order to assess whether these *GFM2* variants cause impairment of *de novo* mitochondrial protein synthesis in growing fibroblast cells as a potential pathomechanism responsible for the observed OXPHOS defects. Cytosolic translation was inhibited through addition of 100 µg/mL emetine to culture media, in order to obtain signal from only protein synthesis occurring within mitochondria. Cells were incubated for one hour with radiolabelled methionine/cysteine, harvested, and separated via SDS-PAGE. The resulting bands correspond to the mtDNA encoded proteins that were synthesised within the 1 hour pulse incubation. In the case of both patients there does not appear to be any effect on the incorporation of radiolabelled methionine/cysteine into newly synthesised mtDNA encoded proteins, except in the case of ND1, where there is no corresponding band in either patient **(Figure 3.7)**. While it appears that signal in the lane containing labelled sample from Patient 2 is generally lower, this is a result of lower loading of total sample as can be seen on the Coomassie stain panel.

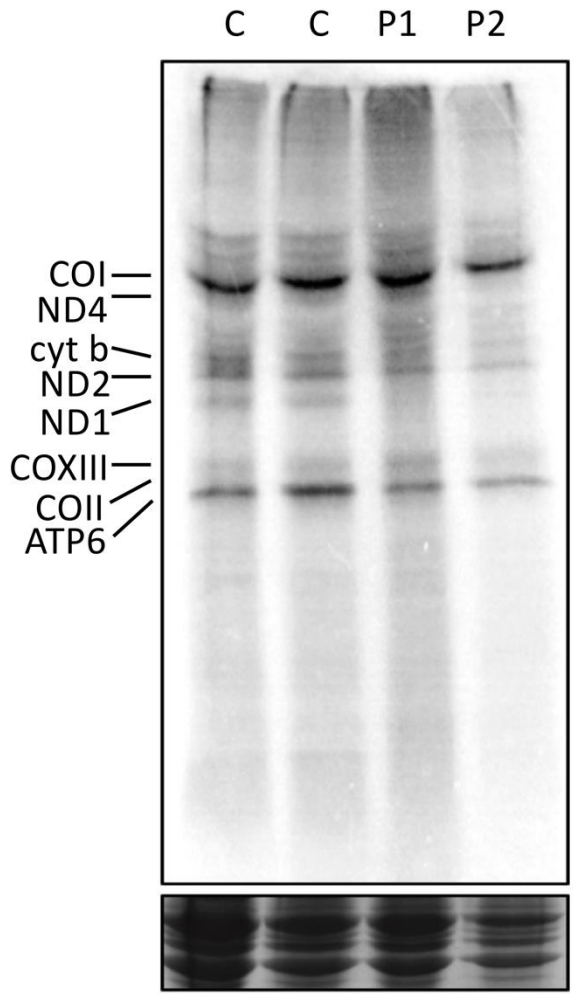

Figure 3.7 [35S] methionine/cysteine incorporation in growing fibroblasts as a measure of *de novo* mitochondrial protein synthesis. Signal detected from fixed and dehydrated SDS-PAGE gel using Typhoon Phosphorimager. Bands are visible for radiolabelled COXI, ND4, cyt b. ND2, ND1, COXIII, COXII and ATP6. Loading is presented through a Coomassie stain on the bottom panel. Figure adopted and amended from (Glasgow *et al.*, 2017).

3.4 *TSFM* Results

3.4.1 Histological, histochemical and biochemical studies

Masson trichrome staining of cardiac tissue from both the right and left ventricles revealed multiple foci of myocardial fibro-adipose replacement **(Figure 3.8A-B)**. Myocytes lost from the RV were mostly replaced with adipose tissue **(Figure 3.8A)**, while myocardial replacement in the LV was mostly fibrous (**Figure 3.6B**). Sequential COX-SDH histochemistry revealed a severe and widespread COX deficiency in explanted cardiac tissue **(Figure 3.8C-D)**.

Biochemical assessment of respiratory chain enzyme activities revealed a severe defect in the activity of complex IV alongside a small decrease in complex I activity that remains within the range of standard deviation **(Figure 3.8E)**.

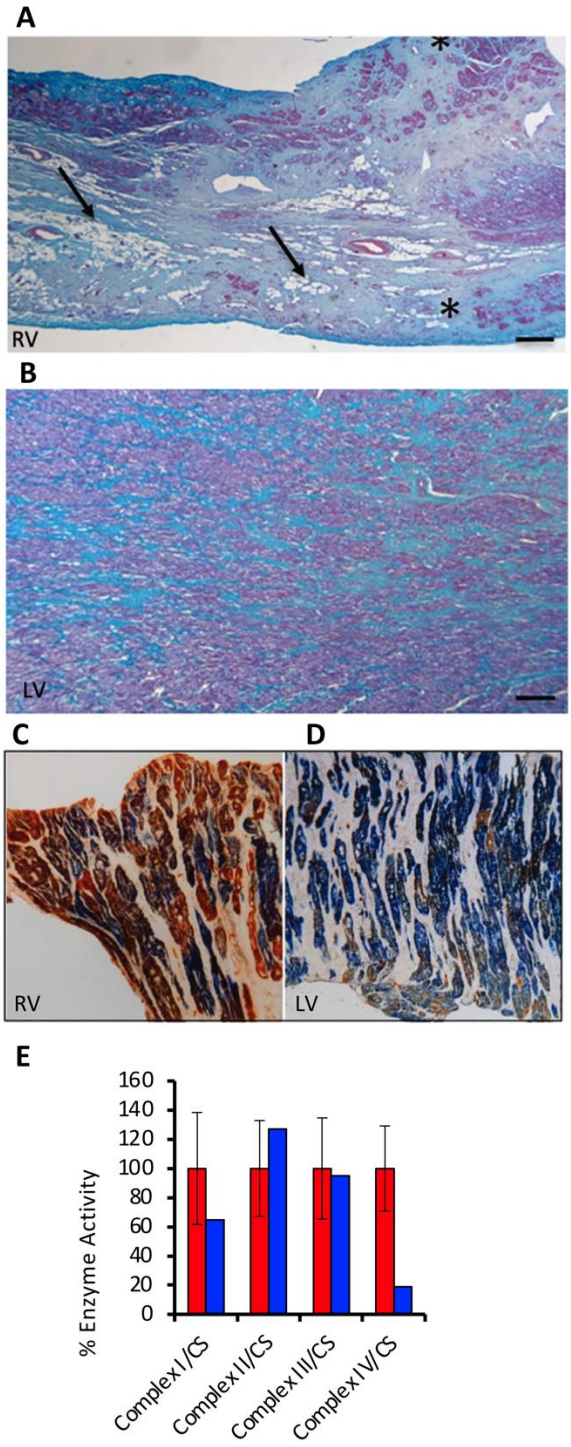

Figure 3.8 Histological, histochemical and biochemical investigation of patient cardiac tissue. Masson trichrome performed on right ventricle (RV) **(A)** shows abundant connective tissue (blue) replacement of cardiomyocytes (red). Arrows denote adipose tissue, asterisks denote fibroadipose replacement. Foci of scarring (blue) are present in the left ventricle (LV) **(B)**. Scale bars are 250um. Combined COX/SDH staining of RV and LV **(C-D)**. Biochemical analysis of mitochondrial respiratory chain enzyme activities performed on cardiac tissue homogenate from proband (blue) and controls (red) **(E)**. Control datasets for fibroblast biochemistry are based on n=25 normal samples, normalised and set to 100% with error bars to represent standard deviation. Data contributed by Elena Perli, Annalinda Pisano and Langping He. Figure adopted and amended from (Perli *et al.*, 2019).

3.4.2 Variant identification, confirmation and segregation

Complete mitochondrial genome sequencing was performed. All variants identified were previously reported non-pathogenic polymorphisms within the MitoMap database (www.mitomap.org), excluding a mtDNA mutation as causative of disease.

Whole exome sequencing lead to the identification of two novel, heterozygous variants in the *TSFM* gene (NM_001172697.1): One missense mutation c.505C>T, p.(Leu169Phe) and one frameshift mutation c.408_409delGT, p.(Leu137Glyfs*24) resulting in a shift in the translational reading frame and the generation of a premature truncation 24 codons downstream of the deletion. Sanger sequencing confirmed the compound heterozygous state of these variants in the proband. The c.505C>T mutation was found to be present in a heterozygous state in the proband's mother. An unaffected sibling had two wild-type *TSFM* alleles. While a paternal DNA sample was not available, the genotyping of the proband's mother and sister is consistent with segregation of recessive *TSFM* variants within the family **(Figure 3.9)**.

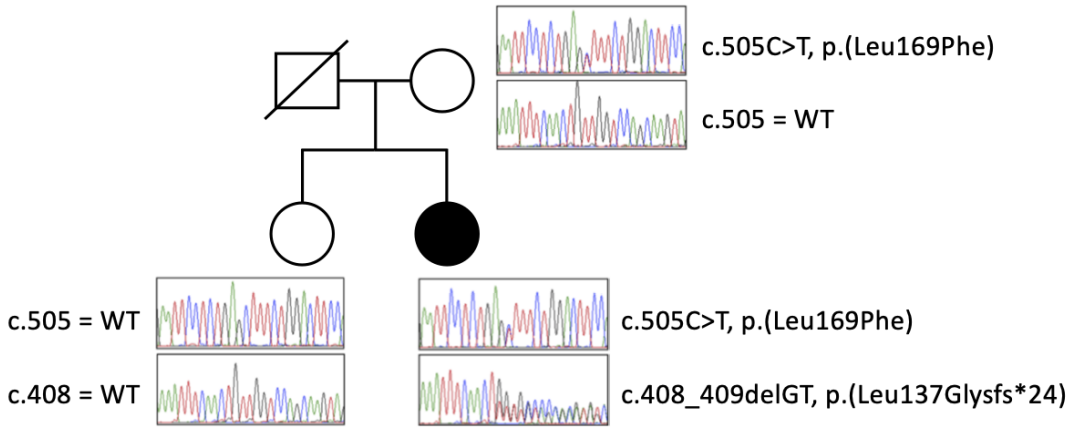

Figure 3.9 Segregation of recessive TSFM variants. Familial pedigree and Sanger sequencing data demonstrating recessive inheritance of compound heterozygous variants in the proband and homozygous wildtype alleles in her unaffected sibling. Figure adopted and amended from (Perli *et al.*, 2019).

3.4.3 Missense residue conservation and *in silico* pathogenicity prediction

The missense c.505C>T mutation identified in this patient has not been reported before and is not present within the gnomAD variant browser (https://gnomad.broadinstitute.org/), nor has it been previously detected in large-scale sequencing studies (http://evs.gs.washington.edu/EVS/). The mutation results in the exchange of a highly conserved leucine residue for phenylalanine **(Figure 3.10)**.

Figure 3.10 Multiple sequence alignment of mtEF-Ts region surrounding missense variant. Mutant and Wildtype human mtEF-Ts sequence aligned alongside orthologs from 7 further species to visualise evolutionary conservation of each affected residue and surrounding sequence.

The use of five different *in silico* pathogenicity prediction tools produced varied results **(Table 3.2)**. Mutation Taster, Polyphen and CADD predict this missense Leu169Phe change to be damaging. The mutation has a CADD score of 26.7, indicating it is among the top 1% of the most deleterious substitutions that could occur within the human genome (https://cadd.gs.washington.edu/). However Align GVGD and SIFT both predict the mutation to be tolerated, and unlikely to affect protein function.

	Mutation Taster	Align GVGD	SIFT	Polyphen	CADD
L169F	'disease causing'	Class C0	'tolerated'	'probably damaging'	26.7

Table 3.2 Assessment of missense *TSFM* variant using a panel of *in silico* pathogenicity prediction tools. Output of each *in silico* pathogenicity prediction tool when assessing missense change c.505C>T, p.(Leu169Phe). Deleterious predictions are shaded in red, tolerated predictions are shaded in green. Align GVGD uses Grantham scores of evolutionary distance alongside sequence conservation to categorise missense changes into one of six classes. Class C0 = class containing variants least likely to interfere with protein function, Combined annotation dependent depletion (CADD) scores are calculated using an array of different tools assessing variants and simulated mutations. A CADD score of 20 classifies a variant as within the top 1% of most deleterious SNVs in the genome. All web-based tools are freely available – see Materials and Methods section **2.1.6**.

3.4.4 Steady-state levels of mtEF-Ts, EF-Tu and mtEF-G1

Western blot analysis was performed by collaborators, Elena Perli and Annalinda Pisano, on patient cardiac tissue lysate alongside non-failing heart (NFH) and failing heart (FH) control lysates to investigate the impact of these compound heterozygous *TSFM* variants on steady-state levels of mtEF-Ts alongside two further elongation factors EF-Tu and mtEF-G1. mtEF-Ts was dramatically decreased in patient cardiac tissue when compared to both NFH and FH. There was also a marked decrease in steady-state EF-Tu protein. Abundance of mtEF-G1 protein, a mitochondrial elongation factor with no direct mtEF-Ts or EF-Tu interaction, was unchanged **(Figure 3.11A)**.

Similarly, mtEF-Ts protein levels in patient fibroblasts were severely decreased. However rather than decreased in abundance, the steady-state level of EF-Tu appeared to be upregulated, though this upregulation is mild when taking into account the overloading of patient sample indicated by GAPDH signal. The steady-state level of mtEF-G1 was unaffected, as also seen in cardiac tissue lysate **(Figure 3.11B)**.

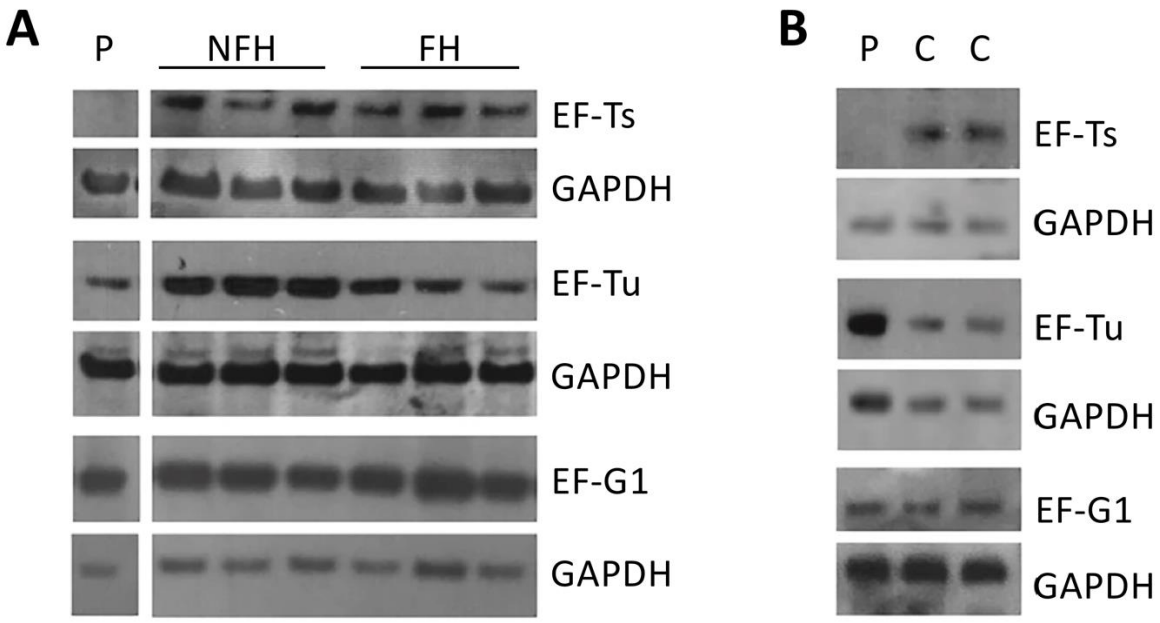

Figure 3.11 Western blot analysis of translation factors in patient cardiac tissue and fibroblasts. Cardiac tissue (A) and fibroblast (B) lysates immunoblotted for mtEF-Ts, EF-Tu and mtEF-G1 alongside GAPDH as a loading control. NFH = non-failing heart control. FH = failing heart control. C = control. Data contributed by Elena Perli and Annalinda Pisano. Figure adopted and amended from (Perli *et al.*, 2019).

3.4.5 Western blot analysis of OXPHOS proteins

Investigation into the stability of OXPHOS subunit proteins was carried out through western blot analysis, performed on patient cardiac tissue and fibroblast lysates alongside age matched controls. There was no decrease in abundance of OXPHOS subunits identified in patient fibroblasts when compared to age-matched controls **(Figure 3.12A)**. However, a marked decrease of NDUFB8 (CI) and an almost complete absence of COXI (CIV) was observed in patient cardiac tissue lysate. **(Figure 3.12B)**.

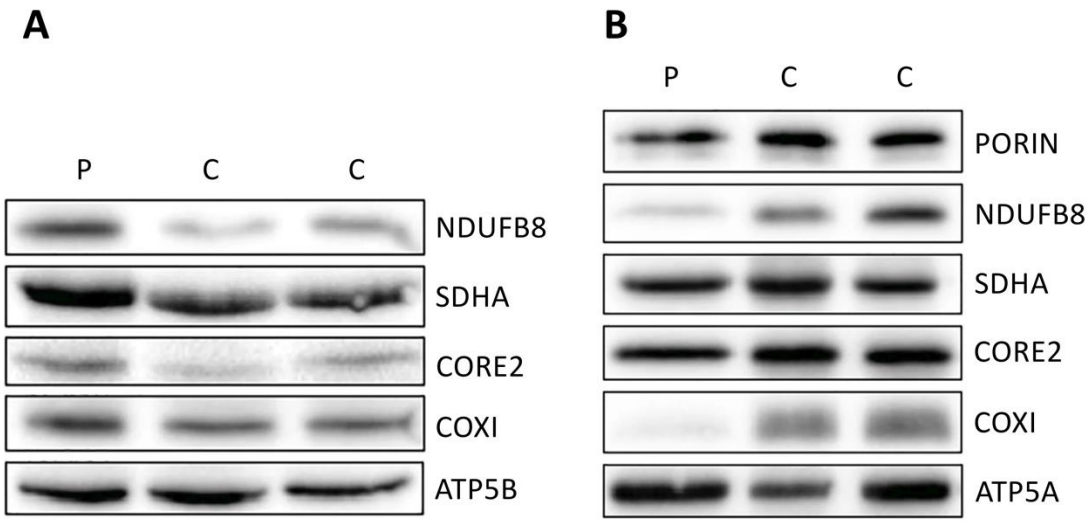

Figure 3.12 Western blot analysis of OXPHOS subunits in patient fibroblasts and cardiac tissue. Patient fibroblast whole cell lysate immunoblotted for NDUFB8, SDHA (loading control), CORE2, COXI and ATP5B (A). Patient cardiac tissue lysate immunoblotted for NDUFB8, SDHA, CORE2, COXI and ATP5A with PORIN as a loading control. Figure adopted and amended from (Perli *et al.*, 2019). Data shown is representative of three independent repeats.

3.5 Discussion

3.5.1 *GFM2*

Western blot analysis of patient fibroblasts demonstrated differential effects at the steady-state protein level for each of these patients. While patient 2 shows decreased steady-state levels of OXPHOS subunits NDUFB8 (CI), CYTB and CORE2 (CIII), and COXI and COXII (CIV), revealing a combined OXPHOS deficiency, steady-state NDUFB8, COXI and COXII levels were only very mildly decreased in Patient 1 when compared to controls **(Figure 3.6A)**. However, the abundance of COXI and COXII protein in the skeletal muscle of Patient 1 was severely decreased, demonstrating a much clearer clear complex IV deficiency **(Figure 3.6B)**. These results are in accordance with the original diagnostic assessment of individual respiratory chain enzyme activities in the skeletal muscle of Patient 1, which detected a complex IV activity of approximately 40% of controls **(Figure 3.3E)**. Tissue specific discrepancies, such as the difference in severity of OXPHOS defect between the fibroblasts and muscle of *GFM2* Patient 1, are not uncommon in defects of mitochondrial translation. Mutations in mt-aaRS genes often demonstrate much clearer OXPHOS deficiencies in high energy tissues than glycolytic fibroblasts, producing tissue-specific manifestations in the heart, skeletal muscle and brain (Boczonadi, Jennings and Horvath, 2018).

The abundance of mtEF-G2 protein the skeletal muscle of Patient 1 was approximately 50% of controls **(Figure 3.6B)**. The c.636delA, p.(Glu213Argfs*3) heterozygous *GFM2* variant identified in Patient 1 results in a frame shift and premature stop codon. It is therefore highly likely to encode a non-functional truncated version of mtEF-G2 that will be targeted for degradation. The 50% residual mtEF-G2 can be consequently be attributed to protein resulting from the allele carrying the c.569G>A, p.(Arg190Gln) variant, suggesting that this missense change affecting residue 190 has no significant impact on mtEF-G2 stability.

Consideration of the levels of sequence conservation at missense residue sites and *in silico* pathogenicity predictions might offer a possible explanation for the distinct difference in the severity of the OXPHOS defect in the fibroblasts of patients 1 and 2. While both missense variants affect residues with strong evolutionary conservation **(Figure 3.5)**, all five of the pathogenicity prediction tools predicted the p.(Tyr92Ser) missense variant to have some deleterious effect on protein function or stability, whereas only three predicted a p.(Arg190Gln) to be as damaging. These tools are predictions only and must be interpreted with caution. However, if the heterozygous p.(Arg190Gln) present in Patient 1 is tolerated slightly more than the homozygous p.(Tyr92Ser) missense change in Patient 2, it may account for the fibroblasts of Patient 1 exhibiting a milder OXPHOS defect.

Despite mtEF-G2 playing an important role in the termination and mitribosome recycling stage of translation, [^{35}S] metabolic labelling revealed no marked decrease in the incorporation of [^{35}S] methionine/cysteine in growing fibroblasts as a measure of *de novo* mitochondrial protein synthesis. A lack of translation defect might have been expected in the fibroblasts of Patient 1, due to there being only a very mild OXPHOS defect in these cells. However, finding the fibroblasts of Patient 2 to have [^{35}S] signal comparable to controls **(Figure 3.7)** was unexpected, considering their clear combined OXPHOS defect upon western blotting **(Figure 3.6A)**. Mitoribosome recycling occurs primarily upon completion of a full protein synthesis cycle, following the release of the nascent peptide, to disassemble the post-termination complex (PoTC) made up of the LSU, SSU, deacylated tRNA and mRNA transcript (Koripella *et al.*, 2019). It is likely that dysfunctional mtEF-G2 would not prevent incorporation of amino acids throughout the synthesis of individual peptides, as the translocase mtEF-G1 functions during elongation but mtEF-G2 does not exert its function until termination has occurred (Christian, Haque and Spremulli, 2009). The incubation period for the [^{35}S] metabolic labelling used in this translation assay was one hour, which may not be long enough for signal resulting from incorporated methionine cysteine to be affected by a quality control system. Repeating the experiment with a one hour pulse followed by several chases of different lengths might reveal differences in the subsequent stability of labelled mtDNA encoded proteins between patient and control cell lines.

The affected missense residues of both Patient 1 and Patient 2 reside within domain 1 of the 5 domains belonging to mtEF-G2. This domain is responsible for guanine nucleotide binding and is very similar to the GTP binding domains of other translational GTPases. Swapping of domain 1 between mtEF-G1 and mtEF-G2 does not affect their translocase and recycling activities respectively (Tsuboi *et al.*, 2009). GTP hydrolysis is not required by mtEF-G2 for the splitting of the PoTC but is necessary for mtEF-G2 release from the LSU that has been freed from the PoTC. Therefore, if the missense changes reported here primarily affect GTP binding, it is possible that mutant mtEF-G2 is less efficient only at its own recycling, remaining bound to the LSU for longer and decreasing the amount of free mtEF-G2 available to other post-termination complexes.

Prior to its identification as a ribosome recycling factor, mtEF-G2 was postulated to play a role in quality-control of mitochondrial translation. Overexpression of mtEF-G2 was demonstrated to suppress a translation and respiratory chain defect phenotype in the myoblasts of a 3243A>G MELAS patient (Sasarman, Antonicka and Shoubridge, 2008). A mechanism for mtEF-G2-mediated quality-control is yet to be investigated. Feedback from mtEF-G2 as an influence on the stability of newly synthesised mtDNA encoded OXPHOS proteins, as is suggested by the overexpression data in MELAS patient myoblasts, might offer an explanation for the discrepancy between the results of the translation assay and the clear OXPHOS defect observed in the fibroblasts of Patient 2.

3.5.2 TSFM

Cardiomyopathy is a common clinical feature of *TSFM* related disease, found in 10 out of the 13 reported patients. However, development of hypertrophic cardiomyopathy in the index patient investigated within this report is unique, due to its manifestation later in adulthood. All previous *TSFM* cardiomyopathies presented in early infancy (Smits *et al.*, 2011a; Calvo *et al.*, 2012; Vedrenne *et al.*, 2012; Smeitink *et al.*, 2006b) or later in childhood (Ahola *et al.*, 2014; Emperador *et al.*, 2017; Scala *et al.*, 2019).

Steady-state levels of mtEF-Ts are severely decreased in both patient fibroblasts and cardiac tissue, indicative of the c.505C>T, p.(Leu169Phe) mutant protein being unstable and the c.408_409delGT, p.(Leu137Glyfs*24) mutation resulting in nonsense mediated mRNA decay. However, while loss of mtEF-Ts in patient cardiac tissue appears to result in a destabilisation of EF-Tu, patient fibroblast cells exhibit increased steady-state EF-Tu protein in comparison with controls **(Figure 3.11)**. Similarly, a combined OXPHOS defect affecting complexes I and IV is observed in patient myocardium, but not in fibroblasts **(Figure 3.12)**. These findings are in accordance with the tissue specific nature of disease in this patient, with a presentation with primarily cardiac involvement alongside very mild and stable form of ataxia.

It was demonstrated in the first report of *TSFM* as a nuclear mitochondrial disease gene that overexpression of EF-Tu was able to rescue a combined OXPHOS defect in patient fibroblasts. This rescue is attributed to the re-stabilisation of the EF-Tu-mtEF-Ts complex due to increased availability of EF-Tu (Smeitink *et al.*, 2006b). Control skin fibroblasts have been shown to be very sensitive to changes in the ratio of EF-Tu and mtEF-Ts. The overexpression of either elongation factor, or the overexpression of both simultaneously, results in a reduction in rate of mitochondrial translation between 20-40% (Antonicka *et al.*, 2006).

Adaptive upregulation of EF-Tu expression has been previously reported and implicated in tissue specific patterns of OXPHOS and translation defects in patients with compound heterozygous mutations in the *GFM1* gene. In this case the upregulation of EF-Tu in patient heart impacted the ratio of EF-Tu:mtEF-Ts, increasing from 1:6 in controls to 1:2 in patient cardiac tissue. The severity of translation defect in these patients varied significantly between tissues, with cardiac tissue being the least affected. The authors hypothesised that this shift in the EF-Tu:EF-TS ratio could slow EF-Tu recycling and bring this stage of elongation in line with the subsequent function of mtEF-G1, thus ameliorating the translation defect within cardiac tissue (Antonicka *et al.*, 2006).

It is possible that the lack of OXPHOS defect in the fibroblasts of the patient presented in this chapter is the result of a compensatory mechanism of EF-Tu overexpression. The exact mechanism underpinning this EF-Tu overexpression remains unclear. A deeper understanding of any post-trancriptional and post-translational modifications of individual mitochondrial translation factors in patient and control cell lines and tissues would be extremely valuable in the study of adaptive responses and tissue specific patterns found within this group of disorders.

3.6 Concluding remarks

In summary, three patients carrying previously unreported variants in the *GFM2* and *TSFM* genes have been identified through the application of WES. The diagnostic and experimental data presented in this chapter have confirmed the segregation of these rare recessive variants and demonstrated the detrimental impact of mutant mtEF-G2 and mtEF-Ts on steady-state levels of oxidative phosphorylation, confirming pathogenicity in all three patients. The tissue-specific differences identified, both within and between patients, illustrates the complexity of the underlying pathomechanisms and highlights the gap in our current understanding of tissue specific adaptation and the compensatory mechanisms present in disorders of mitochondrial translation.

Chapter 4 : A homozygous variant in the *MRPL47* large subunit mitoribosomal gene as a novel cause of mitochondrial disease

4.1 Introduction

Ribosomes are large ribonucleoprotein complexes that are responsible for driving protein synthesis within the cytosol of all eukaryotic and prokaryotic cells. All ribosomes are comprised of two asymmetrical subunits: The SSU recruits mRNA and allows translation of the transcripts by selecting the cognate aminoacyl-tRNA molecules. The LSU contains the peptidyl transfer centre (PTC), the catalytic site responsible for the formation of peptide bonds between amino acids of growing polypeptide chains which then leave the LSU through the polypeptide exit tunnel (Greber and Ban, 2016).

4.1.1 Structure and function of the mitoribosome

The existence of active ribosomes within isolated mitochondria was first noted in 1958 (McLean *et al.*, 1958). Mitochondria possess translation machinery distinct to that of the cytosol, as a remnant of their α-proteobacterial ancestry. Mitoribosomes, required for the synthesis of proteins encoded by the mitochondrial genome, have undergone evolutionary changes in composition, structure and function diverging significantly from their bacterial counterparts. The release of increasingly high-resolution cryo-EM (cryogenic electron microscopy) structural models in the last two decades has shed further light on the specialised features of the mammalian mitoribosome machinery (Sharma *et al.*, 2003; Amunts *et al.*, 2015).

One of the most striking evolutionary adaptations of the mitoribosome can be seen in the relative amounts of protein and ribosomal RNA. Bacterial ribosomes are composed of 70% RNA and 30% protein, whereas this ratio is reversed, at 30% RNA and 70% protein, in the mammalian mitoribosome (Greber and Ban, 2016). This shift

in composition has been driven by the evolutionary loss of large ribosomal RNA domains, the extension of conserved ribosomal proteins and the acquisition of mitochondria-specific ribosomal proteins. Many of the more recently evolutionary acquired MRPs are located on the periphery of the mitoribosome (Brown *et al.*, 2014) **(Figure 4.1)**, which has been postulated to act as a protective barrier shielding the core machinery from damaging ROS, while a few mitochondria-specific proteins fill the structural spaces left behind by lost ribosomal RNA domains (Pietromonaco, Denslow and O'Brien, 1991; Lightowlers, Rozanska and Chrzanowska-Lightowlers, 2014).

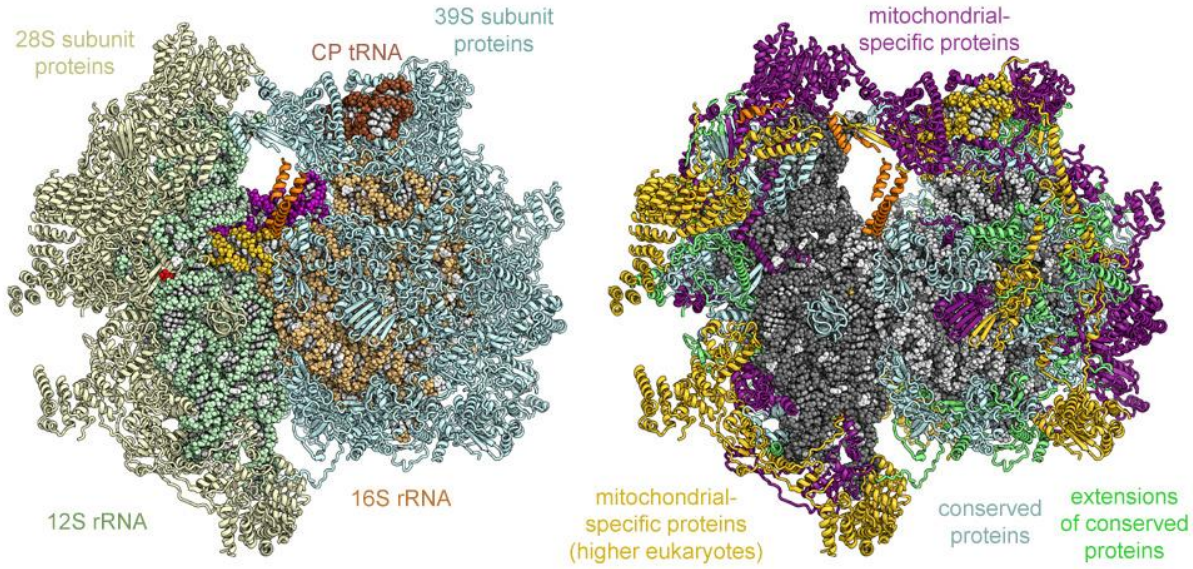

Figure 4.1 Structure and composition of the mammalian mitoribosome. RNA and protein components of the 55S mammalian mitoribosome (left) and evolutionary conservation of mitoribosomal proteins (right). Figure adapted from (Greber *et al.*, 2015) and (Greber and Ban, 2016).

Bacterial ribosomes are built around three ribosomal RNA molecules, a 16S rRNA within the SSU, a 23S rRNA at the core of the LSU and a 5S rRNA within the central protuberance of the LSU. In mammalian mitoribosomes a structural tRNA, mt-tRNA^{Phe} or mt-tRNA^{Val}, is present within the LSU central protuberance, replacing 5S rRNA which is not present within the mammalian mitochondrial genome (Chrzanowska-Lightowlers, Rorbach and Minczuk, 2017). The functional core of the mammalian mitoribosome has remained highly conserved throughout evolution. All tRNA binding

A-, P- and E-sites, that occupy the inter-subunit space of the bacterial ribosome, have been preserved (Greber and Ban, 2016).

Biogenesis of mitoribosomes requires the synthesis and assembly of ~80 proteins and 3 structural RNA molecules in a coordinated fashion. Research into the key factors involved in this process is ongoing and our understanding of the mechanisms underlying mitoribosome biogenesis remains relatively basic. Studies using stable isotope labelling of amino acids in cells (SILAC) followed by sucrose gradient fractionation and proteomics demonstrated that a subset of MRPs associate with the mtDNA nucleoid, indicating that the initial steps of mitoribosome assembly occur proximally to this site (Bogenhagen, Martin and Koller, 2014). An RNA binding GTPase, ERAL1, is believed to bind 12S rRNA for its stabilisation prior to insertion into the SSU (Uchiumi *et al.*, 2010). Three further GTPases have been demonstrated to play roles in mitoribosome assembly. Mtg1 and Mtg2 are membrane bound GTPases that interact with the immature LSU (Kotani *et al.*, 2013), while C4orf14 is believed to be involved in SSU assembly (He *et al.*, 2012). MPV17L12, a protein found within nucleoids that is dependent on mtDNA, is thought to contribute to both the assembly and stability of the mitoribosome at the IMM (Dalla Rosa *et al.*, 2014). Two RNA helicases, DDX28 and DHX30, and a Fas-activated serine-theronine kinase (FASTKD2), each residing within RNA granules, are also thought to be required for mitoribosome biogenesis (Antonicka and Shoubridge, 2015). Depletion of a core RNA granule protein component, GRSF1, results in the accumulation of SSU sub-assemblies, indicating it may also be involved in mitoribosome assembly (Antonicka *et al.*, 2013) .

Mitochondrial mRNA transcripts lack a 5’ UTR (untranslated region) and therefore do not carry Shine-Dalgarno sequences that recruit the ribosome in the initiation stage of bacterial translation. The mechanism by which mitoribosomes recognise start-codons is therefore unique. Binding of a 5’AUG depends on the presence of a formylated $tRNA^{Met}$ and is enhanced by mitochondrial initiation factor 2 ($IF2_{mt}$) (Rudler *et al.*, 2019).

The signal recognition particle system that is employed within the cytosol, coupling the synthesis of hydrophobic proteins with their membrane insertion, is absent in mitochondria (Pool, 2005). To compensate for this, in order to prevent protein aggregation and precipitation, mitoribosomes are anchored to the inner mitochondrial membrane in close proximity to membrane insertion machinery (Liu and Spremulli, 2000). This allows nascent peptides to be rapidly inserted into the IMM as they leave the polypeptide exit site of the mitoribosome.

4.1.2 Mitoribosomal mutations in human disease

An increasing number of MRPs are implicated in mendelian human pathologies. To date, recessive variants in ten SSU genes and four LSU genes have been reported in the literature **(Table 4.1)**. These defects typically result in combined respiratory chain defects and cause a wide, and often severe, range of clinical presentations.

Mammalian mitoribosomal protein nomenclature has historically been determined by the presence of the MRP within either the large subunit (MRPL) or the small subunit (MRPS) of the mitoribosome, followed by an identifying integer. A recently proposed naming system attempts to unify the nomenclature of mitoribosomal proteins with proteins belonging to cytoplasmic, and prokaryotic ribosomes (Greber and Ban, 2016). However, as almost all previously published mitoribosomal disease genes are reported under the original naming system, the same nomenclature will be used throughout the following text.

Gene	Patient	Variant(s)	Onset	Age	Clinical Features	Biochemical findings	OXPHOS findings	Ref
MRPS2 (NM_016034.5)	1	c.328C>T, p.(Arg110Cys); c.340G>A, p.(Asp114Asn)	Infantile	Alive at 11 years	FTT, DD, sensorineural deafness, hypoglycaemia, redundant skin on hands and abdomen, dysmorphic features	↑ lactate, ↑ liver enzymes, ↑ serum alanine, ↑ excretion of Krebs cycle intermediates	Fibroblasts: ↓CIV Muscle: ↓CII, ↓CIII, ↓CIV Liver: ↓CI, ↓CIII, ↓CIV	Gardeitchik et al. (2018)
	2	c.413G>A, p.(Arg138His)	Infantile	Alive at 11 years	DD, sensorineural deafness, hypoglycaemia, ID, exercise intolerance	↑ lactate, ↑ excretion of Krebs cycle intermediates	Fibroblasts: ↑CII, ↓CIII, ↓CIV Muscle: ↑CII, ↓CIV Liver: ↓CI, ↓CII, ↓CIII, ↓CIV	
MRPS7 (NM_015971.4)	1[S]	c.550A>G, p.(Met184Val)	Infantile	Died at 14 years	FTT, sensorineural deafness, hepatomegaly and liver failure, hypoglycaemia, renal dysfunction, encephalopathy	↑ lactate, ↑ fumarate, ↑ 3- hydroxybutyrate, ↑ C6-C10 dicarboxylic acids	Fibroblasts: ↓CI, CIV Muscle: ↓CI Liver: ↓CI, ↓CIII, ↓CIV	Menezes, et al. (2015)

Gene	Patient	Variant(s)	Onset	Age	Clinical Features	Biochemical findings	OXPHOS findings	Ref
	2[S]	c.550A>G, p.(Met184Val)	Infantile	Alive at 17 years	Sensorineural deafness, hypoglycaemia, primary hypogonadism, primary adrenal failure, mild learning difficulties	↑ lactate, ↑TSH, ↑ urea, creatine	Muscle: Normal Liver: ↓CI, ↓CIII	
MRPS14 (NM_022100.3)	1	c.322C>T, p.(Arg108Cys)	Neonatal	Alive at 5 years	HCM (receded by 5 years of age), FTT, DD, dysmorphic features, muscle hypotonia	'Episodic metabolic acidosis'; ↑ lactate, ↑ alanine,	Fibroblasts: ↓CI, ↓CIII, ↓CIV, ↓CV Muscle: ↓CIV	Jackson, et al. (2019)
MRPS16 (NM_016065.4)	1	c.331C>T, p.(Arg111∗)	Neonatal	Died at 3 days	Dilation of cerebral ventricles and agenesis of corpus collosum on foetal ultrasound, FTT, hypotonia, redundant skin on neck	'Severe metabolic acidosis'; ↑ lactate, ↑ liver enzymes	Fibroblasts: ↓CII+III, ↓CIV Muscle: ↓CI, ↓CII+III, ↓CIV, ↓CV Liver: ↓CI, ↓CII+III, ↓CIV	Miller, et al.(2004)

Gene	Patient	Variant(s)	Onset	Age	Clinical Features	Biochemical findings	OXPHOS findings	Ref
MRPS22 (NM_020191.4)	1[S]	c.509G>A, p.(Arg170Cys)	Antenatal	Died before 1 month	Generalised oedema on foetal sonogram, subcutaneous oedema at birth, muscle hypotonia, HCM, renal tubulopathy	↑ lactate, ↑ ammonia	Fibroblasts: ↓CIV Muscle: ↓CI, ↓CIII, ↓CIV, ↓CV	Saada, et al. (2007)
	2[S]	c.509G>A, p.(Arg170Cys)	Antenatal	Died before 1 month	Generalised oedema on foetal sonogram, subcutaneous oedema at birth, muscle hypotonia, HCM, renal tubulopathy	↑ lactate, ↑ ammonia	Lymphocytes: ↓CIV	
	3[S]	c.509G>A, p.(Arg170Cys)	Antenatal	Died before 1 month	'affected similarly to siblings 1 and 2'	'affected similarly to siblings 1 and 2'	N/A	

Gene	Patient	Variant(s)	Onset	Age	Clinical Features	Biochemical findings	OXPHOS findings	Ref
	1	c.644T>C, p.(Leu215Pro)	Antenatal	Alive at 5.5 years	FTT, antenatal microcephaly, stable HCM, Cornelia de Lange-like dysmorphic features, redundant skin on neck, muscle hypotonia, leukoencephalopathy, transient seizures, tetraspasticity and dystonic movements	'Severe metabolic acidosis'; ↑ lactate, ↑ urinary TCA-cycle intermediates	Fibroblasts: ↓CI, ↓CIII, ↓CIV	Smits, et al. (2011)
	1	c.1032_1035dup, p.(Leu346Asnfs*21)	Neonatal	Died at 3 days	Agenesis of the corpus callosum and periventricular cysts, atrial and ventricular septal defects with a coronary artery fistula	'Severe lactic acidosis'; ↑ lactate, ↑ ammonia, ↑ lactaturea	Fibroblasts: ↓CI, ↓CIII, ↓CIV	Baertling, et al. (2015)
	1	c.339+5G>A, p.(?)	Neonatal	Alive at 4 years	DD, hypotonia, mild dysmorphic features, Leigh-like brain lesions, mosaic Down syndrome, oxygen dependence, tetraspasticity, nasogastric tube feeding	↑ lactate, ↑ pyruvate, ↑ urine organic acids	N/A	Kilic, et al. (2017)

Gene	Patient	Variant(s)	Onset	Age	Clinical Features	Biochemical findings	OXPHOS findings	Ref
	1[S,C]	c.605G>A, p.(Arg202His)	Adolescence	Alive at reporting	Delayed puberty, primary ovarian insufficiency with hypergonadotrophic hypergonadism, small uterus, delayed bone age	↑ gonadotropins, ↓ oestrogens	N/A	Chen, et al. (2018)
	2[S,C]	c.605G>A, p.(Arg202His)	Childhood	Alive at reporting	Primary ovarian insufficiency, elevated gonadotrophins, fibrotic ovaries without follicles	↑ gonadotropins, ↓ oestrogens	N/A	
	3[C]	c.605G>A, p.(Arg202His)	Adolescence	Alive at reporting	Delayed puberty, primary ovarian insufficiency with hypergonadotrophic hypergonadism	↑ gonadotropins	N/A	

Gene	Patient	Variant(s)	Onset	Age	Clinical Features	Biochemical findings	OXPHOS findings	Ref
	4	c.404G>A, p.(Arg135Gln)	Adolescence	Alive at reporting	Amenhorroea, mild facial dysmorphism, delayed bone age, delayed puberty, primary ovarian insufficiency with hypergonadotrophic hypergonadism, small uterus, mild osteoporosis, bilateral axonal polyneuropathy	↑ gonadotropins, ↓ oestrogens, ↑ lactate, ↓ ketosteroids, ↑ methemoglobin	N/A	
MRPS23 (NM_016070.4)	1	c.119C>G, p.(Pro40Arg)	Infantile	N/A	Hepatic disease	N/A	'combined respiratory chain deficiency'	Kohda, et al. (2016)

Gene	Patient	Variant(s)	Onset	Age	Clinical Features	Biochemical findings	OXPHOS findings	Ref
MRPS25 (NM_022497.5)	1	c.215C>T, p.(Pro72Leu)	Antenatal	Alive at reporting	Intrauterine growth-restriction, DD, choreoathetoid distal limb movements, muscle weakness and dystonia, dysphagia, partial agenesis of corpus collosum and underdevelopment of frontal and parietal temporal regions on MRI, hip dysplasia, adrenal insufficiency	↑ lactate	Fibroblasts: ↓CI, ↓CIII, ↓CIV M: ↓CIV	Bugiardini, et al. (2019)
MRPS28 (NM_014018.3)	1	c.356A>G, p.(Lys119Arg); c.214_395del, p.(Gly72Glufs*16)	Antenatal	Alive at 30 years	Intrauterine growth retardation, FTT, DD, microcephaly, dysphagia, facial dysmorphism, sensorineural deafness, hepatomegaly, hypoglycaemia, bilateral lesions in globus pallidus and cerebellar atrophy on MRI	↑ lactate, ↑ alanine, ↑ liver enzymes, ↑ urinary TCA cycle metabolites	Fibroblasts: ↓CIV Muscle: ↓CV Liver: ↓CIV	Pulman, et al. (2019)

Gene	Patient	Variant(s)	Onset	Age	Clinical Features	Biochemical findings	OXPHOS findings	Ref
MRPS34 (NM_023936.2)	1	c.321+1G>T, p.(Val100 Gln107del)	Infantile	Died at 9 months	DD, microcephaly, episodic tachypnoea	↑ lactate, ↑ alanine	Fibroblasts: ↓CI, ↓CIV Muscle: ↓CI, ↓CIII, ↓CIV Liver: ↓CI, ↓CIV	Lake, et al. (2017)
	2[S1]	c.322-10G>A, p.(Asn108Leufs∗12/ p.(Asn108Glyfs∗50)	Infantile	Alive at 17 years	Hypotonia, DD, non-verbal, microcephaly, horseshoe kidney, mild coarsening of facial features, extropia and ptosis, kyphoscoliosis, bilateral choreoathetoid movements, atrophy of extremities with hypertonia, contractures at most joints	↑ lactate	Muscle: ↓CI, ↓CIII, ↓CIV	

Gene	Patient	Variant(s)	Onset	Age	Clinical Features	Biochemical findings	OXPHOS findings	Ref
	3[S1]	c.322-10G>A, p.(Asn108Leufs∗12/ p.(Asn108Glyfs∗50)	Infantile	Alive at 14 years	DD, choreoathetoid spastic quadriplegia, abnormal MRI, non-verbal, microcephaly, mild coarsening of facial features, strabismus, scoliosis, dystonia, mild contractures at most joints	↑ lactate	N/A	
	4[S2]	c.322-10G>A, p.(Asn108Leufs∗12/ p.(Asn108Glyfs∗50)	Infantile	Alive at 7 years	Transient nystagmus, intermittent ptosis and alternating extropia, involuntary movements, developmental regression, axial hypotonia, limb hypertonia, contractures at the knees and ankles, non-verbal, suspected sleep apnoea, dysmorphic facies, premature puberty	↑ lactate, ↓ ammonia	Muscle: ↓CI, ↓CII, ↓CIII, ↓CIV	
	5[S2]	c.322-10G>A, p.(Asn108Leufs∗12/ p.(Asn108Glyfs∗50)	Infantile	Alive at 2 years	DD, dysconjugate eye movements, dysphagia, suspected sleep apnoea	↑ lactate	N/A	

Gene	Patient	Variant(s)	Onset	Age	Clinical Features	Biochemical findings	OXPHOS findings	Ref
	6	c.37G>A, p.(Glu13Lys); c.94C>T, p.(Gln32*)	Neonatal	Died at 8 months	Developmental regression, axial hypotonia, pyramidal syndrome of the lower limbs, and dystonia, hemodynamic instability related to tubulopathy	'Transient metabolic acidosis'; ↑ lactate	Fibroblasts: ↓CIV Muscle: ↓CIV	
MRPS39 (NM_017952.6)	1	c.415- 2A>G p.(?); c.1747_1748insCT p.Phe583Serfs*3	Antenatal	Died at 1 year and 4 months	Intrauterine growth defect, limb rigidity, myoclonus, nystagmus, psychomotor regression, bilateral optic atrophy, bilateral hearing loss, bilateral lesions involving ventral side of the medulla, cerebral peduncle thalamus, caudate nucleus, and putamen of the basal ganglia on MRI	N/A	Fibroblasts: ↓CI, ↓CIII, ↓CIV	Borna, et al. (2019)

Gene	Patient	Variant(s)	Onset	Age	Clinical Features	Biochemical findings	OXPHOS findings	Ref
MRPL3 (NM_007208.4)	1[S]	c.950C>G, p.(Pro317Arg); large-scale 225-kb deletion	Infantile	Died at 17 months	FTT, dyspnoea, hypotrophy, hepatomegaly, HCM	↑ lactate, ↑ liver enzymes	Fibroblasts: ↓CIV Muscle: ↓CIII, ↓CIV	Galmiche, et al. (2011)
	2[S]	c.950C>G, p.(Pro317Arg); large-scale 225-kb deletion	Infantile	Died at 15 months	FTT, HCM, similar disease course to sibling	↑ lactate	Fibroblasts: ↓CIV	

Gene	Patient	Variant(s)	Onset	Age	Clinical Features	Biochemical findings	OXPHOS findings	Ref
	3ST	c.950C>G, p.(Pro317Arg); large-scale 225-kb deletion	Infantile	Alive at 3 years	Hepatomegaly, liver dysfunction, HCM (stable), hypergyria of the cortical brain on MRI	↑ lactate, ↑ alanine, ↑ liver enzymes	Fibroblasts: ↓CI, ↓CIV Muscle: ↓CIV	
	4ST	c.950C>G, p.(Pro317Arg); large-scale 225-kb deletion	Infantile	Alive at 3 years	Hepatomegaly, liver dysfunction, HCM (stable), FTT, hypergyria of the cortical brain on MRI	↑ lactate, ↑ alanine, ↑ liver enzymes	Fibroblasts: ↓CI, ↓CIV	

Gene	Patient	Variant(s)	Onset	Age	Clinical Features	Biochemical findings	OXPHOS findings	Ref
MRPL12 (NM_002949.4)	1[S]	c.542C>T, p.(Ala181Val)	Antenatal/ neonatal	Died at 2 years	Severe general hypotrophy, FTT, muscle weakness, psychomotor delay, trunk hypotonia, mild hepatomegaly, intermittent nystagmus, cerebellar ataxia and tremor, mild dysmorphic facial features, tonic seizure, lesions in white matter and basal ganglia on MRI	↑ lactate, ↓ plasma IGF1	Fibroblasts: ↓CI, ↓CIV Muscle: ↓CII+III, ↓CIV Liver: ↓CII+III, ↓CIV	Serre, et al. (2013)
	2[ST]		Antenatal	Pregnancy terminated			Cells from amniotic fluid: ↓CIV	
	3[ST]		Antenatal	Pregnancy terminated			Cells from amniotic fluid: ↓CIV	
MRPL24 (NM_145729.3)	1	c.272T>C, p.(Leu91Pro)	Infantile	Alive at 14 years	Developmental regression, spasticity and dystonic posturing of distal upper and lower limbs, dyskinetic facial grimacing, ID, choreoathetosis of limbs and face, Wolff-Parkinson-White syndrome	↑ lactate	Fibroblasts: ↓CIV Muscle: ↓CI, ↓CIII, ↓CIV, ↓CIV	Di Nottia, et al. (2020)

Gene	Patient	Variant(s)	Onset	Age	Clinical Features	Biochemical findings	OXPHOS findings	Ref
MRPL44 (NM_022915.5)	1[S]	c.467T>G, p.(Leu156Arg)	Infantile	Died at 6 months	HCM, mild steatosis in all cardiomyocytes, steatosis of liver	N/A	Muscle: ↓CIV Heart: ↓CI, ↓CIV	Carroll, et al. (2013)
	2[S]	c.467T>G, p.(Leu156Arg)	Infantile	Alive at 14 years	HCM (stable and asymptomatic after 2 years), steatosis of liver, mild granular pigmentation in the retina	↑ lactate, ↑ liver enzymes	Muscle: ↓CIV	
	1	c.233G>A, p.(Arg78Gln); c.467T>G, p.(Leu156Arg)	Infantile	Alive at 8 years	Feeding difficulties in infancy, exercise intolerance, non-obstructive HCM, mild hepatopathy, muscle weakness	↑ lactate, ↓ free carnitine, ↑ liver enzymes	Fibroblasts: ↓CIV	Distelmaier, et al. (2015)

Gene	Patient	Variant(s)	Onset	Age	Clinical Features	Biochemical findings	OXPHOS findings	Ref
	2	c.467C>T, p.(Leu156Arg)	Neonatal	Alive at 26 years	Exercise intolerance, learning difficulties, hemiplegic migraine, tapetoretinal dystrophy, non-obstructive HCM, Leigh-like lesions in the thalamus, basal ganglia, and cerebellum on MRI	'Metabolic acidosis'	Heart: ↓CI, ↓CIV	

Table 4.1 Mitoribosomal pathologies: Variants reported to date with associated clinical and biochemical presentations. FTT = failure to thrive; DD = developmental delay; HCM = hypertrophic cardiomyopathy; ID = intellectual disability; ^{S} indicates siblings, numbered for distinction where multiple sibships presented within single report; ^{C} indicates cousins; ^{T} indicates twins; ↓ and ↑ used to denote decreases and increases in biochemical markers and OXPHOS enzyme activities or steady-state levels; OXPHOS defect listed where demonstrated biochemically or at the steady-state level.

While the clinical spectrum of these pathologies is broad, there are some clear overlapping features common to a number of different mitoribosomal disorders. Severe lactic acidosis, a common finding in mitochondrial disease, is also a frequently reported clinical feature in mitoribosomal defects. Of the 38 patients currently reported in the literature, 30 individuals suffered from elevated levels of lactate **(Table 4.1)**, while acidosis in a number of cases was fatal (Miller *et al.*, 2004; Baertling *et al.*, 2015). A hypertrophic cardiomyopathy phenotype is reported in cases of *MRPS14*, *MRPS22*, *MRPL3* and *MRPL44* disease, affecting a total of 13 patients (Jackson *et al.*, 2019; Smits *et al.*, 2011b; Saada *et al.*, 2007; Galmiche *et al.*, 2011; Carroll *et al.*, 2013; Distelmaier *et al.*, 2015), while nine MRP patients, harbouring mutations in *MRPS22*, *MRPS34, MRPS39* or *MRPL44* presented with Leigh syndrome or a Leigh-like phenotype (Kilic *et al.*, 2017; Lake *et al.*, 2017; Borna *et al.*, 2019). One of the most striking similarities in this group of pathologies is an extremely early age of disease onset; clinical presentation occurred at the antenatal/neonatal stage or in early infancy in almost all MRP patients, a distinguishing feature from many other forms of mitochondrial disease. Four patients, with missense mutations in the *MRPS22* gene are the only exception to this pattern of early-onset disease, presenting with a distinct phenotype of primary ovarian insufficiency presenting only in later childhood/adolescence (Chen *et al.*, 2018).

4.1.3 Defects of the LSU

The earliest report of a LSU gene implicated in mitochondrial disease describes the use of a combination of SNP genotyping and WES to identify compound heterozygous variants, c.950C>G (p.Pro317Arg) and 225-kb deletion in the MRPL3 gene in four siblings. The clinical presentation of these patients included hypertrophic cardiomyopathy, hepatomegaly and psychomotor retardation. The identified mutations caused a severe decrease in steady-state MRPL3 levels, resulting in the defective assembly of the LSU. Patient fibroblasts and muscle exhibited combined respiratory chain defects at both the enzymatic and steady-state level (Galmiche *et al.*, 2011).

Hypertrophic cardiomyopathy was also reported in all four previously reported cases of *MRPL44* disease. A homozygous c.467T>G (p.Leu156Arg) missense mutation in the *MRPL44* gene was first identified in a sibling pair. While the older sibling died at the age of six months, the hypertrophic cardiomyopathy phenotype in the second sibling became stable and asymptomatic at two years of age. The Leu156Arg change resulted in decreased levels of MRPL44 protein, demonstrated in patient fibroblasts. A combined OXPHOS deficiency was present in patient cardiac and skeletal muscle (Carroll *et al.*, 2013). Two further patients with missense mutations in the *MRPL44* gene are reported, presenting with a slowly-progressing multisystem disease with cardiac, kidney and neurological involvement (Distelmaier *et al.*, 2015).

The third LSU gene to be implicated in mitochondrial disease was *MRPL12.* A homozygous c.542C>T (p.Ala181Val) variant was identified in a patient presenting at birth with severe general hypertrophy and growth defect followed by fatal neurological and cardiac distress (Serre *et al.*, 2013). A combined respiratory chain defect was observed in patient fibroblasts, heart and liver. Steady-state levels of MRPL12 and a number of other LSU proteins were significantly decreased, resulting in a defect of global mitochondrial translation in patient fibroblasts.

Most recently, *MRPL24* was characterised as the fourth LSU gene harbouring mitochondrial disease variants. A homozygous c.272T>C (p.Leu91Pro) mutation was identified in a patient presenting in infancy with a complex movement disorder, intellectual disability and developmental regression. Patient fibroblasts and muscle homogenate demonstrated a dramatic decrease in MRPL24 protein. A defect affecting subunits of OXPHOS complexes I, IV and V was observed in patient muscle. Steady-state levels of several other LSU proteins were also reduced, while sucrose gradient fractionation of mitoribosome in patient fibroblasts revealed significant destabilisation of the LSU (Di Nottia *et al.*, 2020).

4.1.4 Assigning pathogenicity to a variant in a novel LSU gene

Of the ten previously reported SSU genes with reported pathogenic variants, five are core evolutionary conserved subunits with bacterial ribosome homologs (*MRPS2, MRPS7, MRPS14, MRPS16* and *MRPS28),* while the remaining five genes encode mitochondria-specific mitoribosomal proteins (*MRPS22, MRPS23, MRPS25, MRPS34* and *MRPS39*). With 52 protein subunits, the mammalian LSU contains 22 more individual proteins than the mammalian SSU. However, with only four LSU genes published in association with mitochondrial disease to date, defects of LSU MRPs remain extremely rare. Three of these genes, *MRPL3, MRPL12* and *MRPL24*, are conserved from bacterial counterparts, while *MRPL44* is unique to the mitoribosome.

The mammalian *MRPL47* gene, encoding a protein of the same name, is homologous to the bacterial rpmC gene, encoding RPL29. MRPL47 is a constitutive subunit of the ring of proteins that surround the polypeptide exit site of the mitoribosomal LSU (Greber *et al.*, 2014). This ring of proteins surrounding the exit tunnel are highly conserved from the bacterial ribosome, however the sequence of *MRPL47* has undergone significant divergence from bacterial RPL29 such that it is almost past homology detection limits (Smits *et al.*, 2007).

This chapter will outline work undertaken to characterise the molecular mechanisms underlying disease in three unrelated paediatric patients with a novel homozygous nonsense variant in the LSU gene *MRPL47*, not previously implicated in mitochondrial disease.

4.2 Patient reports

4.2.1 Patient 1

Patient 1, a 4 year-old female, is the first child of healthy consanguineous parents of Arab ethnicity from Saudi Arabia. The patient was delivered at term, but required admission to the neonatal intensive care unit for 10 days due to hypoglycaemia, hyperammonaemia and metabolic acidosis. She presented later at the age of 2 years 5 months with hypoglycaemic seizure, occurring while sleeping, with very low blood sugar preceded by mild febrile illness and poor feeding. Neurological examinations have been normal. Laboratory investigations showed low blood sugar on presentation, metabolic acidosis, high ammonia with high ketones and lactate. Her weight and height are normal for her age and there are no motor or language developmental delays. Lactate continues to be persistently high at 3-6 mmol/L (normal <2.5 mmol/L). This patient was referred by Dr.Malak Ali Alghamdi, College of Medicine and University Hospitals, King Saud University.

4.2.2 Patient 2

Patient 2, a 3 year-old female, is the first child of healthy consanguineous parents of Arab ethnicity from Saudi Arabia. Patient 2 was healthy at birth, with weight, height and head circumference measurements within normal ranges. At two days of age the patient was admitted to NICU with hypoglycaemia and metabolic acidosis related to febrile illness and poor oral intake. At 17 months she presented with persistent vomiting preceded by URTI complicated by moderate to severe dehydration and associated with lactic acidosis and metabolic acidosis. Recurrent attacks of hypoglycaemia, keto-acidosis with failure to thrive prompted a genetic and metabolic work up at the age of 17 months. Neurological examinations have been normal. Liver enzymes were modestly elevated and liver ultrasound revealed increased echotexture consistent with hepatic steatosis. At last examination, height and head circumference measurements had fallen to below the 3rd centile. This patient was referred by

Dr.Malak Ali Alghamdi, College of Medicine and University Hospitals, King Saud University.

4.2.3 Patient 3

Patient 3, a 17 year-old female, is the second child of healthy non-consanguineous parents originating from Germany. Born at full term, this patient was healthy at birth but the neonatal period was complicated by hypoglycaemia (1.11 mmol/L, normal range 4.0-6.0 mmol/L). In the context of febrile illness a diagnosis of hypothyroidism was made, but a L-thyroxine supplementation could be stopped in the follow-up appointments. Developmental delay was reported in infancy, with delayed speech and walking. The patient has moderate intellectual disability. Febrile seizures began at three and a half years of age and increased in frequency over time. Despite continued treatment with anti-epileptics, she experiences one (self-limiting after 2-3 minutes) seizure per week. At the age of 15 the patient developed acute liver failure (encephalopathy, vomiting, abdominal pain) which resolved after treatment. This patient was referred by Dr. Saskia Wortmann, Department of Human Genetics, Paracelsus Medical University Salzburg.

4.3 Results

4.3.1 Variant identification

Diagnostic WES, carried out at Centogene (https://www.centogene.com), identified a segregating homozygous nonsense variant in both Patient 1 and 2. The mutation, c.646C>T, is located within the nuclear gene *MRPL47* (NCBI Reference Sequence: NM_020409.2) and produces a premature stop codon resulting in early truncation at the protein level (p.Arg216*). This truncation occurs at amino acid 216 of 250 in exon 7, the final exon, of *MRPL47*.

WES of Patient 3, carried out in the lab of Professor Holger Prokisch at the Institute of Human Genetics, Helmholtz Centre Munich, identified the same c.(646C>T) truncating variant. Trio Sanger sequencing confirmed segregation of this variant **(Figure 4.2)**. This variant is present in the gnomAD browser at an allele frequency of 0.00001205 (3 heterozygous alleles out of 248942), but is not found in a homozygous state.

Skin biopsies for all three patients were obtained and shipped to Newcastle for culture and functional investigation. However, the fibroblasts of Patient 1 did not recover upon arrival. For this reason, the following data has been acquired using the cells of patients 2 and 3 only.

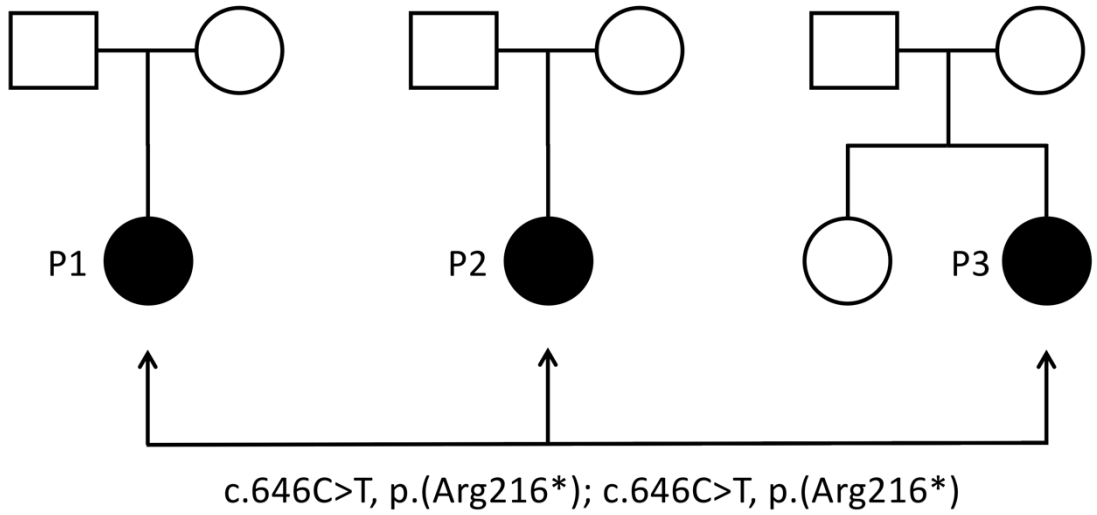

Figure 4.2 Familial pedigrees of *MRPL47* Patients. Familial pedigrees to demonstrate recessive inheritance of the same homozygous c.646C>T, p(Arg218*) truncating variant in each Patient.

4.3.2 Western blot analysis of MRPL47 and OXPHOS proteins

To investigate the impact of c.(646C>T) introducing a premature truncation at position 216 of MRPL47, western blot analysis using a commercially available antibody was carried out. This revealed undetectable levels of full-length MRPL47 protein in the fibroblasts of patients 2 and 3 **(Figure 4.3)**.

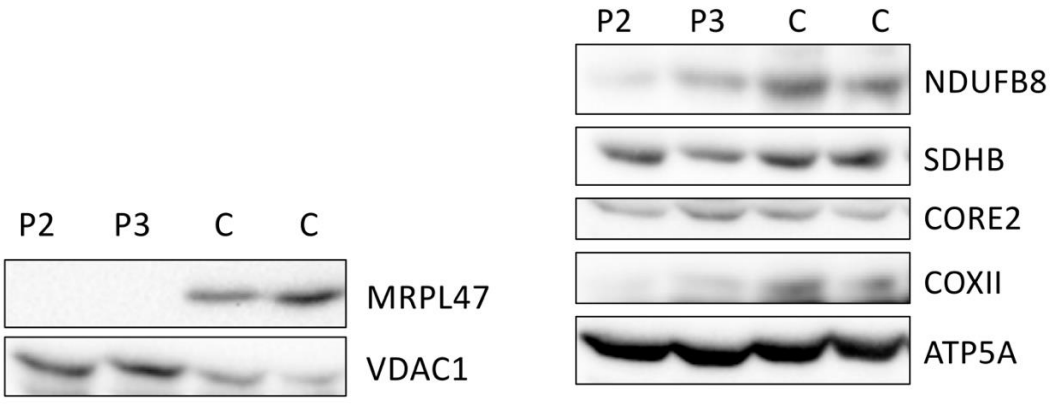

Figure 4.3 Western blot analysis of MRPL47 patient fibroblasts. Whole cell lysates from fibroblasts of Patient 2 and Patient 3 were probed with antibodies against MRPL47 and VDAC1 (loading control) on the left panel. Antibodies targeting NDUFB8, SDHB (loading) CORE2, COXII and ATP5A were applied (right panel). Data shown is representative of three independent repeats.

Investigation into steady-state levels of individual OXPHOS subunits demonstrated moderately decreased NDUFB8 and COXII, indicating a combined OXPHOS defect affecting complexes I and IV **(Figure 4.3)**.

4.3.3 [^{35}S] translation assay in growing fibroblasts

A translation assay using [^{35}S] labelled methionine/cysteine was carried out in order to assess the consequence of a loss of full-length MRPL47 from the tunnel exit region of the mitoribosome in relation to *de novo* protein synthesis in growing patient fibroblasts. This metabolic labelling assay was carried out over a 1 hour incubation period, in the presence of 100 µg/mL emetine for cytosolic translation inhibition. Through the measurement of signal resulting from incorporation of [^{35}S] labelled methionine/cysteine into newly synthesised mitochondrial proteins in the fibroblasts of patients 2 and 3, alongside controls, a generalised defect of mitochondrial translation was detected **(Figure 4.4)**. This defect appears to affect all detectable proteins synthesised by the mitoribosome, suggesting a global decrease in mitochondrial translation.

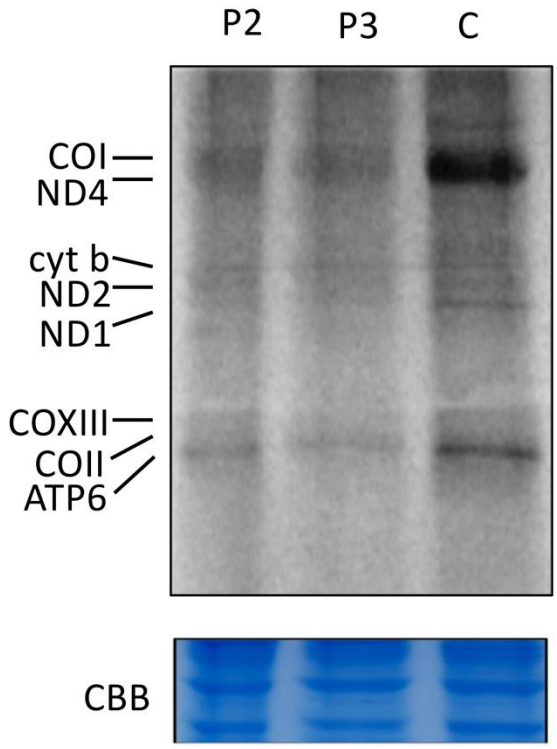

Figure 4.4 [35S] methionine/cysteine incorporation in growing MRPL47 patient fibroblasts as a measure of de novo mitochondrial protein synthesis. Signal detected from fixed and dehydrated SDS-PAGE gel using Typhoon Phosphorimager. Bands are visible for radiolabelled COXI, ND4, cyt b. ND2, ND1, COXIII, COXII and ATP6. Even loading is demonstrated through a Coomassie stain on the bottom panel.

4.3.4 siRNA knock-down of MRPL47 in patient and control cell lines

Investigation into the specificity of a previous commercial MRPL47 antibody through siRNA knockdown of MRPL47 resulted in an incidental finding in the fibroblasts of Patient 2. Treatment of MRPL47 siRNA in the patient cells led to the exacerbation of the combined OXPHOS defect affecting complexes I and IV. Steady-state levels of NDUFB8 and COXI were greatly decreased when Patient 2 fibroblasts were treated with MRPL47 siRNA **(Figure 4.5)**, in comparison with non-targeting siRNA treatment, indicating a much more severe defect upon MRPL47 knockdown. This finding suggests there to be some residual and functional MRPL47 protein in patient fibroblasts, despite full-length protein being undetectable **(Figure 4.3)**. Sample taken from the patient fibroblasts treated with non-targeting siRNA were overloaded in comparison to other fibroblast conditions when using SDHA as an indication of loading.

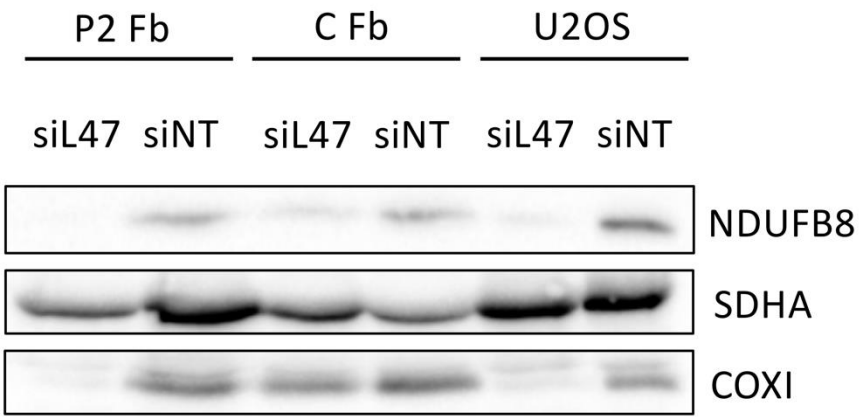

Figure 4.5 siRNA knockdown of MRPL47 in patient fibroblasts, control fibroblasts and U2OS cells. Patient 2 fibroblasts, control fibroblasts and a U2OS cell line were transfected with either MRPL47 siRNA (siL47) or non-targeting siRNA (siNT) with a second transfection on day three and harvested on day six. SDS-PAGE of whole cell lysis was followed by immunoblotting with antibodies againt NDUFB8, SDHA (loading control) and COXI. Data shown is representative of two independent repeats.

4.3.5 Western blot analysis of 25kDa MRPL47 species

In order to identify a truncated protein species that might be mediating the response to MRPL47 siRNA knockdown identified in **4.3.4**, further siRNA studies were carried out using the fibroblasts of patients 2 and 3 alongside controls. In no-treatment, and non-targeting siRNA treatment conditions, the use of MRPL47 antibody and subsequent over-exposure of blot on detection revealed an approximately 25 kDa species. This band disappears in cell lysates harvested from MRPL47 siRNA treatments **(Figure 4.6)**.

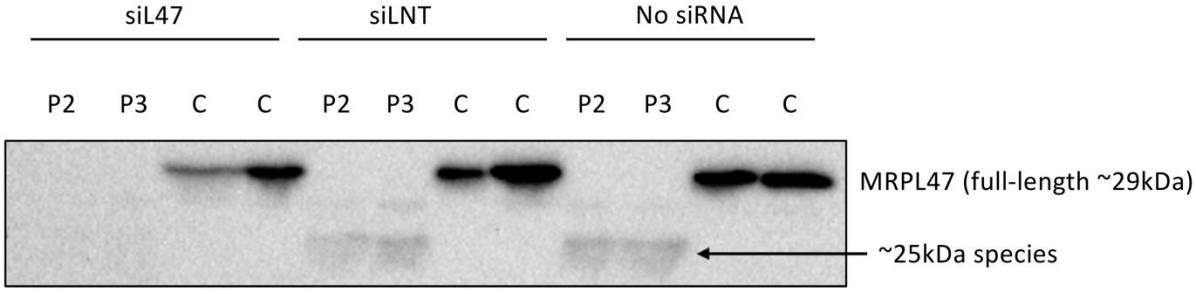

Figure 4.6 Over-exposure of blot with siRNA knockdown of MRPL47 in patient and control fibroblasts. Whole cell lysates of patient and control fibroblasts were harvested following a six-day treatment with MRPL47 or non-targeting siRNA, with no siRNA cells as a second control, were subject to SDS-PAGE and immunblotted for MRPL47 only. A second species corresponding to a 25 kDa MRPL47 protein is present in the lysates taken from patient fibroblasts in the non-targeting and no siRNA conditions only.

Using the commercial antibody, full-length MRPL47 appears on a western blot at approximately 28 kDa. The expected decrease in size resulting from a loss of the final 35 residues of MRPL47 has been estimated using the Science Gateway Protein Molecular Weight Calculator tool

(https://www.sciencegateway.org/tools/proteinmw.htm). Uniprot fasta sequence UniProtKB - Q9HD33 (RM47_HUMAN) was used to calculate the size of full-length and truncated protein. This tool predicted MRPL47 protein corresponding to the full 250 residue sequence to weigh 29.46 kDa and protein generated from a shorter 216 residue sequence to weigh 25.53 kDa **(Figure 4.7)**. Using these predictions, the overall decrease in size resulting from a premature truncation at residue 216 would be 3.93 kDa. The 25 kDA species identified upon over-exposure of blots incubated with MRPL47 antibody is consistent with this estimated size difference **(Figure 4.6)**. This, combined with the decrease in intensity of the bands upon treatment with siRNA targeting *MRPL47* is highly indicative of the truncated version of MRPL47 retaining some stability.

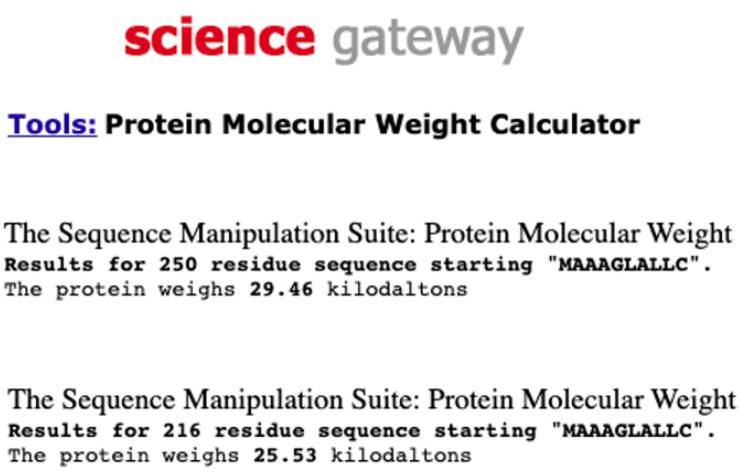

Figure 4.7 Molecular weight predictions of full-length and mutant MRPL47. Science gateway protein molecular weight calculator predictions for sequences corresponding to the 250 residue wild-type MRPL47 protein and a 216 residue truncated MRPL47 protein. Fasta sequence was obtained from the Uniprot website (https://www.uniprot.org/) and corresponds to UniProtKB - Q9HD33 (RM47_HUMAN).

4.3.6 Investigation of MRPL47 assembly within the LSU

Following the identification of the truncated MRPL47 protein stable at low steady-state levels, it was important to ascertain whether this protein retains any function and whether it is incorporated into the LSU of the mitoribosome. Sucrose gradient ultracentrifugation fractionation of samples containing 700 µg of total protein, followed by TCA precipitation of each fraction, was used to address this question. SDS-PAGE of fractions 1-11 and immunoblotting of mitoribosomal subunits determines the sedimentation profiles of the LSU and SSU. DAP3 and MRPL65 antibodies were used to attribute the SSU to fractions 4-5 and LSU to fractions 6-7. Bands corresponding to MRPL47 could be detected in LSU fraction 6 and 7 with low signal strength in comparison to the control **(Figure 4.8)**. This weak signal for MRPL47 was detected at a slightly lower molecular weight in Patient samples when measured using the protein ladder and compared to controls. This confirms that, while severely decreased at the steady-state level, some truncated MRPL47 is successfully assembled within the LSU of the mitoribosome.

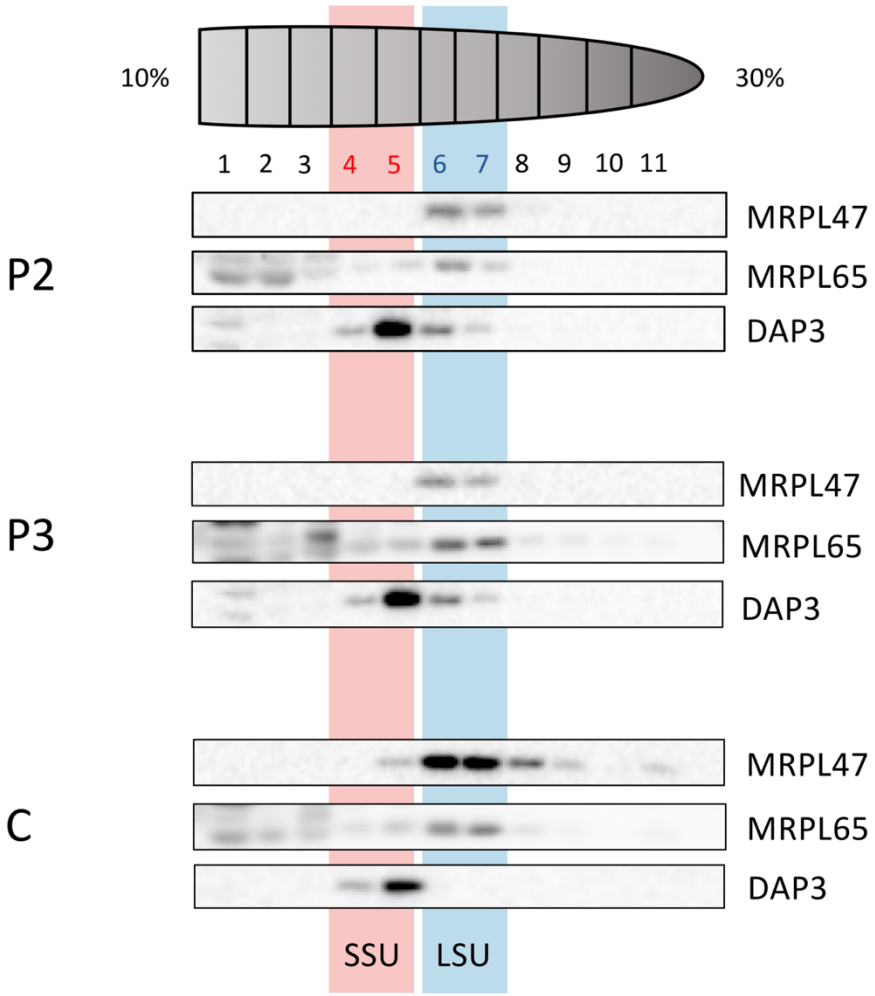

Figure 4.8 Sucrose gradient ultracentrifugation and immunoblotting to investigate MRPL47 in mitoribosome assembly. 700 µg of total protein from the fibroblasts of patients 2 and 3 was separated on a linear 10-30% sucrose gradient. Following ultracentrifugation, eleven fractions were taken and TCA precipitated for protein enrichment, then run on SDS-PAGE gels and immunoblotted for MRPL47, MRPL65 and DAP3. Fractions 4 and 5 (red) contain proteins of the SSU. Fractions 6 and 7 (blue) contain proteins of the LSU. Data shown is representative of two independent repeats.

4.3.7 Investigation into LSU and monosome stability

Further sucrose gradient ultracentrifugation experiments were carried out in order to assess the impact of severely decreased and truncated MRPL47 protein on the stability of the mitoribosomal LSU and monosome. Centrifugation over a longer period of time, followed by the sampling of seventeen fractions allows visualisation of signal corresponding to the monosome alongside the LSU and SSU. The fibroblasts of

Patient 2 consistently exhibit decreased levels of large subunit proteins MRPL3, MRPL37, MRPL12 and MRPL28, within both the LSU and the monosome **(Figure 4.9)**. Immunoblotting for SSU protein MRPS15 reveals no equivalent decrease in the SSU but a comparable decrease in signal in monosomal fractions. These data suggest destabilisation of the LSU and the monosome as a result of the Arg216* MRPL47 mutant protein.

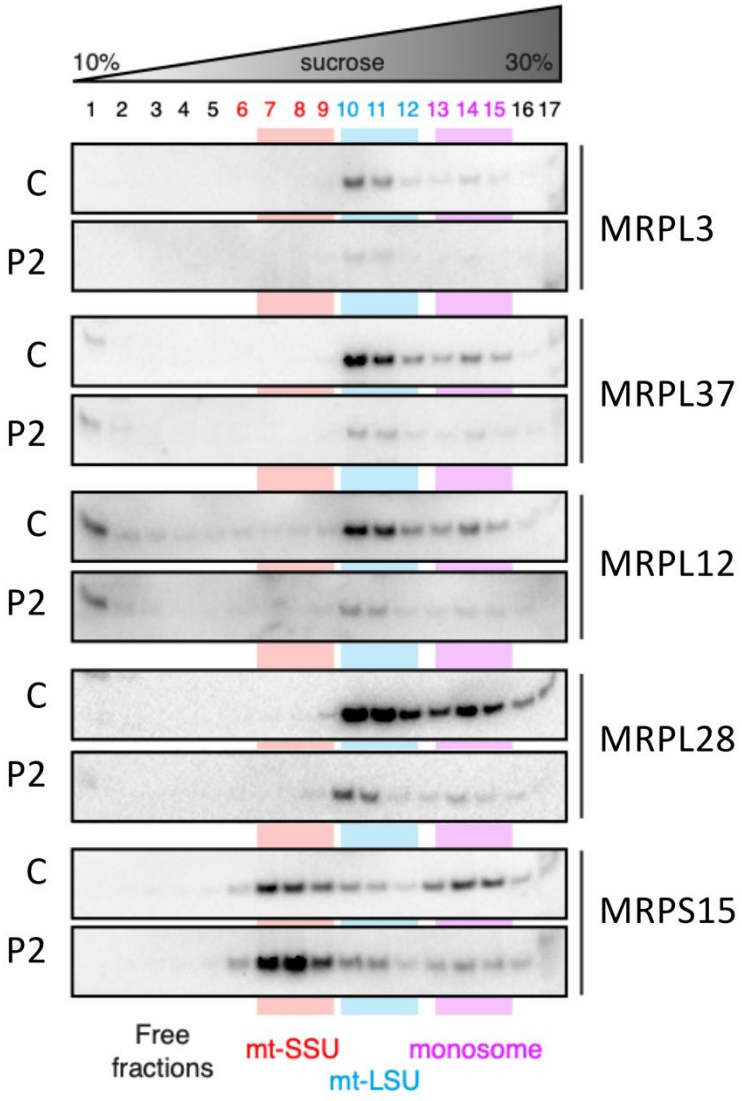

Figure 4.9 Sucrose gradient ultracentrifugation and immunoblotting to investigate LSU and monosome stability. 900 µg of total protein from the fibroblasts of Patient 2 and a control line were separated on a linear 10-30% sucrose gradient. Following centrifugation at 79,000 *g* for 15 hours at 4°C, 17 fractions were taken and subjected to SDS-PAGE. Membranes were immunoblotted for MRPL3, MRPL37, MRPL12, MRPL28 and MRPS15.

4.4 Discussion

The identification of a homozygous c.646C>T (p.Arg216*) variant in three unrelated patients adds to a rare, but growing, number of pathogenic mutations in mitoribosomal proteins. Of the pathogenic variants reported to date in genes encoding mitoribosomal proteins, 14 have been demonstrated to result in a moderate to severe destabilisation and decrease in steady-state levels of the mutant protein (Gardeitchik *et al.*, 2018; Menezes *et al.*, 2015; Miller *et al.*, 2004; Chen *et al.*, 2018; Smits *et al.*, 2011b; Bugiardini *et al.*, 2019; Pulman *et al.*, 2019; Lake *et al.*, 2017; Borna *et al.*, 2019; Galmiche *et al.*, 2011; Serre *et al.*, 2013; Di Nottia *et al.*, 2020; Carroll *et al.*, 2013). In the majority of cases this leads to a destabilisation of the mitoribosomal subunit of which the affected protein is a constituent, and in one *MRPL12* case assembly and stability of both the LSU and SSU is affected (Serre *et al.*, 2013). Interestingly, while variants in all four previously reported LSU genes implicated in mitochondrial disease have resulted in decreased steady-state levels of the affected protein, three of these mutant proteins have been shown to continue be incorporated as a structural component of the mitoribosome (Serre *et al.*, 2013; Di Nottia *et al.*, 2020; Carroll *et al.*, 2013).

While a premature 'stop' codon at MRPL47 residue 216 of 250 results in a complete loss of full length protein **(Figure 4.3)**, a ~25 kDa truncated version of MRPL47 remains stable at very low steady state levels **(Figure 4.6)** and is able to assemble as a structural component of the LSU **(Figure 4.7)**. Despite this, the fibroblasts of patients 2 and 3 exhibit a clear and global defect of mitochondrial translation when subjected to a [^{35}S] metabolic labelling assay **(Figure 4.4)**. This appears be the result of destabilisation of the LSU and mitoribosomal monosome **(Figure 4.9)**, and results in a combined OXPHOS defect affecting subunits of complexes I and IV at the steady-state level **(Figure 4.3)**.

While these data clearly demonstrate the pathogenicity of this novel variant, further work will help to elucidate the precise mechanism underlying the mitochondrial translation defect. At present, it is unclear whether mitoribosomal function is impeded

by a structural impact on the tunnel exit region of the LSU resulting from the incorporation of a truncated version of MRPL47, by decreased availability of mutant MRPL47, or through a combination of both.

To answer this question, I plan to carry out two parallel rescue experiments, over-expressing either wild-type MRPL47 or p.Arg216* mutant MRPL47, in patient fibroblasts. If the translation defect observed in patient fibroblasts can be rescued by over-expression of mutant MRPL47, this would indicate that the pathomechanism is driven primarily by low steady-state levels of MRPL47. If rescue can only be achieved through the expression of wild-type MRPL47, it is most likely that a structural consequence of mutant MRPL47 on the LSU is underpinning this generalised translation defect. It remains possible that both decreased steady-state levels and aberrant folding of MRPL47 within the LSU are contributing to this disorder in translation, in which case one might expect to see a degree of improvement in translation efficiency and restoration of OXPHOS in both rescue experiments.

4.5 Concluding remarks

In conclusion, a novel truncating variant in the *MRPL47* gene has been identified in three unrelated paediatric mitochondrial disease patients presenting in early infancy with overlapping clinical presentations including metabolic acidosis, epilepsy and liver involvement. The data presented within this chapter has demonstrated the impact of this variant on MRPL47 size and stability, confirmed a detrimental impact on the assembly of the LSU and monosome, and revealed a global translation defect that results in a combined OXPHOS defect in patient fibroblasts. These data have assigned pathogenicity to this variant, confirming genetic diagnosis in three families and expanding our current understanding of LSU disorders. Future rescue experiments should be carried out to investigate any impact that truncated MRPL47 might have on the structure of the polypeptide exit site of the mitoribosome.

Chapter 5 : Investigation of novel variants in *MRPL65* encoding a large mitoribosomal subunit

5.1 Introduction

The functional validation of novel and extremely rare disease variants is, for the most part, reliant on the study of patient biopsies and samples. When investigating novel variants to assign pathogenicity it is important to understand the underlying disease pathomechanisms within cells and tissues that are of relevance to the affected patient. However, the acquisition of patient samples for functional testing is not always possible. In such cases, it is important to consider cell line models, or whole-organism options, for the modelling of specific variants in order to obtain evidence of their pathogenicity (Thompson *et al.*, 2019).

5.1.1 CRISPR/Cas9: A genome editing tool

One emerging technique, now extensively used for the generation of cell-line and animal models of disease-causing mutations, is CRISPR/Cas9 genome editing. The CRISPR/Cas system is a naturally occurring adaptive immune response mechanism employed by eubacteria and archaea for the destruction of foreign viral or plasmid DNA or RNA (Horvath and Barrangou, 2010) that has subsequently been modified and optimised for use as a gene-editing tool. CRISPR, standing for Clustered Regularly Interspaced Short Palindromic Repeats, was first identified in 1987 within the genome of *Escherichia coli* as 29 nucleotide repeat fragments of genomic DNA interspaced by 32 nucleotide variable sequence fragments (Ishino *et al.*, 1987). Many of the variable fragments within CRISPR regions were later found to correspond to viral genomic regions (Pourcel, Salvignol and Vergnaud, 2005).

CRISPR associated (Cas) genes, identified due to their proximity to the CRISPR locus (Jansen *et al.*, 2002), encode nucleases with the ability to introduce double strand

breaks (DSBs) in specific and targeted regions of DNA (Garneau *et al.*, 2010). Also adjacent to the CRISPR array is trans activating CRISPR RNA (tracrRNA), that is complimentary to the primary CRISPR array transcript and aids in transcript processing into individual CRISPR RNA (crRNA) molecules carrying ~20 nucleotide sequences complimentary to the target foreign DNA (Deltcheva *et al.*, 2011). The crRNA-tracrRNA complex interacts with the Cas encoded protein to form an active RNA guided nuclease (Karvelis *et al.*, 2013). This ribonuclease complex interacts with a ~2-4 nucleotide protospacer adjacent motif (PAM), lying immediately adjacent to target DNA sequences, where the sequence-specific cleavage is carried out and DSBs are introduced (Mojica *et al.*, 2009). Three different classes of CRISPR/Cas systems exist endogenously, grouped into types I, II and III, based on similarities in the sequences and structures of the constituent Cas proteins (Makarova *et al.*, 2011). The type II CRISPR/Cas system is reliant on a single Cas protein (Cas9) **(Figure 5.1A)**, and has therefore been the most simple to develop into a sophisticated tool for genome editing (Ma, Zhang and Huang, 2014). Cas9 from *Streptococcus pyogenes* possesses two nuclease domains: The HNH domain, for cleavage of the DNA strand complimentary to the crRNA, and the RuvC-like domain for cleavage of the non-complimentary strand (Nishimasu *et al.*, 2014).

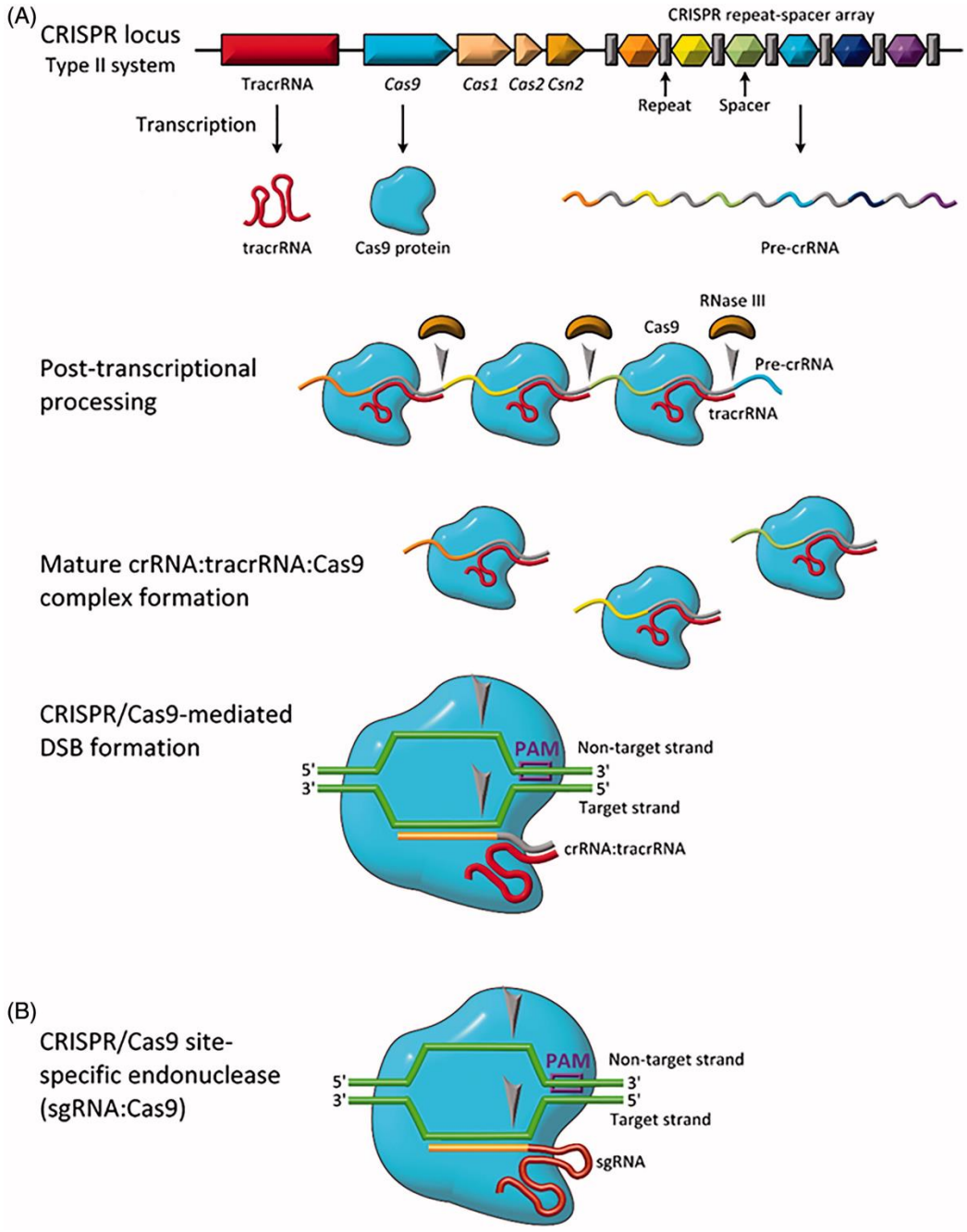

Figure 5.1 Structure and function of the type II CRISPR/Cas9 system. (A) The genomic organisation, transcription processing and assembly of CRISPR/Cas9 elements in an endogenous environment. (B) An engineered CRISPR/Cas9 system used for targeted genome editing directed by a sgRNA. Figure adopted from Lino, Christopher A et al. (2018).

The utilisation of CRISPR/Cas9 as a genome editing tool has been achieved through the design of short guide RNAs (sgRNAs) that encompass both the tracrRNA and crRNA elements of the endogenous CRISPR/Cas system **(Figure 5.1B)** (Jinek *et al.*, 2012). These guide RNA are typically complimentary to genomic DNA 18-24

nucleotides in length, lying adjacent to a 2-4 nucleotide PAM sequence (Zhang, Wen and Guo, 2014). Introduction of a DSB at a precise and targeted region of the nuclear genome triggers a cellular DNA repair by non-homologous end joining (NHEJ) response. NHEJ is an error-prone process and can therefore result in the introductions of insertions and deletions (indels) at the site of DSB repair which have the potential to disrupt or eliminate gene function to generate target gene knock-outs (Iliakis *et al.*, 2004).

Delivery of a CRISPR/Cas9 system into model systems can be achieved via three main routes: A delivery plasmid encoding both the Cas9 nuclease and a guide RNA, a mixture of separate mRNAs encoding the Cas9 nuclease and a guide RNA or a delivery of a Cas9 protein and guide RNA formed as a ribonuclease complex (Lino *et al.*, 2018). The applications of CRISPR/Cas9 technology, both as a basic science research tool and as a therapeutic approach, are continuously expanding (Rodriguez-Rodriguez *et al.*, 2019).

5.1.2 CRISPR/Cas9 studies in mitochondrial research

In the field of mitochondrial research, genome-wide CRISPR/Cas9 death screens and CRISPR interference (CRISPRi) screens have been utilised for the identification and annotation of genes encoding proteins previously unknown to be essential to OXPHOS and energy metabolism (Arroyo *et al.*, 2016; Mendelsohn *et al.*, 2018). Knock-out models of nuclear genes associated with mitochondrial disease are shown to be extremely useful in instances when samples of clinically affected tissues are scarce. Induced pluripotent stem cell (iPSC) lines have been used in the generation of *DGOUK* CRISPR/Cas9 knockout cells. The *DGOUK* gene encodes a mitochondrial kinase required for the phosphorylation of purine deoxyribonucleosides. Patients with DGOUK deficiencies suffer from mitochondrial depletion, often manifesting as progressive liver disease. Differentiation of *DGOUK* CRISPR/Cas9 knockout iPSCs into hepatocyte-like cells has enabled the study of mitochondrial dysfunction and the application of drug screens within a clinically relevant cell type (Jing *et al.*, 2018).

5.1.3 *MRPL65*: A mitoribosomal LSU gene

As discussed in **4.1.3**, pathogenic variants in genes encoding proteins of the mitoribosomal LSU remain extremely rare, with only four LSU genes implicated in mitochondrial disease to date (Galmiche *et al.*, 2011; Carroll *et al.*, 2013; Serre *et al.*, 2013; Di Nottia *et al.*, 2020). Detailed within this chapter are investigations into the molecular mechanism underpinning disease in two unrelated paediatric mitochondrial disease patients harbouring novel variants in the *MRPL65* gene which were deemed to be the likely cause of the patients' clinical presentation. A lack of available patient biopsy material has driven a need to generate an *MRPL65* knockout cell line and this work will focus on the use of a CRISPR/Cas9 genome editing system to achieve that goal. Having previously been believed to be a constituent of the SSU named *MRPS30,* the name of this gene was recently changed to *MRPL65*. Cryo-EM studies of mitoribosomal structure revealed that MRPL65 protein forms a heterodimer with homologous MRPL37, together occupying a void left behind after the evolutionary loss of LSU ribosomal RNA domain III (Brown *et al.*, 2014).

5.2 Patient reports

5.2.1 Patient 1

This female patient was the second child of healthy, non-consanguineous, Lebanese parents. The patient was healthy at birth, but developed jerky eye movements at the age of 2 weeks, which, by the age of 2 months, progressed to nystagmus with poor tracking. An eye examination revealed bilateral optic nerve atrophy. The patient demonstrated axial hypotonia and worsening dystonic limb movements. By 6 months the patient had developed myoclonic limb jerks, which over the course of one month progressed into infantile spasms. At the age of 1 year, she exhibited oromandibular dyskinesia with snouting and tongue thrusting movements. The patient's hypotonia worsened significantly and she developed severe muscle weakness. Head growth was poor, falling off the centiles, and the patient had poor feeding. Lactate was elevated at 6.98mmol/L (normal <2.5mmol/L). The patient died at 3 years of age.

The older sister of the index patient died after exhibiting clinical findings very similar to those described above. Histochemical analysis of a muscle biopsy was carried out in a laboratory at the American University of Beirut at the time and reported to demonstrate COX deficiency, however no tissue has been available for further analysis. Brain MRI was reported as normal.

Diagnostic WES of Patient 1, and a deceased sibling, carried out at Centogene (https://www.centogene.com), identified compound heterozygous variants in the *MRPL65* gene (NCBI Reference Sequence: NM_016640.3). One of the variants, c.(601+5G>A) is a single base substitution located 5 nucleotides into the first intron of *MRPL65* and is therefore predicted as likely to impact splicing. This variant has a CADD score of 21.9, indicating it is in the top 1% of possible damaging single nucleotide variants in the human genome. The second variant is a nonsense mutation, c.(382G>T), resulting in a premature 'stop' codon (p.Glu128*) at amino acid 128 of 439 **(Figure 5.2)**. This variant has a CADD score of 34, indicating it is in the top 0.1%

of deleterious possible mutations. Both of these variants are absent from the gnomAD population database. This patient was referred by Dr.Rose-Mary Boustany and Dr.Rolla Shbarou, Department of Pediatrics and Adolescent Medicine, American University of Beirut.

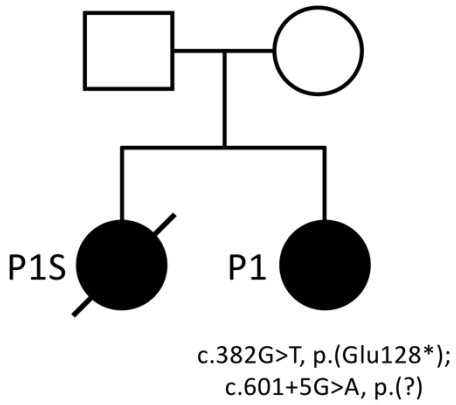

Figure 5.2 Familial pedigree of *MRPL65* Patient 1. Familial pedigree to demonstrate the recessive inheritance of compound heterozygous c.382G>T, p.(Glu128*); c.601+5G>A, p.(?) *MRPL65* variants.

5.2.2 Patient 2

This male patient is the second child of healthy, unrelated parents, both of Lebanese ethnic origin and investigated in the US. The parents of Patient 2 had experienced three prior miscarriages. The patient first presented at 18 months of age with an unsteady gait. A progressive ataxia has persisted throughout childhood, alongside a tremor and mild global developmental delay while optic atrophy and nystagmus were noted in later childhood. Repeat brain MRI studies revealed a progressive cerebellar atrophy and nerve conduction studies identified diffuse axonal sensory neuropathy. The patient is currently alive at 12 years of age. Diagnostic WGS of Patient 2 identified a homozygous c.(601+5G>A) variant in the *MRPL65* gene **(Figure 5.3),** the same splice variant identified in Patient 1. This patient was referred by Dr.Vinod Misra and Mitchell Cunningham, Division of Genetics and Metabolic Disorders, Children's Hospital of Michigan.

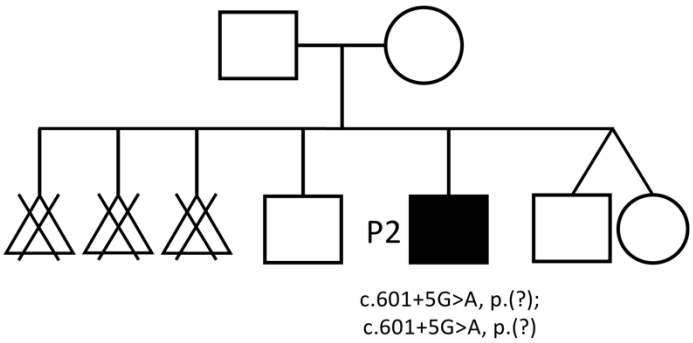

Figure 5.3 Familial pedigree of *MRPL65* Patient 2. Familial pedigree to demonstrate the recessive inheritance of homozygous c.601+5G>A, p.(?) *MRPL65* variants in Patient 2.

5.3 Results

5.3.1 *MRPL65* cDNA studies in Family 1

Given that the truncating *MRPL65* variant present in Patient 1 occurs less than one third of the way into the protein, it is very unlikely to lead to the synthesis of functional MRPL65 protein. Two PCR primer pairs were designed to investigate the impact of the second *MRPL65* variant, c.(601+5G>A), on splicing. The first pair was designed to amplify exons 1-2, and the second to amplify exons 1-4 producing 673bp and 915bp products respectively (**Figure 5.4**). These experiments were conducted using RNA extracted from fixed tissue of Patient 1 and their deceased sibling, which had been shipped to the Newcastle Highly Specialised Mitochondrial Diagnostic Service.

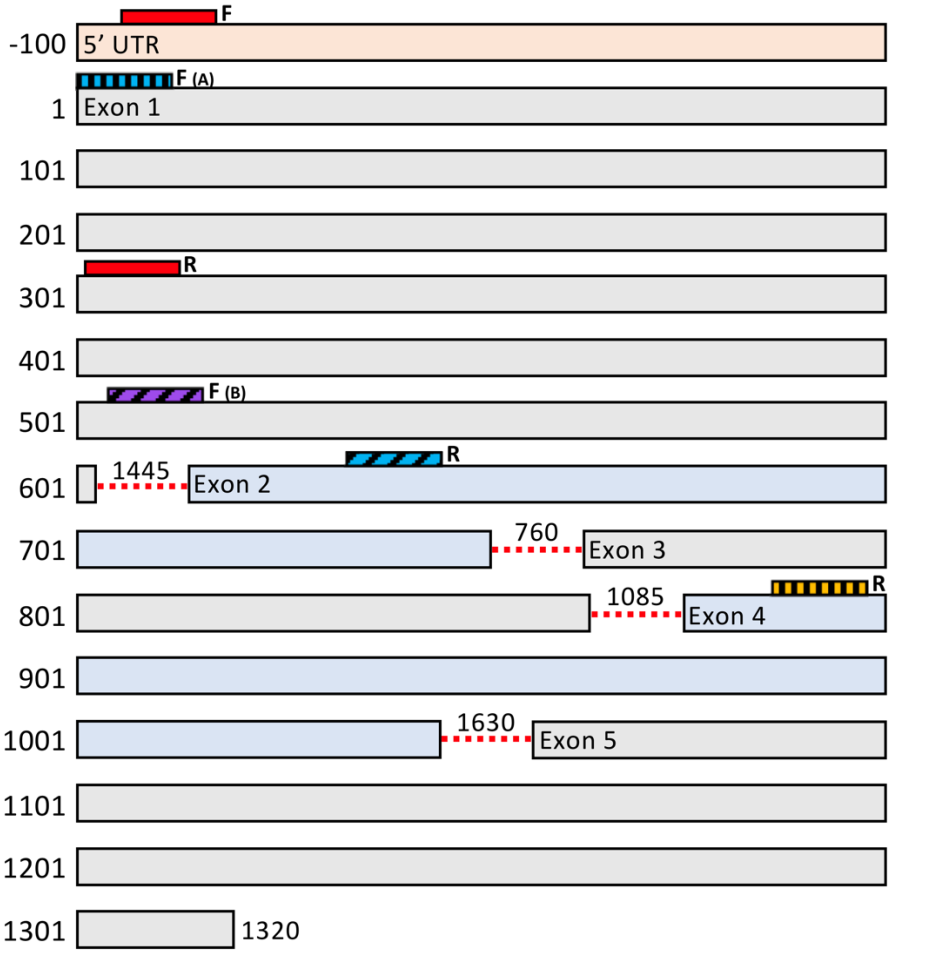

Forward	Reverse	Target Region	Product Size (bp)
		5' UTR Forward - Exon 1 Reverse	401
		Full Forward – Exon 2 Reverse	915
		Exon 1 Forward – Exon 2 Reverse	143
		Full Forward – Exon 4 Reverse	673

Figure 5.4 Schematic of *MRPL65* primers and expected PCR product. Binding sites of each primer targeting *MRPL65* and the size of PCR products resulting from specific primer pairs used throughout chapter. Intronic regions are depicted with red dashed line.

Following reverse transcription and second strand synthesis of cDNA, neither primer pair were able to amplify *MRPL65* product in patient samples**(Figure 5.5).** Both primer

pairs successfully amplified *MRPL65* using cDNA generated from control RNA samples. Patient samples were successfully used as controls for cDNA studies of other genes within the diagnostic service, suggesting that the c.(601+5G>A) variant may result in *MRPL65* aberrantly spliced mRNA transcripts that are targeted for nonsense mediated mRNA decay.

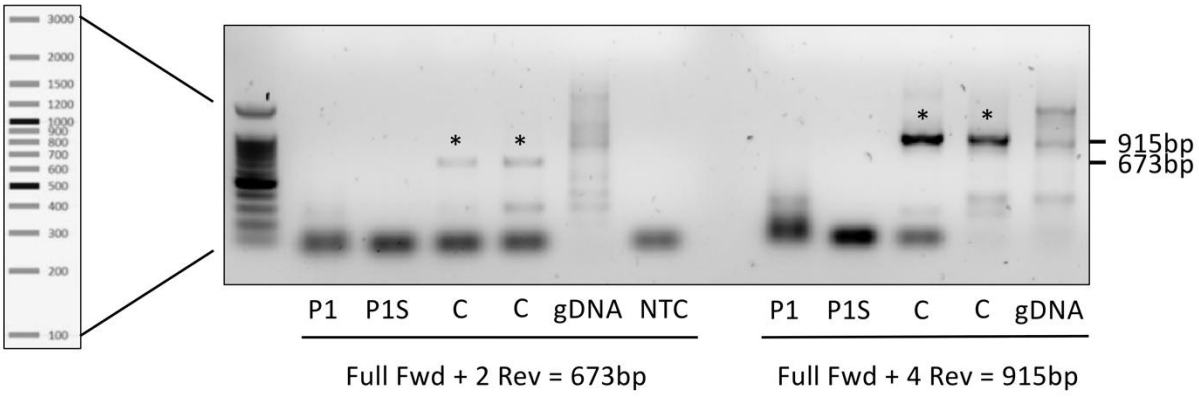

Figure 5.5 cDNA studies in Family 1. RNA samples of Patient 1 (P1) and an affected sibling (P1S) were used for reverse transcription and second strand synthesis to investigate the potential impact of a c.(601+5C>A) variant on splicing of *MRPL65* mRNA transcripts. Two primer pairs were used for the PCR amplification of exons 1-2 (left panel) and exons 1-4 (right panel). Asterisks indicate cDNA bands corresponding to correctly sized PCR products in control samples.

5.3.2 MRPL65 knockdown in U2OS control cells

No skin or tissue biopsies from Patient 1 have been available for further investigation into the effect of these compound heterozygous *MRPL65* variants on mitochondrial function. Due to the inherent pathogenic nature of the truncating variant and the apparent absence of *MRPL65* cDNA, knock-down of MRPL65 expression was carried out to assess the impact of decreased MRPL65 in U2OS cells. Cells treated with an MRPL65 siRNA smart-pool, containing siRNA molecules targeting four different regions of *MRPL65* sequence, demonstrate almost undetectable steady-state levels of COXI and COXII, while NDUFB8 and CORE2 are also decreased **(Figure 5.6)**. This indicates that decreased abundance of MRPL65 protein results in a severe combined OXPHOS defect affecting complexes I, III, and IV. The combined OXPHOS deficiency

is likely to be the result of impaired mitoribosomal function leading to a defect of mitochondrial translation.

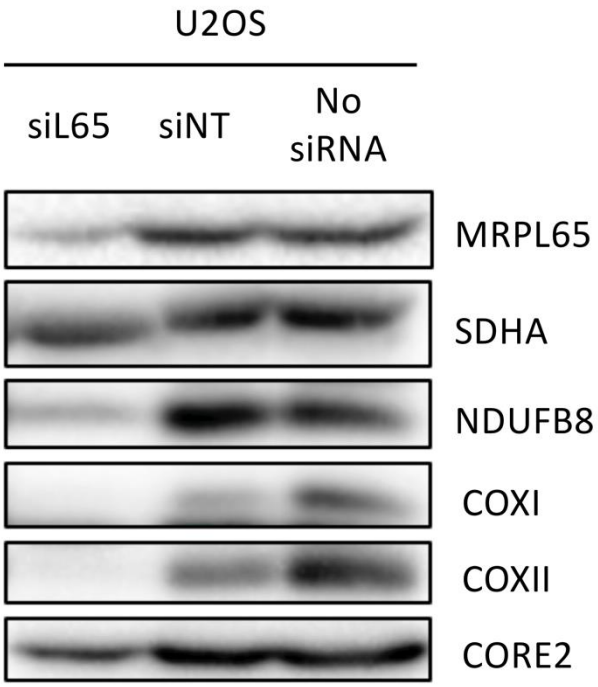

Figure 5.6 Western blot analysis of MRPL65 knock-down U2OS cells. Whole cell lysates from U2OS cells treated with an MRPL65 siRNA smart pool, U2OS cells treated with a non-targeting siRNA and an untreated U2OS control. MRPL65 antibody was applied to confirm successful knock-down. Antibodies detecting SDHA, NDUFB8, COXI, COX II and CORE2 were used to investigate the impact of MRPL65 knockdown on OXPHOS. Data shown is representative of three independent repeats.

5.3.3 Generating an *MRPL65*-targeting PX458 CRISPR/Cas9 plasmid

Due to the clear and very severe, steady-state OXPHOS protein defect resulting from MRPL65 knock-down, and given the lack of available patient cell lines, I decided to generate a MRPL65 CRISPR/Cas9 knockout cell line as the best approach to investigate the potential mechanisms underlying disease in Family 1. As neither *MRPL65* variant carried by patient 1 is missense (being a splice variant and a loss of function truncating variant) an *MRPL65* knock-out cell line was thought to be the best representative model of the combined functional consequences of these two variants. A PX458 plasmid expressing Cas9 from *Streptococcus pyogenes*, 2A-EGFP, and with a cloning backbone for sgRNA insertion was purchased from Addgene. In order to target the Cas9 nuclease to *MRPL65,* four sgRNA sequences were designed for subsequent insertion into the PX458 plasmid through backbone cutting and ligation reactions. Competent DH5α cells were transformed using PX458 inserted with each of the four sgRNA oligos. DH5α clonal colonies were grown from populations transformed with sgRNAs 1, 2 and 4 plasmids, and plasmid DNA isolated. Double restriction digests, using *BbsI* and *EcoRI* restriction enzymes were used to identify plasmids in which sgRNA insertion had been successful. The PX458 plasmid contains one *BbsI* restriction site and two *EcoRI* restriction sites. Insertion of a short guide sequence destroys the PX458 *BbsI* restriction site, resulting in only two digestion products identifiable upon gel electrophoresis. If short guide insertion has not occurred, the plasmid will be digested at the *BbsI* restriction site along with the *EcoRI* site, resulting in three digestion products **(Figure 5.7)**.

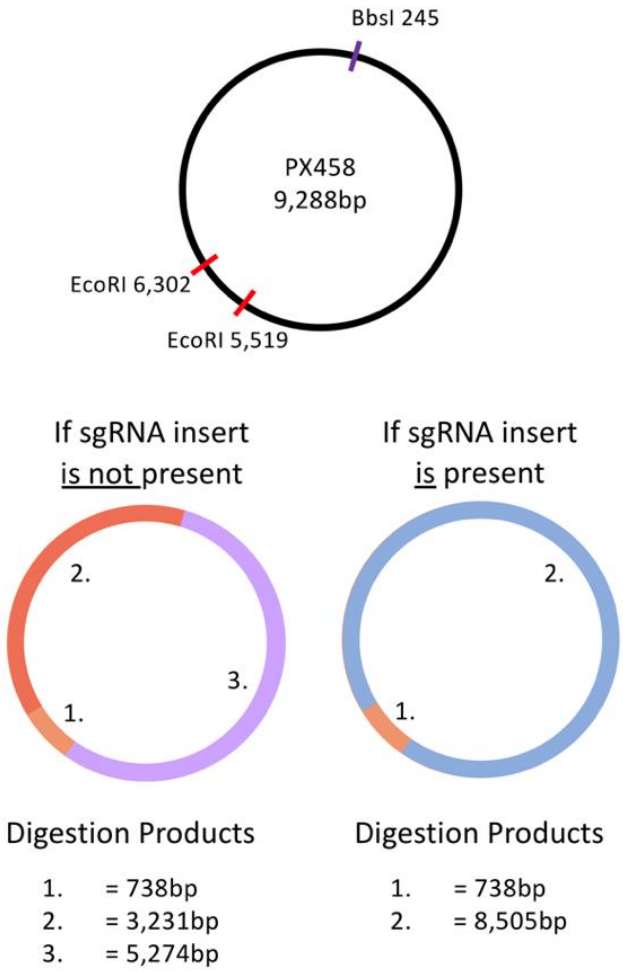

Figure 5.7 Diagram depicting test digest of PX458 plasmid. Px458 plasmids contain a single *BbsI* restriction site and two *EcoRI* restriction sites. *BbsI* was used for backbone cutting for sgRNA insertion. When incubated with *BbsI* and *EcoRI*, sgRNA negative plasmids will be cut into three linear products at 738bp, 3,231bp and 5,274bp in length. The *BbsI* restriction site is destroyed in sgRNA positive plasmids, resulting in only two linear digestion products at 738bp and 8,505bp in size.

Double restriction digests demonstrated that all but one of the purified sgRNA-inserted plasmids were successful. Samples from three clones of PX458 sgRNA 1, two clones of PX458 sgRNA 2 and one clone of PX458 sgRNA 4 each generated two digestion products at 738 and 8,505 base pairs in length. Sample from clone 3 of PX458 sgRNA 2 generated two incorrectly sized bands, indicating that insertion of sgRNA 2 had not been achieved **(Figure 5.8)**.

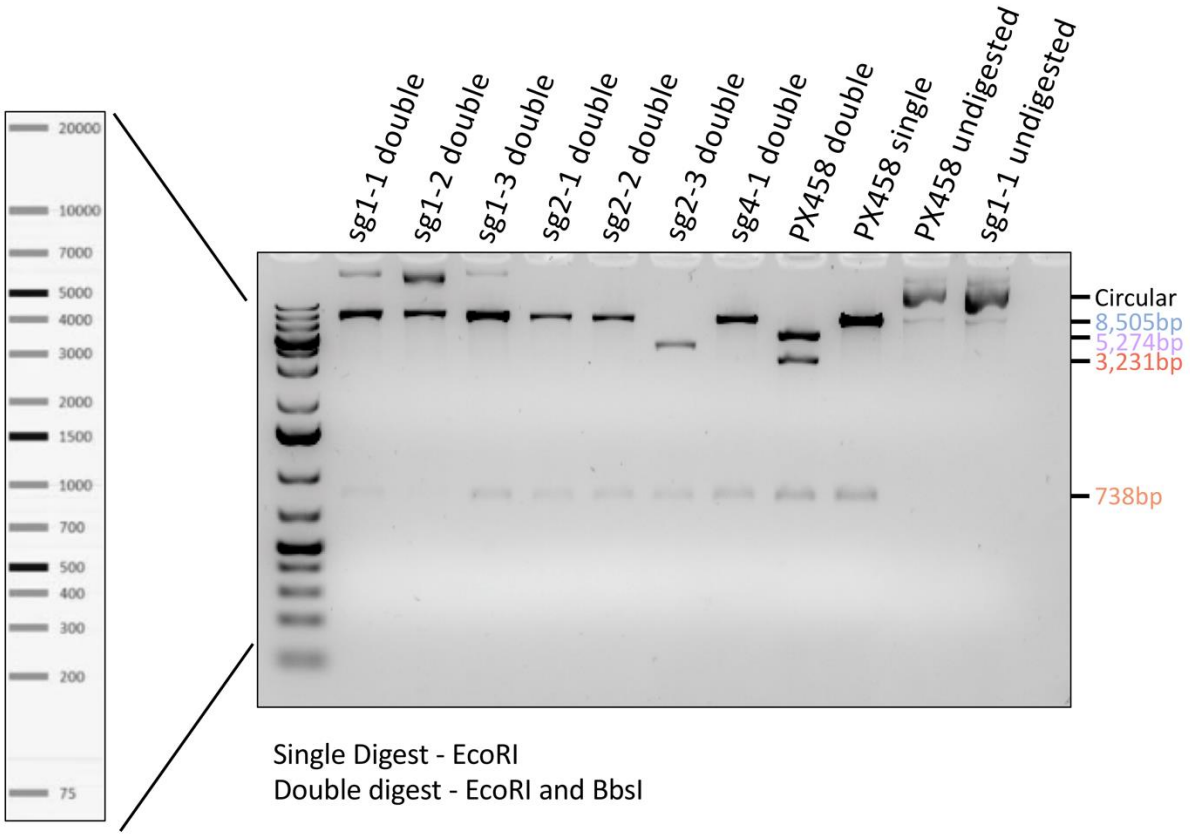

Figure 5.8 Test digest identification of sgRNA positive PX458 plasmids. Product from test double digests of miniprep purified sgRNA-inserted PX458 plasmid DNA and unmodified PX458 plasmid DNA. Single digest unmodified plasmid, undigested unmodified plasmid and undigested sgRNA1-inserted PX458 plasmid were used as negative controls.

5.3.4 Sequencing the *BbsI* region of PX458 plasmid

Sequencing of each sgRNA positive clone was undertaken to check that each full short guide had been inserted without the introduction of any sequence errors. A primer pair targeting the *BbsI* restriction site region of the PX458 plasmid was used for PCR and Sanger sequencing to confirm the presence of each sgRNA sequence **(Figure 5.9)**.

An sgRNA positive clone was confirmed for sgRNAs 1, 2 and 4, each of which were used for the nucleofection of wildtype U2OS cell populations alongside nucleofection of a single U2OS cell population a pmaxGFP Vector as a control. As both the PX458 plasmid and the pmaxGFP control vector express GFP, each transfected population

was sorted into single cell populations using flow cytometry selecting for cells with GFP fluorescence.

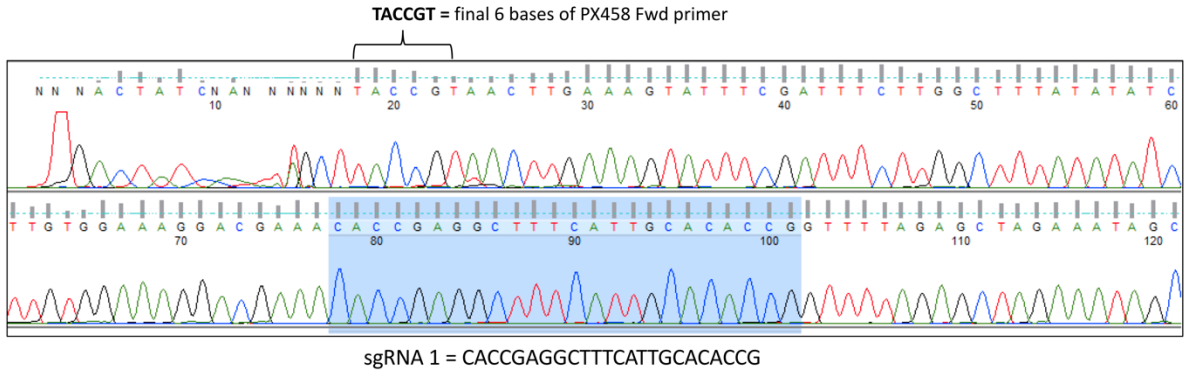

Figure 5.9 Example sequence confirmation of error-free sgRNA 1 insertion into PX458 plasmid. The *BbsI* restriction region of each sgRNA positive PX458 plasmid was sequenced in order to confirm the error-free insertion of full short guide sequences. Sequence traces were searched for the entire sgRNA sequence (highlighted in blue) using FinchTV software.

5.3.5 PCR screens of transfected U2OS clones

PCR screens of *MRPL65* exon 1 were carried out on all clonal populations grown from each single sorted cell to identify clones that generate bands of a different size to isogenic control GFP clones and control genomic DNA, indicating insertions or deletions in *MRPL65*. Lanes containing multiple bands were noted as containing likely heterozygous mutants (red), lanes containing single bands that looked larger or smaller than control bands were noted as possible homozygous mutants (blue) and lanes containing bands identical to control were noted as possible wild-type clones (green) **(Figure 5.10)**.

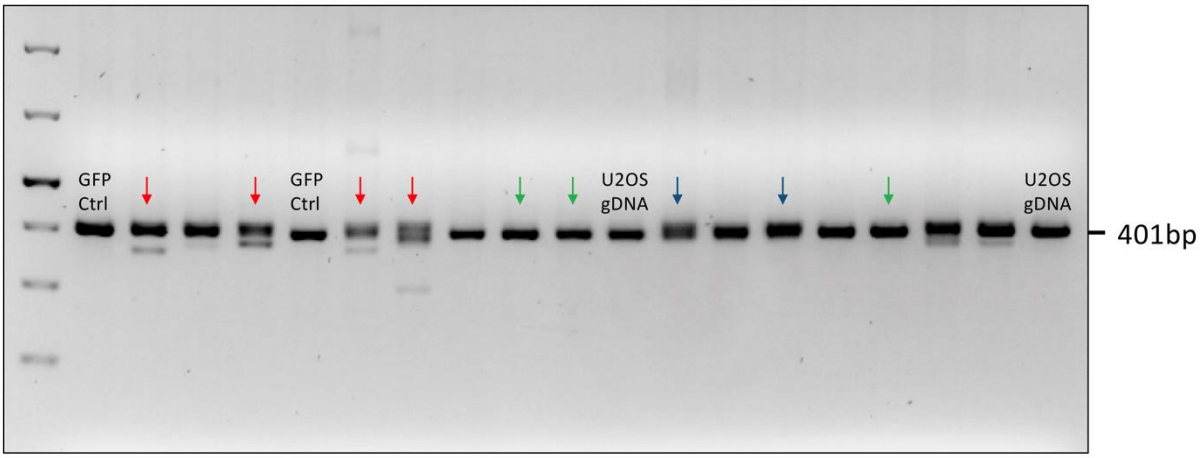

Figure 5.10 PCR screening of post-transfection U2OS clonal populations. Genomic DNA was extracted from each post-transfection clonal population for PCR using primers targeting *MRPL65* exon 1. Samples of genomic DNA extracted from U2OS cells transfected with pmaxGFP vector and wildtype U2OS cells were used as controls. PCR products were run on long 3% agarose gels to maximise resolution between bands with subtle differences in size. Red arrows indicate likely heterozygous mutants that exhibit two *MRPL65* bands of different sizes. Blue arrows depict possible homozygous mutants that run as a single band of a different size to controls. Green arrows highlight suspected wildtype clones that appear to run as bands identical in size to controls. This gel illustrates the PCR screening of 15 out of a total of 96 screened clones.

5.3.6 Sequencing *MRPL65* to identify mutant clones

A total of 18 clones, six targeted with each sgRNA, were selected from the PCR screens for Sanger sequencing of *MRPL65* exon 1. Both suspected mutants and suspected wild-type clones were sequenced. Sequence data demonstrated the introduction of mutations in 12 of the 18 clones and confirmed each sgRNA to be successful in targeting the Cas9 nuclease to exon 1 of *MRPL65.* However, no homozygous mutants were identified. Example chromatograms are shown in **(Figure 5.11, Figure 5.12** and **Figure 5.13)**.

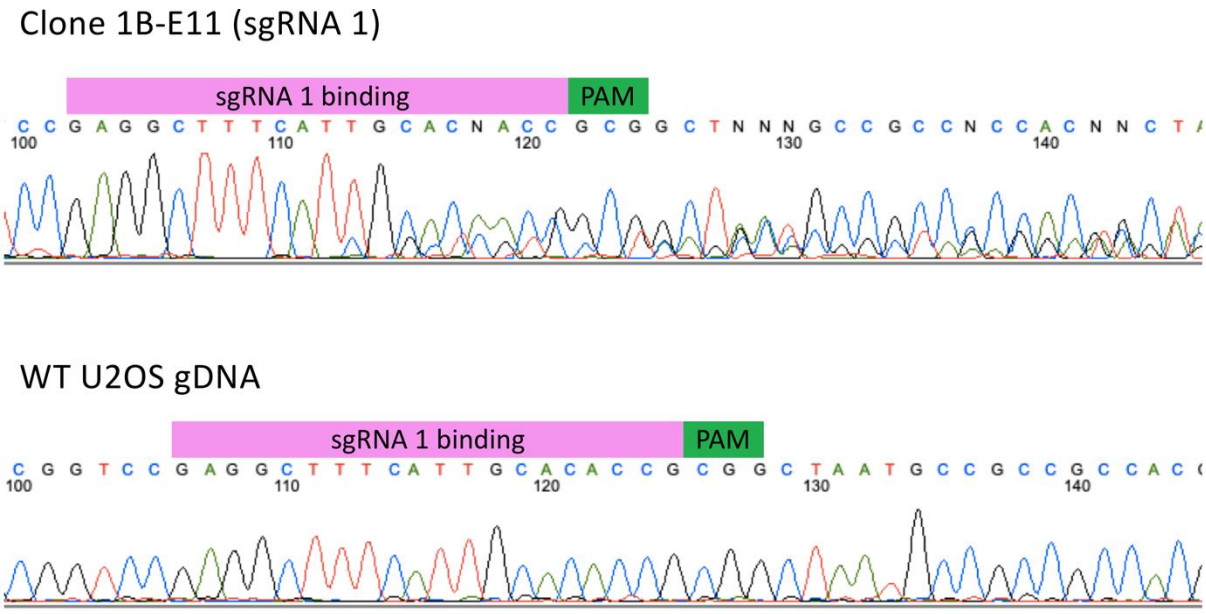

Figure 5.11 Example sequence confirmation of sgRNA 1 targeted *MRPL65* mutation. Sanger sequencing of clone 1B-E11, generated through transfection with sgRNA 1 positive PX458 plasmid, identified the introduction of mutations at the site of sgRNA 1 binding proximal to the PAM site. The resulting sequencing file contains multiple frameshift traces that are not clear enough to resolve the precise nature of the mutations. As neither trace appeared to correspond to wild-type *MRPL65* sequence, this clone was classified as a bi-allelic mutant. Sequence data for wild-type genomic U2OS DNA is provided as a control.

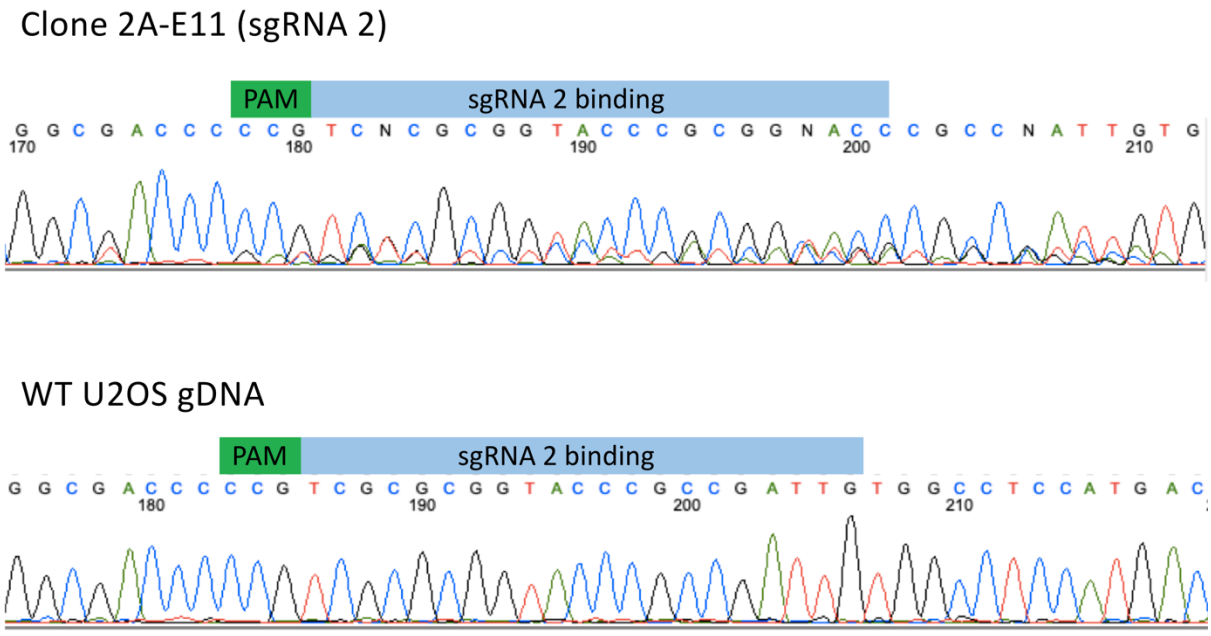

Figure 5.12 Example sequence confirmation of sgRNA 2 targeted *MRPL65* mutation. Sanger sequencing of clone 2A-E11, generated through transfection with sgRNA 2 positive PX458 plasmid, identified the introduction of mutations at the site of sgRNA 2 binding proximal to the PAM site. Two sequence traces are visible at this site, one of which corresponds to wild-type *MRPL65* indicating this clone to be a mono-allelic mutant. Sequence data for wild-type genomic U2OS DNA is provided as a control.

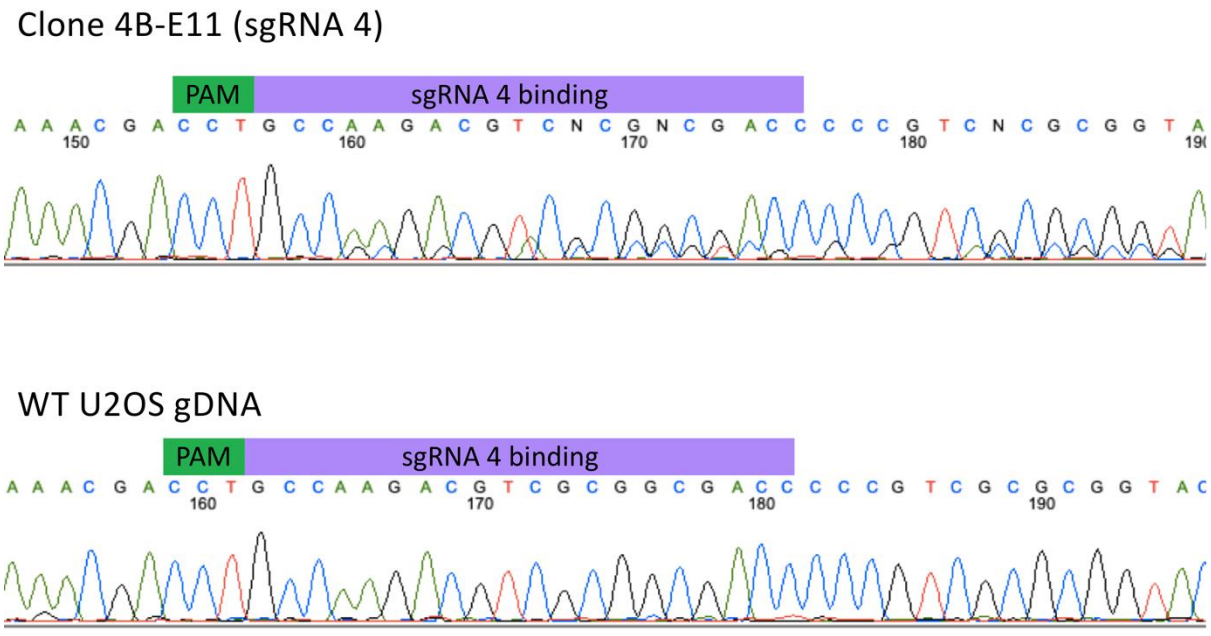

Figure 5.13 Example sequence confirmation of sgRNA 3 targeted *MRPL65* mutation. Sanger sequencing of clone 4B-E11, generated through transfection with sgRNA 4 positive PX458 plasmid, identified the introduction of mutations at the site of sgRNA 4 binding proximal to the PAM site. Two sequence traces are visible at this site, one of which corresponds to wild-type *MRPL65* indicating this clone to be a mono-allelic mutant. Sequence data for wild-type genomic U2OS DNA is provided as a control.

While unable to assign precise genotypes, clones exhibiting sequence traces that corresponded to multiple mutant alleles were classified as ‘bi-allelic mutants’ **(Figure 5.11)** while clones that still displayed one clear wild-type trace were classified as ‘mono-allelic mutants’ **(Figure 5.12, Figure 5.13)**.

5.3.7 Western blot analysis of U2OS clones

In order to identify any successful knock-out clones, six clones were grown for cell lysis and western blotting to investigate the steady state levels of MRPL65. Two bi-allelic and two mono-allelic mutants were investigated, alongside two wild-type clones as isogenic controls. Despite the introduction of suspected deleterious mutations, surprisingly all the mutant cell lines failed to demonstrate the loss of steady-state MRPL65 levels **(Figure 5.14)**.

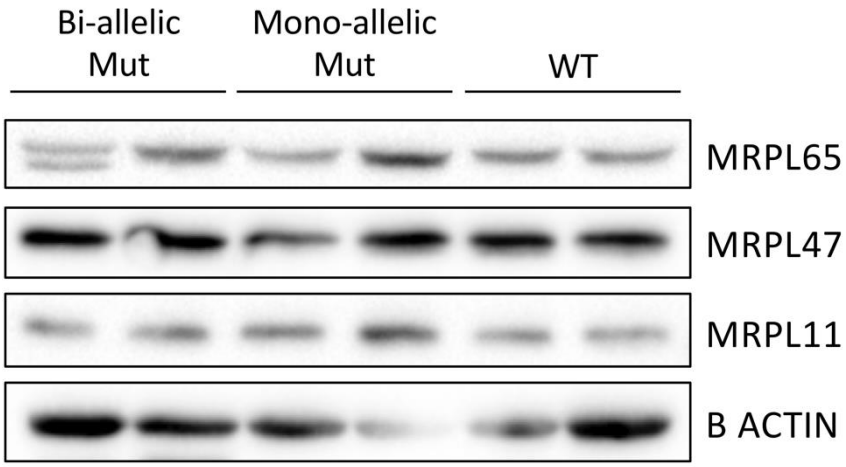

Figure 5.14 Western blot analysis of mitoribosomal proteins in U2OS CRISPR clones. Whole cell lysates were generated from two ‘bi-allelic’ and two ‘mono-allelic’ mutant clones, alongside two clones with a wild-type genotype (confirmed through Sanger sequencing) as isogenic controls. SDS-PAGE and Immunoblotting with MRPL65 antibody was carried out in an attempt to identify a knock-out clone. Antibodies for two other LSU proteins MRPL47 and MRPL11 were also interrogated; Beta-actin was used as a loading control.

One bi-allelic mutant appeared to have two bands corresponding to MRPL65 protein, however, none of the mutants appeared to have decreased levels of other LSU proteins **(Figure 5.14)**, or any protein subunits of OXPHOS complexes **(Figure 5.15)**.

This suggests that, in addition to there being no successful complete knock-out of *MRPL65*, the mutations introduced in each clone did not have any deleterious effects on MRPL65 function or downstream impact on the LSU and OXPHOS.

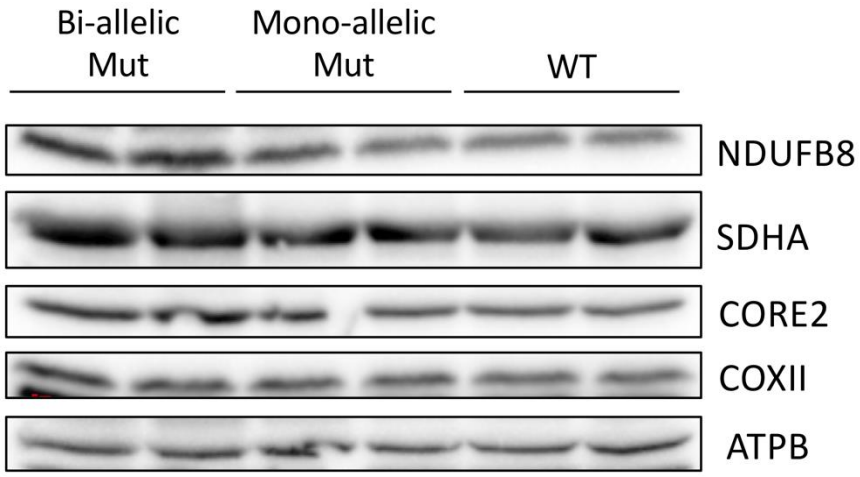

Figure 5.15 Western blot analysis of OXPHOS proteins in U2OS CRISPR clones. Whole cell lysates were generated from two suspected 'bi-allelic' and two suspected 'mono-allelic' mutants alongside two clones with wildtype genotype. SDS-PAGE and immunoblotting with NDUFB8, SDHA, CORE2, COXII and ATPB was used to interrogate the steady state levels of protein subunits of complexes I-IV. SDHA was used as an indication of equal loading.

5.3.8 SNP genotyping of WT U2OS cells

The *MRPL65* gene is located on the P arm of Chromosome 5 (cytogenetic band 5p12). In order to identify any aneuploidy affecting this region within the clones, genomic DNA was extracted from wildtype U2OS cells and sent for single nucleotide polymorphism (SNP) genotyping, kindly carried out by Dr.Simon Zwoliński at the NHS Northern Genetics Service, International Centre for Life, Newcastle upon Tyne. DNA was analysed for 850,000 SNPs using the Illumina CytoSNP-850K v1.2 BeadChip microarray. The results from this array revealed the U2OS population to have an extremely abnormal karyotype, consistent with the known genome instability of cancer derived cell lines, with no fully diploid chromosomes. Copy number across Chromosome 5 was determined using the LogR ratio as a function of B-allele frequency. The entire P arm of Chromosome 5 is within a region of tetraploidy,

meaning that there are four copies of all genes encoded within this region, including the *MRPL65* gene **(Figure 5.16)**.

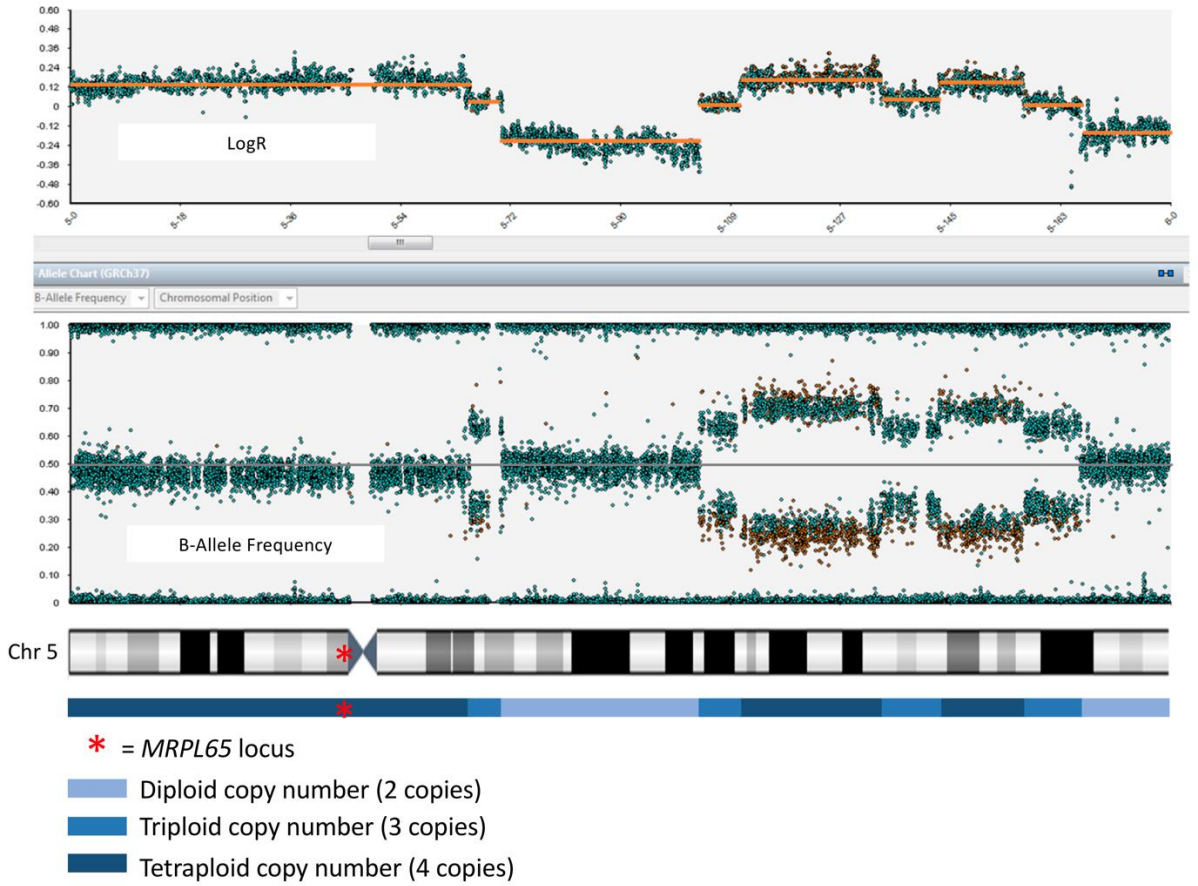

Figure 5.16 SNP genotyping of Chromosome 5 in a wildtype population of U2OS cells. Log R ratio and B-allele frequency across the entirety of Chromosome 5 allows the identification of copy number changes. Areas of homozygosity have B-allele frequencies of either 1 or 0. Areas of allelic balance and heterozygous SNPs have B-allele frequencies of 0.5. Regions of allelic imbalance will have intermediate value B-allele frequencies. LogR ratio corresponds to normalised measure of total probe intensity of all alleles at each given SNP. If a duplication is present, LogR ratio increases. The region of Chromosome 5 containing the *MRPL65* gene has a B-allele frequency indicating balanced heterozygosity and an increased LogR ratio to indicate duplication. From this, the copy number variation of the region is determined as tetraploidy.

To obtain a complete *MRPL65* knock-out cell line using this population of U2OS cells, all four *MRPL65* alleles must be targeted by the Cas9 nuclease to achieve gene disruption through NHEJ. If the starting population of cells had been diploid in this region of Chromosome 5, introduction of indels into all *MRPL65* alleles would be much more likely.

5.3.9 PCR screens of transfected HEK293 clones

Due to the tetraploidy region identified in Chromosome 5 encompassing the *MRPL65* gene in U2OS cells, HEK293 cells were chosen as a second cell line to transfect with each sgRNA positive PX458 plasmid. Cells were GFP sorted and single cell clonal populations were grown. PCR screening of HEK293 clones using primers to amplify exon 1 of *MRPL65* revealed multiple clones producing three bands **(Figure 5.17)**. This indicates that the wild-type HEK293 population are also subject to a copy number duplication in the region of Chromosome 5 containing the *MRPL65* locus.

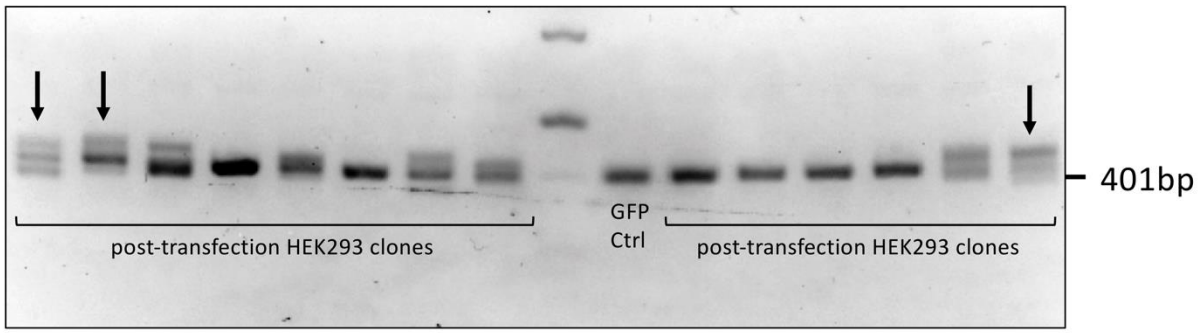

Figure 5.17 PCR screening of post-transfection HEK293 clonal populations. Genomic DNA was extracted from each post-transfection HEK293 clonal population for PCR using primers targeting *MRPL65* exon 1. Genomic DNA extracted from HEK293 cells transfected with pmaxGFP vector was used as an isogenic control. PCR products were run on long 3% agarose gels to maximise resolution between bands with subtle differences in size. The presence of double bands and shifts in product size confirmed the successful sgRNA targeting of Cas9 to *MRPL65* in this cell population. A number of clones ran with three bands (black arrows), suggesting that *MRPL65* is within a region of duplication on HEK293 Chromosome 5.

To acquire the precise karyotype of the wild-type HEK293 cells used for transfection, genomic DNA was once again extracted and sent for SNP genotyping. Copy number analysis confirmed that the 5p12 region in this cell line was also aneuploid, this time lying within a 50Mb region of triploidy.

5.3.10 PCR screens of second round transfected HEK293 clones

Following the confirmation of a triploid *MRPL65* copy number, three suspected mutant HEK293 clones from the first PCR screen were selected for a second round of nucleofection. Each clone was transfected with a plasmid containing the same sgRNA sequence as its original transfection, to increase the likelihood of targeting only wildtype alleles. As above, transfected cells were sorted into single cell wells to obtain clonal populations. However, the recovery rate of these cells was very low and attempts to extract DNA from these populations were often unsuccessful due to very limited cell survival within each well. PCR screens were conducted where possible on surviving cells to identify clones with bands that differed in size to the pmaxGFP vector transfected control **(Figure 5.18)**.

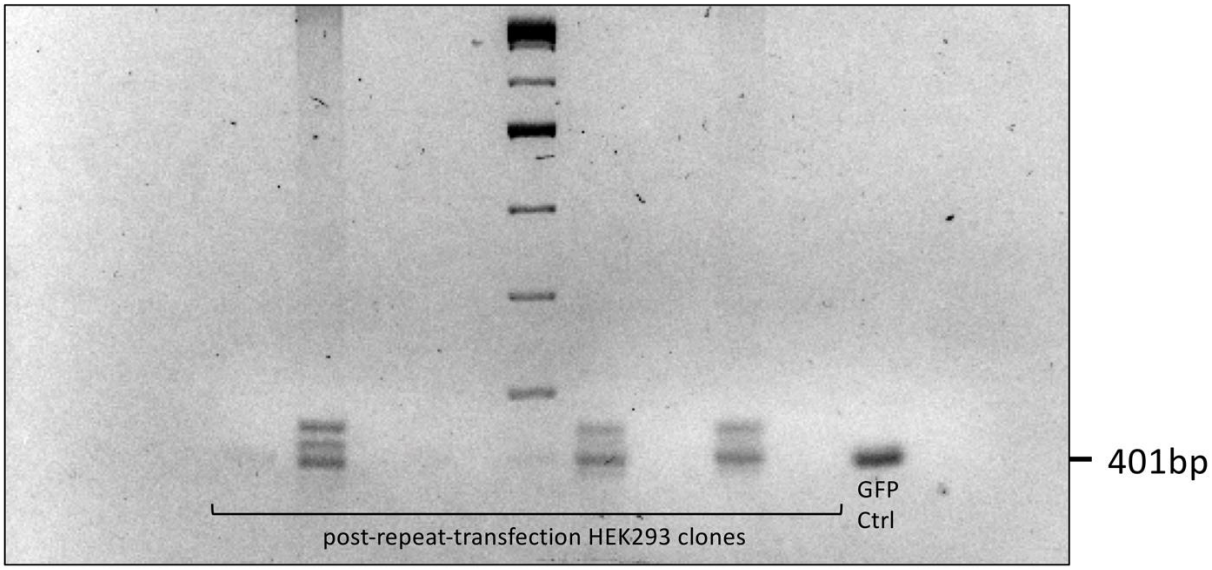

Figure 5.18 PCR screening of surviving second-round post-transfection HEK293 clonal populations. Attempts to amplify *MRPL65* exon 1 using genomic DNA extracted from HEK293 clones following a second round of transfection with sgRNA positive PX458 plasmids was successful in very few clones. Empty lanes correspond to failed PCR reactions. All successful PCR reactions confirmed the presence of *MRPL65* mutations through the presence of bands corresponding to multiple PCR products.

5.3.11 Investigation into steady-state MRPL65 in HEK293 clones

Of the clones that underwent PCR screening following a second round of transfection, only four grew to a confluency that allowed cell lysis for investigation into the steady-state levels of MRPL65. No clone exhibited any significant loss of MRPL65 protein **(Figure 5.19)**. These data suggest that, despite the introduction of mutations within the *MRPL65* gene and repeated rounds of transfection with a CRISPR/Cas9 plasmid, the aneuploid nature of 5p12 prevented the generation of an *MRPL65* knock-out cell line to model the variants identified in Family 1.

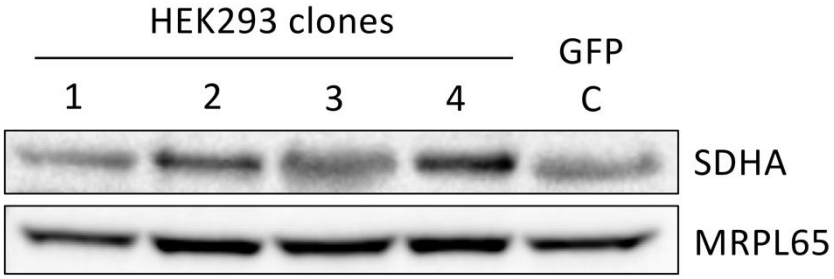

Figure 5.19 Western blot analysis of steady-state MRPL65 levels in four HEK293 CRISPR clones. Whole cell lysates were generated from the four clones that survived a second round of transfection with sgRNA positive PX458 plasmid, alongside a single pmaxGFP transfected clone as a control. SDS-PAGE and immunoblotting with MRPL65 antibody was carried out, alongside SDHA as a loading control. Data shown is representative of two independent repeats.

5.3.12 cDNA studies in Patient 2

Following the identification of a homozygous c.(601+5G>A) variant in a second paediatric patient, fibroblasts were obtained for functional investigation. RNA was extracted from the fibroblasts of Patient 2 for reverse transcription and the synthesis of cDNA, in order to investigate the splicing of *MRPL65* transcripts in this patient using a primer pair targeting exons 1-4 **(Figure 5.4)** producing a product 915bp in size. A faint band was visible in the lane containing cDNA from Patient 2, that was very similar in size to the bands corresponding to *MRPL65* product in controls **(Figure 5.20)**. However, Sanger sequencing and Basic Local Alignment Search Tool analysis of sequence data revealed product to be non-specific and not *MRPL65*.

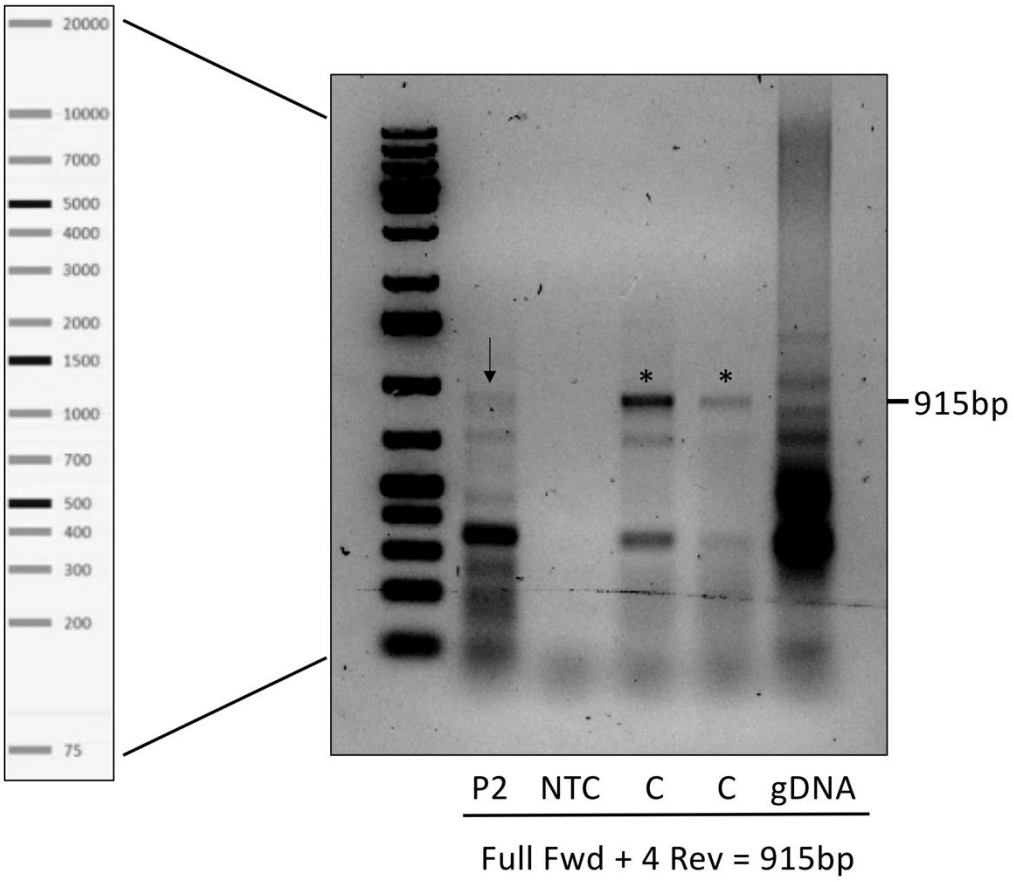

Figure 5.20 *MRPL65* cDNA studies in Patient 2. RNA extracted from the fibroblasts of Patient 2 was used for reverse transcription and second strand synthesis of cDNA, to investigate the potential impact of a homozygous c.(601+5C>A) variant on splicing of *MRPL65* mRNA transcripts. Asterisks indicate product of expected size in control samples, arrow indicates a band of a similar size in the Patient 2 sample, possibly indicating *MRPL65 cDNA* product of a normal size.

A deeper investigation into potentially unstable *MRPL65* transcripts was undertaken by treating growing cells with emetine, a specific inhibitor of nonsense mediated mRNA decay (NMD). A new primer set was designed to amplify a smaller 143bp region surrounding the boundary of exons 1 and 2. Using this primer pair, a larger amplimer between 400-500bp in length becomes visible in the cDNA of Patient 2, both with and without emetine treatment **(Figure 5.21)**. This band is not present in untreated or treated controls.

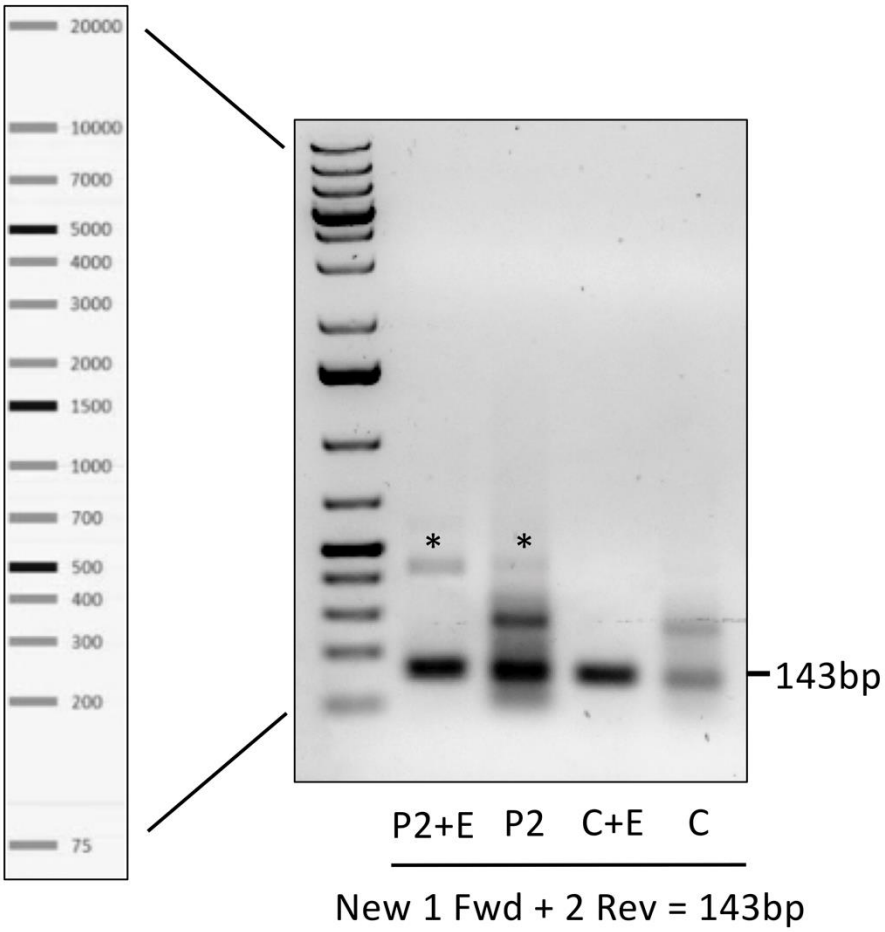

Figure 5.21 *MRPL65* cDNA studies with inhibition of nonsense mediated decay in Patient 2. Patient and control fibroblast cells were cultured in media containing 100ug/mL emetine for 10 hours prior to RNA extraction. RNA was extracted from untreated patient and control cells as a control. RNA was used for reverse transcription and second strand synthesis of cDNA. A primer pair amplifying a 143nt region encompassing the exon 1/ exon 2 boundary was used for PCR and agarose gel electrophoresis. Asterisks indicate a band of increased size present only in patient samples.

5.3.13 Identification of cryptic *MRPL65* splice donor site in Patient 2

The larger *MRPL65* cDNA band which was only present in samples from Patient 2 was subjected to Sanger sequencing, leading to the identification of two unique sequence traces. The smaller of the traces corresponds to the expected product of this primer pair, containing the final 96 nucleotides of exon 1 and the first 47 nucleotides of exon 2. However, the second underlying trace exhibits read-through from the end of exon 1 into intron 1 **(Figure 5.22)**.

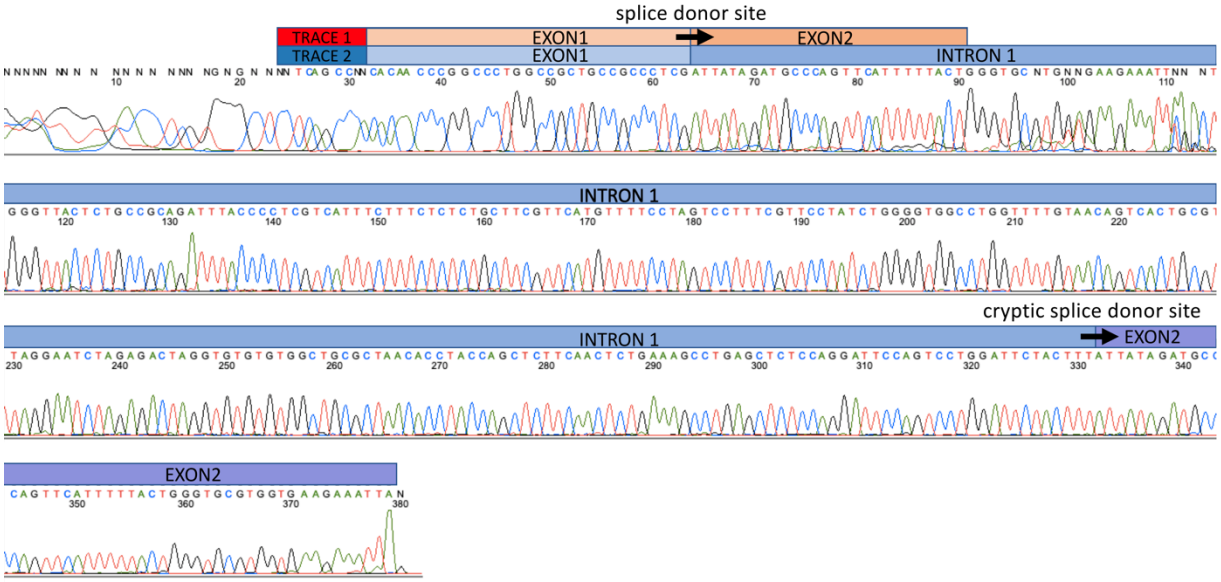

Figure 5.22 Sequencing of larger *MRPL65* product previously identified in Patient 2 cDNA sample. Sanger sequencing of cDNA generated from emetine treated fibroblasts of Patient 2 revealed two individual sequence traces. Trace 1 (red) is a product of normal splicing at the exon 1/ intron 1 and in intron 1/ exon 2 boundaries. This trace ends with the end of the reverse primer, lying 47 base pairs into exon 2. Trace 2 (blue) in the product of loss of processing at the exon 1/intron 1 boundary, resulting in intron retention and generating a longer transcript, corresponding to the larger band seen on the cDNA gel in (**Figure 5.21**).

Two free, online splice site predictor tools Alternative Splice Site Predictor (ASSP - http://wangcomputing.com/assp/) (Wang and Marin, 2006) and Splice Site Prediction by Neural Network (https://www.fruitfly.org/seq_tools/splice.html) (Reese *et al.*, 1997) were used for the analysis of wild-type and mutant *MRPL65* genomic sequences . In the c.(601+5G>A) sequence, prediction of the regular splice donor site at the end of exon 1 was lost **(Figure 5.23)**. Cross-referencing of predicted splice donor sites that aren't typical donor sites with a second sequence trace containing intronic sequence was carried out in order to identify potential cryptic splice donor sites. A predicted donor site 268 nucleotides downstream of the exon 1/intron boundary **(Figure 5.23)** corresponds perfectly in size with the size of band seen on cDNA gels above the 400bp marker in Patient 2 **(Figure 5.21)** as retention of 268bp would result in a PCR product 411bp in size.

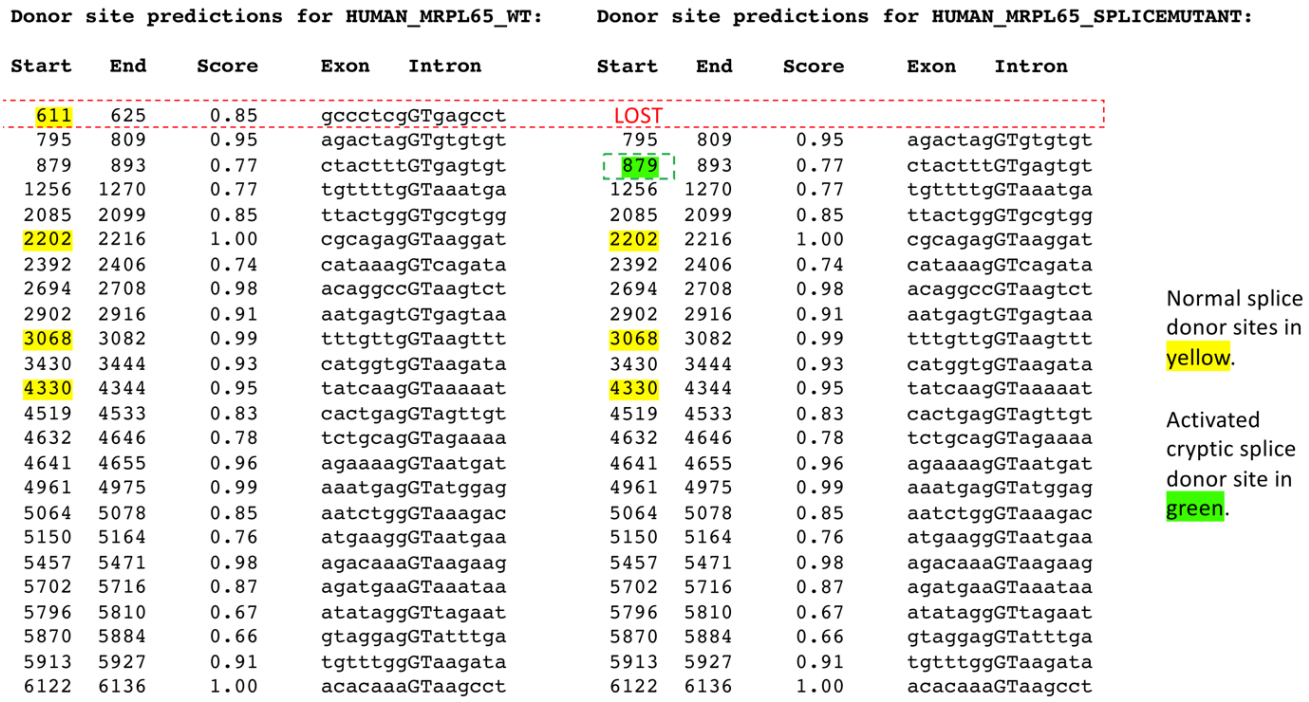

Donor site predictions for HUMAN_MRPL65_WT:

Start	End	Score	Exon	Intron
611	625	0.85	gccctcgGTgagcct	
795	809	0.95	agactagGTgtgtgt	
879	893	0.77	ctactttGTgagtgt	
1256	1270	0.77	tgttttgGTaaatga	
2085	2099	0.85	ttactggGTgcgtgg	
2202	2216	1.00	cgcagagGTaaggat	
2392	2406	0.74	cataaagGTcagata	
2694	2708	0.98	acaggccGTaagtct	
2902	2916	0.91	aatgagtGTgagtaa	
3068	3082	0.99	tttgttgGTaagttt	
3430	3444	0.93	catggtgGTaagata	
4330	4344	0.95	tatcaagGTaaaaat	
4519	4533	0.83	cactgagGTagttgt	
4632	4646	0.78	tctgcagGTagaaaa	
4641	4655	0.96	agaaaagGTaatgat	
4961	4975	0.99	aaatgagGTatggag	
5064	5078	0.85	aatctggGTaaagac	
5150	5164	0.76	atgaaggGTaatgaa	
5457	5471	0.98	agacaaaGTaagaag	
5702	5716	0.87	agatgaaGTaaataa	
5796	5810	0.67	atataggGTtagaat	
5870	5884	0.66	gtaggagGTatttga	
5913	5927	0.91	tgtttggGTaagata	
6122	6136	1.00	acacaaaGTaagcct	

Donor site predictions for HUMAN_MRPL65_SPLICEMUTANT:

Start	End	Score	Exon	Intron
LOST				
795	809	0.95	agactagGTgtgtgt	
879	893	0.77	ctactttGTgagtgt	
1256	1270	0.77	tgttttgGTaaatga	
2085	2099	0.85	ttactggGTgcgtgg	
2202	2216	1.00	cgcagagGTaaggat	
2392	2406	0.74	cataaagGTcagata	
2694	2708	0.98	acaggccGTaagtct	
2902	2916	0.91	aatgagtGTgagtaa	
3068	3082	0.99	tttgttgGTaagttt	
3430	3444	0.93	catggtgGTaagata	
4330	4344	0.95	tatcaagGTaaaaat	
4519	4533	0.83	cactgagGTagttgt	
4632	4646	0.78	tctgcagGTagaaaa	
4641	4655	0.96	agaaaagGTaatgat	
4961	4975	0.99	aaatgagGTatggag	
5064	5078	0.85	aatctggGTaaagac	
5150	5164	0.76	atgaaggGTaatgaa	
5457	5471	0.98	agacaaaGTaagaag	
5702	5716	0.87	agatgaaGTaaataa	
5796	5810	0.67	atataggGTtagaat	
5870	5884	0.66	gtaggagGTatttga	
5913	5927	0.91	tgtttggGTaagata	
6122	6136	1.00	acacaaaGTaagcct	

Normal splice donor sites in yellow.

Activated cryptic splice donor site in green.

Figure 5.23 Output from splice donor site predictor tool analysis of wildtype and mutant *MRPL65*. The analysis of *MRPL65* sequence containing the c.(601+5G>A) variant demonstrates that this mutation is predicted to result in the loss of the typical splice donor site at the end of exon 1. Output from this prediction tool was searched for predicted splice donor sites not typically active, but that if active might result in retention of the length of intron seen via Sanger sequencing. A splice donor site was identified 268 nucleotides downstream of the typical splice site. Activation of this splice donor would result in a transcript identical in size to trace 2 in the sequencing data. Output obtained from (https://www.fruitfly.org/seq_tools/splice.html) (Reese *et al.*, 1997).

I confirmed the activation of this predicted donor site through Sanger sequencing of the intron/exon boundaries, clearly demonstrating a trace corresponding to 268 nucleotides of intronic sequence **(Figure 5.24)**, corroborating its activation as a cryptic splice donor site in *MRPL65* transcripts of Patient 2.

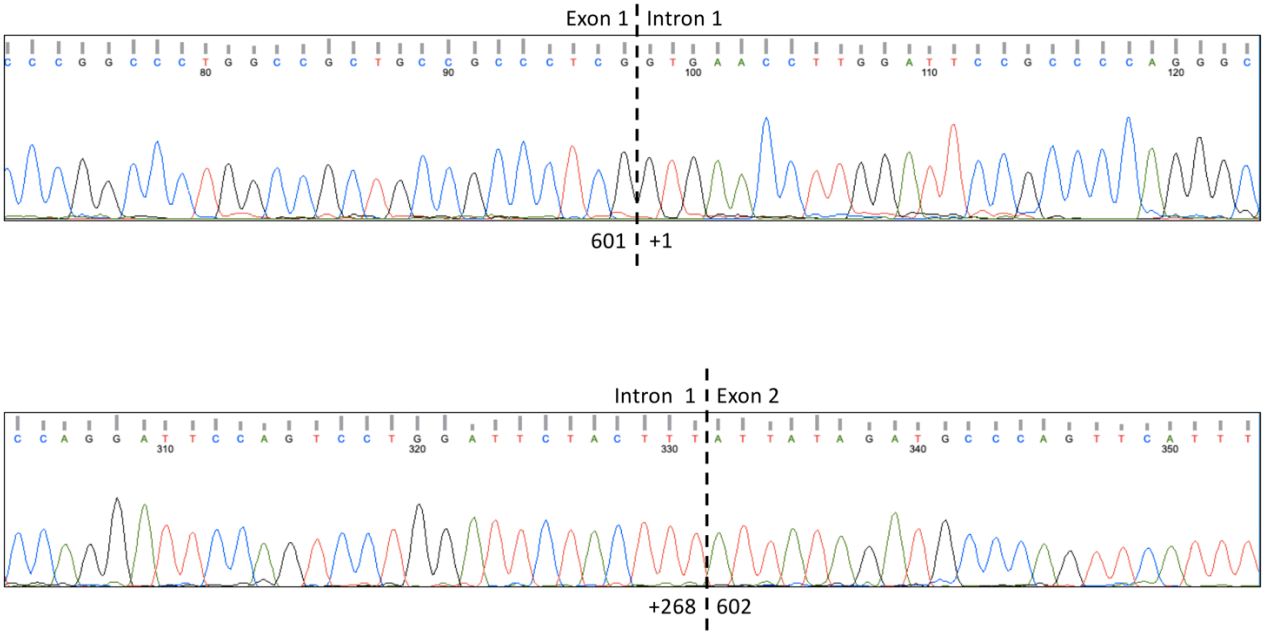

Figure 5.24 Exonic/intronic boundaries in transcript resulting from activation of a cryptic splice donor site. Dashed line on top panel marks boundary between exon 1 and intron 1 at which processing would normally occur to remove intronic sequence. Dashed line on bottom panel marks boundary at which a cryptic splice donor site results in the read-through of sequence belonging to intron 1 back into sequence of exon 2.

5.3.14 Western blot analysis of protein levels in Patient 2 fibroblasts

Western blot analysis was carried out on fibroblast cell lysates of Patient 2, to investigate the impact of this homozygous c.(601+5G>A) splice variant on the steady-state levels of MRPL65 and protein subunits of OXPHOS.

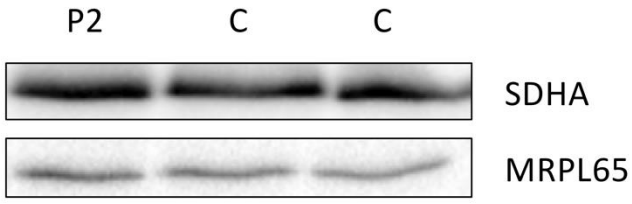

Figure 5.25 Western blot analysis of steady state MRPL65 in fibroblasts of Patient 2. SDS-PAGE and immunoblotting of whole cell lysate from fibroblasts of Patient 2 alongside two paediatric control fibroblasts. MRPL65 antibody was used alongside SDHA as an indication of loading. Data shown is representative of three independent repeats.

The abundance of full-length MRPL65 protein appears to be unaffected in the fibroblasts of Patient 2 **(Figure 5.25)**. There was also no observable OXPHOS defect at the steady-state level in the fibroblasts of Patient 2 **(Figure 5.26)**.

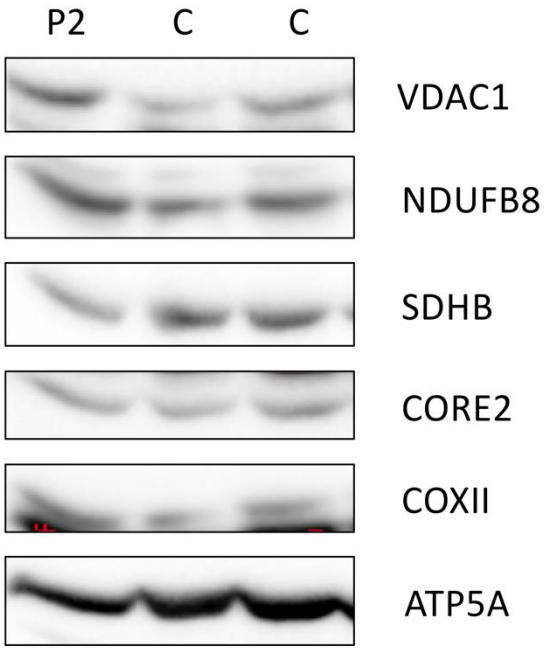

Figure 5.26 Western blot analysis of OXPHOS proteins in fibroblasts of Patient 2. SDS-PAGE and immunoblotting of whole cell lysate from fibroblasts of Patient 2 alongside two paediatric control fibroblasts. An antibody cocktail containing NDUFB8, SDHB, CORE2, COXII and ATP5A was used to investigate OXPHOS complexes I-IV. VDAC1 was used as a loading control. Data shown is representative of three independent repeats.

5.3.15 Investigation of MRPL65 assembly within the LSU

Next, I used sucrose gradient centrifugation and immunoblotting to investigate the assembly of MRPL65 within the LSU. The ultracentrifugation of 700 ug of protein through sucrose gradients allowed the sedimentation of mitoribosomal subunits based on size. SDS-PAGE and western blotting of MRPL45 confirmed the presence of the LSU in lanes six and seven in both Patient 2 and control sample. However, in Patient 2 MRPL65 signal appears to be limited to lanes three and four, containing protein complexes smaller than the mitoribosomal LSU **(Figure 5.27)**. This could indicate that MRPL65 does not assemble successfully within the LSU of the mitoribosome**.**

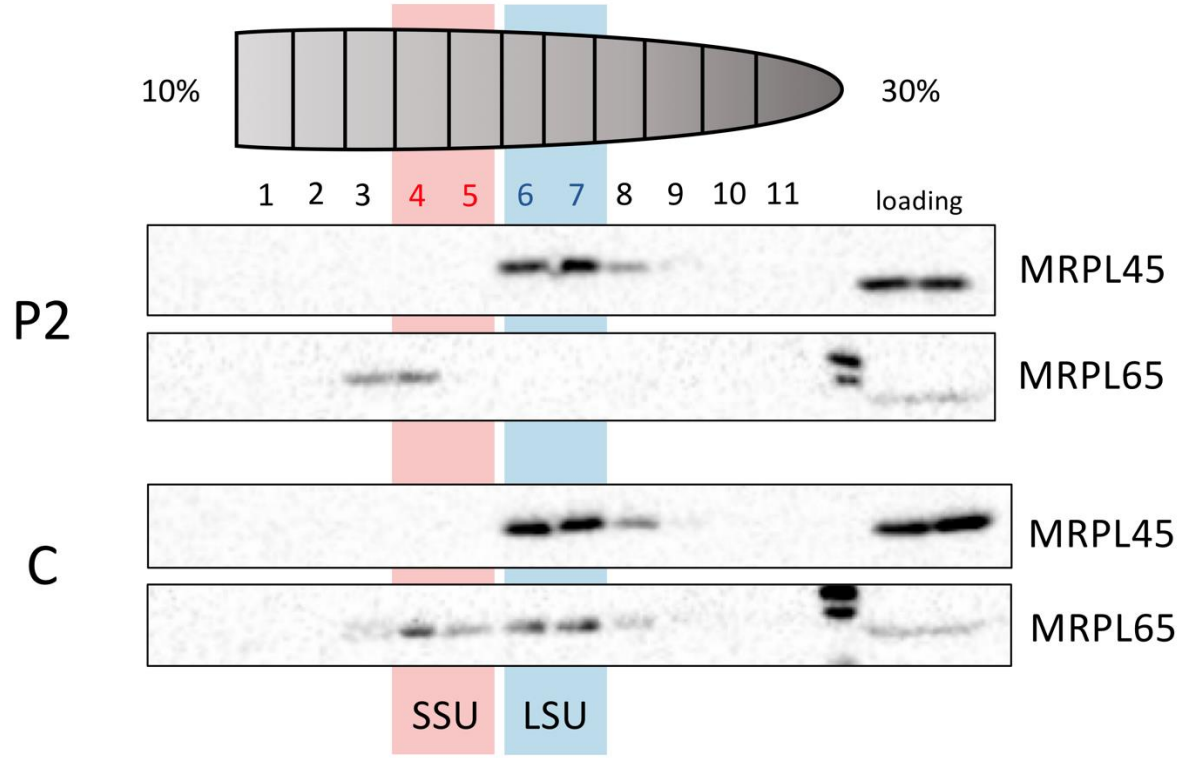

Figure 5.27 Sucrose gradient ultracentrifugation and immunoblotting to investigate MRPL65 in mitoribosome assembly. 700 µg of total protein from the fibroblasts of patients 2 and a paediatric control was separated on a linear 10-30% sucrose gradient. Following ultracentrifugation, eleven fractions were taken to be run on SDS-PAGE gels and immunoblotted for MRPL45 and MRPL65. Fractions 6 and 7 (blue) contain proteins of the LSU, demonstrated through MRPL45 signal. Whole cell lysate used for loading controls. Data shown is representative of three independent repeats.

5.3.16 [^{35}S] translation assay in growing fibroblasts

To assess the impact of a potential loss of MRPL65 from the assembled LSU, metabolic labelling assay using [^{35}S] labelled methionine/cysteine was used to investigate *de novo* protein synthesis in Patient 2 fibroblasts. Incubation of growing patient and control fibroblasts with radiolabelled media for 1 hour was conducted in the presence of 100 µg/mL emetine to inhibit cytosolic translation. Phosphorimaging of the resulting signal revealed a generalised defect of mitochondrial translation in Patient 2. All visible bands, corresponding to newly-synthesised mtDNA encoded OXPHOS proteins, are decreased in signal when compared to signal in the control lane **(Figure 5.28)**.

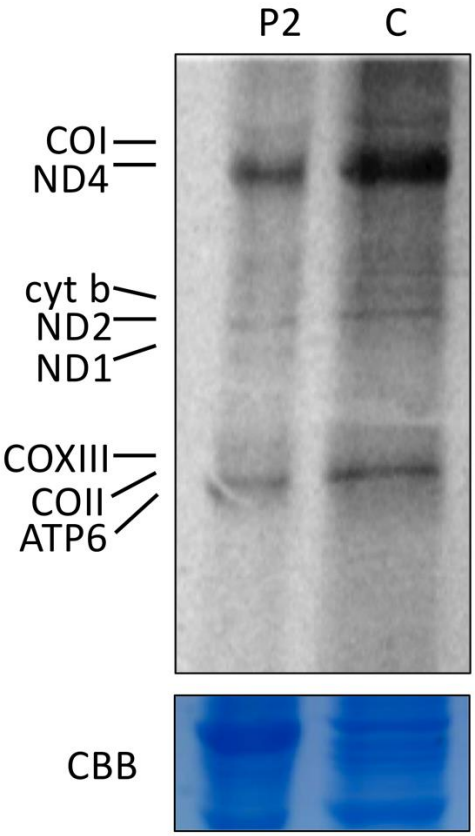

Figure 5.28 [35S] methionine/cysteine incorporation in growing MRPL65 patient fibroblasts as a measure of *de novo* mitochondrial protein synthesis. Signal detected from fixed and dehydrated SDS-PAGE gel using Typhoon Phosphorimager. Bands are visible for radiolabelled COXI, ND4, cyt b. ND2, ND1, COXIII, COXII and ATP6 in Patient 2 and control sample. Loading is demonstrated using the Coomassie Brilliant Blue (CBB) stain on the bottom panel.

5.4 Discussion

5.4.1 Ploidy of cell lines used for CRISPR/Cas9 studies

While cancer derived cell lines such as U2OS and HEK293 are of immense value to biomedical research, they are characteristically genotypically unstable, and often have extremely abnormal karyotypes (Ozaki *et al.*, 2003). As the ploidy of a target region increases, the likelihood of successful CRISPR/Cas9 editing of all target alleles decreases. Despite the successful introduction of indels using PX458 plasmids expressing sgRNAs 1, 3 and 4, no MRPL65 knockout clones were successfully generated **(Figure 5.14, Figure 5.19)**. This is highly likely to be a result of the tetraploid and triploid nature Chromosomal region 5p12 in U2OS and HEK293 cells respectively **(Figure 5.16)**, and highlights the importance of identifying the cell line most amenable to genome editing at a desired target site when still in the early stages of knockout study design.

5.4.2 Resolving specific genotypes of heterozygous CRISPR clones

Due to the random and unpredictable nature of indels introduced upon NHEJ following the introduction of DSBs by Cas9, sequencing of clones with multiple indels can produce chromatograms with multiple frameshift traces **(Figure 5.12)**. As a result, from sequence data alone it is difficult to ascertain the precise mutations that have been introduced. A long-standing method used classically in the resolution of this type of problem is the cloning of the mixture of alleles into bacterial vectors, followed by bacterial transformation and cloning. Sequencing multiple colonies would result in the eventual sequencing of each individual allele, from which a single trace would be obtained, thereby allowing the identification and genotyping of precise insertions or deletions. However, the advent of CRISPR/Cas9 genome editing has resulted in the development of various tools and techniques, such as CRISP-ID, to circumvent this classic approach. CRISP-ID is a tool that allows the detection of exact indel sizes and locations within a given target region, based on Sanger sequencing alone (Dehairs *et*

al., 2016). This tool can resolve multiple frameshift sequences up to a maximum of three traces. Retrospective attempts to analyse the Sanger sequence data of the mutant U2OS CRISPR clones generated within this study using the CRISP-ID online tool, resulted in the detection of four sequences, preventing trace 'unmixing' for these data. Despite being unable to resolve the precise sizes of indels within these tetraploid clones, receiving information regarding the number of individual alleles within a single clone would be of use in the early stages of CRISPR/Cas9 studies, particularly if using a cell line with a normal target gene copy number.

5.4.3 Knock-out Vs knock-in models

Repeated attempts to generate a CRISPR/Cas9 *MRPL65* knockout cell line have proven to be unsuccessful. However, the identification of a second family at a later stage of the functional workflow, through the online GeneMatcher tool (https://genematcher.org/), allowed for more detailed functional validation studies using patient fibroblasts. The fibroblasts of Patient 2 did not exhibit any decrease in steady-state MRPL65. While this finding was surprising, it further highlighted the limitations of knockout studies in the absence of patient cell lines. Had the *MRPL65* knockout studies been successful, they would be used to model a c.(601+5A>G) disease variant that does not result in the loss of *MRPL65* expression (**Figure 5.25**).

In addition to CRISPR/Cas9 knock-out studies using NHEJ, a second DNA repair mechanism, error-free homology directed repair (HDR), can also be triggered by the introduction of DSBs. HDR can be utilised for CRISPR knock-in or precise gene-editing through the delivery of homology-containing donor DNA templates alongside the CRISPR/Cas9 machinery (Ryu, Hur and Kim, 2019). This technique offers a much more precise way of modelling specific variants in cell-lines and whole organisms which, with more time, would have proven to be a very useful tool in the modelling of disease in these patients.

5.4.4 Impact of intron retention on MRPL65 function

The cDNA studies in Patient 2 revealed the specific impact of a c.(601+5G>A) variant on splicing at the donor site of exon 1 in some *MRPL65* transcripts. Some transcripts fail to splice at the constitutive donor site and a downstream cryptic donor site is activated, resulting in the retention of 268 nucleotides of intron 1 **(Figure 5.22)**. This c.(601_602ins601+1_601+268) transcript results in a frameshift, and the introduction of a downstream STOP codon, with the nomenclature p.(Asp201Glyfs*68). These transcripts are therefore extremely unlikely to produce any stable MRPL65 protein. However, steady-state levels of MRPL65 appear to be normal in the fibroblasts of Patient 2 **(Figure 5.25)**. It is therefore difficult to connect the c.(601+5G>A) splice mutation with the translation defect in fibroblast cells **(Figure 5.28)**, and the clinical disease in Patient 2. The antibody used against MRPL65 has been validated through siRNA knock-down studies in U2OS cells **(Figure 5.6)** which should rule out the possibility of a non-specific band being mistaken for full-length MRPL65 in the fibroblasts of Patient 2. However, the siRNA knock-down should be repeated in Patient fibroblasts to confirm with certainty that the visible band represents MRPL65. It would also be interesting to combine siRNA treatment with a [^{35}S] translation assay, to investigate whether MRPL65 knock-down exacerbates the existing translation defect in this cell-line.

Diagnostic RNA sequencing was ordered by the referring clinician of Patient 2. These studies were carried out by MNG Laboratories in the US using RNA extracted by lymphocytes and skin fibroblasts and determined that 24% and 19% of *MRPL65* transcripts remained unprocessed at the affected splice donor site respectively. As the ratio of processed:unprocessed transcripts appears to vary in the two cell types tested, it is possible that the proportion of unprocessed transcripts may be high enough to cause a decrease in steady-state MRPL65 protein in cell types that are clinically relevant to the Patient's disease presentation.

5.4.5 Identification of multiple families through ‘GeneMatcher’

Both patients investigated within this chapter are of Lebanese ethnic origin. The c.(601+5A>G) mutation is present in Patient 1 in a compound heterozygous state and in Patient 2 in a homozygous state. A very recent GeneMatcher ‘hit’ has identified a third family of Lebanese origin, containing three paediatric patients homozygous for the c.(601+5A>G) splice variant and presenting with significantly overlapping clinical features to Patients 1 and 2 including ataxia, developmental delay and nystagmus. So far, this splice variant appears to be ethnically isolated to patients of Lebanese descent and is therefore a potential founder mutation. However, we don’t yet have samples available to prove this in the laboratory.

Chapter 6 : Final discussion

The research within this thesis has contributed new understanding of the mitochondrial pathophysiology and mechanisms associated with two mitochondrial proteins not previously linked to human disease*, MRPL47* and *MRPL65,* thus expanding the list of nuclear genes implicated in mitochondrial presentations. Novel disease variants in two previously reported genes, *GFM2* and *TSFM,* have also been validated. Throughout this thesis I have employed a number of different techniques to assess mitochondrial function using patient cell lines and tissues, as well as working with CRISPR/Cas9 and siRNA in U2OS and HEK293 cell lines, to aid in the validation of these variants. This demonstrates the value of further research-based functional studies in assigning pathogenicity to novel variants as part of the diagnostic algorithm used for mitochondrial disorders.

6.1 Diagnostic algorithm

The investigation and diagnosis of suspected mitochondrial disease requires a dynamic multidisciplinary approach. Due to the vast clinical heterogeneity of mitochondrial disease, a wide range of different clinical and biochemical investigations can indicate disease with a mitochondrial aetiology. Abnormalities identified on brain MRI, nerve conduction studies or electrocardiogram together with metabolic abnormalities such as increased lactate or the presence of urinary 3-methylglutaconic acid could be suggestive of a mitochondrial disorder. However, these presentations are not limited to diseases with underlying mitochondrial dysfunction and thus require further investigation (Thompson *et al.*, 2019). Biochemical and histopathological techniques using patient muscle biopsies are used to identify defects in respiratory chain function or abnormalities in muscle morphology, both of which can also signify a mitochondrial defect (Taylor *et al.*, 2004; Frazier *et al.*, 2020).

Approaches to the diagnosis of mitochondrial disease are steadily adapting as the power of NGS technologies continues to grow. The identification of mitochondrial disease variants via this ‘genetics first’ approach potentially avoids the requirement for

skin or muscle biopsies when identified variants have been previously reported (Wortmann *et al.*, 2017). Further large data-set methods such as proteomics, transcriptomics and metabolomics ('multi-omics') are also increasingly being incorporated into functional characterisation pathways (Stenton and Prokisch, 2020). However, as a result of NGS and 'multi-omic' implementation, the list of nuclear genes implicated in mitochondrial disease is ever-growing. Half of the 14 reported *MRP* mitochondrial disease genes have been reported within the past three years alone **(Table 4.1)**. This rate of gene discovery drives the need for molecular characterisation studies in the investigation of novel variants. The availability of skin and/or tissue biopsies is extremely beneficial to functional studies that allow confirmation of pathogenicity. The studies conducted in the investigation of *MRPL65* variants in **Chapter 5** highlight the advantages of having access to patient biopsies rather than drawing conclusions on the molecular mechanisms of a particular variant based only on knock-down and knock-out experiments. In the absence of a patient cell line, sirRNA and CRISPR/Cas9 studies were carried out working under the assumption that the variants identified in *MRPL65* would result in a loss of steady-state protein. However, subsequent patient samples harbouring one of the same variants demonstrated that this was not the case **(Figure 5.25)**. Biopsies of tissues with clinical relevance to the specific disease presentation in each patient are of particular value, owing to the tissue specificity often observed in mitochondrial disorders, as can be seen in the investigation of novel *TSFM* variant.

6.2 Tissue specificity in mitochondrial disease

Tissue specific patterns of mitochondrial dysfunction and subsequent clinical presentations are frequently observed in mitochondrial disorders of both mtDNA and nuclear genetic origins. While often reported, the mechanisms underlying tissue specificity in mitochondrial disease remain elusive in many cases. Clinical and functional tissue specific features can be seen in the cases presented throughout this thesis, however it was particularly striking in the *TSFM* patient presented in **Chapter 3**. This patient presented with clinical features linked almost exclusively to cardiac dysfunction which was mirrored by the presence of a steady-state level OXPHOS

defect in cardiac tissue but not in fibroblasts **(Figure 3.12)**. While mtEF-Ts levels were decreased in both cardiac tissue and fibroblasts, its interacting elongation factor mtEF-Tu was only decreased in cardiac tissue as patient fibroblasts appeared to exhibit over-expression of mtEF-Tu protein **(Figure 3.11)**. Increased abundance of mtEf-Tu might form a compensatory mechanism that prevents the loss of mtEF-Ts from severely impeding mitochondrial translation. As mtEF-Tu steady-state levels are not increased in the cardiac tissue of this patient, this may offer an explanation for the stark tissue specificity observed.

Fifteen patients with mitochondrial disease arising as a result of variants in the *TSFM* gene have been reported to date (Emperador *et al.*, 2017; Finsterer, 2019; Perli *et al.*, 2019; Scala *et al.*, 2019; Traschutz *et al.*, 2019; Smeitink *et al.*, 2006a; Calvo *et al.*, 2012; Ahola *et al.*, 2014; Vedrenne *et al.*, 2012), including the patient presented here. Hypotrophic cardiomyopathy is common to almost all of these patients, but despite this overlap a number of *TSFM* cases also present with clinical features affecting other organs and systems, such as optic atrophy and ataxia. Interestingly, one of the three *TSFM* patients whose clinical features do not include cardiac involvement exhibits no decrease in of steady-state mtEF-Tu in myoblasts (Ahola *et al.*, 2014), further supporting the theory that increased levels of mtEF-Tu might act as a protective compensatory mechanism in some tissues.

6.3 Mitoribosome biogenesis and stability

Throughout **Chapter 4** and **Chapter 5** I have described the investigation of two mitoribosomal proteins, MRPL47 and MRPL65. The vast majority of reported mitochondrial disease variants in mitoribosomal subunits have been demonstrated to result in the destabilisation of the mitoribosome, leading to a defect of mitochondrial translation (Di Nottia *et al.*, 2020). While it is known that the process of mitoribosome construction is extremely energy-demanding, the precise mechanisms of mitoribosome biogenesis remain relatively poorly understood. High-resolution crystal structures of the mammalian mitoribosome have been obtained through the use of sophisticated cryo-EM techniques, shedding new light on the structural nuances that

distinguish the mitoribosome from its bacterial and cytosolic counterparts (Amunts *et al.*, 2015). Attention has now begun to shift to obtaining a deeper understanding of mitoribosome biogenesis and assembly (Bogenhagen *et al.*, 2018).

Although a handful of mitoribosome assembly factors have been identified, there are likely more to be discovered and characterised. The process of bacterial ribosome assembly requires approximately 20 proteins (Shajani, Sykes and Williamson, 2011), while the number of identified cytoplasmic ribogenesis factors lies at ~200 (Klinge and Woolford, 2019). With a greater understanding of the proteins involved in mitoribosome assembly, it may be possible to elucidate the specific assembly pathways affected by mutations in MRP genes that result in the mitoribosome destabilisation observed in patients. This in turn could identify possible therapeutic targets within the mitoribosome assembly pathway that could be genetically or pharmacologically manipulated to stabilise the mitoribosome. To this end, cell-lines obtained from patients with pathogenic variants in MRP genes and an observable mitoribosome assembly defect are potentially a valuable resource for the identification and/or validation of new mitoribosome assembly factors. I have plans to further investigate the MRP defects presented here while collaborating with Dr. Joanna Rorbach at the Division of Molecular Metabolism, Karolinska Institute. This work will first focus on understanding the precise impact that the truncated MRPL47 has on mitoribosome assembly and function.

6.4 The investigation of splicing mutations

The difficulties encountered in **Chapter 5** when attempting to ascertain the precise impact on splicing of the c.601+5G>A variant highlights the importance of functional validation of variants found at intron/exon boundaries. The process of pre-mRNA transcript splicing is carried out by a large protein-RNA complex named the spliceosome (Zhang *et al.*, 2019). In the majority of cases, the spliceosome recognises and binds *cis* splicing elements in the form of highly conserved GT and AG nucleotides at the 5’ (donor) and 3’ (acceptor) ends of each intron. As the splicing consensus sequences are short, there are many other similar sites found throughout an individual

gene known as pseudo or cryptic splice sites (Green, 1986). Binding of the spliceosome at the correct splice donor and accepter sites is aided by other *cis* splicing elements such as splicing branchpoints (Mercer *et al.*, 2015), polypyrimidine tract sequences (Coolidge, Seely and Patton, 1997) and exonic splicing enhancers (Jobbins *et al.*, 2018). Mutations that occur within *cis* splicing element sequences can result in the skipping of exons/exon fragments or the inclusion of intronic sequence. These changes to splicing may produce a transcript that remains in the same reading frame or cause a shift in the reading frame thus introducing a premature stop codon (Abramowicz and Gos, 2018).

The patients presented in **Chapter 5** harboured a c.601+5A>G splicing mutation in the *MRPL65* gene. The most common splicing mutations are found at the +1 and +2 nucleotides of a splicing donor site, and usually lead to exon skipping (Krawczak *et al.*, 2007). Splicing mutations that occur further from the intron/exon boundary, such as the +5 variant in the *MRPL65* patients presented here, are less commonly identified in disease and the effects are harder to predict. If the affected splice site is weak, a +3/+4/+5/+6 mutation may result in the activation of a cryptic splice site and cause intronic fragment retention or exonic fragment removal (Abramowicz and Gos, 2018). A number of *in silico* tools have been developed to analyse and identify splice consensus sequences using a range of databases and statistical models. However, the results from such *in silico* tools must be treated as predictions only and cannot be used in isolation to assign pathogenicity to a novel splicing mutation (Spurdle *et al.*, 2008).

6.5 Concluding remarks

The work presented within this thesis documents the validation of multiple pathogenic variants in mitochondrial disease cases, and is a product of the increasing rate of gene discovery in mitochondrial disease brought about by NGS implementation into diagnostic pathways. My research has allowed the assignment of pathogenicity to novel variants in four genes, *GFM2*, *TSFM*, *MRPL47* and *MRPL65*, across eight families. Obtaining this information enables the provision of risk recurrence estimates

and reproductive advice to affected families. A genetic diagnosis can be achieved in a higher proportion of mitochondrial disease patients than ever before, with the functional characterisation of novel variants being an integral part of this field of diagnostic research. The further implementation of multi-omic pipelines in this genetics-first era will continue to improve upon diagnostic yields, benefiting an even higher proportion of affected families.

References

Abe, Y., Shodai, T., Muto, T., Mihara, K., Torii, H., Nishikawa, S., Endo, T. and Kohda, D. (2000) 'Structural basis of presequence recognition by the mitochondrial protein import receptor Tom20', *Cell,* 100(5), pp. 551-60.

Abramowicz, A. and Gos, M. (2018) 'Splicing mutations in human genetic disorders: examples, detection, and confirmation', *J Appl Genet,* 59(3), pp. 253-268.

Adams, K. L. and Palmer, J. D. (2003) 'Evolution of mitochondrial gene content: gene loss and transfer to the nucleus', *Mol Phylogenet Evol,* 29(3), pp. 380-95.

Ahola, S., Isohanni, P., Euro, L., Brilhante, V., Palotie, A., Pihko, H., Lonnqvist, T., Lehtonen, T., Laine, J., Tyynismaa, H. and Suomalainen, A. (2014) 'Mitochondrial EFTs defects in juvenile-onset Leigh disease, ataxia, neuropathy, and optic atrophy', *Neurology,* 83(8), pp. 743-51.

Alston, C. L., Compton, A. G., Formosa, L. E., Strecker, V., Olahova, M., Haack, T. B., Smet, J., Stouffs, K., Diakumis, P., Ciara, E., Cassiman, D., Romain, N., Yarham, J. W., He, L., De Paepe, B., Vanlander, A. V., Seneca, S., Feichtinger, R. G., Ploski, R., Rokicki, D., Pronicka, E., Haller, R. G., Van Hove, J. L., Bahlo, M., Mayr, J. A., Van Coster, R., Prokisch, H., Wittig, I., Ryan, M. T., Thorburn, D. R. and Taylor, R. W. (2016) 'Biallelic Mutations in TMEM126B Cause Severe Complex I Deficiency with a Variable Clinical Phenotype', *Am J Hum Genet,* 99(1), pp. 217-27.

Amunts, A., Brown, A., Toots, J., Scheres, S. H. W. and Ramakrishnan, V. (2015) 'The structure of the human mitochondrial ribosome', *Science,* 348(6230), pp. 95-98.

Anderson, S., Bankier, A. T., Barrell, B. G., de Bruijn, M. H., Coulson, A. R., Drouin, J., Eperon, I. C., Nierlich, D. P., Roe, B. A., Sanger, F., Schreier, P. H., Smith, A. J., Staden, R. and Young, I. G. (1981) 'Sequence and organization of the human mitochondrial genome', *Nature,* 290(5806), pp. 457-65.

Antonicka, H., Østergaard, E., Sasarman, F., Weraarpachai, W., Wibrand, F., Pedersen, A. M. B., Rodenburg, R. J., Van Der Knaap, M. S., Smeitink, J. A. M., Chrzanowska-Lightowlers, Z. M. and Shoubridge, E. A. (2010) 'Mutations in C12orf65 in Patients with Encephalomyopathy and a Mitochondrial Translation Defect', *The American Journal of Human Genetics,* 87(1), pp. 115-122.

Antonicka, H., Sasarman, F., Kennaway, N. G. and Shoubridge, E. A. (2006) 'The molecular basis for tissue specificity of the oxidative phosphorylation deficiencies in patients with mutations in the mitochondrial translation factor EFG1', *Human Molecular Genetics,* 15(11), pp. 1835-1846.

Antonicka, H., Sasarman, F., Nishimura, T., Paupe, V. and Shoubridge, E. A. (2013) 'The mitochondrial RNA-binding protein GRSF1 localizes to RNA granules and is required for posttranscriptional mitochondrial gene expression', *Cell Metab,* 17(3), pp. 386-98.

Antonicka, H. and Shoubridge, E. A. (2015) 'Mitochondrial RNA Granules Are Centers for Posttranscriptional RNA Processing and Ribosome Biogenesis', *Cell Rep,* 10(6), pp. 920-932.

Arroyo, J. D., Jourdain, A. A., Calvo, S. E., Ballarano, C. A., Doench, J. G., Root, D. E. and Mootha, V. K. (2016) 'A Genome-wide CRISPR Death Screen Identifies Genes Essential for Oxidative Phosphorylation', *Cell Metab,* 24(6), pp. 875-885.

Asin-Cayuela, J., Schwend, T., Farge, G. and Gustafsson, C. M. (2005) 'The human mitochondrial transcription termination factor (mTERF) is fully active in vitro in the non-phosphorylated form', *J Biol Chem,* 280(27), pp. 25499-505.

Backes, S., Hess, S., Boos, F., Woellhaf, M. W., Godel, S., Jung, M., Muhlhaus, T. and Herrmann, J. M. (2018) 'Tom70 enhances mitochondrial preprotein import efficiency by binding to internal targeting sequences', *J Cell Biol,* 217(4), pp. 1369-1382.

Baertling, F., Haack, T. B., Rodenburg, R. J., Schaper, J., Seibt, A., Strom, T. M., Meitinger, T., Mayatepek, E., Hadzik, B., Selcan, G., Prokisch, H. and Distelmaier, F. (2015) 'MRPS22 mutation causes fatal neonatal lactic acidosis with brain and heart abnormalities', *Neurogenetics,* 16(3), pp. 237-40.

Bai, Y., Srivastava, S. K., Chang, J. H., Manley, J. L. and Tong, L. (2011) 'Structural Basis for Dimerization and Activity of Human PAPD1, a Noncanonical Poly(A) Polymerase', *Molecular Cell,* 41(3), pp. 311-320.

Balasubramaniam, S., Choy, Y. S., Talib, A., Norsiah, M. D., van den Heuvel, L. P. and Rodenburg, R. J. (2012) 'Infantile Progressive Hepatoencephalomyopathy with Combined OXPHOS Deficiency due to Mutations in the Mitochondrial Translation Elongation Factor Gene GFM1', *JIMD Rep,* 5, pp. 113-22.

Balciuniene, J. and Balciunas, D. (2019) 'A Nuclear mtDNA Concatemer (Mega-NUMT) Could Mimic Paternal Inheritance of Mitochondrial Genome', *Front Genet,* 10, pp. 518.

Ban, T., Ishihara, T., Kohno, H., Saita, S., Ichimura, A., Maenaka, K., Oka, T., Mihara, K. and Ishihara, N. (2017) 'Molecular basis of selective mitochondrial fusion by heterotypic action between OPA1 and cardiolipin', *Nat Cell Biol,* 19(7), pp. 856-863.

Banci, L., Bertini, I., Cefaro, C., Ciofi-Baffoni, S., Gallo, A., Martinelli, M., Sideris, D. P., Katrakili, N. and Tokatlidis, K. (2009) 'MIA40 is an oxidoreductase that catalyzes oxidative protein folding in mitochondria', *Nat Struct Mol Biol,* 16(2), pp. 198-206.

Bar-Yaacov, D., Frumkin, I., Yashiro, Y., Chujo, T., Ishigami, Y., Chemla, Y., Blumberg, A., Schlesinger, O., Bieri, P., Greber, B., Ban, N., Zarivach, R., Alfonta, L., Pilpel, Y., Suzuki, T. and Mishmar, D. (2016) 'Mitochondrial 16S rRNA Is Methylated by tRNA Methyltransferase TRMT61B in All Vertebrates', 14(9), pp. e1002557.

Becker, T., Vogtle, F. N., Stojanovski, D. and Meisinger, C. (2008) 'Sorting and assembly of mitochondrial outer membrane proteins', *Biochim Biophys Acta,* 1777(7-8), pp. 557-63.

Beinert, H., Holm, R. H. and Munck, E. (1997) 'Iron-sulfur clusters: nature's modular, multipurpose structures', *Science,* 277(5326), pp. 653-9.

Belostotsky, R., Ben-Shalom, E., Rinat, C., Becker-Cohen, R., Feinstein, S., Zeligson, S., Segel, R., Elpeleg, O., Nassar, S. and Frishberg, Y. (2011) 'Mutations in the Mitochondrial Seryl-tRNA Synthetase Cause Hyperuricemia, Pulmonary Hypertension, Renal Failure in Infancy and Alkalosis, HUPRA Syndrome', *The American Journal of Human Genetics,* 88(2), pp. 193-200.

Benit, P., Lebon, S. and Rustin, P. (2009) 'Respiratory-chain diseases related to complex III deficiency', *Biochim Biophys Acta,* 1793(1), pp. 181-5.

Besse, A., Wu, P., Bruni, F., Donti, T., Brett, William, McFarland, R., Moretti, P., Lalani, S., Kenneth, Robert and Penelope (2015) 'The GABA Transaminase, ABAT, Is Essential for Mitochondrial Nucleoside Metabolism', 21(3), pp. 417-427.

Boczonadi, V., Jennings, M. J. and Horvath, R. (2018) 'The role of tRNA synthetases in neurological and neuromuscular disorders', *FEBS Lett,* 592(5), pp. 703-717.

Bogenhagen, D. F., Martin, D. W. and Koller, A. (2014) 'Initial steps in RNA processing and ribosome assembly occur at mitochondrial DNA nucleoids', *Cell Metab,* 19(4), pp. 618-29.

Bogenhagen, D. F., Ostermeyer-Fay, A. G., Haley, J. D. and Garcia-Diaz, M. (2018) 'Kinetics and Mechanism of Mammalian Mitochondrial Ribosome Assembly', *Cell Rep,* 22(7), pp. 1935-1944.

Boggan, R. M., Lim, A., Taylor, R. W., McFarland, R. and Pickett, S. J. (2019) 'Resolving complexity in mitochondrial disease: Towards precision medicine', *Mol Genet Metab,* 128(1-2), pp. 19-29.

Borna, N. N., Kishita, Y., Kohda, M., Lim, S. C., Shimura, M., Wu, Y., Mogushi, K., Yatsuka, Y., Harashima, H., Hisatomi, Y., Fushimi, T., Ichimoto, K., Murayama, K., Ohtake, A. and Okazaki, Y. (2019) 'Mitochondrial ribosomal protein PTCD3 mutations cause oxidative phosphorylation defects with Leigh syndrome', *Neurogenetics,* 20(1), pp. 9-25.

Borowski, L. S., Dziembowski, A., Hejnowicz, M. S., Stepien, P. P. and Szczesny, R. J. (2013) 'Human mitochondrial RNA decay mediated by PNPase-hSuv3 complex takes place in distinct foci', 41(2), pp. 1223-1240.

Bourgeron, T., Rustin, P., Chretien, D., Birch-Machin, M., Bourgeois, M., Viegas-Pequignot, E., Munnich, A. and Rotig, A. (1995) 'Mutation of a nuclear succinate dehydrogenase gene results in mitochondrial respiratory chain deficiency', *Nat Genet,* 11(2), pp. 144-9.

Brito, S., Thompson, K., Campistol, J., Colomer, J., Hardy, S. A., He, L., Fernã¡Ndez-Marmiesse, A., Palacios, L., Jou, C., Jimã©Nez-Mallebrera, C., Armstrong, J., Montero, R., Artuch, R., Tischner, C., Wenz, T., McFarland, R. and Taylor, R. W. (2015) 'Long-term survival in a child with severe encephalopathy, multiple respiratory chain deficiency and GFM1 mutations', *Frontiers in Genetics,* 6.

Brown, A., Amunts, A., Bai, X. C., Sugimoto, Y., Edwards, P. C., Murshudov, G., Scheres, S. H. W. and Ramakrishnan, V. (2014) 'Structure of the large ribosomal subunit from human mitochondria', 346(6210), pp. 718-722.

Brown, W. M. (1980) 'Polymorphism in mitochondrial DNA of humans as revealed by restriction endonuclease analysis', *Proc Natl Acad Sci U S A,* 77(6), pp. 3605-9.

Bruni, F., Gramegna, P., Oliveira, J. M., Lightowlers, R. N. and Chrzanowska-Lightowlers, Z. M. (2013) 'REXO2 is an oligoribonuclease active in human mitochondria', *PLoS One,* 8(5), pp. e64670.

Brzoska, K., Meczynska, S. and Kruszewski, M. (2006) 'Iron-sulfur cluster proteins: electron transfer and beyond', *Acta Biochim Pol,* 53(4), pp. 685-91.

Bugiardini, E., Mitchell, A. L., Rosa, I. D., Horning-Do, H.-T., Pitmann, A., Poole, O. V., Holton, J. L., Shah, S., Woodward, C., Hargreaves, I., Quinlivan, R., Amunts, A., Wiesner, R. J., Houlden, H., Holt, I. J., Hanna, M. G., Pitceathly, R. D. S. and Spinazzola, A. (2019) 'MRPS25 mutations impair mitochondrial translation and cause encephalomyopathy', *Human Molecular Genetics*.

Cai, Y. C., Bullard, J. M., Thompson, N. L. and Spremulli, L. L. (2000) 'Interaction of Mitochondrial Elongation Factor Tu with Aminoacyl-tRNA and Elongation Factor Ts', 275(27), pp. 20308-20314.

Calvo, S. E., Clauser, K. R. and Mootha, V. K. (2016) 'MitoCarta2.0: an updated inventory of mammalian mitochondrial proteins', *Nucleic Acids Res,* 44(D1), pp. D1251-7.

Calvo, S. E., Compton, A. G., Hershman, S. G., Lim, S. C., Lieber, D. S., Tucker, E. J., Laskowski, A., Garone, C., Liu, S., Jaffe, D. B., Christodoulou, J., Fletcher, J. M., Bruno, D. L., Goldblatt, J., Dimauro, S., Thorburn, D. R. and Mootha, V. K. (2012) 'Molecular diagnosis of infantile mitochondrial disease with targeted next-generation sequencing', *Sci Transl Med,* 4(118), pp. 118ra10.

Carroll, C. J., Isohanni, P., Poyhonen, R., Euro, L., Richter, U., Brilhante, V., Gotz, A., Lahtinen, T., Paetau, A., Pihko, H., Battersby, B. J., Tyynismaa, H. and Suomalainen, A. (2013) 'Whole-exome sequencing identifies a mutation in the mitochondrial ribosome protein MRPL44 to underlie mitochondrial infantile cardiomyopathy', *J Med Genet,* 50(3), pp. 151-9.

Carroll, J., Fearnley, I. M., Skehel, J. M., Shannon, R. J., Hirst, J. and Walker, J. E. (2006) 'Bovine complex I is a complex of 45 different subunits', *J Biol Chem,* 281(43), pp. 32724-7.

Cerritelli, S. M., Frolova, E. G., Feng, C., Grinberg, A., Love, P. E. and Crouch, R. J. (2003) 'Failure to produce mitochondrial DNA results in embryonic lethality in Rnaseh1 null mice', *Mol Cell,* 11(3), pp. 807-15.

Chaban, Y., Boekema, E. J. and Dudkina, N. V. (2014) 'Structures of mitochondrial oxidative phosphorylation supercomplexes and mechanisms for their stabilisation', *Biochim Biophys Acta,* 1837(4), pp. 418-26.

Chan, D. C. (2012) 'Fusion and fission: interlinked processes critical for mitochondrial health', *Annu Rev Genet,* 46, pp. 265-87.

Chen, A., Tiosano, D., Guran, T., Baris, H. N., Bayram, Y., Mory, A., Shapiro-Kulnane, L., Hodges, C. A., Akdemir, Z. C., Turan, S., Jhangiani, S. N., van den Akker, F., Hoppel, C. L., Salz, H. K., Lupski, J. R. and Buchner, D. A. (2018) 'Mutations in the mitochondrial ribosomal protein MRPS22 lead to primary ovarian insufficiency', *Hum Mol Genet,* 27(11), pp. 1913-1926.

Chinnery, P. F., DiMauro, S., Shanske, S., Schon, E. A., Zeviani, M., Mariotti, C., Carrara, F., Lombes, A., Laforet, P., Ogier, H., Jaksch, M., Lochmuller, H., Horvath, R., Deschauer, M., Thorburn, D. R., Bindoff, L. A., Poulton, J., Taylor, R. W., Matthews, J. N. and Turnbull, D. M. (2004) 'Risk of developing a mitochondrial DNA deletion disorder', *Lancet,* 364(9434), pp. 592-6.

Chiron, S., Suleau, A. and Bonnefoy, N. (2005) 'Mitochondrial translation: elongation factor tu is essential in fission yeast and depends on an exchange factor conserved in humans but not in budding yeast', *Genetics,* 169(4), pp. 1891-901.

Christian, B., Haque, E. and Spremulli, L. (2009) 'Ribosome shifting or splitting: it is all up to the EF-G', *Mol Cell,* 35(4), pp. 400-2.

Christian, B. E. and Spremulli, L. L. (2009) 'Evidence for an active role of IF3mt in the initiation of translation in mammalian mitochondria', *Biochemistry,* 48(15), pp. 3269-78.

Christian, B. E. and Spremulli, L. L. (2010) 'Preferential selection of the 5'-terminal start codon on leaderless mRNAs by mammalian mitochondrial ribosomes', *J Biol Chem,* 285(36), pp. 28379-86.

Christian, B. E. and Spremulli, L. L. (2012) 'Mechanism of protein biosynthesis in mammalian mitochondria', 1819(9-10), pp. 1035-1054.

Chrzanowska-Lightowlers, Z., Rorbach, J. and Minczuk, M. (2017) 'Human mitochondrial ribosomes can switch structural tRNAs – but when and why?', *RNA Biology,* 14(12), pp. 1668-1671.

Chujo, T., Ohira, T., Sakaguchi, Y., Goshima, N., Nomura, N., Nagao, A. and Suzuki, T. (2012) 'LRPPRC/SLIRP suppresses PNPase-mediated mRNA decay and promotes polyadenylation in human mitochondria', *Nucleic Acids Res,* 40(16), pp. 8033-47.

Clay Montier, L. L., Deng, J. J. and Bai, Y. (2009) 'Number matters: control of mammalian mitochondrial DNA copy number', *Journal of Genetics and Genomics,* 36(3), pp. 125-131.

Clayton, D. A. (1982) 'Replication of animal mitochondrial DNA', *Cell,* 28(4), pp. 693-705.

Coenen, M. J., Antonicka, H., Ugalde, C., Sasarman, F., Rossi, R., Heister, J. G., Newbold, R. F., Trijbels, F. J., van den Heuvel, L. P., Shoubridge, E. A. and Smeitink, J. A. (2004) 'Mutant mitochondrial elongation factor G1 and combined oxidative phosphorylation deficiency', *N Engl J Med,* 351(20), pp. 2080-6.

Coolidge, C. J., Seely, R. J. and Patton, J. G. (1997) 'Functional analysis of the polypyrimidine tract in pre-mRNA splicing', *Nucleic Acids Res,* 25(4), pp. 888-96.

Cory, S. and Adams, J. M. (2002) 'The Bcl2 family: regulators of the cellular life-or-death switch', *Nat Rev Cancer,* 2(9), pp. 647-56.

Cramer, W. A., Hasan, S. S. and Yamashita, E. (2011) 'The Q cycle of cytochrome bc complexes: a structure perspective', *Biochim Biophys Acta,* 1807(7), pp. 788-802.

D'Souza, A. R. and Minczuk, M. (2018) 'Mitochondrial transcription and translation: overview', *Essays In Biochemistry,* 62(3), pp. 309-320.

Dahout-Gonzalez, C. (2006) 'Molecular, Functional, and Pathological Aspects of the Mitochondrial ADP/ATP Carrier', 21(4), pp. 242-249.

Dalla Rosa, I., Durigon, R., Pearce, S. F., Rorbach, J., Hirst, E. M., Vidoni, S., Reyes, A., Brea-Calvo, G., Minczuk, M., Woellhaf, M. W., Herrmann, J. M., Huynen, M. A., Holt, I. J. and Spinazzola, A. (2014) 'MPV17L2 is required for ribosome assembly in mitochondria', *Nucleic Acids Res,* 42(13), pp. 8500-15.

Dallabona, C., Diodato, D., Kevelam, S. H., Haack, T. B., Wong, L. J., Salomons, G. S., Baruffini, E., Melchionda, L., Mariotti, C., Strom, T. M., Meitinger, T., Prokisch, H., Chapman, K., Colley, A., Rocha, H., K, Schiffmann, R., Salsano, E., Savoiardo, M., Hamilton, E. M., Abbink, T. E. M., Wolf, N. I., Ferrero, I., Lamperti, C., Zeviani, M., Vanderver, A., Ghezzi, D. and Van Der Knaap, M. S. (2014) 'Novel (ovario) leukodystrophy related to AARS2 mutations', *Neurology,* 82(23), pp. 2063-2071.

Dayan, D., Bandel, M., Gunsel, U., Nussbaum, I., Prag, G., Mokranjac, D., Neupert, W. and Azem, A. (2019) 'A mutagenesis analysis of Tim50, the major receptor of the TIM23 complex, identifies regions that affect its interaction with Tim23', *Sci Rep,* 9(1), pp. 2012.

Dehairs, J., Talebi, A., Cherifi, Y. and Swinnen, J. V. (2016) 'CRISP-ID: decoding CRISPR mediated indels by Sanger sequencing', *Sci Rep,* 6, pp. 28973.

Deltcheva, E., Chylinski, K., Sharma, C. M., Gonzales, K., Chao, Y., Pirzada, Z. A., Eckert, M. R., Vogel, J. and Charpentier, E. (2011) 'CRISPR RNA maturation by trans-encoded small RNA and host factor RNase III', *Nature,* 471(7340), pp. 602-7.

Di Nottia, M., Marchese, M., Verrigni, D., Mutti, C. D., Torraco, A., Oliva, R., Fernandez-Vizarra, E., Morani, F., Trani, G., Rizza, T., Ghezzi, D., Ardissone, A., Nesti, C., Vasco, G., Zeviani, M., Minczuk, M., Bertini, E., Santorelli, F. M. and Carrozzo, R. (2020) 'A homozygous MRPL24 mutation causes a complex movement disorder and affects the mitoribosome assembly', *Neurobiol Dis,* 141, pp. 104880.

Dimmer, K. S., Papic, D., Schumann, B., Sperl, D., Krumpe, K., Walther, D. M. and Rapaport, D. (2012) 'A crucial role for Mim2 in the biogenesis of mitochondrial outer membrane proteins', *J Cell Sci,* 125(Pt 14), pp. 3464-73.

Distelmaier, F., Haack, T. B., Catarino, C. B., Gallenmuller, C., Rodenburg, R. J., Strom, T. M., Baertling, F., Meitinger, T., Mayatepek, E., Prokisch, H. and Klopstock, T. (2015) 'MRPL44 mutations cause a slowly progressive multisystem disease with childhood-onset hypertrophic cardiomyopathy', *Neurogenetics,* 16(4), pp. 319-23.

Dixon-Salazar, T. J., Silhavy, J. L., Udpa, N., Schroth, J., Bielas, S., Schaffer, A. E., Olvera, J., Bafna, V., Zaki, M. S., Abdel-Salam, G. H., Mansour, L. A., Selim, L., Abdel-Hadi, S., Marzouki, N., Ben-Omran, T., Al-Saana, N. A., Sonmez, F. M., Celep, F., Azam, M., Hill, K. J., Collazo, A., Fenstermaker, A. G., Novarino, G., Akizu, N., Garimella, K. V., Sougnez, C., Russ, C., Gabriel, S. B. and Gleeson, J. G. (2012) 'Exome Sequencing Can Improve Diagnosis and Alter Patient Management', 4(138), pp. 138ra78-138ra78.

Echevarria, L., Clemente, P., Hernandez-Sierra, R., Gallardo, M. E., Fernandez-Moreno, M. A. and Garesse, R. (2014) 'Glutamyl-tRNAGln amidotransferase is essential for mammalian mitochondrial translation in vivo', *Biochem J,* 460(1), pp. 91-101.

Efremov, R. G. and Sazanov, L. A. (2011) 'Respiratory complex I: 'steam engine' of the cell?', *Curr Opin Struct Biol,* 21(4), pp. 532-40.

El-Hattab, A. W., Craigen, W. J. and Scaglia, F. (2017) 'Mitochondrial DNA maintenance defects', *Biochimica et Biophysica Acta (BBA) - Molecular Basis of Disease,* 1863(6), pp. 1539-1555.

Elson, J. L., Swalwell, H., Blakely, E. L., McFarland, R., Taylor, R. W. and Turnbull, D. M. (2009) 'Pathogenic mitochondrial tRNA mutations--which mutations are inherited and why?', *Hum Mutat,* 30(11), pp. E984-92.

Emperador, S., Bayona-Bafaluy, M. P., Fernández-Marmiesse, A., Pineda, M., Felgueroso, B., López-Gallardo, E., Artuch, R., Roca, I., Ruiz-Pesini, E., Couce, M. L. and Montoya, J. (2017) 'Molecular-genetic characterization and rescue of a TSFM mutation causing childhood-onset ataxia and nonobstructive cardiomyopathy', *European Journal of Human Genetics,* 25(1), pp. 153-156.

Falkenberg, M. (2018) 'Mitochondrial DNA replication in mammalian cells: overview of the pathway', *Essays In Biochemistry,* 62(3), pp. 287-296.

Falkenberg, M., Gaspari, M., Rantanen, A., Trifunovic, A., Larsson, N.-G. and Gustafsson, C. M. (2002) 'Mitochondrial transcription factors B1 and B2 activate transcription of human mtDNA', 31(3), pp. 289-294.

Faxen, K., Gilderson, G., Adelroth, P. and Brzezinski, P. (2005) 'A mechanistic principle for proton pumping by cytochrome c oxidase', *Nature,* 437(7056), pp. 286-9.

Fernandez-Vizarra, E. and Zeviani, M. (2018) 'Mitochondrial complex III Rieske Fe-S protein processing and assembly', *Cell Cycle,* 17(6), pp. 681-687.

Finsterer, J. (2019) 'Extensive clinical and genetic workup is worthwhile in patients with Leigh-like syndrome due to the TSFM variant c.547G>A', *Neurogenetics*.

Frazier, A. E., Thorburn, D. R. and Compton, A. G. (2019) 'Mitochondrial energy generation disorders: genes, mechanisms, and clues to pathology', *J Biol Chem,* 294(14), pp. 5386-5395.

Frazier, A. E., Vincent, A. E., Turnbull, D. M., Thorburn, D. R. and Taylor, R. W. (2020) 'Assessment of mitochondrial respiratory chain enzymes in cells and tissues', *Methods Cell Biol,* 155, pp. 121-156.

Fukumura, S., Ohba, C., Watanabe, T., Minagawa, K., Shimura, M., Murayama, K., Ohtake, A., Saitsu, H., Matsumoto, N. and Tsutsumi, H. (2015) 'Compound heterozygous GFM2 mutations with Leigh syndrome complicated by arthrogryposis multiplex congenita', *J Hum Genet,* 60(9), pp. 509-13.

Fusté, J. M., Wanrooij, S., Jemt, E., Granycome, C. E., Cluett, T. J., Shi, Y., Atanassova, N., Holt, I. J., Gustafsson, C. M. and Falkenberg, M. (2010) 'Mitochondrial RNA Polymerase Is Needed for Activation of the Origin of Light-Strand DNA Replication', 37(1), pp. 67-78.

Galkin, A. and Moncada, S. (2017) 'Modulation of the conformational state of mitochondrial complex I as a target for therapeutic intervention', *Interface Focus,* 7(2), pp. 20160104.

Galmiche, L., Serre, V., Beinat, M., Assouline, Z., Lebre, A. S., Chretien, D., Nietschke, P., Benes, V., Boddaert, N., Sidi, D., Brunelle, F., Rio, M., Munnich, A. and Rotig, A. (2011) 'Exome sequencing identifies MRPL3 mutation in mitochondrial cardiomyopathy', *Hum Mutat,* 32(11), pp. 1225-31.

Galmiche, L., Serre, V., Beinat, M., Zossou, R., Assouline, Z., Lebre, A. S., Chretien, F., Shenhav, R., Zeharia, A., Saada, A., Vedrenne, V., Boddaert, N., de Lonlay, P., Rio, M., Munnich, A. and Rotig, A. (2012) 'Toward genotype phenotype correlations in GFM1 mutations', *Mitochondrion,* 12(2), pp. 242-7.

Garcia-Diaz, B., Mario, Sanna-Cherchi, S., Emmanuele, V., Hasan, Claudia, Horvath, R., Tadesse, S., Nader, Dimauro, S., Darryl, Shokr, A., Hirano, M. and Catarina (2012) 'Infantile Encephaloneuromyopathy and Defective Mitochondrial Translation Are Due to a Homozygous RMND1 Mutation', 91(4), pp. 729-736.

Gardeitchik, T., Mohamed, M., Ruzzenente, B., Karall, D., Guerrero-Castillo, S., Dalloyaux, D., van den Brand, M., van Kraaij, S., van Asbeck, E., Assouline, Z., Rio, M., de Lonlay, P., Scholl-Buergi, S., Wolthuis, D., Hoischen, A., Rodenburg, R. J., Sperl, W., Urban, Z., Brandt, U., Mayr, J. A., Wong, S., de Brouwer, A. P. M., Nijtmans, L., Munnich, A., Rotig, A., Wevers, R. A., Metodiev, M. D. and Morava, E. (2018) 'Bi-allelic Mutations in the Mitochondrial Ribosomal Protein MRPS2 Cause Sensorineural Hearing Loss, Hypoglycemia, and Multiple OXPHOS Complex Deficiencies', *Am J Hum Genet,* 102(4), pp. 685-695.

Garneau, J. E., Dupuis, M. E., Villion, M., Romero, D. A., Barrangou, R., Boyaval, P., Fremaux, C., Horvath, P., Magadan, A. H. and Moineau, S. (2010) 'The CRISPR/Cas bacterial immune system cleaves bacteriophage and plasmid DNA', *Nature,* 468(7320), pp. 67-71.

Gebert, N., Chacinska, A., Wagner, K., Guiard, B., Koehler, C. M., Rehling, P., Pfanner, N. and Wiedemann, N. (2008) 'Assembly of the three small Tim proteins precedes docking to the mitochondrial carrier translocase', *EMBO Rep,* 9(6), pp. 548-54.

Giachin, G., Bouverot, R., Acajjaoui, S., Pantalone, S. and Soler-Lopez, M. (2016) 'Dynamics of Human Mitochondrial Complex I Assembly: Implications for Neurodegenerative Diseases', *Front Mol Biosci,* 3, pp. 43.

Giles, R. E., Blanc, H., Cann, H. M. and Wallace, D. C. (1980) 'Maternal inheritance of human mitochondrial DNA', *Proc Natl Acad Sci U S A,* 77(11), pp. 6715-9.

Giorgi, C., Marchi, S. and Pinton, P. (2018) 'The machineries, regulation and cellular functions of mitochondrial calcium', *Nat Rev Mol Cell Biol,* 19(11), pp. 713-730.

Glasgow, R. I. C., Thompson, K., Barbosa, I. A., He, L., Alston, C. L., Deshpande, C., Simpson, M. A., Morris, A. A. M., Neu, A., Lobel, U., Hall, J., Prokisch, H., Haack, T. B., Hempel, M., McFarland, R. and Taylor, R. W. (2017) 'Novel GFM2 variants associated with early-onset neurological presentations of mitochondrial disease and impaired expression of OXPHOS subunits', *Neurogenetics,* 18(4), pp. 227-235.

Gohil, V. M. and Greenberg, M. L. (2009) 'Mitochondrial membrane biogenesis: phospholipids and proteins go hand in hand', *J Cell Biol,* 184(4), pp. 469-72.

Gorman, G. S., Chinnery, P. F., DiMauro, S., Hirano, M., Koga, Y., McFarland, R., Suomalainen, A., Thorburn, D. R., Zeviani, M. and Turnbull, D. M. (2016) 'Mitochondrial diseases', *Nat Rev Dis Primers,* 2, pp. 16080.

Gorman, G. S., Schaefer, A. M., Ng, Y., Gomez, N., Blakely, E. L., Alston, C. L., Feeney, C., Horvath, R., Yu-Wai-Man, P., Chinnery, P. F., Taylor, R. W., Turnbull, D. M. and McFarland, R. (2015) 'Prevalence of nuclear and mitochondrial DNA mutations related to adult mitochondrial disease', *Annals of Neurology,* 77(5), pp. 753-759.

Gotz, A., Tyynismaa, H., Euro, L., Ellonen, P., Hyotylainen, T., Ojala, T., Hamalainen, R. H., Tommiska, J., Raivio, T., Oresic, M., Karikoski, R., Tammela, O., Simola, K. O., Paetau, A., Tyni, T. and Suomalainen, A. (2011) 'Exome sequencing identifies mitochondrial alanyl-tRNA synthetase mutations in infantile mitochondrial cardiomyopathy', *Am J Hum Genet,* 88(5), pp. 635-42.

Grady, J. P., Campbell, G., Ratnaike, T., Blakely, E. L., Falkous, G., Nesbitt, V., Schaefer, A. M., McNally, R. J., Gorman, G. S., Taylor, R. W., Turnbull, D. M. and McFarland, R. (2014) 'Disease progression in patients with single, large-scale mitochondrial DNA deletions', *Brain,* 137(Pt 2), pp. 323-34.

Gray, M. W. (2012) 'Mitochondrial evolution', *Cold Spring Harb Perspect Biol,* 4(9), pp. a011403.

Gray, M. W., Burger, G. and Lang, B. F. (1999) 'Mitochondrial evolution', *Science,* 283(5407), pp. 1476-81.

Greber, B. J. and Ban, N. (2016) 'Structure and Function of the Mitochondrial Ribosome', *Annu Rev Biochem,* 85, pp. 103-32.

Greber, B. J., Bieri, P., Leibundgut, M., Leitner, A., Aebersold, R., Boehringer, D. and Ban, N. (2015) 'The complete structure of the 55S mammalian mitochondrial ribosome', *Science,* 348(6232), pp. 303-8.

Greber, B. J., Boehringer, D., Leitner, A., Bieri, P., Voigts-Hoffmann, F., Erzberger, J. P., Leibundgut, M., Aebersold, R. and Ban, N. (2014) 'Architecture of the large subunit of the mammalian mitochondrial ribosome', *Nature,* 505(7484), pp. 515-9.

Green, M. R. (1986) 'Pre-mRNA splicing', *Annu Rev Genet,* 20, pp. 671-708.

Gustafsson, C. M., Falkenberg, M. and Larsson, N. G. (2016) 'Maintenance and Expression of Mammalian Mitochondrial DNA', *Annu Rev Biochem,* 85, pp. 133-60.

Haack, T. B., Gorza, M., Danhauser, K., Mayr, J. A., Haberberger, B., Wieland, T., Kremer, L., Strecker, V., Graf, E., Memari, Y., Ahting, U., Kopajtich, R., Wortmann, S. B., Rodenburg, R. J., Kotzaeridou, U., Hoffmann, G. F., Sperl, W., Wittig, I., Wilichowski, E., Schottmann, G., Schuelke, M., Plecko, B., Stephani, U., Strom, T. M., Meitinger, T., Prokisch, H. and Freisinger, P. (2014) 'Phenotypic spectrum of eleven patients and five novel MTFMT mutations identified by exome sequencing and candidate gene screening', 111(3), pp. 342-352.

Hadrava Vanova, K., Kraus, M., Neuzil, J. and Rohlena, J. (2020) 'Mitochondrial complex II and reactive oxygen species in disease and therapy', *Redox Rep,* 25(1), pp. 26-32.

Hahn, A. and Zuryn, S. (2019) 'Mitochondrial Genome (mtDNA) Mutations that Generate Reactive Oxygen Species', *Antioxidants (Basel),* 8(9).

Hammarsund, M., Wilson, W., Corcoran, M., Merup, M., Einhorn, S., Grander, D. and Sangfelt, O. (2001) 'Identification and characterization of two novel human mitochondrial elongation factor genes, hEFG2 and hEFG1, phylogenetically conserved through evolution', *Hum Genet,* 109(5), pp. 542-50.

Haque, M. E., Spremulli, L. L. and Fecko, C. J. (2010) 'Identification of Protein-Protein and Protein-Ribosome Interacting Regions of the C-terminal Tail of Human Mitochondrial Inner Membrane Protein Oxa1L', 285(45), pp. 34991-34998.

Haute, L. V., Hendrick, A. G., D'Souza, A. R., Powell, C. A., Rebelo-Guiomar, P., Harbour, M. E., Ding, S., Fearnley, I. M., Andrews, B. and Minczuk, M. (2019) 'METTL15 introduces N4-methylcytidine into human mitochondrial 12S rRNA and is required for mitoribosome biogenesis', *Nucleic Acids Research*.

Hawlitschek, G., Schneider, H., Schmidt, B., Tropschug, M., Hartl, F. U. and Neupert, W. (1988) 'Mitochondrial protein import: identification of processing peptidase and of PEP, a processing enhancing protein', *Cell,* 53(5), pp. 795-806.

He, J., Cooper, H. M., Reyes, A., Di Re, M., Kazak, L., Wood, S. R., Mao, C. C., Fearnley, I. M., Walker, J. E. and Holt, I. J. (2012) 'Human C4orf14 interacts with the mitochondrial nucleoid and is involved in the biogenesis of the small mitochondrial ribosomal subunit', *Nucleic Acids Res,* 40(13), pp. 6097-108.

Hebbar, M., Girisha, K. M., Srivastava, A., Bielas, S. and Shukla, A. (2017) 'Homozygous c.359del variant in MGME1 is associated with early onset cerebellar ataxia', *European Journal of Medical Genetics,* 60(10), pp. 533-535.

Hikmat, O., Tzoulis, C., Chong, W. K., Chentouf, L., Klingenberg, C., Fratter, C., Carr, L. J., Prabhakar, P., Kumaraguru, N., Gissen, P., Cross, J. H., Jacques, T. S., Taanman, J. W., Bindoff, L. A. and Rahman, S. (2017) 'The clinical spectrum and natural history of early-onset diseases due to DNA polymerase gamma mutations', *Genet Med,* 19(11), pp. 1217-1225.

Hillen, H. S., Parshin, A. V., Agaronyan, K., Morozov, Y. I., Graber, J. J., Chernev, A., Schwinghammer, K., Urlaub, H., Anikin, M., Cramer, P. and Temiakov, D. (2017) 'Mechanism of Transcription Anti-termination in Human Mitochondria', *Cell,* 171(5), pp. 1082-1093 e13.

Hillen, H. S., Temiakov, D. and Cramer, P. (2018) 'Structural basis of mitochondrial transcription', *Nature Structural & Molecular Biology,* 25(9), pp. 754-765.

Hirokawa, G., Demeshkina, N., Iwakura, N., Kaji, H. and Kaji, A. (2006) 'The ribosome-recycling step: consensus or controversy?', *Trends Biochem Sci,* 31(3), pp. 143-9.

Holt, I. J. (2009) 'Mitochondrial DNA replication and repair: all a flap', *Trends in Biochemical Sciences,* 34(7), pp. 358-365.

Holt, I. J., Lorimer, H. E. and Jacobs, H. T. (2000) 'Coupled Leading- and Lagging-Strand Synthesis of Mammalian Mitochondrial DNA', *Cell,* 100(5), pp. 515-524.

Horvath, P. and Barrangou, R. (2010) 'CRISPR/Cas, the immune system of bacteria and archaea', *Science,* 327(5962), pp. 167-70.

Iliakis, G., Wang, H., Perrault, A. R., Boecker, W., Rosidi, B., Windhofer, F., Wu, W., Guan, J., Terzoudi, G. and Pantelias, G. (2004) 'Mechanisms of DNA double strand break repair and chromosome aberration formation', *Cytogenet Genome Res,* 104(1-4), pp. 14-20.

Ishino, Y., Shinagawa, H., Makino, K., Amemura, M. and Nakata, A. (1987) 'Nucleotide sequence of the iap gene, responsible for alkaline phosphatase isozyme conversion in Escherichia coli, and identification of the gene product', *J Bacteriol,* 169(12), pp. 5429-33.

Ivanova, E., Jowitt, T. A. and Lu, H. (2008) 'Assembly of the mitochondrial Tim9-Tim10 complex: a multi-step reaction with novel intermediates', *J Mol Biol,* 375(1), pp. 229-39.

Jackson, C. B., Huemer, M., Bolognini, R., Martin, F., Szinnai, G., Donner, B. C., Richter, U., Battersby, B. J., Nuoffer, J. M., Suomalainen, A. and Schaller, A. (2019) 'A variant in MRPS14 (uS14m) causes perinatal hypertrophic cardiomyopathy with neonatal lactic acidosis, growth retardation, dysmorphic features and neurological involvement', *Hum Mol Genet,* 28(4), pp. 639-649.

Janer, A., Prudent, J., Paupe, V., Fahiminiya, S., Majewski, J., Sgarioto, N., Des Rosiers, C., Forest, A., Lin, Z. Y., Gingras, A. C., Mitchell, G., McBride, H. M. and Shoubridge, E. A. (2016) 'SLC25A46 is required for mitochondrial lipid homeostasis and cristae maintenance and is responsible for Leigh syndrome', *EMBO Mol Med,* 8(9), pp. 1019-38.

Janer, A., Van Karnebeek, C. D., Sasarman, F., Antonicka, H., Al Ghamdi, M., Shyr, C., Dunbar, M., Stockler-Ispiroglu, S., Ross, C. J., Vallance, H., Dionne, J., Wasserman, W. W. and Shoubridge, E. A. (2015) 'RMND1 deficiency associated with neonatal lactic acidosis, infantile onset renal failure, deafness, and multiorgan involvement', 23(10), pp. 1301-1307.

Jansen, R., Embden, J. D., Gaastra, W. and Schouls, L. M. (2002) 'Identification of genes that are associated with DNA repeats in prokaryotes', *Mol Microbiol,* 43(6), pp. 1565-75.

Jinek, M., Chylinski, K., Fonfara, I., Hauer, M., Doudna, J. A. and Charpentier, E. (2012) 'A programmable dual-RNA-guided DNA endonuclease in adaptive bacterial immunity', *Science,* 337(6096), pp. 816-21.

Jing, R., Corbett, J. L., Cai, J., Beeson, G. C., Beeson, C. C., Chan, S. S., Dimmock, D. P., Lazcares, L., Geurts, A. M., Lemasters, J. J. and Duncan, S. A. (2018) 'A Screen Using iPSC-Derived Hepatocytes Reveals NAD(+) as a Potential Treatment for mtDNA Depletion Syndrome', *Cell Rep,* 25(6), pp. 1469-1484 e5.

Jobbins, A. M., Reichenbach, L. F., Lucas, C. M., Hudson, A. J., Burley, G. A. and Eperon, I. C. (2018) 'The mechanisms of a mammalian splicing enhancer', *Nucleic Acids Res,* 46(5), pp. 2145-2158.

Johansson, M. and Karlsson, A. (1996) 'Cloning and expression of human deoxyguanosine kinase cDNA', 93(14), pp. 7258-7262.

Johansson, M. and Karlsson, A. (1997) 'Cloning of the cDNA and Chromosome Localization of the Gene for Human Thymidine Kinase 2', 272(13), pp. 8454-8458.

Jonckheere, A. I., Smeitink, J. A. and Rodenburg, R. J. (2012) 'Mitochondrial ATP synthase: architecture, function and pathology', *J Inherit Metab Dis,* 35(2), pp. 211-25.

Jourdain, A. A., Koppen, M., Wydro, M., Rodley, C. D., Lightowlers, R. N., Chrzanowska-Lightowlers, Z. M. and Martinou, J. C. (2013) 'GRSF1 regulates RNA processing in mitochondrial RNA granules', *Cell Metab,* 17(3), pp. 399-410.

Joyce, N. C., Oskarsson, B. and Jin, L. W. (2012) 'Muscle biopsy evaluation in neuromuscular disorders', *Phys Med Rehabil Clin N Am,* 23(3), pp. 609-31.

Jukes, T. H. (1983) 'Evolution of the amino acid code: inferences from mitochondrial codes', *J Mol Evol,* 19(3-4), pp. 219-25.

Karvelis, T., Gasiunas, G., Miksys, A., Barrangou, R., Horvath, P. and Siksnys, V. (2013) 'crRNA and tracrRNA guide Cas9-mediated DNA interference in Streptococcus thermophilus', *RNA Biol,* 10(5), pp. 841-51.

Kasiviswanathan, R., Collins, T. R. and Copeland, W. C. (2012) 'The interface of transcription and DNA replication in the mitochondria', *Biochim Biophys Acta,* 1819(9-10), pp. 970-8.

Kilic, M., Oguz, K. K., Kilic, E., Yuksel, D., Demirci, H., Sagiroglu, M. S., Yucel-Yilmaz, D. and Ozgul, R. K. (2017) 'A patient with mitochondrial disorder due to a novel mutation in MRPS22', *Metab Brain Dis,* 32(5), pp. 1389-1393.

Kispal, G., Csere, P., Prohl, C. and Lill, R. (1999) 'The mitochondrial proteins Atm1p and Nfs1p are essential for biogenesis of cytosolic Fe/S proteins', *EMBO J,* 18(14), pp. 3981-9.

Klinge, S. and Woolford, J. L., Jr. (2019) 'Ribosome assembly coming into focus', *Nat Rev Mol Cell Biol,* 20(2), pp. 116-131.

Kluck, R. M., Bossy-Wetzel, E., Green, D. R. and Newmeyer, D. D. (1997) 'The release of cytochrome c from mitochondria: a primary site for Bcl-2 regulation of apoptosis', *Science,* 275(5303), pp. 1132-6.

Koehler, C. M., Jarosch, E., Tokatlidis, K., Schmid, K., Schweyen, R. J. and Schatz, G. (1998) 'Import of mitochondrial carriers mediated by essential proteins of the intermembrane space', *Science,* 279(5349), pp. 369-73.

Kohda, M., Tokuzawa, Y., Kishita, Y., Nyuzuki, H., Moriyama, Y., Mizuno, Y., Hirata, T., Yatsuka, Y., Yamashita-Sugahara, Y., Nakachi, Y., Kato, H., Okuda, A., Tamaru, S., Borna, N. N., Banshoya, K., Aigaki, T., Sato-Miyata, Y., Ohnuma, K., Suzuki, T., Nagao, A., Maehata, H., Matsuda, F., Higasa, K., Nagasaki, M., Yasuda, J., Yamamoto, M., Fushimi, T., Shimura, M., Kaiho-Ichimoto, K., Harashima, H., Yamazaki, T., Mori, M., Murayama, K., Ohtake, A. and Okazaki, Y. (2016) 'A Comprehensive Genomic Analysis Reveals the Genetic Landscape of Mitochondrial Respiratory Chain Complex Deficiencies', *PLoS Genet,* 12(1), pp. e1005679.

Kondadi, A. K., Anand, R. and Reichert, A. S. (2019) 'Functional Interplay between Cristae Biogenesis, Mitochondrial Dynamics and Mitochondrial DNA Integrity', *Int J Mol Sci,* 20(17).

Koripella, R. K., Sharma, M. R., Risteff, P., Keshavan, P. and Agrawal, R. K. (2019) 'Structural insights into unique features of the human mitochondrial ribosome recycling', *Proc Natl Acad Sci U S A,* 116(17), pp. 8283-8288.

Korr, H., Kurz, C., Seidler, T. O., Sommer, D. and Schmitz, C. (1998) 'Mitochondrial DNA synthesis studied autoradiographically in various cell types in vivo', *Brazilian Journal of Medical and Biological Research,* 31(2), pp. 289-298.

Kotani, T., Akabane, S., Takeyasu, K., Ueda, T. and Takeuchi, N. (2013) 'Human G-proteins, ObgH1 and Mtg1, associate with the large mitochondrial ribosome subunit and are involved in translation and assembly of respiratory complexes', *Nucleic Acids Res,* 41(6), pp. 3713-22.

Kowluru, A., Tannous, M. and Chen, H.-Q. (2002) 'Localization and Characterization of the Mitochondrial Isoform of the Nucleoside Diphosphate Kinase in the Pancreatic β Cell: Evidence for Its Complexation with Mitochondrial Succinyl-CoA Synthetase', 398(2), pp. 160-169.

Kraus, F. and Ryan, M. T. (2017) 'The constriction and scission machineries involved in mitochondrial fission', *J Cell Sci,* 130(18), pp. 2953-2960.

Krawczak, M., Thomas, N. S., Hundrieser, B., Mort, M., Wittig, M., Hampe, J. and Cooper, D. N. (2007) 'Single base-pair substitutions in exon-intron junctions of human genes: nature, distribution, and consequences for mRNA splicing', *Hum Mutat,* 28(2), pp. 150-8.

Kuhl, I., Miranda, M., Posse, V., Milenkovic, D., Mourier, A., Siira, S. J., Bonekamp, N. A., Neumann, U., Filipovska, A., Polosa, P. L., Gustafsson, C. M. and Larsson, N. G. (2016) 'POLRMT regulates the switch between replication primer formation and gene expression of mammalian mtDNA', *Sci Adv,* 2(8), pp. e1600963.

Lake, N. J., Webb, B. D., Stroud, D. A., Richman, T. R., Ruzzenente, B., Compton, A. G., Mountford, H. S., Pulman, J., Zangarelli, C., Rio, M., Boddaert, N., Assouline, Z., Sherpa, M. D., Schadt, E. E., Houten, S. M., Byrnes, J., McCormick, E. M., Zolkipli-Cunningham, Z., Haude, K., Zhang, Z., Retterer, K., Bai, R., Calvo, S. E., Mootha, V. K., Christodoulou, J., Rotig, A., Filipovska, A., Cristian, I., Falk, M. J., Metodiev, M. D. and Thorburn, D. R. (2017) 'Biallelic Mutations in MRPS34 Lead to Instability of the Small Mitoribosomal Subunit and Leigh Syndrome', *Am J Hum Genet,* 101(2), pp. 239-254.

Lee, K. W. and Bogenhagen, D. F. (2014) 'Assignment of 2'-O-methyltransferases to modification sites on the mammalian mitochondrial large subunit 16 S ribosomal RNA (rRNA)', *J Biol Chem,* 289(36), pp. 24936-42.

Lee, K. W., Okot-Kotber, C., LaComb, J. F. and Bogenhagen, D. F. (2013) 'Mitochondrial ribosomal RNA (rRNA) methyltransferase family members are positioned to modify nascent rRNA in foci near the mitochondrial DNA nucleoid', *J Biol Chem,* 288(43), pp. 31386-99.

Lee, Y.-S., Kennedy, W. D. and Yin, Y. W. (2009) 'Structural Insight into Processive Human Mitochondrial DNA Synthesis and Disease-Related Polymerase Mutations', 139(2), pp. 312-324.

Lightowlers, R. N. and Chrzanowska-Lightowlers, Z. M. (2010) 'Terminating human mitochondrial protein synthesis: a shift in our thinking', *RNA Biol,* 7(3), pp. 282-6.

Lightowlers, R. N., Rozanska, A. and Chrzanowska-Lightowlers, Z. M. (2014) 'Mitochondrial protein synthesis: figuring the fundamentals, complexities and complications, of mammalian mitochondrial translation', *FEBS Lett,* 588(15), pp. 2496-503.

Lino, C. A., Harper, J. C., Carney, J. P. and Timlin, J. A. (2018) 'Delivering CRISPR: a review of the challenges and approaches', *Drug Deliv,* 25(1), pp. 1234-1257.

Litonin, D., Sologub, M., Shi, Y., Savkina, M., Anikin, M., Falkenberg, M., Gustafsson, C. and Temiakov, D. (2010) 'Human mitochondrial transcription revisited: only TFAM and TFB2M are required for transcription of the mitochondrial genes in vitro', 285(24), pp. jbc.C110.128918.

Liu, M. and Spremulli, L. (2000) 'Interaction of mammalian mitochondrial ribosomes with the inner membrane', *J Biol Chem,* 275(38), pp. 29400-6.

Loeffen, J. L., Smeitink, J. A., Trijbels, J. M., Janssen, A. J., Triepels, R. H., Sengers, R. C. and van den Heuvel, L. P. (2000) 'Isolated complex I deficiency in children: clinical, biochemical and genetic aspects', *Hum Mutat,* 15(2), pp. 123-34.

Loson, O. C., Song, Z., Chen, H. and Chan, D. C. (2013) 'Fis1, Mff, MiD49, and MiD51 mediate Drp1 recruitment in mitochondrial fission', *Mol Biol Cell,* 24(5), pp. 659-67.

Lott, M. T., Leipzig, J. N., Derbeneva, O., Xie, H. M., Chalkia, D., Sarmady, M., Procaccio, V. and Wallace, D. C. (2013) 'mtDNA Variation and Analysis Using Mitomap and Mitomaster', *Curr Protoc Bioinformatics,* 44, pp. 1 23 1-26.

Luckey, J. A., Drossman, H., Kostichka, A. J., Mead, D. A., D'Cunha, J., Norris, T. B. and Smith, L. M. (1990) 'High speed DNA sequencing by capillary electrophoresis', *Nucleic Acids Res,* 18(15), pp. 4417-21.

Luo, S., Valencia, C. A., Zhang, J., Lee, N. C., Slone, J., Gui, B., Wang, X., Li, Z., Dell, S., Brown, J., Chen, S. M., Chien, Y. H., Hwu, W. L., Fan, P. C., Wong, L. J., Atwal, P. S. and Huang, T. (2018) 'Biparental Inheritance of Mitochondrial DNA in Humans', *Proc Natl Acad Sci U S A,* 115(51), pp. 13039-13044.

Luo, S. M., Ge, Z. J., Wang, Z. W., Jiang, Z. Z., Wang, Z. B., Ouyang, Y. C., Hou, Y., Schatten, H. and Sun, Q. Y. (2013) 'Unique insights into maternal mitochondrial inheritance in mice', *Proc Natl Acad Sci U S A,* 110(32), pp. 13038-43.

Lutz-Bonengel, S. and Parson, W. (2019) 'No further evidence for paternal leakage of mitochondrial DNA in humans yet', *Proc Natl Acad Sci U S A,* 116(6), pp. 1821-1822.

Ma, Y., Zhang, L. and Huang, X. (2014) 'Genome modification by CRISPR/Cas9', *FEBS J,* 281(23), pp. 5186-93.

Magnusson, J., Orth, M., Lestienne, P. and Taanman, J. W. (2003) 'Replication of mitochondrial DNA occurs throughout the mitochondria of cultured human cells', *Exp Cell Res,* 289(1), pp. 133-42.

Mai, N., Chrzanowska-Lightowlers, Z. M. A. and Lightowlers, R. N. (2017) 'The process of mammalian mitochondrial protein synthesis', *Cell and Tissue Research,* 367(1), pp. 5-20.

Makarova, K. S., Haft, D. H., Barrangou, R., Brouns, S. J., Charpentier, E., Horvath, P., Moineau, S., Mojica, F. J., Wolf, Y. I., Yakunin, A. F., van der Oost, J. and Koonin, E. V. (2011) 'Evolution and classification of the CRISPR-Cas systems', *Nat Rev Microbiol,* 9(6), pp. 467-77.

Marinoni, E. N., de Oliveira, J. S., Nicolet, Y., Raulfs, E. C., Amara, P., Dean, D. R. and Fontecilla-Camps, J. C. (2012) '(IscS-IscU)2 complex structures provide insights into Fe2S2 biogenesis and transfer', *Angew Chem Int Ed Engl,* 51(22), pp. 5439-42.

Martikainen, M. H. and Chinnery, P. F. (2015) 'Mitochondrial disease: mimics and chameleons', *Pract Neurol,* 15(6), pp. 424-35.

Mayr, J. A., Haack, T. B., Freisinger, P., Karall, D., Makowski, C., Koch, J., Feichtinger, R. G., Zimmermann, F. A., Rolinski, B., Ahting, U., Meitinger, T., Prokisch, H. and Sperl, W. (2015) 'Spectrum of combined respiratory chain defects', *J Inherit Metab Dis,* 38(4), pp. 629-40.

McLean, J. R., Cohn, G. L., Brandt, I. K. and Simpson, M. V. (1958) 'Incorporation of labeled amino acids into the protein of muscle and liver mitochondria', *J Biol Chem,* 233(3), pp. 657-63.

McMillan, H. J., Schwartzentruber, J., Smith, A., Lee, S., Chakraborty, P., Bulman, D. E., Beaulieu, C. L., Majewski, J., Boycott, K. M. and Geraghty, M. T. (2014) 'Compound heterozygous mutations in glycyl-tRNA synthetase are a proposed cause of systemic mitochondrial disease', *BMC Medical Genetics,* 15(1), pp. 36.

McWilliams, T. G. and Suomalainen, A. (2019) 'Mitochondrial DNA can be inherited from fathers, not just mothers', *Nature,* 565(7739), pp. 296-297.

Meera Krishna, B., Khan, M. A. and Khan, S. T. (2019) 'Next-Generation Sequencing (NGS) Platforms: An Exciting Era of Genome Sequence Analysis', in Tripathi, V., Kumar, P., Tripathi, P., Kishore, A. and Kamle, M. (eds.) *Microbial Genomics in Sustainable Agroecosystems: Volume 2*. Singapore: Springer Singapore, pp. 89-109.

Mendelsohn, B. A., Bennett, N. K., Darch, M. A., Yu, K., Nguyen, M. K., Pucciarelli, D., Nelson, M., Horlbeck, M. A., Gilbert, L. A., Hyun, W., Kampmann, M., Nakamura, J. L. and Nakamura, K. (2018) 'A high-throughput screen of real-time ATP levels in individual cells reveals mechanisms of energy failure', *PLoS Biol,* 16(8), pp. e2004624.

Menezes, M. J., Guo, Y., Zhang, J., Riley, L. G., Cooper, S. T., Thorburn, D. R., Li, J., Dong, D., Li, Z., Glessner, J., Davis, R. L., Sue, C. M., Alexander, S. I., Arbuckle, S., Kirwan, P., Keating, B. J., Xu, X., Hakonarson, H. and Christodoulou, J. (2015) 'Mutation in mitochondrial ribosomal protein S7 (MRPS7) causes congenital sensorineural deafness, progressive hepatic and renal failure and lactic acidemia', *Hum Mol Genet,* 24(8), pp. 2297-307.

Mercer, T. R., Clark, M. B., Andersen, S. B., Brunck, M. E., Haerty, W., Crawford, J., Taft, R. J., Nielsen, L. K., Dinger, M. E. and Mattick, J. S. (2015) 'Genome-wide discovery of human splicing branchpoints', *Genome Res,* 25(2), pp. 290-303.

Metodiev, M. D., Lesko, N., Park, C. B., Cámara, Y., Shi, Y., Wibom, R., Hultenby, K., Gustafsson, C. M. and Larsson, N.-G. (2009) 'Methylation of 12S rRNA Is Necessary for In Vivo Stability of the Small Subunit of the Mammalian Mitochondrial Ribosome', 9(4), pp. 386-397.

Metodiev, M. D., Spåhr, H., Loguercio Polosa, P., Meharg, C., Becker, C., Altmueller, J., Habermann, B., Larsson, N.-G. and Ruzzenente, B. (2014) 'NSUN4 Is a Dual Function Mitochondrial Protein Required for Both Methylation of 12S rRNA and Coordination of Mitoribosomal Assembly', 10(2), pp. e1004110.

Metodiev, M. D., Thompson, K., Charlotte, Andrew, He, L., Assouline, Z., Rio, M., Bahi-Buisson, N., Pyle, A., Griffin, H., Siira, S., Filipovska, A., Munnich, A., Patrick, McFarland, R., Rötig, A. and Robert (2016) 'Recessive Mutations in TRMT10C Cause

Defects in Mitochondrial RNA Processing and Multiple Respiratory Chain Deficiencies', 98(5), pp. 993-1000.

Milenkovic, D., Matic, S., Kuhl, I., Ruzzenente, B., Freyer, C., Jemt, E., Park, C. B., Falkenberg, M. and Larsson, N. G. (2013) 'TWINKLE is an essential mitochondrial helicase required for synthesis of nascent D-loop strands and complete mtDNA replication', *Human Molecular Genetics,* 22(10), pp. 1983-1993.

Miller, C., Saada, A., Shaul, N., Shabtai, N., Ben-Shalom, E., Shaag, A., Hershkovitz, E. and Elpeleg, O. (2004) 'Defective mitochondrial translation caused by a ribosomal protein (MRPS16) mutation', *Ann Neurol,* 56(5), pp. 734-8.

Minczuk, M., Piwowarski, J., Papworth, M. A., Awiszus, K., Schalinski, S., Dziembowski, A., Dmochowska, A., Bartnik, E., Tokatlidis, K., Stepien, P. P. and Borowski, P. (2002) 'Localisation of the human hSuv3p helicase in the mitochondrial matrix and its preferential unwinding of dsDNA', *Nucleic Acids Res,* 30(23), pp. 5074-86.

Miralles Fusté, J., Shi, Y., Wanrooij, S., Zhu, X., Jemt, E., Persson, Ö., Sabouri, N., Gustafsson, C. M. and Falkenberg, M. (2014) 'In Vivo Occupancy of Mitochondrial Single-Stranded DNA Binding Protein Supports the Strand Displacement Mode of DNA Replication', *PLoS Genetics,* 10(12), pp. e1004832.

Mitchell, P. (1961) 'Coupling of phosphorylation to electron and hydrogen transfer by a chemi-osmotic type of mechanism', *Nature,* 191, pp. 144-8.

Mizuguchi, T., Nakashima, M., Kato, M., Yamada, K., Okanishi, T., Ekhilevitch, N., Mandel, H., Eran, A., Toyono, M., Sawaishi, Y., Motoi, H., Shiina, M., Ogata, K., Miyatake, S., Miyake, N., Saitsu, H. and Matsumoto, N. (2017) 'PARS2 and NARS2 mutations in infantile-onset neurodegenerative disorder', *J Hum Genet,* 62(5), pp. 525-529.

Mojica, F. J. M., Diez-Villasenor, C., Garcia-Martinez, J. and Almendros, C. (2009) 'Short motif sequences determine the targets of the prokaryotic CRISPR defence system', *Microbiology,* 155(Pt 3), pp. 733-740.

Montoya, J., Christianson, T., Levens, D., Rabinowitz, M. and Attardi, G. (1982) 'Identification of initiation sites for heavy-strand and light-strand transcription in human mitochondrial DNA', 79(23), pp. 7195-7199.

Nakajima, J., Eminoglu, T. F., Vatansever, G., Nakashima, M., Tsurusaki, Y., Saitsu, H., Kawashima, H., Matsumoto, N. and Miyake, N. (2014) 'A novel homozygous YARS2 mutation causes severe myopathy, lactic acidosis, and sideroblastic anemia 2', 59(4), pp. 229-232.

Ng, Y. S., Alston, C. L., Diodato, D., Morris, A. A., Ulrick, N., Kmoch, S., Houstek, J., Martinelli, D., Haghighi, A., Atiq, M., Gamero, M. A., Garcia-Martinez, E., Kratochvilova, H., Santra, S., Brown, R. M., Brown, G. K., Ragge, N., Monavari, A., Pysden, K., Ravn, K., Casey, J. P., Khan, A., Chakrapani, A., Vassallo, G., Simons, C., McKeever, K., O'Sullivan, S., Childs, A. M., Ostergaard, E., Vanderver, A., Goldstein, A., Vogt, J., Taylor, R. W. and McFarland, R. (2016) 'The clinical, biochemical and genetic features associated with RMND1-related mitochondrial disease', *J Med Genet,* 53(11), pp. 768-775.

Nicholls, T. J., Nadalutti, C. A., Motori, E., Sommerville, E. W., Gorman, G. S., Basu, S., Hoberg, E., Turnbull, D. M., Chinnery, P. F., Larsson, N. G., Larsson, E., Falkenberg, M., Taylor, R. W., Griffith, J. D. and Gustafsson, C. M. (2018)

'Topoisomerase 3alpha Is Required for Decatenation and Segregation of Human mtDNA', *Mol Cell,* 69(1), pp. 9-23 e6.

Nicholls, T. J., Zsurka, G., Peeva, V., Scholer, S., Szczesny, R. J., Cysewski, D., Reyes, A., Kornblum, C., Sciacco, M., Moggio, M., Dziembowski, A., Kunz, W. S. and Minczuk, M. (2014) 'Linear mtDNA fragments and unusual mtDNA rearrangements associated with pathological deficiency of MGME1 exonuclease', 23(23), pp. 6147-6162.

Nishimasu, H., Ran, F. A., Hsu, P. D., Konermann, S., Shehata, S. I., Dohmae, N., Ishitani, R., Zhang, F. and Nureki, O. (2014) 'Crystal structure of Cas9 in complex with guide RNA and target DNA', *Cell,* 156(5), pp. 935-49.

Ojala, D., Montoya, J. and Attardi, G. (1981) 'tRNA punctuation model of RNA processing in human mitochondria', *Nature,* 290(5806), pp. 470-474.

Oliveira, M. T. and Kaguni, L. S. (2010) 'Functional Roles of the N- and C-Terminal Regions of the Human Mitochondrial Single-Stranded DNA-Binding Protein', 5(10), pp. e15379.

Osellame, L. D., Blacker, T. S. and Duchen, M. R. (2012) 'Cellular and molecular mechanisms of mitochondrial function', *Best Pract Res Clin Endocrinol Metab,* 26(6), pp. 711-23.

Ozaki, T., Neumann, T., Wai, D., Schafer, K. L., van Valen, F., Lindner, N., Scheel, C., Bocker, W., Winkelmann, W., Dockhorn-Dworniczak, B., Horst, J. and Poremba, C. (2003) 'Chromosomal alterations in osteosarcoma cell lines revealed by comparative genomic hybridization and multicolor karyotyping', *Cancer Genet Cytogenet,* 140(2), pp. 145-52.

Parikh, S. (2010) 'The neurologic manifestations of mitochondrial disease', *Dev Disabil Res Rev,* 16(2), pp. 120-8.

Pearce, S., Nezich, C. L. and Spinazzola, A. (2013) 'Mitochondrial diseases: translation matters', *Mol Cell Neurosci,* 55, pp. 1-12.

Pena, J. A., Lotze, T., Yang, Y., Umana, L., Walkiewicz, M., Hunter, J. V. and Scaglia, F. (2016) 'Methionyl-tRNA Formyltransferase (MTFMT) Deficiency Mimicking Acquired Demyelinating Disease', 31(2), pp. 215-219.

Penque, B. A., Su, L., Wang, J., Ji, W., Bale, A., Luh, F., Fulbright, R. K., Sarmast, U., Sega, A. G., Konstantino, M., Spencer-Manzon, M., Pierce, R., Yen, Y. and Lakhani, S. A. (2018) 'A homozygous variant in RRM2B is associated with severe metabolic acidosis and early neonatal death', *European Journal of Medical Genetics*.

Perli, E., Pisano, A., Glasgow, R. I. C., Carbo, M., Hardy, S. A., Falkous, G., He, L., Cerbelli, B., Pignataro, M. G., Zacara, E., Re, F., Della Monica, P. L., Morea, V., Bonnen, P. E., Taylor, R. W., D'Amati, G. and Giordano, C. (2019) 'Novel compound mutations in the mitochondrial translation elongation factor (TSFM) gene cause severe cardiomyopathy with myocardial fibro-adipose replacement', *Scientific Reports,* 9(1).

Pietromonaco, S. F., Denslow, N. D. and O'Brien, T. W. (1991) 'Proteins of mammalian mitochondrial ribosomes', *Biochimie,* 73(6), pp. 827-35.

Ponnalagu, D. and Singh, H. (2017) 'Anion Channels of Mitochondria', *Handb Exp Pharmacol,* 240, pp. 71-101.

Pontarin, G., Fijolek, A., Pizzo, P., Ferraro, P., Rampazzo, C., Pozzan, T., Thelander, L., Reichard, P. A. and Bianchi, V. (2008) 'Ribonucleotide reduction is a cytosolic

process in mammalian cells independently of DNA damage', 105(46), pp. 17801-17806.

Pool, M. R. (2005) 'Signal recognition particles in chloroplasts, bacteria, yeast and mammals (review)', *Mol Membr Biol,* 22(1-2), pp. 3-15.

Posse, V., Hoberg, E., Dierckx, A., Shahzad, S., Koolmeister, C., Larsson, N. G., Wilhelmsson, L. M., Hallberg, B. M. and Gustafsson, C. M. (2014) 'The amino terminal extension of mammalian mitochondrial RNA polymerase ensures promoter specific transcription initiation', *Nucleic Acids Res,* 42(6), pp. 3638-47.

Posse, V., Shahzad, S., Falkenberg, M., Hallberg, B. M. and Gustafsson, C. M. (2015) 'TEFM is a potent stimulator of mitochondrial transcription elongation in vitro', *Nucleic Acids Res,* 43(5), pp. 2615-24.

Pourcel, C., Salvignol, G. and Vergnaud, G. (2005) 'CRISPR elements in Yersinia pestis acquire new repeats by preferential uptake of bacteriophage DNA, and provide additional tools for evolutionary studies', *Microbiology,* 151(Pt 3), pp. 653-663.

Pronicka, E., Piekutowska-Abramczuk, D., Ciara, E., Trubicka, J., Rokicki, D., Karkucińska-Więckowska, A., Pajdowska, M., Jurkiewicz, E., Halat, P., Kosińska, J., Pollak, A., Rydzanicz, M., Stawinski, P., Pronicki, M., Krajewska-Walasek, M. and Płoski, R. (2016) 'New perspective in diagnostics of mitochondrial disorders: two years' experience with whole-exome sequencing at a national paediatric centre', *Journal of Translational Medicine,* 14(1).

Pulman, J., Ruzzenente, B., Bianchi, L., Rio, M., Boddaert, N., Munnich, A., Rotig, A. and Metodiev, M. D. (2019) 'Mutations in the MRPS28 gene encoding the small mitoribosomal subunit protein bS1m in a patient with intrauterine growth retardation, craniofacial dysmorphism and multisystemic involvement', *Hum Mol Genet,* 28(9), pp. 1445-1462.

Pulst, S. M. (1999) 'Genetic linkage analysis', *Arch Neurol,* 56(6), pp. 667-72.

Rabbani, B., Tekin, M. and Mahdieh, N. (2014) 'The promise of whole-exome sequencing in medical genetics', *J Hum Genet,* 59(1), pp. 5-15.

Rahman, S. and Copeland, W. C. (2019) 'POLG-related disorders and their neurological manifestations', *Nature Reviews Neurology,* 15(1), pp. 40-52.

Rapp, G., Klaudiny, J., Hagendorff, G., Luck, M. R. and Scheit, K. H. (1989) 'Complete sequence of the coding region of human elongation factor 2 (EF-2) by enzymatic amplification of cDNA from human ovarian granulosa cells', *Biol Chem Hoppe Seyler,* 370(10), pp. 1071-5.

Reese, M. G., Eeckman, F. H., Kulp, D. and Haussler, D. (1997) 'Improved splice site detection in Genie', *J Comput Biol,* 4(3), pp. 311-23.

Reyes, A., Kazak, L., Wood, S. R., Yasukawa, T., Jacobs, H. T. and Holt, I. J. (2013) 'Mitochondrial DNA replication proceeds via a 'bootlace' mechanism involving the incorporation of processed transcripts', *Nucleic Acids Res,* 41(11), pp. 5837-50.

Richardson, D. R., Lane, D. J., Becker, E. M., Huang, M. L., Whitnall, M., Suryo Rahmanto, Y., Sheftel, A. D. and Ponka, P. (2010) 'Mitochondrial iron trafficking and the integration of iron metabolism between the mitochondrion and cytosol', *Proc Natl Acad Sci U S A,* 107(24), pp. 10775-82.

Richter, R., Rorbach, J., Pajak, A., Smith, P. M., Wessels, H. J., Huynen, M. A., Smeitink, J. A., Lightowlers, R. N. and Chrzanowska-Lightowlers, Z. M. (2010) 'A

functional peptidyl-tRNA hydrolase, ICT1, has been recruited into the human mitochondrial ribosome', 29(6), pp. 1116-1125.

Riley, L. G., Menezes, M. J., Rudinger-Thirion, J., Duff, R., De Lonlay, P., Rotig, A., Tchan, M. C., Davis, M., Cooper, S. T. and Christodoulou, J. (2013) 'Phenotypic variability and identification of novel YARS2 mutations in YARS2 mitochondrial myopathy, lactic acidosis and sideroblastic anaemia', 8(1), pp. 193.

Robberson, D. L., Kasamatsu, H. and Vinograd, J. (1972) 'Replication of Mitochondrial DNA. Circular Replicative Intermediates in Mouse L Cells', *Proceedings of the National Academy of Sciences,* 69(3), pp. 737-741.

Rocha, M. C., Grady, J. P., Grunewald, A., Vincent, A., Dobson, P. F., Taylor, R. W., Turnbull, D. M. and Rygiel, K. A. (2015) 'A novel immunofluorescent assay to investigate oxidative phosphorylation deficiency in mitochondrial myopathy: understanding mechanisms and improving diagnosis', *Sci Rep,* 5, pp. 15037.

Rodnina, M. V., Stark, H., Savelsbergh, A., Wieden, H. J., Mohr, D., Matassova, N. B., Peske, F., Daviter, T., Gualerzi, C. O. and Wintermeyer, W. (2000) 'GTPases mechanisms and functions of translation factors on the ribosome', *Biol Chem,* 381(5-6), pp. 377-87.

Rodriguez-Rodriguez, D. R., Ramirez-Solis, R., Garza-Elizondo, M. A., Garza-Rodriguez, M. L. and Barrera-Saldana, H. A. (2019) 'Genome editing: A perspective on the application of CRISPR/Cas9 to study human diseases (Review)', *Int J Mol Med,* 43(4), pp. 1559-1574.

Roger, A. J., Munoz-Gomez, S. A. and Kamikawa, R. (2017) 'The Origin and Diversification of Mitochondria', *Curr Biol,* 27(21), pp. R1177-R1192.

Rorbach, J., Boesch, P., Gammage, P. A., Nicholls, T. J., Pearce, S. F., Patel, D., Hauser, A., Perocchi, F. and Minczuk, M. (2014) 'MRM2 and MRM3 are involved in biogenesis of the large subunit of the mitochondrial ribosome', *Mol Biol Cell,* 25(17), pp. 2542-55.

Rudler, D. L., Hughes, L. A., Perks, K. L., Richman, T. R., Kuznetsova, I., Ermer, J. A., Abudulai, L. N., Shearwood, A. J., Viola, H. M., Hool, L. C., Siira, S. J., Rackham, O. and Filipovska, A. (2019) 'Fidelity of translation initiation is required for coordinated respiratory complex assembly', *Sci Adv,* 5(12), pp. eaay2118.

Ruhanen, H., Ushakov, K. and Yasukawa, T. (2011) 'Involvement of DNA ligase III and ribonuclease H1 in mitochondrial DNA replication in cultured human cells', *Biochimica et Biophysica Acta (BBA) - Molecular Cell Research,* 1813(12), pp. 2000-2007.

Ryu, S. M., Hur, J. W. and Kim, K. (2019) 'Evolution of CRISPR towards accurate and efficient mammal genome engineering', *BMB Rep,* 52(8), pp. 475-481.

Saada, A., Shaag, A., Arnon, S., Dolfin, T., Miller, C., Fuchs-Telem, D., Lombes, A. and Elpeleg, O. (2007) 'Antenatal mitochondrial disease caused by mitochondrial ribosomal protein (MRPS22) mutation', *J Med Genet,* 44(12), pp. 784-6.

Salinas-Giege, T., Giege, R. and Giege, P. (2015) 'tRNA biology in mitochondria', *Int J Mol Sci,* 16(3), pp. 4518-59.

Sallevelt, S. C., de Die-Smulders, C. E., Hendrickx, A. T., Hellebrekers, D. M., de Coo, I. F., Alston, C. L., Knowles, C., Taylor, R. W., McFarland, R. and Smeets, H. J. (2017) 'De novo mtDNA point mutations are common and have a low recurrence risk', *J Med Genet,* 54(2), pp. 73-83.

Salvesen, G. S. and Dixit, V. M. (1997) 'Caspases: intracellular signaling by proteolysis', *Cell,* 91(4), pp. 443-6.

Samanta, K., Mirams, G. R. and Parekh, A. B. (2018) 'Sequential forward and reverse transport of the Na(+) Ca(2+) exchanger generates Ca(2+) oscillations within mitochondria', *Nat Commun,* 9(1), pp. 156.

Sanger, F., Nicklen, S. and Coulson, A. R. (1977) 'DNA sequencing with chain-terminating inhibitors', *Proc Natl Acad Sci U S A,* 74(12), pp. 5463-7.

Sasarman, F., Antonicka, H. and Shoubridge, E. A. (2008) 'The A3243G tRNALeu(UUR) MELAS mutation causes amino acid misincorporation and a combined respiratory chain assembly defect partially suppressed by overexpression of EFTu and EFG2', *Hum Mol Genet,* 17(23), pp. 3697-707.

Satoh, M. and Kuroiwa, T. (1991) 'Organization of multiple nucleoids and DNA molecules in mitochondria of a human cell', *Exp Cell Res,* 196(1), pp. 137-40.

Scala, M., Brigati, G., Fiorillo, C., Nesti, C., Rubegni, A., Pedemonte, M., Bruno, C., Severino, M., Derchi, M., Minetti, C. and Santorelli, F. M. (2019) 'Novel homozygous TSFM pathogenic variant associated with encephalocardiomyopathy with sensorineural hearing loss and peculiar neuroradiologic findings', *Neurogenetics,* 20(3), pp. 165-172.

Schafer, E., Seelert, H., Reifschneider, N. H., Krause, F., Dencher, N. A. and Vonck, J. (2006) 'Architecture of active mammalian respiratory chain supercomplexes', *J Biol Chem,* 281(22), pp. 15370-5.

Schagger, H. and Pfeiffer, K. (2000) 'Supercomplexes in the respiratory chains of yeast and mammalian mitochondria', *EMBO J,* 19(8), pp. 1777-83.

Schiller, D. (2009) 'Pam17 and Tim44 act sequentially in protein import into the mitochondrial matrix', *Int J Biochem Cell Biol,* 41(11), pp. 2343-9.

Schubert Baldo, M. and Vilarinho, L. (2020) 'Molecular basis of Leigh syndrome: a current look', *Orphanet J Rare Dis,* 15(1), pp. 31.

Schwartz, M. and Vissing, J. (2002) 'Paternal inheritance of mitochondrial DNA', *N Engl J Med,* 347(8), pp. 576-80.

Serre, V., Rozanska, A., Beinat, M., Chretien, D., Boddaert, N., Munnich, A., Rotig, A. and Chrzanowska-Lightowlers, Z. M. (2013) 'Mutations in mitochondrial ribosomal protein MRPL12 leads to growth retardation, neurological deterioration and mitochondrial translation deficiency', *Biochim Biophys Acta,* 1832(8), pp. 1304-12.

Shadel, G. S. and Clayton, D. A. (1997) 'Mitochondrial DNA Maintenance In Vertibrates', 66(1), pp. 409-435.

Shajani, Z., Sykes, M. T. and Williamson, J. R. (2011) 'Assembly of bacterial ribosomes', *Annu Rev Biochem,* 80, pp. 501-26.

Shamseldin, H. E., Alshammari, M., Al-Sheddi, T., Salih, M. A., Alkhalidi, H., Kentab, A., Repetto, G. M., Hashem, M. and Alkuraya, F. S. (2012) 'Genomic analysis of mitochondrial diseases in a consanguineous population reveals novel candidate disease genes', *J Med Genet,* 49(4), pp. 234-41.

Sharma, M. R., Koc, E. C., Datta, P. P., Booth, T. M., Spremulli, L. L. and Agrawal, R. K. (2003) 'Structure of the mammalian mitochondrial ribosome reveals an expanded functional role for its component proteins', *Cell,* 115(1), pp. 97-108.

Shimazaki, H., Takiyama, Y., Ishiura, H., Sakai, C., Matsushima, Y., Hatakeyama, H., Honda, J., Sakoe, K., Naoi, T., Namekawa, M., Fukuda, Y., Takahashi, Y., Goto, J., Tsuji, S., Goto, Y. I. and Nakano, I. (2012) 'A homozygous mutation of C12orf65 causes spastic paraplegia with optic atrophy and neuropathy (SPG55)', 49(12), pp. 777-784.

Shoubridge, E. A. and Wai, T. (2007) 'Mitochondrial DNA and the mammalian oocyte', *Curr Top Dev Biol,* 77, pp. 87-111.

Sideris, D. P., Petrakis, N., Katrakili, N., Mikropoulou, D., Gallo, A., Ciofi-Baffoni, S., Banci, L., Bertini, I. and Tokatlidis, K. (2009) 'A novel intermembrane space-targeting signal docks cysteines onto Mia40 during mitochondrial oxidative folding', *J Cell Biol,* 187(7), pp. 1007-22.

Simon, M. T., Ng, B. G., Friederich, M. W., Wang, R. Y., Boyer, M., Kircher, M., Collard, R., Buckingham, K. J., Chang, R., Shendure, J., Nickerson, D. A., Bamshad, M. J., Van Hove, J. L. K., Freeze, H. H. and Abdenur, J. E. (2017) 'Activation of a cryptic splice site in the mitochondrial elongation factor GFM1 causes combined OXPHOS deficiency'.

Sissler, M., Gonzalez-Serrano, L. E. and Westhof, E. (2017) 'Recent Advances in Mitochondrial Aminoacyl-tRNA Synthetases and Disease', *Trends Mol Med,* 23(8), pp. 693-708.

Skladal, D., Halliday, J. and Thorburn, D. R. (2003) 'Minimum birth prevalence of mitochondrial respiratory chain disorders in children', *Brain,* 126(Pt 8), pp. 1905-12.

Smeitink, J. A., Elpeleg, O., Antonicka, H., Diepstra, H., Saada, A., Smits, P., Sasarman, F., Vriend, G., Jacob-Hirsch, J., Shaag, A., Rechavi, G., Welling, B., Horst, J., Rodenburg, R. J., van den Heuvel, B. and Shoubridge, E. A. (2006a) 'Distinct clinical phenotypes associated with a mutation in the mitochondrial translation elongation factor EFTs', *Am J Hum Genet,* 79(5), pp. 869-77.

Smeitink, J. A. M., Elpeleg, O., Antonicka, H., Diepstra, H., Saada, A., Smits, P., Sasarman, F., Vriend, G., Jacob-Hirsch, J., Shaag, A., Rechavi, G., Welling, B., Horst, J., Rodenburg, R. J., Van Den Heuvel, B. and Shoubridge, E. A. (2006b) 'Distinct Clinical Phenotypes Associated with a Mutation in the Mitochondrial Translation Elongation Factor EFTs', 79(5), pp. 869-877.

Smith, K. R., Bromhead, C. J., Hildebrand, M. S., Shearer, A. E., Lockhart, P. J., Najmabadi, H., Leventer, R. J., McGillivray, G., Amor, D. J., Smith, R. J. and Bahlo, M. (2011) 'Reducing the exome search space for mendelian diseases using genetic linkage analysis of exome genotypes', *Genome Biol,* 12(9), pp. R85.

Smits, P., Antonicka, H., Van Hasselt, P. M., Weraarpachai, W., Haller, W., Schreurs, M., Venselaar, H., Rodenburg, R. J., Smeitink, J. A. and Van Den Heuvel, L. P. (2011a) 'Mutation in subdomain G' of mitochondrial elongation factor G1 is associated with combined OXPHOS deficiency in fibroblasts but not in muscle', 19(3), pp. 275-279.

Smits, P., Saada, A., Wortmann, S. B., Heister, A. J., Brink, M., Pfundt, R., Miller, C., Haas, D., Hantschmann, R., Rodenburg, R. J., Smeitink, J. A. and van den Heuvel, L. P. (2011b) 'Mutation in mitochondrial ribosomal protein MRPS22 leads to Cornelia de Lange-like phenotype, brain abnormalities and hypertrophic cardiomyopathy', *Eur J Hum Genet,* 19(4), pp. 394-9.

Smits, P., Smeitink, J. and van den Heuvel, L. (2010) 'Mitochondrial translation and beyond: processes implicated in combined oxidative phosphorylation deficiencies', *J Biomed Biotechnol,* 2010, pp. 737385.

Smits, P., Smeitink, J. A., van den Heuvel, L. P., Huynen, M. A. and Ettema, T. J. (2007) 'Reconstructing the evolution of the mitochondrial ribosomal proteome', *Nucleic Acids Res,* 35(14), pp. 4686-703.

Sommerville, E. W., Zhou, X.-L., Oláhová, M., Jenkins, J., Euro, L., Konovalova, S., Hilander, T., Pyle, A., He, L., Habeebu, S., Saunders, C., Kelsey, A., Morris, A. A. M., McFarland, R., Suomalainen, A., Gorman, G. S., Wang, E.-D., Thiffault, I., Tyynismaa, H. and Taylor, R. W. (2018) 'Instability of the mitochondrial alanyl-tRNA synthetase underlies fatal infantile-onset cardiomyopathy', *Human Molecular Genetics*.

Song, Z., Ghochani, M., McCaffery, J. M., Frey, T. G. and Chan, D. C. (2009) 'Mitofusins and OPA1 mediate sequential steps in mitochondrial membrane fusion', *Mol Biol Cell,* 20(15), pp. 3525-32.

Spurdle, A. B., Couch, F. J., Hogervorst, F. B., Radice, P., Sinilnikova, O. M. and Group, I. U. G. V. W. (2008) 'Prediction and assessment of splicing alterations: implications for clinical testing', *Hum Mutat,* 29(11), pp. 1304-13.

Stenton, S. L. and Prokisch, H. (2020) 'Genetics of mitochondrial diseases: Identifying mutations to help diagnosis', *EBioMedicine,* 56, pp. 102784.

Stewart, J. B. and Chinnery, P. F. (2015) 'The dynamics of mitochondrial DNA heteroplasmy: implications for human health and disease', *Nat Rev Genet,* 16(9), pp. 530-42.

Sun, F., Huo, X., Zhai, Y., Wang, A., Xu, J., Su, D., Bartlam, M. and Rao, Z. (2005) 'Crystal structure of mitochondrial respiratory membrane protein complex II', *Cell,* 121(7), pp. 1043-57.

Sutovsky, P., Van Leyen, K., McCauley, T., Day, B. N. and Sutovsky, M. (2004) 'Degradation of paternal mitochondria after fertilization: implications for heteroplasmy, assisted reproductive technologies and mtDNA inheritance', *Reprod Biomed Online,* 8(1), pp. 24-33.

Suzuki, T., Nagao, A. and Suzuki, T. (2011) 'Human Mitochondrial tRNAs: Biogenesis, Function, Structural Aspects, and Diseases', 45(1), pp. 299-329.

Suzuki, T. and Suzuki, T. (2014) 'A complete landscape of post-transcriptional modifications in mammalian mitochondrial tRNAs', *Nucleic Acids Res,* 42(11), pp. 7346-57.

Szczesny, R. J., Borowski, L. S., Brzezniak, L. K., Dmochowska, A., Gewartowski, K., Bartnik, E. and Stepien, P. P. (2010) 'Human mitochondrial RNA turnover caught in flagranti: involvement of hSuv3p helicase in RNA surveillance', *Nucleic Acids Res,* 38(1), pp. 279-98.

Takeuchi, N., Kawakami, M., Omori, A., Ueda, T., Spremulli, L. L. and Watanabe, K. (1998) 'Mammalian mitochondrial methionyl-tRNA transformylase from bovine liver. Purification, characterization, and gene structure', *J Biol Chem,* 273(24), pp. 15085-90.

Taylor, R. W., McDonnell, M. T., Blakely, E. L., Chinnery, P. F., Taylor, G. A., Howell, N., Zeviani, M., Briem, E., Carrara, F. and Turnbull, D. M. (2003) 'Genotypes from patients indicate no paternal mitochondrial DNA contribution', *Ann Neurol,* 54(4), pp. 521-4.

Taylor, R. W., Pyle, A., Griffin, H., Blakely, E. L., Duff, J., He, L., Smertenko, T., Alston, C. L., Neeve, V. C., Best, A., Yarham, J. W., Kirschner, J., Schara, U., Talim, B., Topaloglu, H., Baric, I., Holinski-Feder, E., Abicht, A., Czermin, B., Kleinle, S., Morris,

A. A. M., Vassallo, G., Gorman, G. S., Ramesh, V., Turnbull, D. M., Santibanez-Koref, M., McFarland, R., Horvath, R. and Chinnery, P. F. (2014) 'Use of Whole-Exome Sequencing to Determine the Genetic Basis of Multiple Mitochondrial Respiratory Chain Complex Deficiencies', 312(1), pp. 68.

Taylor, R. W., Schaefer, A. M., Barron, M. J., McFarland, R. and Turnbull, D. M. (2004) 'The diagnosis of mitochondrial muscle disease', *Neuromuscul Disord,* 14(4), pp. 237-45.

Taylor, R. W. and Turnbull, D. M. (2005) 'Mitochondrial DNA mutations in human disease', *Nat Rev Genet,* 6(5), pp. 389-402.

Temperley, R. J., Wydro, M., Lightowlers, R. N. and Chrzanowska-Lightowlers, Z. M. (2010) 'Human mitochondrial mRNAs—like members of all families, similar but different', 1797(6-7), pp. 1081-1085.

Terzioglu, M., Ruzzenente, B., Harmel, J., Mourier, A., Jemt, E., Lopez, M. D., Kukat, C., Stewart, J. B., Wibom, R., Meharg, C., Habermann, B., Falkenberg, M., Gustafsson, C. M., Park, C. B. and Larsson, N. G. (2013) 'MTERF1 binds mtDNA to prevent transcriptional interference at the light-strand promoter but is dispensable for rRNA gene transcription regulation', *Cell Metab,* 17(4), pp. 618-26.

Thompson, K., Collier, J. J., Glasgow, R. I. C., Robertson, F. M., Pyle, A., Blakely, E. L., Alston, C. L., Olahova, M., McFarland, R. and Taylor, R. W. (2019) 'Recent advances in understanding the molecular genetic basis of mitochondrial disease', *J Inherit Metab Dis,* 43(1), pp. 36-50.

Thompson, K., Mai, N., Oláhová, M., Scialó, F., Formosa, L. E., Stroud, D. A., Garrett, M., Lax, N. Z., Robertson, F. M., Jou, C., Nascimento, A., Ortez, C., Jimenez-Mallebrera, C., Hardy, S. A., He, L., Brown, G. K., Marttinen, P., McFarland, R., Sanz, A., Battersby, B. J., Bonnen, P. E., Ryan, M. T., Chrzanowska-Lightowlers, Z. M., Lightowlers, R. N. and Taylor, R. W. (2018) 'OXA1L mutations cause mitochondrial encephalopathy and a combined oxidative phosphorylation defect', *EMBO Molecular Medicine*, pp. e9060.

Tolkunova, E., Park, H., Xia, J., King, M. P. and Davidson, E. (2000) 'The human lysyl-tRNA synthetase gene encodes both the cytoplasmic and mitochondrial enzymes by means of an unusual alternative splicing of the primary transcript', *J Biol Chem,* 275(45), pp. 35063-9.

Traschutz, A., Hayer, S. N., Bender, B., Schols, L., Biskup, S. and Synofzik, M. (2019) 'TSFM mutations cause a complex hyperkinetic movement disorder with strong relief by cannabinoids', *Parkinsonism Relat Disord,* 60, pp. 176-178.

Tsuboi, M., Morita, H., Nozaki, Y., Akama, K., Ueda, T., Ito, K., Nierhaus, K. H. and Takeuchi, N. (2009) 'EF-G2mt is an exclusive recycling factor in mammalian mitochondrial protein synthesis', *Mol Cell,* 35(4), pp. 502-10.

Tucker, E. J., Hershman, S. G., Kohrer, C., Belcher-Timme, C. A., Patel, J., Goldberger, O. A., Christodoulou, J., Silberstein, J. M., McKenzie, M., Ryan, M. T., Compton, A. G., Jaffe, J. D., Carr, S. A., Calvo, S. E., RajBhandary, U. L., Thorburn, D. R. and Mootha, V. K. (2011) 'Mutations in MTFMT underlie a human disorder of formylation causing impaired mitochondrial translation', *Cell Metab,* 14(3), pp. 428-34.

Uchiumi, T., Ohgaki, K., Yagi, M., Aoki, Y., Sakai, A., Matsumoto, S. and Kang, D. (2010) 'ERAL1 is associated with mitochondrial ribosome and elimination of ERAL1 leads to mitochondrial dysfunction and growth retardation', *Nucleic Acids Res,* 38(16), pp. 5554-68.

Uhler, J. P. and Falkenberg, M. (2015) 'Primer removal during mammalian mitochondrial DNA replication', 34, pp. 28-38.

Valente, L., Shigi, N., Suzuki, T. and Zeviani, M. (2009) 'The R336Q mutation in human mitochondrial EFTu prevents the formation of an active mt-EFTu.GTP.aa-tRNA ternary complex', *Biochim Biophys Acta,* 1792(8), pp. 791-5.

Valente, L., Tiranti, V., Marsano, R. M., Malfatti, E., Fernandez-Vizarra, E., Donnini, C., Mereghetti, P., De Gioia, L., Burlina, A., Castellan, C., Comi, G. P., Savasta, S., Ferrero, I. and Zeviani, M. (2007) 'Infantile Encephalopathy and Defective Mitochondrial DNA Translation in Patients with Mutations of Mitochondrial Elongation Factors EFG1 and EFTu', *The American Journal of Human Genetics,* 80(1), pp. 44-58.

Vedrenne, V., Galmiche, L., Chretien, D., de Lonlay, P., Munnich, A. and Rotig, A. (2012) 'Mutation in the mitochondrial translation elongation factor EFTs results in severe infantile liver failure', *J Hepatol,* 56(1), pp. 294-7.

Verrigni, D., Diodato, D., Di Nottia, M., Torraco, A., Bellacchio, E., Rizza, T., Tozzi, G., Verardo, M., Piemonte, F., Tasca, G., D'Amico, A., Bertini, E. and Carrozzo, R. (2017) 'Novel mutations in KARS cause hypertrophic cardiomyopathy and combined mitochondrial respiratory chain defect', *Clinical Genetics,* 91(6), pp. 918-923.

Von Ballmoos, C., Wiedenmann, A. and Dimroth, P. (2009) 'Essentials for ATP synthesis by F1F0 ATP synthases', *Annu Rev Biochem,* 78, pp. 649-72.

Wai, T., Ao, A., Zhang, X., Cyr, D., Dufort, D. and Shoubridge, E. A. (2010) 'The role of mitochondrial DNA copy number in mammalian fertility', *Biol Reprod,* 83(1), pp. 52-62.

Walberg, M. W. and Clayton, D. A. (1981) 'Sequence and properties of the human KB cell and mouse L cell D-loop regions of mitochondrial DNA', *Nucleic Acids Res,* 9(20), pp. 5411-21.

Wang, L. (2016) 'Mitochondrial purine and pyrimidine metabolism and beyond', *Nucleosides, Nucleotides and Nucleic Acids,* 35(10-12), pp. 578-594.

Wang, M. and Marin, A. (2006) 'Characterization and prediction of alternative splice sites', *Gene,* 366(2), pp. 219-27.

Wanrooij, S. and Falkenberg, M. (2010) 'The human mitochondrial replication fork in health and disease', *Biochimica et Biophysica Acta (BBA) - Bioenergetics,* 1797(8), pp. 1378-1388.

Webb, B. D., Wheeler, P. G., Hagen, J. J., Cohen, N., Linderman, M. D., Diaz, G. A., Naidich, T. P., Rodenburg, R. J., Houten, S. M. and Schadt, E. E. (2015) 'Novel, Compound Heterozygous, Single-Nucleotide Variants in MARS2 Associated with Developmental Delay, Poor Growth, and Sensorineural Hearing Loss', *Human Mutation,* 36(6), pp. 587-592.

Wei, W., Pagnamenta, A. T., Gleadall, N., Sanchis-Juan, A., Stephens, J., Broxholme, J., Tuna, S., Odhams, C. A., Genomics England Research, C., BioResource, N., Fratter, C., Turro, E., Caulfield, M. J., Taylor, J. C., Rahman, S. and Chinnery, P. F. (2020) 'Nuclear-mitochondrial DNA segments resemble paternally inherited mitochondrial DNA in humans', *Nat Commun,* 11(1), pp. 1740.

Wiedemann, N., Kozjak, V., Chacinska, A., Schonfisch, B., Rospert, S., Ryan, M. T., Pfanner, N. and Meisinger, C. (2003) 'Machinery for protein sorting and assembly in the mitochondrial outer membrane', *Nature,* 424(6948), pp. 565-71.

Wiedemann, N. and Pfanner, N. (2017) 'Mitochondrial Machineries for Protein Import and Assembly', *Annu Rev Biochem,* 86, pp. 685-714.

Wilson, D. F. (2017) 'Oxidative phosphorylation: regulation and role in cellular and tissue metabolism', *J Physiol,* 595(23), pp. 7023-7038.

Wintermeyer, W. and Rodnina, M. V. (2000) 'Translational elongation factor G: a GTP-driven motor of the ribosome', *Essays Biochem,* 35, pp. 117-29.

Woodbridge, P., Liang, C., Davis, R. L., Vandebona, H. and Sue, C. M. (2013) 'POLG mutations in Australian patients with mitochondrial disease', *Internal Medicine Journal,* 43(2), pp. 150-156.

Wortmann, S. B., Mayr, J. A., Nuoffer, J. M., Prokisch, H. and Sperl, W. (2017) 'A Guideline for the Diagnosis of Pediatric Mitochondrial Disease: The Value of Muscle and Skin Biopsies in the Genetics Era', *Neuropediatrics,* 48(4), pp. 309-314.

Xia, D., Yu, C.-A., Zhou, F. and Esser, L. (2018) 'Ubiquinol-Cytochrome c Oxidoreductase (Complex III)', in Roberts, G. and Watts, A. (eds.) *Encyclopedia of Biophysics*. Berlin, Heidelberg: Springer Berlin Heidelberg, pp. 1-8.

Xu, F., Ackerley, C., Maj, M. C., Addis, J. B., Levandovskiy, V., Lee, J., Mackay, N., Cameron, J. M. and Robinson, B. H. (2008) 'Disruption of a mitochondrial RNA-binding protein gene results in decreased cytochrome b expression and a marked reduction in ubiquinol-cytochrome c reductase activity in mouse heart mitochondria', *Biochem J,* 416(1), pp. 15-26.

Yakes, F. M. and Van Houten, B. (1997) 'Mitochondrial DNA damage is more extensive and persists longer than nuclear DNA damage in human cells following oxidative stress', *Proc Natl Acad Sci U S A,* 94(2), pp. 514-9.

Yellen, G. (2018) 'Fueling thought: Management of glycolysis and oxidative phosphorylation in neuronal metabolism', *J Cell Biol,* 217(7), pp. 2235-2246.

Zaganelli, S., Rebelo-Guiomar, P., Maundrell, K., Rozanska, A., Pierredon, S., Powell, C. A., Jourdain, A. A., Hulo, N., Lightowlers, R. N., Chrzanowska-Lightowlers, Z. M., Minczuk, M. and Martinou, J.-C. (2017) 'The Pseudouridine Synthase RPUSD4 Is an Essential Component of Mitochondrial RNA Granules', *Journal of Biological Chemistry,* 292(11), pp. 4519-4532.

Zhang, F., Wen, Y. and Guo, X. (2014) 'CRISPR/Cas9 for genome editing: progress, implications and challenges', *Hum Mol Genet,* 23(R1), pp. R40-6.

Zhang, L., Vielle, A., Espinosa, S. and Zhao, R. (2019) 'RNAs in the spliceosome: Insight from cryoEM structures', *Wiley Interdiscip Rev RNA,* 10(3), pp. e1523.

Zickermann, V., Wirth, C., Nasiri, H., Siegmund, K., Schwalbe, H., Hunte, C. and Brandt, U. (2015) 'Structural biology. Mechanistic insight from the crystal structure of mitochondrial complex I', *Science,* 347(6217), pp. 44-9.

Zong, S., Wu, M., Gu, J., Liu, T., Guo, R. and Yang, M. (2018) 'Structure of the intact 14-subunit human cytochrome c oxidase', *Cell Res,* 28(10), pp. 1026-1034.